

# TECHNISCHE UNIVERSITÄT MÜNCHEN

Lehrstuhl für Experimentelle Genetik

## *In vivo* and *in vitro* analysis of *Dll1* and *Pax6* function in the adult mouse pancreas

Davide Cavanna

Vollständiger Abdruck der von der Fakultät Wissenschaftszentrum Weihenstephan für Ernährung, Landnutzung und Umwelt der Technischen Universität München zur Erlangung des akademischen Grades eines

Doktors der Naturwissenschaften

genehmigten Dissertation.

Vorsitzender: Univ.-Prof. Dr. D. Langosch

Prüfer der Dissertation:

1. Univ.-Prof. Dr. M. Hrabé de Angelis
2. Univ.-Prof. A. Schnieke, Ph.D.

Die Dissertation wurde am 03.07.2013 bei der Technischen Universität München eingereicht und durch die Fakultät Wissenschaftszentrum Weihenstephan für Ernährung, Landnutzung und Umwelt am 10.12.2013 angenommen.

# I. Table of contents

<b>I.</b>	<b>TABLE OF CONTENTS</b>	<b>I</b>
<b>II.</b>	<b>FIGURES AND TABLES</b>	<b>V</b>
<b>III.</b>	<b>ABBREVIATIONS</b>	<b>VIII</b>
<b>IV.</b>	<b>PUBLICATIONS, TALKS, AND POSTERS</b>	<b>XI</b>
<b>V.</b>	<b>ACKNOWLEDGMENTS</b>	<b>XII</b>
<b>VI.</b>	<b>AFFIRMATION</b>	<b>XIV</b>
<b>1.</b>	<b>SUMMARY/ZUSAMMENFASSUNG</b>	<b>1</b>
<b>2.</b>	<b>INTRODUCTION</b>	<b>3</b>
<b>2.1</b>	<b>Notch signaling</b>	<b>3</b>
2.1.1	Notch signaling components and function	3
2.1.2	Ligand-side non-canonical Notch signaling	6
<b>2.2</b>	<b>The pancreas and the insulin-producing <math>\beta</math>-cells</b>	<b>8</b>
2.2.1	Organ development	8
2.2.1.1	Pancreatic endocrine development	8
2.2.1.2	Notch signaling in pancreatic development	10
2.2.2	The adult pancreas	14
2.2.2.1	Pancreatic anatomy	14
2.2.2.2	Pancreatic $\beta$ -cell function	15
<b>2.3</b>	<b>Diabetes Mellitus</b>	<b>18</b>
2.3.1	Overview	18
2.3.2	The $\beta$ -cell in Type 2 diabetes	19
2.3.3	Notch signaling in diabetes and the adult pancreas	21
<b>2.4</b>	<b>The <i>Pax6</i><sup><i>Leca2</i></sup> mouse model</b>	<b>23</b>
<b>2.5</b>	<b>Thesis outline</b>	<b>25</b>
<b>3.</b>	<b>MATERIALS AND METHODS</b>	<b>26</b>
<b>3.1</b>	<b>Materials</b>	<b>26</b>
3.1.1	Chemicals	26
3.1.2	Buffers and solutions	26
3.1.3	Enzymes and antibodies	29
3.1.4	Molecular biology reagents	29
3.1.5	Kits	30

3.1.6	Plasmids .....	30
3.1.7	Oligonucleotide primers .....	31
3.1.7.1	Mus musculus primers .....	31
3.1.7.1.1	Primers for qRT-PCR (housekeeping genes) .....	31
3.1.7.1.2	Primers for qRT-PCR (genes of interest) .....	32
3.1.7.1.3	Primers for PCR .....	33
3.1.7.2	Rattus Norvegicus primers .....	33
3.1.7.2.1	Primers for qRT-PCR (housekeeping genes) .....	33
3.1.7.2.2	Primers for qRT-PCR (genes of interest) .....	34
3.1.8	Mouse strains .....	34
3.1.9	Cell lines .....	34
<b>3.2</b>	<b>Methods .....</b>	<b>35</b>
3.2.1	Isolation and purification methods .....	35
3.2.1.1	DNA isolation .....	35
3.2.1.2	RNA isolation .....	35
3.2.1.3	Protein isolation .....	36
3.2.2	Molecular methods .....	36
3.2.2.1	Polymerase Chain Reaction (PCR) .....	36
3.2.2.2	cDNA synthesis .....	37
3.2.2.3	Quantitative real-time PCR (qRT-PCR) .....	38
3.2.2.3.1	General strategy .....	38
3.2.2.3.2	Reaction conditions .....	39
3.2.2.3.3	Data analysis .....	40
3.2.2.4	Whole transcriptome microarray analysis .....	41
3.2.2.5	SDS Polyacrylamide Gel Electrophoresis (SDS-PAGE) .....	46
3.2.2.6	Western Blot .....	46
3.2.2.7	Mouse Insulin ELISA .....	47
3.2.3	Cell culture methods .....	48
3.2.3.1	INS-1E cell culture .....	48
3.2.3.2	INS-1E pseudo-islets .....	48
3.2.3.3	Transfection of INS-1E cells .....	48
3.2.3.4	Islet isolation and culture .....	49
3.2.3.5	Glucose-stimulated insulin secretion (GSIS) .....	50
3.2.3.6	Determination of islet oxygen consumption rate (OCR) .....	51
3.2.4	Immunohistochemistry .....	52
3.2.4.1	Immunohistochemistry on pancreatic cryosections .....	52
3.2.4.2	Whole mount staining of isolated islets .....	52
3.2.5	Mouse methods .....	53

3.2.5.1	Animal housing .....	53
3.2.5.2	Generation of Dll1-βKO mice.....	53
3.2.5.3	Genotyping .....	53
3.2.5.4	Blood plasma collection.....	54
3.2.5.5	Blood glucose evaluation.....	54
3.2.5.6	Intraperitoneal glucose tolerance test (ipGTT) .....	54
<b>4.</b>	<b>RESULTS .....</b>	<b>55</b>
<b>4.1</b>	<b><i>In vitro</i> analysis of <i>Dll1</i> and Notch signaling .....</b>	<b>55</b>
4.1.1	Isolated islets of Langerhans.....	55
4.1.2	Insulinoma-derived cell line INS-1E.....	56
<b>4.2</b>	<b>The Dll1-βKO .....</b>	<b>63</b>
4.2.1	Conditional deletion of Dll1 in adult pancreatic β-cells .....	63
4.2.2	Expression analysis of Notch signaling components and targets .....	65
4.2.3	Islet physiology.....	67
4.2.4	In vitro glucose-stimulated insulin secretion (GSIS).....	69
4.2.5	Transcriptomics analysis .....	69
4.2.5.1	Expression profiling of Dll1-βKO islets.....	69
4.2.5.2	Expression profiling of Dll1-βKO islets with a revised approach .....	71
4.2.6	Metabolic phenotyping.....	76
<b>4.3</b>	<b>Dll1_T720A.....</b>	<b>86</b>
<b>4.4</b>	<b><i>Pax6</i><sup>Leca2</sup> .....</b>	<b>90</b>
<b>4.5</b>	<b>Islet cell culture: general findings.....</b>	<b>97</b>
<b>5.</b>	<b>DISCUSSION .....</b>	<b>100</b>
<b>5.1</b>	<b>Dll1 .....</b>	<b>100</b>
5.1.1	In vitro analysis of Dll1 .....	100
5.1.2	Dll1-βKO .....	100
5.1.2.1	Effects of Ins2-controlled expression of Cre in pancreatic β-cells.....	100
5.1.2.2	Metabolic phenotyping .....	104
5.1.2.3	Gene expression analyses.....	105
5.1.3	Conclusion and future perspective .....	108
<b>5.2</b>	<b><i>Pax6</i><sup>Leca2</sup> .....</b>	<b>110</b>
5.2.1	PAX6 <sup>R128C</sup> has direct effects on the global gene expression pattern of adult islets .....	110
5.2.2	PAX6 <sup>R128C</sup> modulates the interaction of the RED subdomain with ETS transcription factors .....	113
5.2.3	PAX6-regulated islet marker genes in <i>Pax6</i> <sup>Leca2</sup> islets .....	114
5.2.4	β-cell dedifferentiation in <i>Pax6</i> <sup>Leca2</sup> islets .....	116
5.2.5	Conclusion and future perspective .....	122
<b>5.3</b>	<b>General comments about islet isolation.....</b>	<b>124</b>
<b>5.4</b>	<b>Closing remarks.....</b>	<b>126</b>

<b>6. APPENDIX .....</b>	<b>127</b>
<b>6.1 Supplementary Figures .....</b>	<b>127</b>
<b>6.2 Supplementary Tables.....</b>	<b>130</b>
<b>7. REFERENCES .....</b>	<b>172</b>

## II. Figures and tables

Figure 1. The canonical Notch pathway. ....	5
Figure 2. Schematic representation of pancreatic development. ....	9
Figure 3. Stepwise differentiation of multipotent pancreatic progenitors into mature islet cells. ....	10
Figure 4. Schematic representation of pancreatic anatomy. ....	15
Figure 5. Glucose-stimulated insulin secretion. ....	16
Figure 6. Role of $\beta$ -cell defects in the etiology of Type 2 Diabetes. ....	21
Figure 7. Schematic representation of PAX6. ....	23
Figure 8. Overview of the procedure for Affymetrix whole transcriptome microarray analysis. From GeneChip® WT Terminal Labeling and Controls Kit user manual. ....	42
Figure 9. Freshly isolated islets. ....	50
Figure 10. Expression of Notch signaling genes in isolated primary C3HeB/FeJ islets. ....	55
Figure 11. Time-dependent regulation of Notch signaling genes in isolated primary C3HeB/FeJ islets. ....	56
Figure 12. Notch signaling activity in INS-1E cells. ....	57
Figure 13. qRT-PCR analysis of INS-1E cells grown in monolayers and as pseudo-islets. ....	58
Figure 14. qRT-PCR analysis of INS-1E cells incubated with the GLP-1 agonist Exendin-4 (Ex4). ....	59
Figure 15. DLL1 overexpression in INS-1E cells. ....	61
Figure 16. <i>In vitro</i> GSIS in INS-1E cells transiently overexpressing DLL1 and DLL1 $\Delta$ A7EV. ....	62
Figure 17. Schematic representation of the <i>Dll1</i> locus and its recombination in $\beta$ -cells of the Dll1- $\beta$ KO mouse. ....	63
Figure 18. Analysis of recombination in the <i>Dll1</i> locus by PCR on genomic DNA. ....	64
Figure 19. Downregulation of <i>Dll1</i> expression in Dll1- $\beta$ KO islets. ....	65
Figure 20. qRT-PCR analysis of isolated islets from 8-weeks old Dll1- $\beta$ KO and CreN mice. ....	66
Figure 21. Relative <i>p21</i> expression in islets of 8-weeks old CreY and CreN <i>Dll1</i> <sup>+/+</sup> mice. ....	67
Figure 22. Immunohistochemical analysis of pancreata in 8-weeks old Dll1- $\beta$ KO and CreN mice. ....	68
Figure 23. Immunohistochemical analysis of pancreata in 40-weeks old Dll1- $\beta$ KO and CreN mice. ....	68
Figure 24. Immunohistochemical analysis of islet vascularization in 12-weeks old Dll1- $\beta$ KO and CreN mice. ....	69
Figure 25. <i>In vitro</i> GSIS in isolated islets from Dll1- $\beta$ KO and CreN mice. ....	69
Figure 26. qRT-PCR analysis of fibrosis-related genes in isolated islets from 37 weeks old mice. ....	71
Figure 27. Pre-selection of Dll1- $\beta$ KO, CreN, and CreY samples for gene expression profiling. ....	72
Figure 28. Regulated genes between Dll1- $\beta$ KO and CreN islets in two different experimental runs. ....	73
Figure 29. Cluster analysis of Dll1- $\beta$ KO, CreN, and CreY islets samples in the second gene expression profiling experiment. ....	74
Figure 30. <i>Ptsg2</i> expression in INS-1E cells incubated with DAPT. ....	76
Figure 31. Strategy for the metabolic phenotyping of the Dll1- $\beta$ KO. ....	77
Figure 32. Weight and body composition of 10-weeks old Dll1- $\beta$ KO, CreN, and CreY mice at the onset of the experiment. ....	78
Figure 33. Body weight of Dll1- $\beta$ KO and control mice over the course of six months. ....	79

Figure 34. Fasted blood glucose levels of Dll1-βKO and control mice over the course of six months.....	81
Figure 35. Blood glucose increase between the high fat and standard diet groups of Dll1-βKO and CreN male mice. ....	82
Figure 36. Plasma insulin levels of Dll1-βKO and control mice. ....	83
Figure 37. Plasma levels of triglycerides and NEFAs in 34-weeks old Dll1-βKO and CreN mice. ....	84
Figure 38. Intraperitoneal Glucose-tolerance test (GTT) on Dll1-βKO mice and controls. ....	85
Figure 39. qRT-PCR analysis of isolated islets from 16-weeks old Dll1_T720A and wild type mice.....	86
Figure 40. Relative <i>Amy2a1</i> expression in Dll1_T720A and wild-type islet samples used for whole genome transcriptomics.....	87
Figure 41. qRT-PCR analysis of selected transcriptomics targets in 16-weeks old Dll1_T720A and wild type mice. ....	88
Figure 42. Genome-wide expression analysis of <i>Pax6</i> <sup>Leca2</sup> mutant islets. ....	91
Figure 43. qRT-PCR analysis of selected genes in islets from 4-weeks old <i>Pax6</i> <sup>Leca2</sup> (n=5), heterozygous (n=6), and WT (n=3) mice. ....	95
Figure 44. Insulin content of islets isolated from 13-weeks old <i>Pax6</i> <sup>Leca2</sup> mice and wild-type littermates. ....	96
Figure 45. Relative expression of <i>Amy2a1</i> (A) and <i>Ins2</i> (B) in isolated C3HeB/FeJ islets after 24, 48, and 72 hours culture, as measured by qRT-PCR.....	97
Figure 46. Oxygen consumption rate (OCR) of islets isolated from BL6J wild-type mice. ....	98
Figure 47. Architecture of an isolated, intact C3HeB/FeJ islet, assessed with a laser scanning microscope.....	99
Figure 48. Venn diagram depicting the overlap between the dysregulated genes in <i>Pax6</i> <sup>Leca2</sup> islets and those genes reported by Xie <i>et al.</i> <sup>216</sup> to be directly bound by PAX6. ....	110
Supplementary Figure 1. qRT-PCR analysis of selected genes in islets from Dll1-βKO, CreY, and CreN mice. ....	127
Supplementary Figure 2. Fat and lean mass of 10-weeks old Dll1-βKO, CreN, and CreY mice, both males (m) and females (f), plotted against their weight (4.2.6).....	128
Supplementary Figure 3. Weight of Dll1-βKO and CreN male mice fed with a standard chow and aged 31 weeks. ....	128
Supplementary Figure 4. Relative <i>Amy2a1</i> expression in homozygous <i>Pax6</i> <sup>Leca2</sup> , heterozygous <i>Pax6</i> <sup>Leca2/wt</sup> and wild-type islets.....	129
Supplementary Figure 5. qRT-PCR analysis of selected genes in islets from 20-weeks old homozygous <i>Pax6</i> <sup>Leca2</sup> and WT mice. ....	129
Table 1. Major components of Notch signaling in mammals <sup>1,3</sup> . ....	3
Table 2. Dll1 overexpression constructs. ....	59
Table 3. <i>Dll1</i> -dependent differentially regulated genes. ....	75
Table 4. Number of animals involved in metabolic phenotyping by genotype, sex and diet. ....	78
Table 5. GeneRanker analysis of genes co-cited with the differentially regulated genes between 4-weeks old homozygous <i>Pax6</i> <sup>Leca2</sup> and wild-type mice. ....	92

Table 6. GeneRanker analysis of tissues associated with the differentially regulated genes between 4-weeks old homozygous <i>Pax6<sup>Leca2</sup></i> and wild-type mice. ....	93
Table 7. GeneRanker analysis of disease annotated with the differentially regulated genes between 4-weeks old homozygous <i>Pax6<sup>Leca2</sup></i> and wild-type mice. ....	94
Table 8. List of genes whose expression is controlled by PAX6 in pancreatic islet cells of rat, mouse, or human origin. ....	114
Supplementary Table 1. Differentially expressed genes in isolated islets from Dll1-βKO and CreN mice (4.2.5.1) filtered for a fold change of at least 1.5 and (FDR <10%). ....	130
Supplementary Table 2. GeneRanker analysis of the gene set displayed in Supplementary Table 1. Only the most significant tissues, cellular components, and disease are included. ....	139
Supplementary Table 3. Differentially expressed genes in isolated islets from Dll1-βKO and CreN mice of the second transcriptomics experiment (4.2.5.2), filtered for a fold change of at least 1.5 (FDR <10%). ....	139
Supplementary Table 4. GeneRanker analysis of certified Cre-dependent genes (4.2.5.2). ....	145
Supplementary Table 5. Differentially expressed genes in isolated islets from Dll1_T720A mice and wild-type controls, filtered for a fold change of at least 1.5 and a FDR of <10% (4.3). Acinar-related genes were excluded. ....	146
Supplementary Table 6. Differentially expressed genes in islets isolated from <i>Pax6<sup>Leca2</sup></i> and wild-type mice aged four weeks, filtered for a fold change of at least 2 and a FDR of <10% (4.4). Acinar-related genes were excluded. ....	150
Supplementary Table 7. Differentially expressed genes in islets isolated from <i>Pax6<sup>Leca2/wt</sup></i> and wild-type mice aged four weeks, filtered for a fold change of at least 2 and a FDR of <10% (4.4). Acinar-related genes were excluded. ....	153
Supplementary Table 8. Differentially expressed genes in islets isolated from <i>Pax6<sup>Leca2</sup></i> and <i>Pax6<sup>Leca2/wt</sup></i> mice aged four weeks, filtered for a fold change of at least 2 and a FDR of <10% (4.4). Acinar-related genes were excluded. ....	154
Supplementary Table 9. Differentially expressed genes in islets isolated from <i>Pax6<sup>Leca2</sup></i> and wild-type mice aged 20 weeks, filtered for a fold change of at least 2 and a FDR of <10% (4.4). Acinar-related genes were excluded. ....	155
Supplementary Table 10. List of genes both differentially regulated in 4-weeks old <i>Pax6<sup>Leca2</sup></i> islets and reported by Xie <i>et al.</i> <sup>216</sup> to be directly bound by PAX6. Gene names in bold refer to those promoter regions that were occupied by PAX6 in β-TC3 cells, whereas the rest were bound in chromatin from lens and forebrain. ....	168
Supplementary Table 11. List of genes both differentially regulated in 20-weeks old <i>Pax6<sup>Leca2</sup></i> islets and reported by Xie <i>et al.</i> <sup>216</sup> to be directly bound by PAX6. Gene names in bold refer to those promoter regions that were occupied by PAX6 in β-TC3 cells, whereas the rest were bound in chromatin from lens and forebrain. ....	168

### III. Abbreviations

A	Alanine
A	Adenine
ANOVA	Analysis of variance
APS	ammonium persulfate
ATP	Adenosine triphosphate
bp	Base pair
BSA	Bovine serum albumin
C	Cytosine
cAMP	Cyclic adenosine monophosphate
cDNA	Complementary deoxyribonucleic acid
ChIP	Chromatin Immunoprecipitation
CO <sub>2</sub>	Carbon dioxide
Cp	Crossing point
CreN	Cre- Dll1 <sup>fl/fl</sup> mice
CreY	Cre+ Dll1 <sup>wt/wt</sup> mice
cRNA	Copy ribonucleic acid
DNA	Deoxyribonucleic acid
DAPI	4'6-diamidino-2'-phenylindole
ddH <sub>2</sub> O	double-distilled water
DICD	Delta-like 1 intracellular domain
Dll1	Delta-like 1
Dll1- $\beta$ KO	Inducible, $\beta$ -cell specific Dll1 knockdown
DMSO	dimethyl sulfoxid
dNTP	Dinucleotide triphosphate
DTT	Dithiothreitol
ECM	Extracellular matrix
EDTA	Ethylene diamine tetraacetic acid
ELISA	Enzyme-linked immunosorbant assay
etc	Etcetera
FCS	Fetal calf serum
FDR	False discovery rate
FELASA	Federation of laboratory animal science association
G	Guanine
G	Centrifugal force
gDNA	Genomic deoxyribonucleic acid

GSIS	Glucose-stimulated insulin secretion
GWAS	Genome wide association studies
H	Histidine
HEPES	4-(2-hydroxyethyl)-1-piperazin-ethanesulfonic acid
IHC	Immunohistochemistry
ipGTT	Intraperitoneal glucose tolerance test
KRBH	Krebs Ringer bicarbonate buffer
LADA	Latent autoimmune diabetes of adulthood
Leca2	Lens corneal adhesion 2
mKRBH	Modified Krebs Ringer bicarbonate buffer
mRNA	Messenger ribonucleic acid
NaOH	Sodium hydroxide
NECD	Notch extracellular domain
NEFA	Non-esterified fatty acids
NEU	N-ethyl-N-nitrosurea
NICD	Notch intracellular domain
NMR	Nuclear magnetic resonance
NTMICD	Notch transmembrane and intracellular domain
OCR	Oxygen consumption rate
PAGE	Polyacrylamide gel electrophoresis
Pax6	Paired-box gene 6
Pax6 <sup>Leca2</sup>	Homozygous Pax6 <sup>Leca2</sup> mice
Pax6 <sup>Leca2/wt</sup>	Heterozygous Pax6 <sup>Leca2</sup> mice
PBS	Phosphate buffered saline
PBST	Phosphate buffered saline with 0.05% Tween-20
PCR	Polymerase chain reaction
PFA	Paraformaldehyde
PVDF	Polyvinylidene fluoride
qRT-PCR	Quantitative real-time PCR
R	Arginine
RIPA	Radioimmunoprecipitation assay buffer
RNA	Ribonucleic acid
Rnase	Ribonuclease
rpm	Revolutions per minute
RPMI	Roswell Park Memorial Institute
RT	Room temperature
SDS	Sodium dodecyl sulfate
SEM	Standard error of the mean

SPF	Specific-pathogen-free
T	Threonine
T	Tyrosine
T1DM	Type 1 Diabetes Mellitus
T2DM	Type 2 Diabetes Mellitus
TAE	Tris base, acetic acid and EDTA
TAM	Tamoxifen
TBS	Tris-buffered saline
TBST	Tris-buffered saline with 0.05% Tween-20
TEMED	N,N,N',N'-tetramethylethylenediamine
TMB	3,3',5,5'-Tetramethylbenzidine
WHO	World Health Organization
wt	Wild type

## 1. Summary/Zusammenfassung

Diabetes Mellitus is a global epidemic made particularly dangerous by its rapidly rising incidence. While many different lifestyle and genetic factors contribute to the disease, a better understanding of the biology of the insulin-producing  $\beta$ -cells, and particularly of  $\beta$ -cell dysfunction, will clearly be pivotal to the currently ongoing research efforts to lessen the burden represented by the disease for human welfare. Given new insights about *in vivo*  $\beta$ -cell dedifferentiation in Type 2 Diabetes (T2DM), one interesting approach is the analysis of endocrine developmental genes in the adult islet of Langerhans.

Two different genes, *Dll1* and *Pax6*, were selected and investigated in an *in vivo* murine context. An inducible,  $\beta$ -cell specific *Dll1* knockdown (Dll1- $\beta$ KO) was generated with Cre-lox technology and phenotyped. Knockdown of DLL1 was shown to induce mild hyperglycemia in males, and whole genome transcriptomics of isolated islets identified a small set of differentially regulated genes in Dll1- $\beta$ KO mice that explain this finding by establishing a link between *Dll1* and genes known to mediate  $\beta$ -cell dysfunction. Comparable analysis of an ENU-generated *Dll1* mutant (DI11\_T720A) proved this role to be at least in part dependent on the DLL1 intracellular domain.

Furthermore, an ENU-generated mutant of *Pax6* (*Pax6*<sup>Leca2</sup>), whose  $\beta$ -cell-loss phenotype was already established, was analyzed with regard to the gene expression network of islets at different ages. Experiments presented in this thesis established that said phenotype is most likely due to  $\beta$ -cell dedifferentiation, and provided mechanistic insights.

In conclusion, the analysis of islets of Langerhans of two different mouse models provided information about the role of developmental genes in adult insulin homeostasis, and serves as a basis for the identification of novel targets.

Diabetes Mellitus ist eine globale Epidemie, die aufgrund der ständig zunehmenden Inzidenz als besonders gefährlich eingestuft wird. Das Zusammenspiel von unterschiedlichen Pathomechanismen und hochkomplexen Gen-Umwelt-Interaktionen kann zum gemeinsamen Endpunkt des klinisch manifesten Typ2 Diabetes (T2DM) führen. Ein besseres Verständnis der Physiologie der insulinproduzierenden  $\beta$ -Zellen, insbesondere deren Fehlfunktion, ist dabei von entscheidender Bedeutung für die intensiven Bemühungen der Forschung, neue Wege in der Prävention und Behandlung des Diabetes zu finden. In Anbetracht der steigenden Bedeutung, die der *in vivo*  $\beta$ -Zell-Dedifferenzierung zugemessen wird, ist die Analyse von Entwicklungsgenen in der adulten Langerhans'schen Insel ein interessanter Ansatz.

Zwei unterschiedliche Gene, *Dll1* und *Pax6*, wurden diesbezüglich ausgesucht und *in vivo* in Mäusen untersucht. Ein induzierbarer,  $\beta$ -Zell-spezifischer *Dll1* Knockdown (Dll1- $\beta$ KO) wurde mittels Cre-lox Technologie generiert und phänotypisiert. Der Knockdown von DLL1 verursacht milde Hyperglykämie in Männchen. Die transkriptomische Analyse von isolierten Inseln konnte passend dazu zeigen, dass die Expression einer kleinen Gruppe von Genen, die bei der  $\beta$ -Zell-Dysfunktion eine Rolle spielen, in Dll1- $\beta$ KO Tieren differenziell reguliert war. Ein ähnliches Experiment mit einer ENU-induzierten Mutante von *Dll1* (Dll1\_T720A) zeigte, dass diese Funktion von DLL1 zumindest teilweise durch dessen intrazelluläre Domäne vermittelt wird.

Darüber hinaus wurde das Genexpressionsmuster von Langerhans'schen Inseln aus einer anderen ENU-induzierten Mutante untersucht, der *Pax6*<sup>Leca2</sup> Mauslinie, deren Phänotyp aus einem graduellen Verlust Insulin-positiver Zellen bereits beschrieben ist. Die Daten dieser Dissertation zeigen, dass dieser Phänotyp durch  $\beta$ -Zell-Dedifferenzierung verursacht wird, und tragen zu dessen mechanistischen Verständnis bei.

Zusammenfassend konnte in dieser Dissertation gezeigt werden, dass die Untersuchung von Entwicklungsgenen in der adulten Langerhans'schen Insel eine praktikable Herangehensweise ist, um neue Targets in der Bekämpfung des Diabetes zu identifizieren.

## 2. Introduction

### 2.1 Notch signaling

#### 2.1.1 Notch signaling components and function

The Notch signaling pathway is present in all metazoan species studied to date and is mainly responsible for cell-cell communication during development<sup>1</sup>. While most pathways that transmit signals from the cell membrane to the nucleus involve a complicated cascade of different proteins and secondary messengers, Notch acts both at the cell surface as a receptor and in the nucleus to directly regulate gene expression. The core pathway apparatus is formed by three components: a ligand, a Notch receptor and a CSL transcription factor (named after CBF1/RBPJ, Su(H) and LAG-1, the proteins filling this role in mammals, *D. melanogaster* and *C. elegans*, respectively)<sup>1,2</sup>. Major mammalian components of Notch signaling are listed in Table 1.

Component type	Mammalian proteins
Ligand	Delta-like 1, 3-4 (DLL1, 3-4) Jagged 1-2 (JAG1-2)
Receptor	Notch 1-4
CSL	RBPJ/CBF1, RBPJL
Co-activator	Mastermind-like 1-3 (MAML1-3)
Target genes	<i>Hes1, Hes5, Hes7, Hey1-2, HeyL</i> (Hairy/enhance-of-split family)

**Table 1. Major components of Notch signaling in mammals<sup>1,3</sup>.**

Notch receptors are single-pass transmembrane proteins that are cleaved during biosynthesis by furin-like convertases within an unstructured loop (designated site S1 for site of first cleavage). This process generates a heterodimer formed by the Notch extracellular domain and the Notch transmembrane and intracellular domain (respectively NECD and NTM1CD), held together by non-covalent interactions<sup>4</sup>. The canonical Notch ligands (termed DSL for Delta, Serrate and LAG2, the first discovered ligands in *Drosophila* and *C. elegans*) are type I transmembrane proteins as well, and the extracellular domains of both Notch and DSL ligands are formed by multiple tandem epidermal growth factor (EGF) repeats<sup>5</sup>. Signals are elicited when a DSL ligand, located on the signal-sending cell, binds a Notch receptor on a neighboring cell, an interaction mediated by specific EGF repeats<sup>6</sup>. The binding event induces a conformational change in the receptor that exposes the cleavage site S2, located in the

short extracellular stub of NTM1CD<sup>7</sup>. S2 is cleaved by a metalloprotease (ADAM10 or ADAM17 in mammals<sup>8,9</sup>), resulting in shedding of the ectodomain and production of the N $\beta$  peptide (Figure 1). A second proteolysis follows, catalyzed by the intramembrane  $\gamma$ -secretase complex that cleaves the receptor progressively from S3 to S4 and thus releases the soluble Notch intracellular domain (NICD)<sup>10</sup>. NICD translocates to the nucleus and interacts with the CSL transcription factor. In absence of NICD, CSL occupies the promoter region of target genes in complex with a co-repressor, actively suppressing them. Upon translocation of NICD, the co-repressor is displaced and co-activators are recruited to the complex together with NICD, which now drives expression of Notch target genes<sup>11,12</sup> (Figure 1). The best characterized targets are *Hairy/Enhancer-of-Split* genes in *Drosophila* and their homologue *Hes* and *Hey* gene families in mammals (see Table 1 for details), which all encode for basic helix-loop helix (bHLH) transcriptional repressors and are ultimately responsible for the effects of Notch signaling<sup>3</sup>.

Since most cells undergoing Notch signaling synthesize both receptors and ligands, their segregation in signal-sending and signal-receiving cells is not a trivial process. The crucial factor that decides the fate of a given cell is the relative expression ratio of ligands and receptors. Small differences in the reciprocal amounts of the two components are amplified by different means to generate mutually exclusive signaling states. The most important of these means is *cis*-inhibition, a phenomenon by which DSL-Notch interactions on the same cell inhibit signaling<sup>13,14</sup>. When the concentration of DSL is higher than the concentration of Notch, excess ligands are capable of inactivating almost all of the receptors on that cell, which consequently loses the ability to receive signals and becomes a dedicated signal-sending cell. By the same token, if Notch concentration is higher than DSL, excess Notch inactivates all ligands, resulting in a cell that can only receive, but not send, signals<sup>15</sup>. This feature is central for lateral inhibition, one of the mechanisms by which Notch signaling determines cell fate decisions during development. In the lateral inhibition model, different fates are adopted within a roughly equivalent population of cells when Notch signal-sending cells are established (with the aid of *cis*-inhibition) that prevent the signal-receiving cells from differentiating through the expression of *Hes* and *Hey* transcriptional repressors, whereas the signal-sending cells do not experience signaling themselves and commit to a specific

lineage<sup>16</sup> (for a detailed review of the Notch pathway in development, which is beyond the scope of this introduction, see<sup>2</sup>).

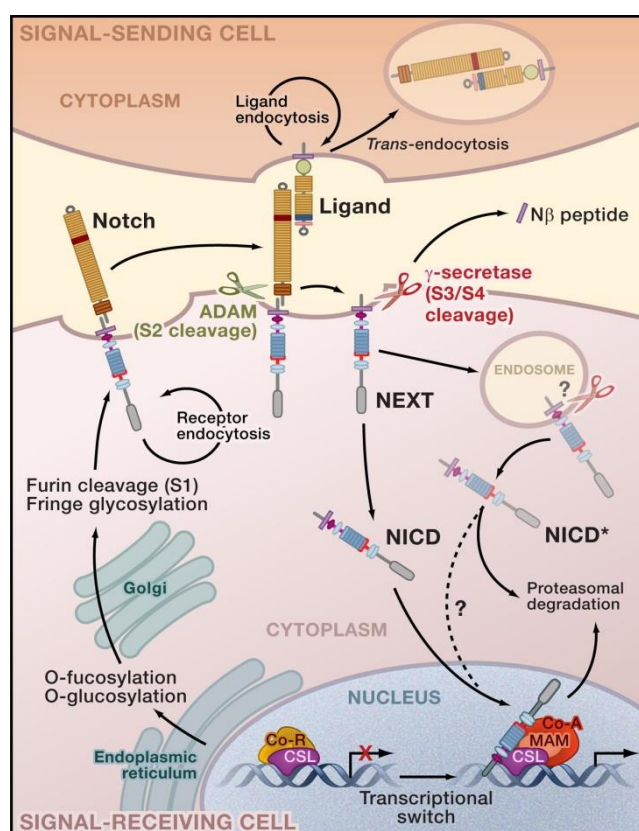


**Figure 1. The canonical Notch pathway.**

Binding between a ligand and a receptor on adjacent cells result in a proteolytic cascade that involves two steps, S2 cleavage by a metalloprotease and S3/S4 cleavage by  $\gamma$ -secretase. The Notch intracellular domain (NICD) is released and localizes to the nucleus where it binds the transcription factor CSL together with a co-activator, and drives expression of target genes. Additionally required processes, such as endocytosis and receptor glycosylation, are also depicted. Illustration adopted from<sup>4</sup>.

The activation of specific targets is tightly regulated and differs greatly between tissues. The ability of the pathway to specifically activate different targets is explained in part by the fact that the four mammalian Notch paralogs do not have fully overlapping functions. They all bind CBF1/RBPJ, but show different specificity depending on the associated promoter regions, and hence may have preferred targets<sup>17</sup>. Furthermore, NOTCH3 is actually an inhibitor of NOTCH1: its intracellular domain (N3ICD) competes with N1ICD for CBF1/RBPJ binding and modulates NOTCH1 activity in a dominant-negative fashion<sup>18</sup>.

In addition to this differences in function, the expression patterns of ligand and receptor paralogs are partly divergent, although not enough to fully explain the observed specificity in signaling activities<sup>19</sup>. Several mechanisms have been described that regulate both ligand and

receptor availability on the cell membrane and their ability to form productive interactions, and may provide for additional fine-tuning of signaling. One of these mechanisms is endocytosis and endosomal trafficking<sup>20</sup>. Endocytosis of ligands is initiated by ubiquitination, catalyzed by the E3 ubiquitin ligases Neuralized and Mindbomb. After endocytosis, ligands return to the cell surface in a more active state, and while the mechanism is yet poorly understood, ligand endocytosis is required for signaling<sup>20,21</sup>. One of several interesting possibilities that have been raised to explain this finding is that ligand endocytosis may generate a mechanical pulling force on a bound receptor, thereby causing the conformational changes that expose the S2 site and initiate the proteolytic cascade. This hypothesis seems supported by the fact that NECD is trans-endocytosed into the signal-sending cell while bound to the ligand<sup>22</sup> (Figure 1). Other hypotheses cannot be discarded, however, and include the clustering of ligands through ubiquitylation or a role for trafficking in the insertion of ligands into specific membrane regions that are more conducive to binding<sup>23</sup> (reviewed in<sup>1</sup>). Notch receptors undergo endosomal trafficking as well and can either be directed back to the cell membrane (recycling) or towards lysosomal degradation, with resulting complex effects on signaling<sup>21</sup>.

Another important post-translational modification that modulates signaling is receptor glycosylation. Notch receptors are large glycoproteins that contain fucose, glucose and N-glycans at specific EGF positions. The exact composition of the sugars bound to the receptor defines both strength and specificity of receptor-ligand interactions<sup>24</sup>.

Finally and possibly most importantly, Notch signaling depends on the cellular context in which it takes place. *Hes* and *Hey* genes are under the control of other pathways as well, suggesting that crosstalk and signal integration between this pathways and Delta/Notch ultimately determines the result of the signaling event<sup>25,26</sup>.

### **2.1.2 Ligand-side non-canonical Notch signaling**

The picture of the canonical Notch pathway presented thus far is further complicated by the finding that signaling may be bidirectional. Proteolytic cleavage of a DSL ligand by the same metalloprotease that processes Notch was first reported for Delta in *Drosophila* more than a decade ago<sup>27</sup>. While the function of this proteolytic event remains debated, at least in some cases it may be an integral part of canonical signaling. *In vitro* experiments support the

hypothesis that Delta processing is an additional mechanism by which ligands are downregulated in signal-receiving cells, thereby maintaining if not enhancing the asymmetrical distribution of ligands and receptors and ensuring unidirectional Notch signaling<sup>28,29</sup>. In accordance with this model, Delta processing has been reported to be Notch-induced and therefore mainly taking place in signal-receiving cells. Interestingly, the same paper reported a nuclear localization of the Delta intracellular domain<sup>30</sup>.

In mammals, ligands undergo essentially the same proteolytic cascade of their receptor counterparts, with cleavage by an ADAM protease followed by  $\gamma$ -secretase processing reported for DLL1 among others<sup>31,32</sup>. The production of a soluble intracellular domain (DlCD in the case of DLL1) seems to be dispensable for some well-described Notch functions such as T-cell development<sup>33</sup> or angiogenesis<sup>34</sup>, but proteolysis itself is critical for muscle cell differentiation. In this latter case, DLL1 shedding is again instrumental to achieve an asymmetry in Notch signaling in an initially homogenous population of myogenic cells, and is therefore playing a role in the canonical pathway<sup>35</sup>.

Other reports, on the other hand, point to a cell-autonomous function for DlCD that may be Notch-independent. Firstly, DlCD harbors a nuclear translocation sequence, which accounts for its nuclear localization<sup>32</sup>, and can participate directly in transcriptional regulation<sup>36,37</sup>. Taken together, these results can be interpreted by postulating that proteolysis of DSL ligands in mammals can, depending on the context, either enhance canonical Notch signaling or initiate reverse signaling.

The latter is additionally supported by the fact that the intracellular domain of most mammalian DSL ligands (the only exceptions are DLL3 and JAG2) have PDZ-binding motifs that mediate interaction with PDZ-containing scaffolding proteins<sup>38</sup>. Several PDZ-proteins were identified as specific interaction partners of DLL1<sup>39-43</sup>. Further research will be required to determine if the interaction with PDZ proteins is involved in ligand-side signaling<sup>41</sup>, or if the binding of PDZ-proteins stabilizes DLL1 at the cell membrane enhancing Notch activation<sup>42,43</sup>, or if both mechanism are in effect depending on the binding partner and the cellular context.

## 2.2 The pancreas and the insulin-producing $\beta$ -cells

### 2.2.1 Organ development

#### 2.2.1.1 Pancreatic endocrine development

During mouse development, the pancreas is first macroscopically visible at gestational day 9.5 (E9.5) as a thickening in the posterior foregut region of the dorsal endodermal germ layer, followed 12 hours later by a corresponding evagination of the ventral domain<sup>44</sup>. These structures, called the pancreatic buds, are preceded on the cellular level by gene expression of the transcription factors *Pdx1* and *Ptf1a*, which are both required for specification of the pancreatic fate, beginning at E8.5<sup>45</sup>. All pancreatic cell lineages, exocrine and endocrine, will be later derived from these initial patches of PDX1<sup>+</sup>PTF1A<sup>+</sup> cells<sup>45,46</sup>.

With the appearance of the buds at E9.5, the primary transition begins, a phase originally defined on morphological criteria and characterized by the emergence of low levels of both acinar and endocrine cells, the latter expressing mostly glucagon<sup>47</sup>. These glucagon<sup>+</sup> and insulin<sup>+</sup> cells, however, are not the precursors of mature islet cells, and their function is unclear<sup>48</sup>. After a period of growth, branching morphogenesis starts around E11.5, during which the developing pancreas generates tree-like epithelial protrusions into the surrounding mesenchyme<sup>44</sup>. At this stage, the pancreatic epithelium is already divided into two functional, spatially defined domains, the tip and the trunk. The tip domain comprises cells in the distal tips of the epithelial tree, while the trunk domain is composed by cells nearer to the center of the buds<sup>49,50</sup>. Lineage-tracing experiments have provided compelling evidence that the cells in the tip domain, defined genetically by expression of *Pdx1*, *Ptf1a*, *cMyc* and *Cpa1*, are multipotent pancreatic progenitors with the potential to give rise to endocrine and exocrine cells, whereas the trunk is formed by more lineage-restricted progeny of the tip cells, namely endocrine and duct progenitors<sup>49</sup>. While the exact molecular cues that guide this patterning into tip and trunk regions are not yet fully understood, the reciprocal repression between PTF1A and NKX6.1/NKX6.2 plays an important role. They eventually become mutually exclusive, with PTF1a restricted to the tip domain while the NKX6 factors determine the trunk fate<sup>51</sup>.

The most important marker of endocrine lineages is *Neurog3* (previously known as *Ngn3*), a basic helix-loop-helix (bHLH) transcription factor. NEUROG3<sup>+</sup> cells are the endocrine

progenitors that give rise to all hormone-secreting pancreatic cells, as shown by lineage-tracing<sup>46</sup> as well as transgenic overexpression of *Neurog3* in pancreatic progenitors, which leads to precocious endocrine differentiation at the expense of exocrine development<sup>52</sup>. Mice deficient for *Neurog3* fail to develop any islet cells and die postnatally of diabetes<sup>53</sup>. In accordance to the domain patterning described above, expression of *Neurog3* is confined to the trunk domain at any time and is first detectable at E9.5. It peaks at around E15.5 during the secondary transition, a synchronized wave of endocrine and exocrine differentiation, and then fades rapidly after birth<sup>54</sup>: in adult islets, *Neurog3* expression is almost undetectable, and rises only in pathological conditions of  $\beta$ -cell dedifferentiation<sup>55</sup>. The precise mechanisms by which NEUROG3<sup>+</sup> cells are directed towards different lineages are not completely elucidated, but seem to be dependent on the developmental context at different time points. NEUROG3<sup>+</sup> progenitors experience discrete competence time-windows with distinct differentiation abilities: early during development, they mostly give rise to  $\alpha$ -cells, whereas  $\beta$ - and PP-cells are not generated in significant numbers until the start of the secondary transition between E13.5 and E14.5, and  $\delta$ -cells appear even later<sup>56,57</sup> (summarized in Figure 2).

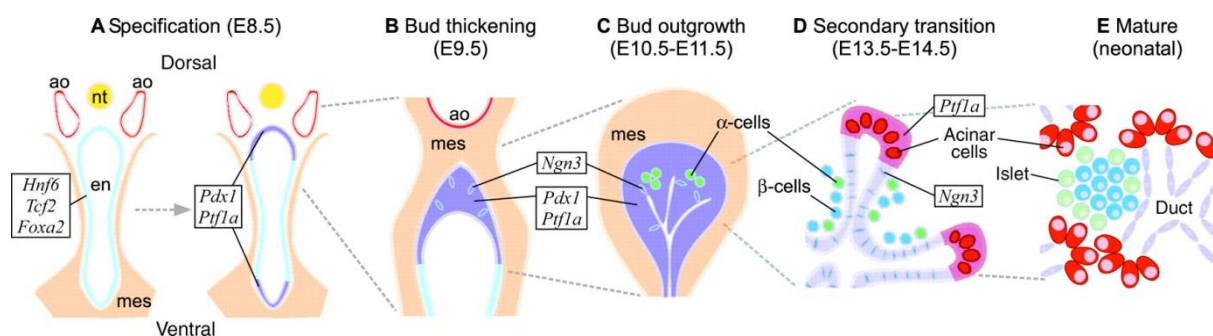


**Figure 2. Schematic representation of pancreatic development.**

**(A)** Pancreatic specification begins at E8.5 through the expression of *Pdx1* and *Ptf1a* in two endoderm (en) cell patches, a process promoted by signaling from nearby tissues such as notochord (nt) and aorta (ao). **(B, C)** The two resulting buds grow and branch into the surrounding mesenchyme (mes), and the first *Neurog3* (*Ngn3*) expressing endocrine progenitors surface. **(D)** The bulk of pancreatic lineages, including  $\beta$ -cells, appear during the secondary transition. Illustration adopted from<sup>57</sup>.

There are several transcription factors that act downstream of NEUROG3 to specify distinct endocrine lineages, including PAX4, ARX, NEUROD1 and NKX6.1<sup>58</sup>. Among these, NEUROD1 binds directly to the promoter of the paired and homeodomain containing transcription factor gene *Pax6* and enhances its expression<sup>59</sup>. PAX6 was first identified as essential for the development of  $\alpha$ -cells<sup>60</sup>, but is indeed required for the differentiation of all endocrine

lineages and for the correct organization of the forming islets. Its role persists in adulthood as a transcriptional activator of the insulin, glucagon and somatostatin promoters<sup>61</sup>. PAX6 has been found by pulse-chase lineage tracing experiments to mark cells that are further in the endocrine specification program than early NEUROG3<sup>+</sup> cells but are still multipotent for all islet fates and are therefore termed late endocrine progenitors<sup>49</sup> (Figure 3).

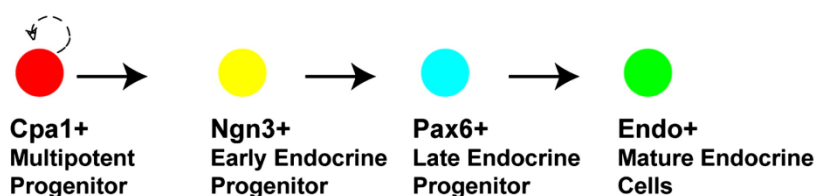


**Figure 3. Stepwise differentiation of multipotent pancreatic progenitors into mature islet cells.**

All pancreatic lineages derive from multipotent progenitors in the tip domain that express *Cpa1* (depicted here) in addition to *Pdx1*, *Ptf1a* and *cMyc*. This pool of cells is capable of self-renewal and generation of *Neurog3*(*Ngn3*)-expressing endocrine progenitors. Endocrine specification progresses through expression of *Pax6* before terminal differentiation ensues. Illustration adopted from<sup>49</sup>.

Two other targets of NEUROG3, *Pax4* and *Arx*, are co-expressed with *Pax6* in late endocrine progenitors and contribute decisively to their partition by repressing each other. Eventually, their expression becomes mutually exclusive. *Pax4* marks  $\beta$ - and  $\delta$ -cells, whereas *Arx* is expressed in  $\alpha$ - and  $\epsilon$ -cells<sup>62,63</sup>. By E18, all endocrine lineages are present and organized into islet clusters<sup>54</sup>.

The Notch signaling pathway plays a crucial role in multiple steps of the processes outlined above. Since the pathway itself is the major focus of this thesis, its role in pancreatic development is discussed in depth in the following chapter. For a more detailed review of pancreatic development, which is beyond the scope of this introduction, see<sup>54,57,58</sup>.

### **2.2.1.2 Notch signaling in pancreatic development**

Several Notch pathway components are expressed in the early mouse pancreas, including NOTCH1-3, DLL1, DLL3, JAG1-2 and HES1<sup>64</sup>. They play a crucial role in pancreatic development, controlling multiple steps and possibly operating through different mechanisms.

The involvement of Notch signaling was first conclusively demonstrated by gene knockouts of *Dll1* and *Rbpj*, encoding a Notch ligand and an intracellular mediator, respectively (see

2.1.1 for details). The phenotype of these mice is roughly identical to the effects of transgenic *Neurog3* overexpression in pancreatic progenitors, with a massively accelerated differentiation of endocrine cells at the expense of organ growth and other cell fates due to depletion of the progenitor pool<sup>52</sup>. Inactivation of *Rbpj* specifically in PDX1<sup>+</sup> pancreatic progenitors (as opposed to the generic knockout described above) results in a similar phenotype of precocious endocrine differentiation (particularly of  $\alpha$ - and PP-cells) and, while non-lethal, caused severe pancreatic hypoplasia<sup>65</sup>. Deficiency of the Notch target *Hes1* renders the pancreas hypoplastic as well, again the effect of increased endocrine cell numbers at the early stages of development at the expense of multipotent progenitors<sup>64</sup>.

Taken together, these results show that loss-of-function at different nodes of the Notch pathway, namely ligand expression<sup>52</sup>, function of NICD<sup>52,65</sup> or expression of target genes<sup>64</sup>, invariably leads to an upregulation of *Neurog3* and a premature endocrine differentiation wave that depletes pancreatic progenitors.

Gain-of-function experiments corroborate this picture by producing opposite phenotypes. Transgenic overexpression of the constitutively active intracellular domain of Notch1 (*Notch1<sup>ICD</sup>*) keeps PDX1<sup>+</sup> progenitors trapped in an undifferentiated state. When activated at a later time point in NEUROG3<sup>+</sup> endocrine progenitors, NOTCH1<sup>ICD</sup> blocks them from further differentiating as well, thus demonstrating that Notch signaling controls several steps of pancreatic development<sup>66</sup>. Notably, activated NOTCH1 not only affects endocrine development, but also fully prevents exocrine differentiation<sup>67</sup>, and always acts in a cell-autonomous fashion<sup>66,67</sup>. Genetic lineage-tracing, which labels all cells that experienced NOTCH1 proteolysis (by substituting the NOTCH1 intracellular domain with a Cre recombinase), reveals that progeny of these cells is scattered throughout the endocrine and exocrine pancreas, consistent with a role for *Notch1* in progenitors that will contribute to both lineages<sup>68</sup>.

Results in both zebrafish<sup>69</sup> and chicken<sup>70</sup> fully recapitulate the mouse phenotypes described so far. Hence, a model emerges in which Notch signaling acts on different pools of progenitors (PDX1<sup>+</sup> pan-pancreatic progenitors as well as NEUROG3<sup>+</sup> endocrine progenitors) through an evolutionarily conserved mechanism of suppressive maintenance, blocking differentiation and thus enabling the expansion of said progenitors until a critical mass is achieved that is necessary for morphogenesis.

Notch action in the embryonic pancreas is mediated to a large extent by *Hes1*, whose expression is activated by the interaction of DELTA1 and NOTCH1<sup>71</sup>. *Hes1* encodes for a bHLH transcriptional repressor, a family of proteins capable of counteracting the activity of bHLH transcriptional activators such as NEUROG3<sup>3</sup>. Promoter reporter assays proved that HES1 binds directly and with high affinity to the *Neurog3* proximal promoter, repressing its transcription<sup>72</sup>. This provides a straightforward explanation for the enhanced and precocious *Neurog3* expression in knockouts of *Dll1*, *Rbpj* and *Hes1* described above<sup>52,64</sup>, since DELTA1- and NOTCH1-mediated activation of *Hes1* is absent in these models, leading to de-repression of the *Neurog3* gene. This mechanism accounts at least in part for the suppressive maintenance of PDX1<sup>+</sup> progenitor cells.

Additionally, HES1 is capable of influencing the function of PTF1A<sup>69</sup>, which during development first plays a role in progenitors and is later required for acinar specification<sup>73</sup>. Underlying the Notch-dependent repression of acinar differentiation is not, as with *Neurog3*, a transcriptional mechanism, but rather a protein-protein interaction between HES1 (and HEY2, another Notch effector) and PTF1A that inhibits the function of the latter<sup>74</sup> and explains the NOTCH1-induced stop to exocrine specification<sup>67</sup>.

Another mode of action by which HES1 controls pancreatic development is demonstrated by its interaction with CDKN1C (alias p57), a cyclin-dependent kinase inhibitor and thus a negative regulator of proliferation. The precocious differentiation in *Hes1*<sup>-/-</sup> embryos, and probably in most loss-of-function modulations of Notch signaling described above, is accompanied by an increased expression of *Cdkn1c* by pancreatic progenitors, followed by cell cycle exit and differentiation. In wild types, HES1 binds the *Cdkn1c* promoter directly and represses its transcription, delaying this phenomenon. Indeed, embryos deficient for both *Hes1* and *Cdkn1c*, while lethal after E11.5 due to pleiotropic effects, are rescued with respect to the balance of proliferation and differentiation of PDX1<sup>+</sup> progenitors up to that point<sup>75</sup>. Thus, Notch signaling, by way of HES1 and its transcriptional regulation of *Cdkn1c*, controls the binary decision of pancreatic progenitors to either self-renew or exit the cell cycle initiating terminal differentiation. The balance between proliferation and controlled cell cycle exit is not only critical to ensure the correct size and shape of developing organs, but also to prevent the aberrant proliferative characteristics typical of cancer. In light of the fact that Notch signaling controls this balance throughout pancreatic development, it is not

surprising that it has been implicated in pancreatic tumorigenesis<sup>76</sup> and, more generally, in other cancers as well, where depending on the circumstances it can act as an activator or suppressor<sup>77</sup>.

Lineage-tracing experiments designed to examine the fate of HES1<sup>+</sup> cells at different time points further developed this picture. Early HES1<sup>+</sup> cells are multipotent progenitors that contribute to all major pancreatic lineages, consistent with the transcriptional repression of both *Neurog3* and *Cdkn1c*. In contrast, HES1<sup>+</sup> cells at later time points (E13.5-E15.5) are restricted to an exocrine cell fate. It has therefore been proposed that cells with activated Notch signaling are multipotent before the start of the secondary transition (~E13.5) and switch later to mark bi-potent acinar/duct progenitors due to continued transcriptional repression of *Neurog3*. Continued elevated NOTCH1 activity in these bi-potent cells promotes duct development, possibly as a consequence of PTF1A functional inhibition<sup>78</sup>.

In summary, Notch signaling in the early developing pancreas maintains the proliferative capacity of progenitors by inhibiting *Cdkn1c* expression and further blocks exocrine and endocrine differentiation by inhibiting PTF1A activity and *Neurog3* expression. At some point before the secondary transition, Notch activated cells become restricted to the exocrine lineage, where they favor duct development. These functions are elicited to a large extent along the DLL1-NOTCH1-HES1 axis.

This conventional view has been complicated somewhat by recent reports. Firstly, mice with a targeted deficiency for both presenilin genes in NEUROG3<sup>+</sup> cells surprisingly exhibit a redirection of the endocrine progenitors to an acinar fate<sup>79</sup>. *Psen1* and *Psen2* encode for the catalytic core of the  $\gamma$ -secretase, and are therefore essential for Notch signaling. Inactivation of Notch signaling in NEUROG3<sup>+</sup> cells could rather be expected to be inconsequential, since pathway activity has already faded by the time *Neurog3* is upregulated<sup>78</sup>. This result suggests a hitherto unknown role for the pathway: indeed, the authors propose a novel function for *Notch2* in the established endocrine progenitors<sup>79</sup>, although a Notch-independent effect of the  $\gamma$ -secretase knockout cannot be ruled out.

In addition, Notch has been implicated in patterning between the tip and trunk domain (see 2.2.1.1). In a further loss-of-function model of Notch signaling, in which a dominant-negative form of *Mam1* (a required co-activator) was expressed under the control of the *Pdx1* promoter, Notch-suppressed cells lost expression of trunk marker genes such as *Nkx6.1*

and were directed towards a tip fate<sup>80</sup>. Interestingly, no precocious differentiation was observed, in stark contrast to previous results<sup>52,64,65</sup>. These contradictions may be caused by differences in the experimental setups, since both the reports about *Psen1-2* and the dominant-negative *Maml1* analyzed models of mosaic loss of Notch signaling<sup>79,80</sup>, whereas the classical view derived from global knockouts<sup>52,64,65</sup>. Mosaic loss of activity may have revealed new roles for Notch in addition to suppressive maintenance, but further research will be needed to incorporate this new knowledge into the existing, well-supported consensus model.

## **2.2.2 The adult pancreas**

### **2.2.2.1 Pancreatic anatomy**

The pancreas is a glandular organ, which belongs to both the exocrine and endocrine systems. Its exocrine compartment forms 98% of the parenchyma and is composed by digestive enzyme-secreting acinar cells that are connected via centro-acinar cells to a highly branched system of ducts. The ductal tree fuses into the major pancreatic duct, channeling the released enzymes into the duodenum<sup>81</sup>. The endocrine compartment is formed by the islets of Langerhans, specialized micro-organs with a mean diameter of between 100 and 200  $\mu\text{m}$  in mammals, which lie scattered throughout the pancreatic tissue and control blood glucose levels by releasing hormones directly into the blood stream. To this end, they are diffused with a dense network of blood vessels (five to tenfold higher than the rest of the organ) and are encapsulated by a thin sheet of collagen and glial cells<sup>82</sup>. Global pancreatic anatomy is summarized in Figure 4.

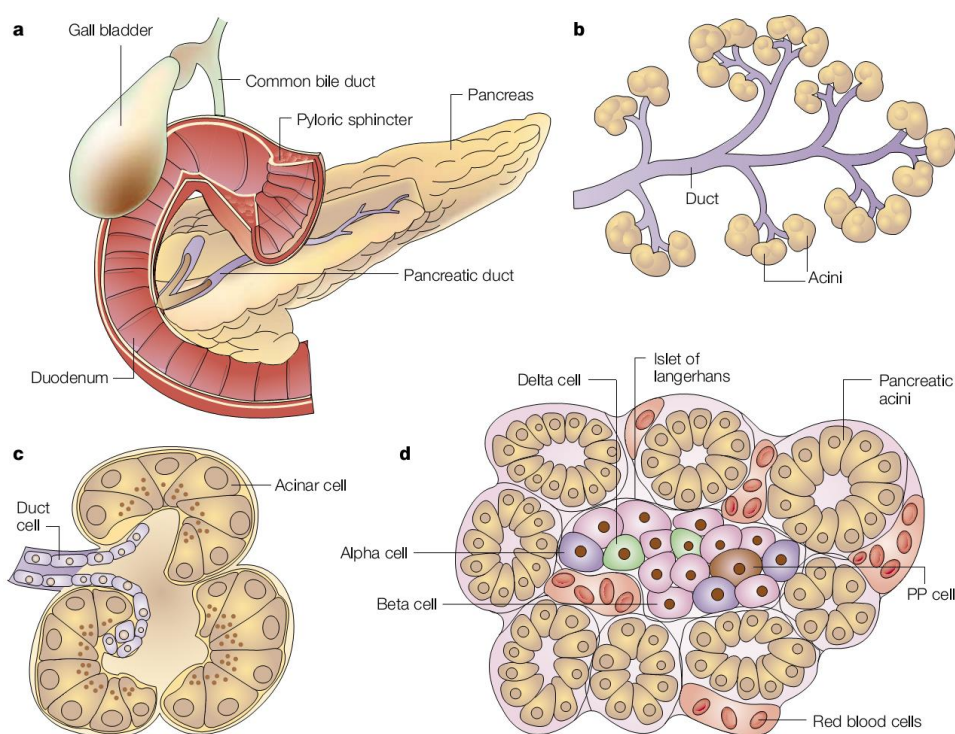


**Figure 4. Schematic representation of pancreatic anatomy.**

(A) Outline of pancreatic anatomy. The pancreas has a curved, elongated shape and lies next to the duodenum. (B) The exocrine pancreas comprising the acini and the ductal tree. (C) A single acinus and its connection to the ducts. (D) An islet of Langerhans embedded within the acinar tissue. Illustration adopted from<sup>83</sup>.

Islets are composed by five different endocrine cell types: glucagon-secreting  $\alpha$ -cells, insulin-secreting  $\beta$ -cells, somatostatin-secreting  $\delta$ -cells, pancreatic polypeptide-secreting PP-cells and ghrelin-secreting  $\epsilon$ -cells<sup>82</sup>.

Anatomically, the pancreas is divided into two distinct lobes, the head and the tail. Probably due to slight differences in the developmental specification programs of the lobes<sup>84–86</sup>, islets show regional differences in cell composition: PP-cells are more common in the head lobe whereas  $\alpha$ -cells are more common in the tail, in both humans and rodents<sup>87,88</sup>.

### 2.2.2.2 Pancreatic $\beta$ -cell function

The pancreatic  $\beta$ -cells constantly monitor blood glucose and control it through the secretion of insulin. The physiological processes underlying this function have been studied extensively and are now fairly well understood. Insulin secretion takes place in response to a complex cellular algorithm that integrates inputs from glucose, amino acid and fatty acid metabolism to generate metabolic coupling factors such as ATP and cAMP that control the exocytosis of insulin secretory granules<sup>89</sup>.

Stimulus-secretion coupling is most extensively studied in the context of glucose-stimulated insulin secretion (GSIS), and the consensus model holds that an increase in glucose metabolism is almost entirely directed towards oxidative phosphorylation, resulting in a rise of the cytosolic ATP/ADP ratio, which prompts the closure of ATP-sensitive potassium channels ( $K_{ATP}$ ) and membrane depolarization<sup>89,90</sup>.

In rodents and humans, glucose is rapidly taken up via the facilitated glucose transporter, SLC2A2 and SLC2A1, respectively, and then becomes phosphorylated by the enzyme glucokinase (GCK), which catalyzes the rate-limiting step of glucose metabolism. The  $K_{ATP}$  channel, whose different subunits are encoded for by the genes *Kcnj11* and *Abcc8* (best known under *Kir6.2* and *Sur1*, respectively), is the key regulator coupling glucose sensing and insulin exocytosis. At low plasma glucose levels, these channels are open and enable  $K^+$  efflux from the cytoplasm into the extracellular space, thereby ensuring membrane hyperpolarization. As a consequence, voltage-gated  $Ca^{2+}$  channels remain closed and insulin secretion is prevented to a large extent. ATP-dependent closure of  $K_{ATP}$  channels results in membrane depolarization, opening of  $Ca^{2+}$  channels, calcium influx and subsequent exocytosis of insulin secretory granules<sup>91</sup> (Figure 5).

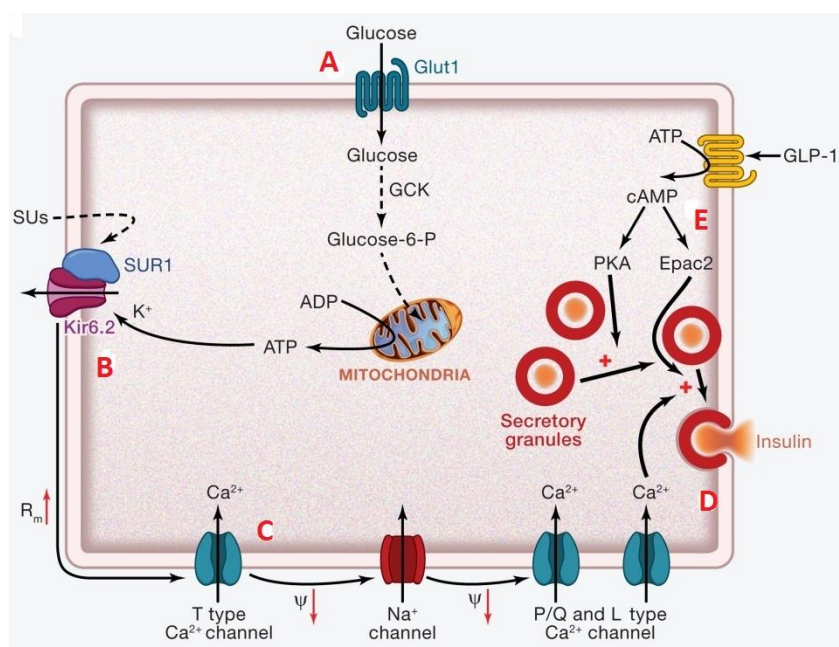


**Figure 5. Glucose-stimulated insulin secretion.**

**(A)** Glucose is taken up by the active transporter GLUT1 (SLC2A2/GLUT2 in rodents) and metabolized to generate ATP. Increased ATP concentration closes the  $K_{ATP}$  channel formed by SUR1 and KIR6.2 **(B)**, leading to membrane depolarization and opening of voltage-gated  $Ca^{2+}$  channels of different types **(C)**. The increased

intracellular  $\text{Ca}^{2+}$  concentration activates the exocytosis of insulin secretory granules **(D)**. **(E)** GLP-1 acts on PKA- and EPAC1-dependent mechanisms to enhance exocytosis. Illustration modified from<sup>92</sup>.

Additional modulators of GSIS are neurotransmitters like acetylcholine and hormones such as the incretins GLP-1 (glucagon-like peptide-1) and GIP (glucose-dependent insulintropic polypeptide), both secreted from the intestine in a glucose-dependent fashion and estimated to account for approximately half of the released insulin during the postprandial phase<sup>93</sup>. Incretin signaling in  $\beta$ -cells is elicited by binding to specific receptors on the plasma membrane and results in increased production of cAMP, another important metabolic coupling factor that acts both on protein kinase A (PKA)-dependent and independent pathways to amplify the release competence of insulin granules<sup>94</sup>. Amino acid and fatty acid metabolism can further augment GSIS, but are not discussed here (reviewed in<sup>89</sup>).

In addition to this core cellular mechanism, glucose has also been shown to directly regulate insulin gene expression and insulin mRNA stability, thus enhancing insulin biosynthesis in addition to its secretion<sup>95</sup>.

While the GSIS mechanism summarized here focuses on individual  $\beta$ -cells, it has to be noted that cell-cell communication within islets inhibits basal insulin secretion and enhances stimulated secretion, thereby dramatically increasing the difference between these two states with important consequences in the maintenance of glucose homeostasis<sup>96</sup>. Both effects are mediated by bidirectional signaling between adjacent  $\beta$ -cells through a receptor tyrosine kinase and its ligand in the EphA-EphrinA pathway. At low glucose concentrations, EphA forward signaling predominates and suppresses secretory granules exocytosis, whereas at high glucose concentrations the balance is shifted towards EphrinA reverse signaling, which enhances secretion<sup>97</sup>.

Summarizing, pancreatic  $\beta$ -cells act as metabolic fuel sensors of the organism and are therefore essential for its survival. Interestingly, the same high metabolic sensitivity that is a prerequisite for this function, also renders  $\beta$ -cells more vulnerable than others to excessive nutrient supply, which becomes particularly relevant in diabetes-related pathophysiology<sup>98</sup> (see 2.3.2).

## 2.3 Diabetes Mellitus

### 2.3.1 Overview

According to the latest report by the International Diabetes Federation, more than 371 million people were estimated to be living with diabetes as of November 2012, 50% of which so far undiagnosed. 4.8 million people died as a consequence of the disease in 2012, up from 4.6 the previous year<sup>99</sup>. The incidence of diabetes is increasing in every country, with the fastest increase expected to be in the developing world, a trend that lead to diabetes being the first noninfectious disease declared a global threat by the United Nations<sup>100</sup>. Furthermore, diabetes represents a major economic and policy problem, with 471 billion US dollars spent due to diabetes in 2012 alone, a third thereof in Europe<sup>99</sup>.

The circulating blood glucose level is one of the most important physiological parameters, and is essentially determined by three factors: intestinal absorption of nutrients, hepatic glucose production, and glucose uptake in peripheral organs such as muscle and adipose tissue. In the bi-hormonal model of glucose maintenance, glucagon drives glycogenolysis to maintain blood glucose in the fasting state. After a meal, insulin stimulates glucose clearance in the periphery, acts directly on the liver to suppress both glycogenolysis and gluconeogenesis, and diminishes glucagon secretion in the pancreas (a detailed review of glycemic control, including the role of additional glucoregulatory hormones, can be found in<sup>101</sup>).

Normoglycemia is defined as a fasting plasma glucose level <110 mg/dl in humans<sup>102</sup> (<150 mg/dl in mice)<sup>103</sup>. Whenever insulin production is insufficient to meet the demands of the peripheral organs, these levels cannot be maintained and the result is diabetes, a group of metabolic diseases characterized by a state of hyperglycemia. This condition can arise from multiple underlying causes and involves defects in insulin secretion, insulin action, or both. Type 1 diabetes (T1DM) is caused by a T-cell mediated autoimmune destruction of the insulin-producing  $\beta$ -cells and accounts for fewer than 10% of all diabetes cases. Type 2 diabetes (T2DM), on the other hand, is characterized by defects in  $\beta$ -cell mass and function as well as insulin resistance in peripheral tissues such as liver, fat, and muscle. T2DM patients are a rather diverse group, with clinical manifestations that range from

predominant insulin resistance with relative insulin deficiency for some cases, to a predominantly insulin secretory defect with accompanying insulin resistance for others. T2DM is by far the most common form of diabetes, accounting for at least 90% of all cases. Known risk factors are diverse and comprise a family history of T2DM, age, ethnicity, insulin resistance and lifestyle habits such as diet composition and physical activity<sup>104</sup>.

The third main form, gestational diabetes, consists of hyperglycemia in pregnant women, develops in one out of 25 pregnancies and presents a high risk of progression to T2DM<sup>104</sup>. Other, monogenic forms of diabetes exist<sup>92</sup>.

The historically precise distinction between T1DM and T2DM has been called into question after the discovery that 10 to 20% of T2DM patients present autoimmunity in the form of anti-islet cell antibodies. This disease subtype has been classified as latent autoimmune diabetes of adulthood (LADA)<sup>105</sup> and has sparked a debate about the role of immunity in other T2DM forms<sup>106,107</sup>. To further blur the distinction between disease types, obesity has been found to be a risk factor for T1DM<sup>108</sup>. Unifying classifications of diabetes have already been proposed<sup>109</sup> and are currently debated in the scientific and medical communities.

### **2.3.2 The $\beta$ -cell in Type 2 diabetes**

While obesity and insulin resistance are associated with T2DM, a large percentage of obese, insulin-resistant individuals do not develop diabetes. In these subjects, pancreatic  $\beta$ -cells retain the ability to enhance insulin production and compensate for both the increased insulin demand and its reduced efficiency<sup>110</sup>. This finding gradually shifted the general view of T2DM, which for many years was attributed solely to insulin resistance and is now recognized as a clinical condition that requires defects in both  $\beta$ -cell function and insulin sensitivity<sup>109</sup>.

The  $\beta$ -cell dysfunction evident in T2DM involves several cellular mechanisms. Not only is the maximum insulin secretory capacity of individual  $\beta$ -cells dramatically reduced, secretory kinetics are disturbed as well, since the pulsatile and oscillatory nature of insulin secretion is disrupted. Insulin biosynthesis is also perturbed, resulting in a greater proportion of unprocessed, biologically inactive proinsulin being released into the blood stream<sup>111</sup>. Average insulin content in islets from T2DM patients is reduced compared to islets from healthy controls, likely an additional result of slowed biosynthesis. Insulin content, however,

does not account for the reduction of insulin secretion, implying that functional defects of the secretory machinery are more important<sup>92</sup>. Crucially, these instances of  $\beta$ -cell dysfunction commence before diabetes is clinically manifest, suggesting that they at least contribute to the etiology of T2DM<sup>111</sup>.

In addition to  $\beta$ -cell function,  $\beta$ -cell mass, defined as both the volume of single  $\beta$ -cells and their number, is decreased in T2DM as a consequence of increased apoptosis<sup>112</sup> and possibly dedifferentiation<sup>55</sup>, further contributing to insulin deficiency. The major driving force behind loss of  $\beta$ -cell mass has been suggested to be hyperglycemia itself<sup>109</sup>, leading to the proposition that  $\beta$ -cell mass may be less important than insulin secretion in T2DM<sup>92</sup>, though differing views persist<sup>113</sup>.

The precise etiology of T2DM, hence, remains debated, but a consensus model is emerging with regard to the role of the pancreatic  $\beta$ -cell. When obesity and insulin resistance arise as a consequence of genetic predisposition and lifestyle, normal  $\beta$ -cells increase both functional responsiveness and mass and maintain normal glucose tolerance by inducing compensatory hyperinsulinemia. By contrast,  $\beta$ -cells of susceptible individuals are unable to respond and become dysfunctional and apoptotic, decreasing both secreted insulin per cell and total mass. A reinforcing feedback loop between insulin sensitivity and secretory deficiency then ensues that ultimately result in impaired glucose tolerance and T2DM<sup>110</sup>.

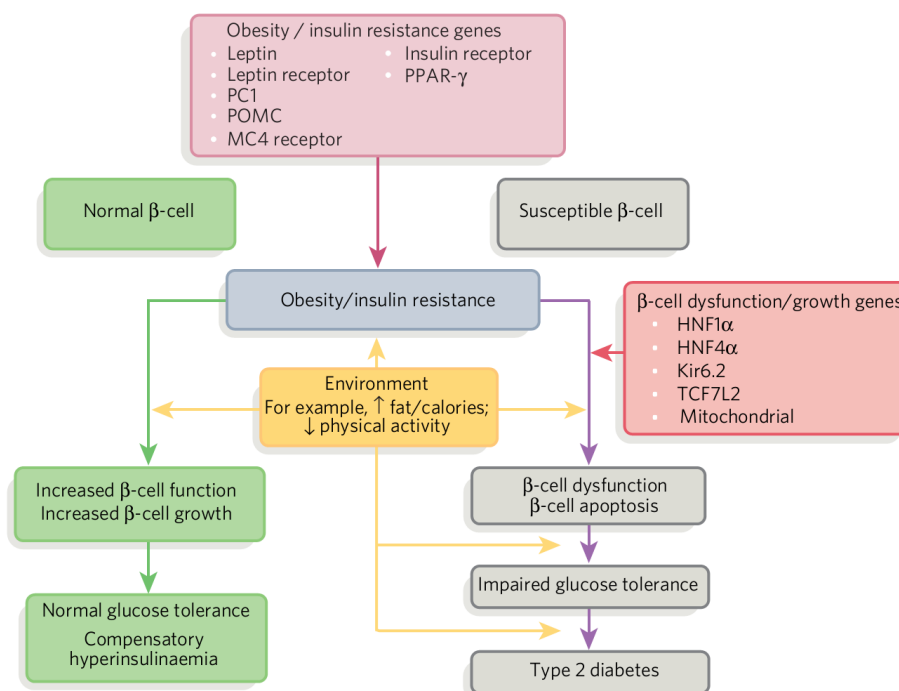


**Figure 6. Role of  $\beta$ -cell defects in the etiology of Type 2 Diabetes.**

Obesity-related insulin resistance does not always result in T2DM: its effect depends on the susceptibility of the  $\beta$ -cell and its ability to compensate with hyperinsulinemia. Failure to do so can cause  $\beta$ -cell dysfunction and diabetes. Environmental factors such as physical activity and caloric intake can act at every step to contribute to the ultimate result. Illustration adopted from<sup>110</sup>.

Implied in this model is the suggestion that genetic susceptibility of pancreatic  $\beta$ -cells may remain without consequences in individuals that do not develop insulin resistance. The complex interplay between these two different parameters and different organs likely explains why already more than 40 genes have been related to T2DM in genome wide association studies (GWAS)<sup>92</sup>.

**2.3.3 Notch signaling in diabetes and the adult pancreas**

While the function of the Notch pathway in the prenatal pancreas has been researched extensively, an emerging consensus from recent literature points to a possible role in the adult pancreas as well. First of all, genome wide association studies (GWAS) in the human population have identified *NOTCH2* as locus robustly associated with T2DM<sup>114</sup>. The mechanism and the functional relevance of this association remain unknown, since evaluation of *NOTCH2* common variants in diabetes-related intermediary traits revealed no impact on either insulin release or insulin action<sup>115</sup>.

Moreover, several pathway components and effectors are expressed in adult murine islets of Langerhans, including all four receptors, several Delta-like and Jagged ligands, and the target gene *Hes1*, proving that Notch signaling remains active in endocrine cells postnatally. *In vitro* experiments on isolated islets of both human and rodent origin exclude any involvement of Delta/Notch in glucose stimulated insulin secretion<sup>116</sup>, fitting to the association studies mentioned above. However, chemical inhibition of  $\gamma$ -secretase activity suggests a role for Notch in suppressing  $\beta$ -cell apoptosis, with possible repercussions for diabetes<sup>116</sup>.

Considering the pivotal role played by Notch signaling in pancreatic and endocrine differentiation, its implication in  $\beta$ -cell dedifferentiation is not surprising. Most of the evidence comes from *in vitro* attempts to expand primary  $\beta$ -cells. *Ex-vivo* expansion of human  $\beta$ -cells has long been considered a promising strategy for obtaining sufficient material for replacement therapy in T1DM. Isolated human  $\beta$ -cells, however, display limited *in vitro* proliferation potential and are subjected to rapid dedifferentiation: they lose insulin

expression, which renders them useless for transplantation (reviewed in<sup>117</sup>). Mouse  $\beta$ -cells behave in a similar fashion<sup>118</sup>. Cell culture analysis of dissociated human islets showed that transcript levels of *NOTCH1* and *HES1* are upregulated in correlation with  $\beta$ -cell dedifferentiation, whereas ligands *DLL1* and *JAG1* are downregulated. Importantly, *HES1* upregulation precedes downregulation of its target *CDKN1C*. These results clearly suggest that the same Notch signaling machinery involved during endocrine development is at work in *in vitro* adult dedifferentiation: upregulation of *HES1* represses the cell cycle inhibitor *CDKN1C* allowing cell cycle re-entry and, given the tight link between the mutually exclusive states of proliferation and insulin expression in  $\beta$ -cells, causing dedifferentiation<sup>119</sup>. *HES6*, a Notch-independent repressor of *HES1*, can restore insulin expression in a cell culture model, further confirming the importance of *HES1* action in controlling the differentiated state of mature  $\beta$ -cells<sup>120</sup>.

Cell culture-induced, *ex-vivo* dedifferentiation is a somewhat artificial context, but Notch signaling has been involved in other instances of loss of  $\beta$ -cell phenotype. Microarray analysis of rat primary islets exposed to cytokines showed that inflammation-induced downregulation of  $\beta$ -cell markers is again accompanied by increased expression of Notch components and targets<sup>121</sup>. Crucially, a comparison of human islets isolated from T2DM patients and non-diabetic individuals also suggested Notch-mediated differences. In an *in vitro* model of  $\beta$ -cell plasticity, islets from non-diabetics retained a pronounced re-differentiation potential whereas islets from diabetic donors were deficient in this respect while showing overexpression of *HES1* and decreased *NEUROG3* frequency<sup>122</sup>.

Taken together, these results clearly point to the fact that Notch signaling retains the potential of controlling endocrine terminal differentiation even in the mature pancreas. Parallel to developmental processes, this function is still largely mediated by *HES1* and its transcriptional control of *Neurog3* and *Cdkn1c*.

Recently, *in vivo*  $\beta$ -cell dedifferentiation has been implicated in the pathophysiology of diabetes. While an involvement of Notch signaling in these events remains to be elucidated, upregulation of *Neurog3* at least suggests this possibility<sup>55</sup>. To date, however, almost all results regarding Notch signaling in adult islets derive from *in vitro* experiments, highlighting the need for further research.

## 2.4 The *Pax6*<sup>Leca2</sup> mouse model

The *Pax6* gene encodes for the paired-box protein 6 (PAX6), a transcription factor with pleiotropic functions contributing to the development of the eye, central nervous system, olfactory epithelium and pancreas<sup>123,124</sup>, where PAX6 marks late endocrine progenitors (see Figure 3 and 2.2.1.1 for details). PAX6 consists of an amino-terminal paired domain (PD) containing two different helix-turn-helix subdomains (referred to as PAI and RED), a linker region, a homeodomain (HD) and a C-terminal transactivation domain<sup>125</sup> (Figure 7). The paired- and homeodomain are responsible for DNA binding<sup>126,127</sup>, while the transactivation domain determines target gene expression<sup>128</sup>. Two different forms of PAX6 are encoded by mammalian genes: the canonical isoform 1 and the alternative splicing variant 5a, that contains a 14 amino acid insertion in the PAI subdomain, rendering it non-functional<sup>129,130</sup>. PAX proteins, including PAX6, exhibit different modes of DNA binding by utilizing different domain combinations to recognize a handful of diverse specific sites<sup>131</sup>.

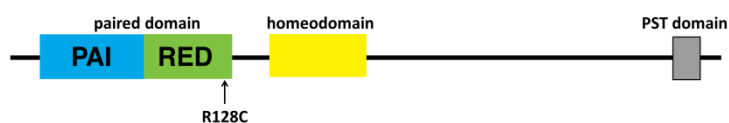


**Figure 7. Schematic representation of PAX6.**

The DNA-binding domains are the paired domain, subdivided in the PAI and RED helix-turn-helix motifs, and the homeodomain. The proline/serine/threonine (PST) domain is responsible for transactivation. In the *Pax6*<sup>Leca2</sup> mutant, a single point mutation leads to the R128C exchange at the third-to-last amino acid position of the RED subdomain (sequence information refers to the canonical isoform 1)<sup>132</sup>. Illustration modified from<sup>131</sup>.

The *Pax6*<sup>Leca2</sup> mutant was first identified in a genome-wide screen of *N*-ethyl-*N*-nitrosurea (ENU)-induced mutations with eye phenotypes, hence the name *Leca* that stands for lens corneal adhesion. A single point mutation is located in exon 7 and leads to an arginine to cysteine exchange at the third-to-last amino acid position of the RED subdomain, R128C in the canonical isoform 1 (see Figure 7)<sup>132</sup>.

While the original paper described the eye phenotype, PAX6 is a major player in pancreatic development and homeostasis<sup>60,133,134</sup> (see 2.2.1.1 and Figure 3), and the effect of the *Leca2* mutation on these processes is hitherto uncharacterized. Moreover, *Pax6*<sup>Leca2</sup> mice are a unique model in that, contrary to other mutations of the paired domain such as the *Pax6*<sup>Aey18</sup> line<sup>135</sup>, they are homozygous viable and have a normal life span. Previous histological studies

performed in our group by Daniel Gradinger established that pancreatic development in *Pax6<sup>Leca2</sup>* animals is indistinguishable from wild types. At the E18.5 time point the gross morphology of *Pax6<sup>Leca2</sup>* pancreata is unchanged, as are both  $\alpha$ - and  $\beta$ -cell numbers. However, phenotypic abnormalities are evident later and comprise mild islet disorganization, with  $\alpha$ -cells closer to the center of the islet contrary to their typical peripheral position, and a considerable reduction of  $\beta$ -cells combined with islet degeneration that worsens with age<sup>136</sup>. Whole genome transcriptome analyses of isolated islets were therefore devised within the framework of this thesis to contribute to these findings on a molecular level and generate hypotheses about the mechanism underlying them, specifically with regard to adult homeostasis.

## 2.5 Thesis outline

*In vitro* experiments with isolated murine islets and the rat insulinoma cell line INS-1E proved that Notch signaling is active in adult  $\beta$ -cells. To better investigate the hitherto unknown role for both canonical and non-canonical Notch signaling in adult  $\beta$ -cell homeostasis in an *in vivo* situation, an inducible,  $\beta$ -cell specific *Dll1* knockdown (Dll1- $\beta$ KO) was generated using existing Cre-Lox transgenic lines<sup>137,138</sup> and phenotyped *in vivo*. A whole genome transcriptomics approach on islets isolated from Dll1- $\beta$ KO mice and mice harboring a point mutation in the intracellular domain of Dll1 (Dll1\_T720A) was used to integrate these results and generate mechanistic hypotheses.

The *Pax6*<sup>Leca2</sup> mouse line is an ENU-induced mutant that harbors a point mutation in exon 7, leading to an arginine to cysteine substitution in the paired domain of the protein<sup>132</sup>. PAX6 plays a crucial role in endocrine development (see 2.2.1.1) and has been implicated in  $\beta$ -cell homeostasis in the adult pancreas<sup>133,134</sup>, and *Pax6*<sup>Leca2</sup> mice were shown by our group to have a unique phenotype in this respect<sup>136</sup>. The methods established during the course of this thesis regarding islet isolation and culture were used to analyze the gene expression network of *Pax6*<sup>Leca2</sup> islets and elucidate the mechanistic involvement of PAX6 in  $\beta$ -cell homeostasis. These efforts were part of a combined project within our group to dissect the pancreatic phenotype of *Pax6*<sup>Leca2</sup> mice. All experiments presented and discussed here were planned and performed in the course of this thesis.

### 3. Materials and Methods

#### 3.1 Materials

##### 3.1.1 Chemicals

Unless stated otherwise, standard chemicals were obtained from the following companies: Sigma Aldrich, Merck, Applichem, Qiagen, Roche, and Invitrogen.

##### 3.1.2 Buffers and solutions

###### G-solution for islet isolation

500 ml Hanks' Balanced Salt Solution (Lonza Verviers)  
+ 5 ml antibiotic antimycotic solution  
+ 5 g BSA  
dissolved and sterile filtered, stored at 4 °C for up to a month

###### 40% Optiprep®

20 ml 60% Optiprep®  
9.7 ml DBPS (Lonza Verviers)  
300 µl 1M HEPES (Lonza Verviers)  
stored at 4 °C for up to a week

###### 15% Optiprep®

5 ml 40% Optiprep®  
3 ml 10% RPMI1640 (Lonza Verviers) in HBSS (Lonza Verviers)  
freshly prepared on the day of use

###### Modified Krebs Ringer Bicarbonate Buffer (mKRBH) (10x)

14 g NaCl  
0.7 g KCl  
0.7 g CaCl<sub>2</sub>·2H<sub>2</sub>O  
0.23 g MgCl<sub>2</sub>  
ddH<sub>2</sub>O added to a final volume of 200 ml  
stored sterile filtered at 4 °C for up to two months

###### acid ethanol (0.18M HCl in 71% ethanol)

375 ml absolute ethanol

117.5 ml ddH<sub>2</sub>O

7.5 ml concentrated HCl

store at 4°C

mKRBH (1x)

approx. 75 ml of ddH<sub>2</sub>O

20 ml 10x mKRBH

2 ml 1M HEPES

9.6 ml 0.5M NaHCO<sub>3</sub> (freshly prepared)

components added in the exact order detailed above and adjusted to pH 7.4

20 ml 1% BSA in ddH<sub>2</sub>O

ddH<sub>2</sub>O added to a final volume of 200 ml

2M glucose added for 1.5mM, 2.8 mM, and 16.7 mM final concentrations as appropriate

freshly prepared on the day of use

PBS (10x)

80 g NaCl

2 g KCl

17.8 g Na<sub>2</sub>HPO<sub>4</sub>·2H<sub>2</sub>O

2.72 g KH<sub>2</sub>PO<sub>4</sub>

dissolved in ddH<sub>2</sub>O and adjusted to pH 7.3

ddH<sub>2</sub>O added to a final volume of 1 l

PBST

100 ml 10x PBS

500 µl Tween20

900 ml ddH<sub>2</sub>O

Tris-Acetate-EDTA (TAE) Buffer (10x) (for agarose gel electrophoresis)

48.4 g Trizma Base

11.4 ml glacial acetic acid (17.4 M)

3.7 g EDTA·Na·2H<sub>2</sub>O

ddH<sub>2</sub>O added to a final volume of 1 l

stored at 4°C

4×Tris·Cl/SDS pH 6.8 (for protein electrophoresis stacking gels)

6.05 g Trizma Base

dissolved in 40 ml ddH<sub>2</sub>O and adjusted to pH 6.8  
ddH<sub>2</sub>O added to a final volume of 100 ml  
add 0.4 g SDS  
stored at 4°C for up to one month

4xTris-Cl/SDS pH 8.8 (for protein electrophoresis separating gels)

91 g Trizma Base  
dissolved in 300 ml ddH<sub>2</sub>O and adjusted to pH 8.8  
ddH<sub>2</sub>O added to a final volume of 500 ml  
add 2 g SDS  
stored at 4°C for up to one month

6x SDS loading buffer

3 ml Glycerol  
7 ml 4xTris-Cl/SDS pH 6.8  
3 mg Bromphenol blue  
375 µl β-mercaptoethanol  
1 g SDS  
stored at 4°C

5x SDS electrophoresis running buffer

15.1 g Trizma base  
72.0 g Glycine  
5.0 g SDS  
ddH<sub>2</sub>O added to a final volume of 1 l  
stored at 4°C for up to one month

10x western blotting transfer buffer

30.03 g Trizma base  
144.1 g Glycine  
ddH<sub>2</sub>O added to a final volume of 1 l  
stored at 4°C for up to one month

1x western blotting transfer buffer

100 ml 10x Transfer buffer  
200 ml Methanol  
700 ml ddH<sub>2</sub>O

Paraformaldehyde fixative (20% stock)

stock prepared under a fume hood

70 ml PBS

8 g PFA

heat to 70°C

add 1 drop of concentrated NaOH until the solution is clear

remove from the heat

add 30 ml PBS, cool to room temperature

adjust pH to 7.2 with HCl

store at -20°C, dilute to 4% before use

**3.1.3 Enzymes and antibodies**

<b>enzymes</b>	<b>Company</b>	<b>Reference number</b>
Taq DNA Polymerase	Qiagen	201205
SuperScript® II Reverse Transcriptase	Invitrogen	18064-014
<b>primary antibodies</b>		
guinea pig-anti-insulin	Abcam	ab7842
rabbit-anti-glucagon	Invitrogen	18-0064
sheep-anti-DLL1	LsBio	LS-C150273
rabbit-anti-DLL1 H-265	Santa Cruz	sc-9102
<b>secondary antibodies</b>		
goat-anti-rabbit HRP-conjugated	Invitrogen	656120
donkey-anti-sheep HRP-conjugated	R&D Systems	HAF016
Alexa Fluor® goat-anti-guinea pig 488	Invitrogen	11073
Alexa Fluor® donkey-anti-rabbit 594	Invitrogen	21207

**3.1.4 Molecular biology reagents**

	<b>Company</b>	<b>Reference number</b>
Lipofectamine® LTX & Plus Reagent	Invitrogen	15338-100

GeneRuler® 1 kb DNA Ladder	Thermo Scientific	SM0312
GeneRuler® 100 bp DNA Ladder	Thermo Scientific	SM0241
RIPA Lysis and Extraction Buffer	Thermo Scientific	89900
cOmplete® Mini Protease Inhibitor Cocktail	Roche	11836153001
Spectra Multicolor Broad Range Protein Ladder	Thermo Scientific	26624
Random Primer Mix	NEB	S1330S
RNaseOUT®	Invitrogen	10777-019
LightCycler® 480 DNA SYBR Green I Master	Roche	04887352001

### 3.1.5 Kits

	<b>Company</b>	<b>Reference number</b>
QIAamp® DNA Mini Kit	Qiagen	51304
RNeasy® Plus Micro Kit	Qiagen	74034
Agilent RNA 6000 Pico Kit	Agilent Technologies	5067-1513
Ambion® WT Expression Kit	Ambion	4411974
GeneChip® Poly-A RNA Control Kit	Affymetrix	900433
GeneChip® WT Terminal Labeling and Controls Kit	Affymetrix	901525
GeneChip® Hybridization, Wash, and Stain Kit	Affymetrix	900720
GeneChip® Mouse Gene 1.0 ST Array	Affymetrix	901169
BCA Protein Assay Reagent	Thermo Scientific	23227
Western Lightning® Plus-ECL Kit	Perkin Elmer	NEL103001EA
Mouse Insulin ELISA	Mercodia	10-1247-01

### 3.1.6 Plasmids

<b>Vector Name</b>	<b>Description</b>	<b>Comment</b>
pDest26	his-tag control vector	Invitrogen 11809-019
pcDNA6.2-EmGFP	EmGFP control vector	Invitrogen K360-20
pDest-Dll1-His	expression of his-tagged, full length DLL1	constructed by Benjamin Moritz
PDest-Dll1ΔATEV	expression of his-tagged DLL1 without the intracellular PDZ-binding motif ATEV	constructed by Benjamin Moritz

pcDNA6.2-Dll1-EmGFP	co-cistronic expression of full length DLL1 and EmGFP	constructed by Benjamin Moritz
pcDNA6.2-Dll1ΔATEV-EmGFP	co-cistronic expression of DLL1 without the intracellular PDZ-binding motif ATEV and EmGFP	constructed by Benjamin Moritz

### 3.1.7 Oligonucleotide primers

Unless otherwise specified, primers were designed in the course of this thesis.

#### 3.1.7.1 *Mus musculus* primers

##### 3.1.7.1.1 Primers for qRT-PCR (housekeeping genes)

Gene		sequence	comments
<i>Ywhaz</i>	F	TGCAAAAACAGCTTTCGATG	
	R	TCCGATGTCCACAATGTTAAGT	
<i>Rpl13a</i>	F	TGAAGCCTACCAGAAAAGTTTGC	
	R	GCCTGTTTCCGTAACCTCAA	
<i>Sdha</i>	F	GCAATTTCTACTCAATACCCAGTG	
	R	CTCCCTGTGCTGCAACAGTA	
<i>Ubc</i>	F	AGCCCAGTGTTACCACCAAG	
	R	ACCAAGAACAAGCACAAGG	
<i>Hmbs</i>	F	GCTGAAAGGGCTTTTCTGAG	
	R	TGCCATCTTTCATCACTGT	
<i>Tbp</i>	F	CCCCACAACCTTCCATTCT	
	R	GCAGGAGTGATAGGGGTCAT	
<i>Fbxw2</i>	F	ATGGGTCACCAAGGTGGTT	
	R	TCCAATTGGCCAAATCTT	
<i>Hprt</i>	F	CCTAAGATGAGCGCAAGTTGAA	
	R	CCACAGGACTAGAACACCTGCTAA	
<i>Tuba1a</i>	F	AAGGAGGATGCTGCCAATAA	
	R	GCTGTGGAAAACCAAGAAGC	
<i>Zfp91</i>	F	TTGCAGCACCACATTAATAC	
	R	ATCCCTCTGGTCTGTATGATG	
<i>Cyc1</i>	F	GTTTCGAGCTAGGCATGGTG	
	R	CGGGAAAGTAAGGGTTGAAATAG	
<i>Atp5b</i>	F	GGTTTGACCGTTGCTGAATAC	
	R	TAAGGCAGACACCTCTGAGC	
<i>B2m</i>	F	GCTATCCAGAAAACCCCTCA	
	R	GGGGTGAATTCAGTGTGAGC	
<i>Actb</i>	F	GCCACCAGTTCGCCAT	designed by Christian Cohrs
	R	CATCACACCCTGGTGCCTA	
<i>Pgk1</i>	F	GAGCCCATAGCTCCATGGT	designed by Christian Cohrs
	R	ACTTTAGCGCTCCAAGA	
<i>Gapdh</i>	F	TGGAGAAACCTGCCAAGTATG	designed by Christian Cohrs
	R	CATTGTCATACCAGGAAATGAGC	

## 3.1.7.1.2 Primers for qRT-PCR (genes of interest)

Gene		sequence	comments
<b>Ins2</b>	F	CAGCAAGCAGGAAGCCTATC	
	R	GCTCCAGTTGTGCCACTTGT	
<b>Ins1</b>	F	GCAAGCAGGTCATTGTTTCA	
	R	CACTTGTGGGTCCTCCACTT	
<b>Gcg</b>	F	AGGCTCACAAGGCAGAAAAA	
	R	CAATGTTGTTCCGGTTCCTC	
<b>MafA</b>	F	CAGCAGCGGCACATTCTG	from Thorel <i>et al.</i> <sup>139</sup>
	R	GCCCGCCAATTCTCGTAT	
<b>Neurog3</b>	F	GTCGGGAGAAGTAGGATGGC	from Thorel <i>et al.</i> <sup>139</sup>
	R	GGAGCAGTCCCTAGGTATG	
<b>Pdx1</b>	F	CAGTGGGCAGGAGGTGCTTA	from Thorel <i>et al.</i> <sup>139</sup>
	R	GCCCGGGTGTAGGCAGTAC	
<b>Nkx6.1</b>	F	CCTGTACCCCATCAAGGAT	
	R	GGAACCAGACCTTGACCTGA	
<b>NeuroD1</b>	F	AACAGGAAGTGGAAACATGACC	
	R	TCTTCTCCTCCTCCTCTCC	
<b>Pcsk1</b>	F	TGCTGTTGGAACCAGCACT	
	R	TTCATTTTGCATTCTTCCAGA	
<b>Cdkn1a</b>	F	GCAGACCAGCCTGACAGATT	
	R	CACACAGAGTGAGGGCTAAGG	
<b>Hey1</b>	F	GAAAAGACGGAGAGGCATCA	
	R	AGCAGATCCCTGCTTCTCAA	
<b>Hey2</b>	F	ATTACCCTGGGCACGCTAC	
	R	TTTTCTATGATCCCTCTCCTTTTC	
<b>Ucn3</b>	F	AAGCTGCAACCCTGAACAGT	
	R	AGCATCGCTCCCTGTAAGTG	
<b>Msln</b>	F	ACCTGCTGCTCTTCTCAAC	
	R	CATACACGCCCTGGCACT	
<b>Aldh1a2</b>	F	GGAGGAGATCTTTGGTCTCG	
	R	TGTAACAATTGATCCAAACTGTCC	
<b>Ptgs2</b>	F	TGTGCTGACATCCAGATCAT	
	R	AAGCTCCTTATTTCCCTTCA	
<b>Sfrp1</b>	F	AGCCTTAAGCCCAAGGTA	
	R	TCATCCTCAGTGCAAACCTG	
<b>Amy2a1</b>	F	AACAATGTTGGTGTCCGTATT	
	R	CAGACGACAATTTCTGACCTGA	
<b>Ctrl</b>	F	GCCTGTAACGGAGACTCTGG	
	R	TTGTATTTTCTCCTTGATCCAGTC	
<b>Tgfb1</b>	F	TGCTTCAGCTCCACAGAGAA	
	R	CCTTGCTGTAAGTGTGTGCTCA	
<b>Bgn</b>	F	ACAGGTTGGGCTTAGGTCAC	
	R	GCAGATAGACAACCTGGAGGA	
<b>Acta2</b>	F	AGCCATCTTTCATTGGGATG	
	R	GGGCAATGATCTTGATCTTCA	
<b>Fn1</b>	F	GGTTGTGACTGTGGGCAAC	

	R	TCATGGCACCATTAGATGAA	
<b>Tnc</b>	F	TTTACCACAGACCTCGATTCC	
	R	CCCACAATGACTTCCTTGACT	
<b>Notch1</b>	F	ATCCGTGGCTCCATTGTCTA	
	R	CTCACTCTTCACGGCCTCA	
<b>Jag2</b>	F	GCCAGGAAGTGGTCATATTCA	
	R	ATCCGCACCATACCTTGCTA	
<b>Jag1</b>	F	GCCAGACTGCAGGATAAACA	
	R	CCCTGAAACTTCATGGCACT	
<b>Notch2</b>	F	GCAGTGGATGACCATGGAA	
	R	GGTGTCTCTTCTTATTGTCCTG	
<b>Notch3</b>	F	TGCACTGGGAATGAAGAACA	
	R	CCGGCTCCTCTACCTTCAGT	
<b>Dll4</b>	F	CACAGTGAGAAGCCAGAGTGTC	
	R	TCCTGCCTTATACCTCTGTGG	
<b>Dll1</b>	F	TGGCCAGGTACCTTCTCTCT	
	R	TCTTTCTGGGTTTTCTGTTGC	
<b>Hes1</b>	F	GAGCACAGAAAGTCATCAAAGC	
	R	ATGCCGGGAGCTATCTTTCT	
<b>Notch4</b>	F	GGATAAAAGGGGAAAACTGC	
	R	CGTCTGTTCCCTACTGTCTCG	
<b>Tacr3</b>	F	GCTTAAGGCTAAACGAAAGGTTG	
	R	TGAAGCCTGCACGAAATCTT	
<b>Gcgr</b>	F	GGCCTCAGGAAGCTGCAC	
	R	CCCCTCACTGAGCCAGAC	
<b>Ctgf</b>	F	AGTGTGCACTGCCAAAGATG	designed by Christian Cohrs
	R	TTCCAGTCGGTAGGCAGCTA	
<b>Timp1</b>	F	ACTCGGACCTGGTCATAAGG	designed by Christian Cohrs
	R	TCCTTTAGCATCTTAGTCATCTTGA	

### 3.1.7.1.3 Primers for PCR

Name		sequence
<b>Dll1_recombination</b>	F	CTGAAAGGTCTGAATGCTTCC
	R	CGCTCAAAGGATATGGGAAA
<b>Cre_genotyping</b>	F	AACCTGGATAGTGAAACAGGGGC
	R	TTCCATGGAGCGAACGACGAGACC

### 3.1.7.2 Rattus Norvegicus primers

#### 3.1.7.2.1 Primers for qRT-PCR (housekeeping genes)

Gene		sequence
<b>Actb</b>	F	TAGGCACCAGGGTGTGATG
	R	CATGATCTGGGTCATCTTTCA
<b>B2m</b>	F	TCAGAAAACTCCCAAATTCA
	R	TACATGTCTCGGTCCAGGT

<b>Gapdh</b>	F	GTCGGTGTGAACGGATTTG
	R	GATCTCGCTCCTGGAAGATG
<b>Hprt</b>	F	CATGGACTGATTATGGACAGGA
	R	CCCGTTGACTGGTCATTACA
<b>Ppia</b>	F	CAAAGTTCAAAGACAGCAGAA
	R	AGCCACTCAGTCTTGGCAGT
<b>Sdha</b>	F	CGCGATTTCTACCCAGTACC
	R	CCGTAATTTTCTAGCTCAACCAC
<b>Ubc</b>	F	GCTGGGCATGCAGATCTTT
	R	AGGGTGGACTCCTTCTGGAT

### 3.1.7.2.2 Primers for qRT-PCR (genes of interest)

Gene		sequence
<b>Hes1</b>	F	GAGCACAGAAAGTCATCAAAGC
	R	CTCGGGTCTGTGCTGAGAG
<b>Ins2</b>	F	GACCCACAAGTGGCACAAC
	R	AGAGCAGATGCTGGTGCAG
<b>Notch1</b>	F	TGTATATGTATGCCAGGTTATGAGG
	R	CACAGAAGGTTACACGGGGA
<b>Dll1</b>	F	ACTGCACTGACCCATTTGT
	R	CAGATCCTGGTTGCAGAAGAG
<b>Ptgs2</b>	F	CGTGTTGACGTCCAGATCA
	R	GGAAGTTCCTTATTCCTTTCACA

### 3.1.8 Mouse strains

The STOCK Tg(Ins2-cre/ERT)1Dam/J mouse line was purchased from the Jackson Laboratory (JAX), while the Dll1<tm1Mjo> line was a kind gift from Prof. Dr. Julian Lewis. *Pax6*<sup>Leca2</sup> animals were provided by Prof. Dr. Magdalena Götz and Dr. Ninkovic as part of a scientific collaboration between our laboratories. Dll1\_T720A mutants were generated in the Munich ENU mutagenesis screen<sup>140</sup>.

### 3.1.9 Cell lines

The INS-1E cell line was a kind gift by Prof Dr. Claes Wollheim.

## 3.2 Methods

### 3.2.1 Isolation and purification methods

#### 3.2.1.1 DNA isolation

Islet genomic DNA (gDNA) was isolated with the QIAamp® DNA Mini Kit (Qiagen). Islets corresponding to one sample were hand-picked under a microscope with a 200 µl micropipette and collected in a 1.5 ml reaction tube. After centrifugation at 12,000 rpm for 1 minute at room temperature, the medium was removed carefully to avoid disturbance of the islet pellet, which was washed once with PBS. Samples were centrifuged again under the same conditions, the supernatant discarded, and islets resuspended in 200 µl PBS without Ca<sup>2+</sup> and Mg<sup>2+</sup> (Lonza Verviers) (the absence of these cations facilitates the dissociation and lysis of the islets but is optional). The procedure was then continued according to the manufacturer's recommendations, starting with step 3 of the protocol "DNA Purification from Blood or Body Fluids" and including all optional steps. The elution was performed in 50 µl ddH<sub>2</sub>O and the incubation time elongated to 5 minutes at room temperature. Samples were stored at -20°C until further use.

#### 3.2.1.2 RNA isolation

Islets were hand-picked under a microscope with a 200 µl micropipette and collected in a 1.5 ml reaction tube, and stored on ice until all samples were ready. For a successful RNA isolation, it is advisable never to pick less than 50 islets for any one sample. After centrifugation at 12,000 rpm for 1 minute at room temperature, the medium was removed carefully with a micropipette, and the islets immediately lysed by adding 350 µl of RLT Buffer Plus with β-mercaptoethanol (10µl/ml). The lysate was homogenized by vortexing for 1 minute, and all subsequent steps were performed according to the manufacturer's manual. Briefly, the homogenized lysates were transferred to a gDNA eliminator spin column and centrifuged for 30 seconds at 12,000 rpm. After the addition of 350 µl 100% ethanol, samples were transferred to an RNeasy MinElute spin column and centrifuged for 15 seconds at 12,000 rpm. The bounded RNA was sequentially washed with 700 µl RW1 buffer, 500 µl RPE buffer and 500 µl 80% ethanol, always followed by centrifugations steps at 12,000 rpm for 15 seconds and for 2 minutes after adding ethanol. Contrary to the

manufacturer's protocol, the collection tube was changed after every step to enhance purity. After a final centrifugation at full speed for 5 minutes, the RNA was eluted with 14-20  $\mu$ l RNase-free water (provided in the kit) and stored until use at  $-80^{\circ}\text{C}$ .

### 3.2.1.3 Protein isolation

Islets were hand-picked under a microscope with a 200  $\mu$ l micropipette and collected in a 1.5 ml reaction tube, and stored on ice until all samples were ready. For western blot analysis, it is advisable not to pick less than 100 islets per sample. After centrifugation at 12,000 rpm for 1 minute at room temperature the medium was removed carefully with a micropipette. The pellet was washed once with PBS without  $\text{Ca}^{2+}$  and  $\text{Mg}^{2+}$  (Lonza Verviers) and then centrifuged again at 12,000 rpm for 1 minute. The supernatant was discarded and the islets resuspended in 100  $\mu$ l ice-cold RIPA Lysis and Extraction Buffer (Thermo Scientific) supplemented with 1x cOmplete<sup>®</sup> Mini Protease Inhibitor Cocktail (Roche) and shaken for 30 minutes at 1,400 rpm and  $4^{\circ}\text{C}$ . Afterwards, samples were centrifuged at 13,000 rpm and  $4^{\circ}\text{C}$  for 10 minutes in order to dispose of insoluble material. The supernatant was transferred to a new 1.5 ml reaction tube and stored at  $-80^{\circ}\text{C}$  until use.

## 3.2.2 Molecular methods

### 3.2.2.1 Polymerase Chain Reaction (PCR)

PCR was performed with 1.5 U *Taq* DNA polymerase and 5-50 ng DNA template. The reaction was as follows:

Component	Volume	Final concentration
CoralLoad PCR Buffer (10x)	2.5 $\mu$ l	1x
dNTPs (10 mM)	0.5 $\mu$ l	200 $\mu$ M
Forward primer (10 $\mu$ M)	1.0 $\mu$ l	0.4 $\mu$ M
Reverse primer (10 $\mu$ M)	1.0 $\mu$ l	0.4 $\mu$ M
Taq (5U/ $\mu$ l)	0.3 $\mu$ l	1.5 U
DNA	1.0 $\mu$ l	
Ampuwa	18.7 $\mu$ l	
<b>Final volume</b>	<b>25.0 <math>\mu</math>l</b>	

Cycling conditions were chosen according to the manufacturer's instructions:

94°C	4 min		
94°C	30s	}	35 cycles
60°C	30s		
72°C	40s		
72°C	7 min		
12°C	until end		

Both annealing temperature and time were adjusted depending on the specific primers used. In the case of the recombination analysis in the *Dll1* locus (see Figure 18), 55°C and 5s were chosen. PCR products were analytically separated via electrophoresis in agarose gels consisting of 2 % (w/v) agarose in TAE buffer and containing 0.5 µg/ml ethidium bromide, and then visualized under UV light.

### 3.2.2.2 cDNA synthesis

cDNA was synthesized from RNA using the SuperScript® II reverse transcriptase enzyme (Invitrogen) and a random primer mix (NEB) containing both random hexamers and anchored dT<sub>23</sub> primers to maximize reaction yields. RNA was mixed with the primers and pre-annealed as follows:

RNA (20-500 ng)	variable
random primer mix (60µM)	2 µl
dNTPs (10 mM)	1 µl
nuclease-free H <sub>2</sub> O	filled to 12 µl

---

pre-annealing at 65°C for 5 minutes

Afterwards, samples were chilled on ice for at least 5 minutes and the following components were added to the test tubes:

---

pre-annealing mix	12 $\mu$ l
5x First-Strand Buffer	4 $\mu$ l
0.1 M DTT	2 $\mu$ l
RNaseOUT®	1 $\mu$ l
SuperScript® II	1 $\mu$ l
<b>final volume</b>	<hr/> 20 $\mu$ l

---

gentle mixing, 10 min incubation at 25°C

Reverse transcription was performed in a thermal cycler for 60 minutes at 42°C. Enzyme inactivation, essential for subsequent applications, was achieved by an additional incubation step at 70°C for 15 minutes. The cDNA samples were stored at -20°C until use.

### **3.2.2.3 Quantitative real-time PCR (qRT-PCR)**

#### *3.2.2.3.1 General strategy*

Quantitative real-time PCR (qRT-PCR) is an umbrella term that summarizes a variety of different experimental procedures and strategies, as has been noted before<sup>141</sup>. For the purposes of this thesis, qRT-PCR was used for the relative quantification of genes in islet cDNA samples, using the fluorescent cyanine dye SYBR Green I included in the LightCycler® 480 DNA SYBR Green I Master (Roche). Each sample was measured in four technical replicates to assure measurement quality.

All primer sequences used were specifically designed to cross exon/exon boundaries, hereby preventing the coamplification of genomic DNA, and to produce an amplicon within the size range of 50-300 bp for optimal results. Sequence information for the primer design was obtained from the Ensembl Genome Browser<sup>142</sup> (<http://www.ensembl.org>), while the design itself was performed with the online tool Primer3 (<http://primer3.wi.mit.edu/>). Primer-BLAST (<http://www.ncbi.nlm.nih.gov/tools/primer-blast/>) was then used to check if the designed primers might recognize cDNA from different genes in addition to the desired target. This is particularly relevant for genes that have homologue sequences, i.e. the *Dll* or *Notch* genes: if several exons have the same sequence, even designing primers across exon/exon boundaries is not enough to assure specificity for only one gene. Since amplicons from homologues might have the exact same size, the bioinformatic control with

Primer-BLAST is the only way to exclude this error source with certainty. Primers were ordered from Metabion and tested in a PCR format to assure the amplification of the right product size (see for 3.1.7.1.1 and 3.1.7.1.2 for primer sequences). Moreover, a dissociation curve analysis was performed as a part of every qRT-PCR experiment to again check that only the specific product was produced.

Given the relative nature of the quantification, normalization is possibly the most essential component of the assay, and its disregard is a serious problem affecting many experimental results<sup>141,143</sup>. The most prevalent mistake is the use of the same housekeeping genes for every tissue and experiment without previously empirically validating their utility for the design at hand. To avoid this glaring mistake, the experiments described in this thesis were carried out according to the strategy outlined by Vandesompele *et al.*<sup>144</sup>, meaning that for every new experimental setup (e.g. the comparison between islet samples isolated from new genotypes or, from mice of a different age, or if the culture conditions were different, etc.) a set of 15 candidate housekeeping genes (3.1.7.1.1) was analyzed with regard to the suitability of said candidates as references. The analysis is based on the assumption that the expression ratio between two ideal housekeeping genes should be identical at all times and between all samples. Calculating the average pairwise variation of the ratios for a candidate with all other candidates (M) enables to numerically determine the divergence to the ideal for every tested gene<sup>144</sup>. The two most stable housekeeping genes, determined with this method using the geNorm<sup>®</sup> 3.5 software, were selected for the qRT-PCR experiment.

#### 3.2.2.3.2 Reaction conditions

For qRT-PCR reactions, 50-500 ng of islet cDNA were usually applied. The reaction mix was as follows:

<b>Component</b>	<b>final concentration</b>	<b>volume</b>
gene-specific primers F+R (3 $\mu$ M)	0.3 $\mu$ M	2 $\mu$ l
cDNA		x $\mu$ l ( <b>max. 0.4</b> )
LightCycler <sup>®</sup> 480 DNA SYBR Green I Master (2x)	1x	10 $\mu$ l
Ampuwa		8-x $\mu$ l
		<hr/> 20 $\mu$ l

In order to achieve maximum reproducibility, the primer solution, containing both the forward and reverse primer, was pipetted first into the required wells of a LightCycler® 480 Multiwell Plate 384 (Roche). A master mix was then prepared for each individual sample (as well as for a no-template negative control) containing cDNA, Ampuwa and the LightCycler® 480 DNA SYBR Green I Master (Roche). 18 µl of this master mix were added to each individual well and the reaction performed on the LightCycler® 480 instrument as described below.

95°C	10 min	} 45 cycles
94°C	15s	
60°C	1 min	
55°C-95°C	dissociation curve	

The volume of cDNA varied between individual experiments depending on the RNA quantity deployed for the synthesis as well as the specific genes to be assayed, meaning the volume of Ampuwa had to be adjusted accordingly. As depicted above, it is crucial that the volume of the undiluted cDNA sample in the final reaction does not exceed 0.4 µl, since a higher amount was found to have a negative effect on the qRT-CR reaction (data not shown). The reverse transcriptase (RT) enzyme and its buffer are known inhibitors of the qRT-PCR reaction, especially when a small amount of RNA is used in the RT reaction<sup>145</sup>, which is always the case with isolated islets due to material restrictions. The existence of an upper limit to the volume of RT reaction that is applicable without inhibition is consistent with previous reports<sup>146</sup>. While dilution of the cDNA represents an alternative strategy, the outcome is essentially identical, meaning for instance that the final volume of a 1:10 diluted sample should not exceed 4 µl, and so forth.

### 3.2.2.3.3 Data analysis

Crossing point (Cp) values were obtained by the automatic Cp analysis of the LightCycler® 480 software (Roche) by the second derivative maximum method. All subsequent data analysis was performed in Microsoft Excel. Technical replicates were averaged and their

standard deviation was determined to assure data quality. The results were determined using the equations outlined in the geNorm® 3.5 user manual, which are mathematically identical to the  $2^{-\Delta\Delta C_p}$  method<sup>147</sup>. Finally, relative expression levels were rescaled to the mean expression level of wild-type controls, which was set to one. Differences were considered statistically significant at  $P < 0.05$  using a heteroscedastic two-tailed Student's t-test and the following significance-ranking was used: \* =  $p < 0.05$ , \*\* =  $p < 0.01$ , \*\*\* =  $p < 0.001$ .

#### **3.2.2.4 Whole transcriptome microarray analysis**

A small aliquot of the RNA samples was diluted to a concentration  $<50$  pg/ $\mu$ l and analyzed with the Agilent RNA 6000 Pico Kit (Agilent Technologies) to ensure the high quality of the RNA. The evaluation was conducted according to the manufacturer's instructions using the Agilent 2100 Bioanalyzer platform (Agilent Technologies), and samples with an RNA Integrity Number (RIN) higher than 9 (10 corresponds to a completely intact total RNA preparation) were selected for subsequent use.

250 ng of total islet RNA were spiked with poly-A control RNA from the GeneChip® Poly-A RNA Control Kit (Affymetrix) and further processed using the Ambion® WT Expression Kit, the GeneChip® WT Terminal Labeling and Controls Kit and the GeneChip® Hybridization, Wash, and Stain Kit. All samples pertaining to the same experiment were handled in parallel at all times. For the purpose of clarity, the two-cycle target labeling strategy that was pursued is summarized in Figure 8.

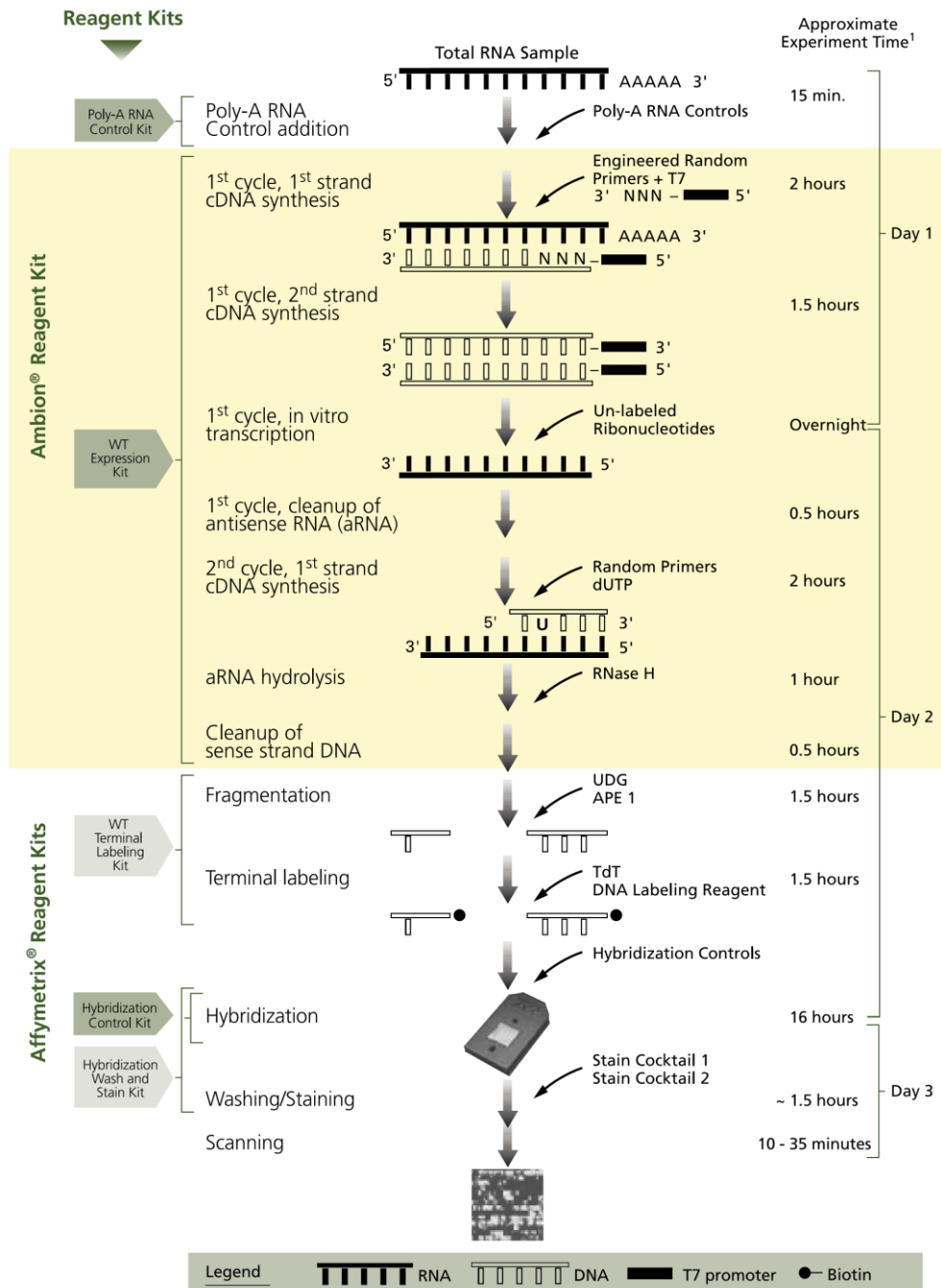


**Figure 8. Overview of the procedure for Affymetrix whole transcriptome microarray analysis.** From GeneChip® WT Terminal Labeling and Controls Kit user manual.

Firstly, samples were amplified through successive reactions. The RNA was reverse transcribed to first strand cDNA, the second strand was synthesized, and copyRNA (cRNA) was transcribed *in vitro* from the resulting double-stranded cDNA. Finally, the cRNA was again reverse transcribed to second-cycle cDNA and the RNA template hydrolyzed with RNase H. Reaction and thermal cycling conditions for the various steps were as follows:

<b>(1) First strand cDNA synthesis</b>	
spiked RNA (40 ng/ $\mu$ l)	5 $\mu$ l
first strand buffer mix	4 $\mu$ l
first strand enzyme mix	1 $\mu$ l
final volume	<u>10 <math>\mu</math>l</u>
thermal cycling	
25°C	1 hour
42°C	1 hour
4°C	2 min

<b>(2) Second strand cDNA synthesis</b>	
nuclease-free H <sub>2</sub> O	32.5 $\mu$ l
second strand buffer mix	12.5 $\mu$ l
second strand enzyme mix	5 $\mu$ l
	<u>50 <math>\mu</math>l</u>
add to the first strand cDNA sample for a final volume of 60 $\mu$ l	
thermal cycling	
16°C	1 hour
65°C	10 min
4°C	2 min

<b>(3) cRNA in vitro transcription (IVT)</b>	
IVT buffer mix	24 $\mu$ l
IVT enzyme mix	6 $\mu$ l
	<u>30 <math>\mu</math>l</u>
add to the second strand cDNA sample for a final volume of 90 $\mu$ l	
thermal cycling	
25°C	1 hour
40°C	16 hours

<b>(4) second-cycle cDNA synthesis</b>	
cRNA (10 µg)	22 µl
random primers	2 µl
final volume	24 µl
thermal cycling (cRNA denaturation)	
70°C	5 min
25°C	5 min
4°C	2 min
add	
second-cycle buffer mix	8 µl
second-cycle enzyme mix	8 µl
final volume	40 µl
thermal cycling	
25°C	10 min
42°C	90 min
70°C	10 min
add	
RNase H	2 µl
thermal cycling	
37°C	45 min
95°C	5 min
4°C	2 min

The reaction buffer for the synthesis of single-stranded second-cycle cDNA importantly contained dUTP nucleotides, leading to their inclusion in the product. This enabled the fragmentation of the cDNA precisely at these unnatural dUTP residues by employing the enzymes uracil-DNA glycosylase (UDG) and apurinic/apyrimidinic (AP) endonuclease 1 (APE1) in combination. UDG recognizes uracil bases and excises them from the DNA, thereby generating AP sites that are recognized by APE1, which cleaves the phosphodiester backbone and breaks the cDNA molecule apart. Subsequently, and additional enzymatic

reaction by the terminal deoxynucleotidyl transferase (TdT) leads to the biotinylation of each individual fragment. The reactions in question were performed according to these protocols:

<b>(5) Fragmentation of 2nd-cycle cDNA</b>	
cDNA (5.5 µg)	31.2 µl
10x fragmentation buffer	4.8 µl
UDG (10 U/µl)	1 µl
APE 1 (1000 U/µl)	1 µl
nuclease-free water	10 µl
total volume	48 µl
thermal cycling	
37°C	1 hour
93°C	2 min
4°C	2 min

<b>(6) Labeling</b>	
Fragmented cDNA	45 µl
5x TdT Buffer	12 µl
TdT	2 µl
DNA Labeling Reagent	1 µl
total volume	60 µl
thermal cycling	
37°C	1 hour
70°C	10 min
4°C	2min

The fragmented and biotinylated cDNA was combined with the controls and buffers provided in the GeneChip® Hybridization, Wash, and Stain Kit to form the hybridization cocktail. Each individual cocktail, corresponding to one sample, was then loaded on a GeneChip® Mouse Gene 1.0 ST Array cartridge and incubated for 17 hours at 45°C and 60 rpm in a hybridization oven. Next, the array cartridges were sequentially stained and washed automatically using the GeneChip® Fluidics Station 450 (Affymetrix), and finally scanned with the GeneChip® Scanner 3000 (Affymetrix) to obtain the probe array images. Mean foreground intensities were obtained for each spot with the Expression Console™ Software (Affymetrix). The data was normalized and array metrics and quality controls, such as the hybridization controls and the poly-A spikes, which should yield equal results on all arrays handled in parallel, were analyzed. Further analysis of the microarray results to detect the differentially expressed genes was performed with CARMAweb (Comprehensive R-based Microarray Analysis web service), a free online R-package designed by Rainer *et al.*<sup>148</sup>. Specifically, a moderated t-test (limma) was applied, and the false discovery rate (FDR) calculated according to Benjamini & Hochberg<sup>149</sup>.

### 3.2.2.5 SDS Polyacrylamide Gel Electrophoresis (SDS-PAGE)

Proteins were separated by SDS-PAGE as described by Gallagher<sup>150</sup>. Protein samples were heated to 95 °C for 10 min in an SDS-containing loading dye and loaded on a 10% polyacrylamide gel. The electrophoretic separation was carried out at 60V during focusing in the stacking gel (usually 30 minutes) and then 80-100V until the bromophenol blue indicator reached the lower end of the gel.

#### separating gel

Acrylamide/Bis-acrylamide, 30% solution	5 ml
4×Tris•Cl/SDS pH 8.8	3.75 ml
ddH <sub>2</sub> O	6.25 ml
10% (w/v) ammonium persulfate	100 µl
TEMED	20 µl

#### stacking gel

Acrylamide/Bis-acrylamide, 30% solution	650 µl
4×Tris•Cl/SDS pH 6.8	1.25 ml
ddH <sub>2</sub> O	3.05 ml
10% (w/v) ammonium persulfate	50 µl
TEMED	10 µl

### 3.2.2.6 Western Blot

After SDS-PAGE, proteins were blotted on a Hybond-P PVDF membrane (GE Healthcare) according to the protocol delineated by Gallagher *et al.*<sup>151</sup> for a tank transfer system. The membrane was activated in methanol for 10 seconds, washed in ddH<sub>2</sub>O, and equilibrated in transfer buffer with Whatman<sup>®</sup> paper (Biometra) for at least one hour during electrophoresis. The transfer sandwich was assembled as follows:

**cathode side**

Whatman® paper, 4 layers

gel

membrane

Whatman® paper, 4 layers

**anode side**

Blotting was performed at 200 mA for 2 hours and checked by reversible staining with Ponceau S. Subsequently, the membrane was incubated overnight in 10% skimmed milk in TBST at 4°C, under gentle shaking in order to avoid clotting. Next to at least five washing steps of 10 minutes each in TBST, primary antibodies, diluted in 10% skimmed milk in TBST according to manufacturer's recommendations, were applied directly to the side of the membrane with the bound proteins and again incubated overnight at 4°C under gentle shaking. The membrane was then washed as before and incubated with HRP-conjugated secondary antibodies for 1 hour at room temperature. After washing five times in TBST, protein bands were visualized using the HRP luminescent substrate provided in the Western Lightning® Plus-ECL Kit (Perkin Elmer) and detected with the Fusion FX7 scanner (Vilber).

**3.2.2.7 Mouse Insulin ELISA**

Insulin measurements were performed with the ELISA kit purchased from Mercodia and were required in two different contexts, namely the measurement of plasma insulin from mice and the assessment of *in vitro* glucose-stimulated insulin secretion (GSIS) from isolated islets. In the case of plasma insulin, the procedure was carried out according to the manufacturer's manual. Briefly, plasma was thawed on ice and 10 µl were mixed with 10 µl calibrator solution in the pre-coated wells provide in the kit. 100 µl enzyme conjugate were added and the plate incubate for two hours at room temperature and 800 rpm. After six manual washing steps with each 300 µl washing buffer, 200 µl TMB substrate were added and the reaction incubated for 15 minutes at room temperature. 50 µl stop solution were used to halt the reaction and the OD<sub>450</sub> was measured immediately thereafter in a plate reader (GeniusPRO, Tecan). The standards provided by the kit were used to calculate sample concentrations.

GSIS samples were diluted in calibrator 0 as follows:

---

<b>sample</b>	<b>dilution</b>
islet lysate	1:200
supernatant from high glucose samples	1:2 – 1:5
supernatant from low glucose samples	1:2

The rest of the procedure was performed as described above.

### **3.2.3 Cell culture methods**

#### **3.2.3.1 INS-1E cell culture**

The clonal  $\beta$ - cell line INS-1E was cultured in RPMI 1640 medium (Lonza Verviers) supplemented with 10% fetal calf serum (Invitrogen), 1mM sodium pyruvate (Lonza Verviers), 50  $\mu$ M beta-mercaptoethanol (Lonza Verviers), 10 mM HEPES and 1x penicillin/streptomycin solution (Sigma Aldrich). Cells were grown in monolayers in 75-cm<sup>2</sup> Falcon cell culture bottles (BD Biosciences) in 20-22 ml medium and kept in a sterile incubator at 37°C with 5% CO<sub>2</sub> infusion and humidified air at all times. Passaging was carried out once a week by gentle trypsinization. To this end, the cell monolayer was rinsed once with sterile PBS w/o Ca<sup>2+</sup>/Mg<sup>2+</sup> (Lonza Verviers) and then incubated in 3 ml Trypsin w/o Ca<sup>2+</sup>/Mg<sup>2+</sup> (Sigma Aldrich) at 37°C for 5 min. Trypsin was inactivated by the addition of culture medium and the cells were split 1/3 in a new cell culture bottle. For all experiments presented here, 1.5·10<sup>5</sup> INS-1E cells were seeded in Falcon 24-well plates (BD Biosciences) in 500  $\mu$ l medium and cultured for 2 days before use.

#### **3.2.3.2 INS-1E pseudo-islets**

For the formation of pseudo-islets, 10<sup>6</sup> INS-1E cells were seeded in 10 ml medium in non-treated suspension culture dishes (Corning®, #430591) and cultured for 2 days before use.

#### **3.2.3.3 Transfection of INS-1E cells**

Transfection of INS-1E cells was carried out with Lipofectamine® LTX & Plus Reagent (Invitrogen) according to the manufacturer's instructions and using 1  $\mu$ g of plasmid DNA.

#### **3.2.3.4 Islet isolation and culture**

Mice were euthanized by CO<sub>2</sub>, readily dissected to expose the inner organs, and placed under a dissecting microscope. The gut and the liver were pushed aside with surgical forceps, thereby exposing the common bile duct that was clamped at its junction with the duodenum with a micro bulldog clamp (Roboz, Germany) and subsequently cannulated. The pancreas was distended via the injection of 3-5 ml collagenase solution, removed from the cadaver, and immediately placed on ice in a 15-ml falcon tube containing further 3 ml of the same collagenase solution. When processing more than one animal, organs should not be stored on ice longer than 30 minutes before proceeding to the next step, allowing for the preparation of approximately 4 animals by one experimenter.

Samples were incubated in a 37 °C water bath for 15 minutes and shaken gently once after 7.5 minutes. All remaining steps were performed under a sterile working bench. 10 ml ice-cold G-solution were added to the digested pancreas followed by centrifugation for 2 minutes at 290G (all centrifugation steps were performed at room temperature). The supernatant, containing mainly fat tissue that remained attached to the pancreas during removal as well as loose exocrine tissue, was discarded and the pellet resuspended in further 10-12 ml ice-cold G-solution. The suspension was then filtered through a pre-wet small metal mesh (pore size approx. 1 mm) to separate undigested tissue chunks, and collected in a 50-ml falcon tube. Both the 15-ml tube originally containing the pancreatic suspension and the metal mesh were rinsed with additional G-solution to avoid islet loss. The filtrate was then centrifuged again at 290G for 2 minutes. The supernatant, made up mostly by acinar cells, was discarded and the pellet resuspended in 5.5 ml of a 15% Optiprep® solution prepared as described and stored at 4°C until use. This suspension was pipetted carefully onto 2.5 ml of 15% Optiprep® in a new falcon tube, producing two distinct layers of different density. This gradient was then overlaid again with 6 ml G-solution and incubated for 10 minutes at room temperature followed by 15 minutes centrifugation at 290-300G (depending on a visual inspection of the thickness of the middle layer), with the brake turned off to avoid mixing of the gradient during deceleration. The islets, now located at the interface between the first and second layer, were collected with a serological pipette and filtrated through a 70 µm cell strainer to loose remaining acinar cells. The strainer was turned over a petri dish and rinsed with RPMI 1640 (Lonza Verviers) to liberate the islets that

were hand-picked under a microscope with a 200  $\mu$ l micropipette to further enhance purity. Islets were plated into non-treated suspension culture dishes (Corning®, #430591) to avoid attachment and kept at a maximum density of 50 islets per dish to prevent competition for nutrients and the appearance of hypoxic centers. Culture was carried out in 10 ml 5.5 mM glucose RPMI 1640 (Lonza Verviers) supplemented with 10% fetal calf serum (Invitrogen) and 1x antibiotic antimycotic solution (Sigma Aldrich). Islet dishes were kept in a sterile incubator at 37°C with 5% CO<sub>2</sub> infusion and humidified air at all times. A representative photograph of freshly isolated islets is presented in Figure 9. Unless specified otherwise, islets were cultured overnight and then used.

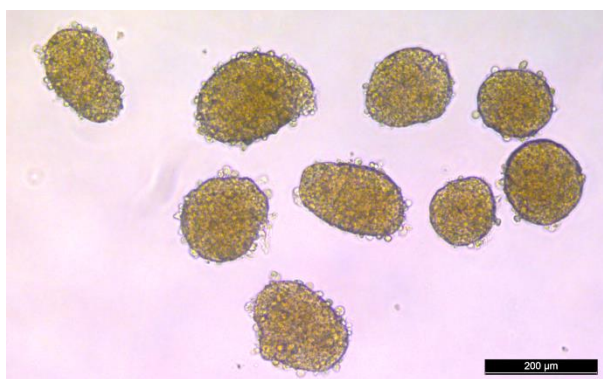


**Figure 9. Freshly isolated islets.**

The transparent cells attached to the islet surface represent remaining acinar cells.

The procedure detailed here is a combined and modified version of those previously reported by Li *et al.*<sup>152</sup> and Carter *et al.*<sup>153</sup>.

### **3.2.3.5 Glucose-stimulated insulin secretion (GSIS)**

All buffers were warmed to room temperature before the start of the procedure. Islets corresponding to one sample were hand-picked under a microscope and collected in a 1.5 ml reaction tube, using a 20  $\mu$ l micropipette to minimize carryover of culture medium (it is essential to only use islets with a diameter < 150  $\mu$ m). The reaction tube was then filled with 1.5 mM glucose/mKRBH, and the islets were allowed to settle to the bottom of the tube for 5 minutes. 1.4 ml of the supernatant were carefully removed using a 1000  $\mu$ l micropipette and without disturbing the islet pellet and 1 ml 1.5 mM glucose/mKRBH was added. After 5 minutes, 1 ml was carefully removed and an additional washing step was performed by again

adding 1 ml 1.5 mM glucose/mKRBH and removing it after 5 minutes. Using a 200  $\mu$ l micropipette, islets were transferred to one well of a 6 well-plate containing 5 ml of 1.5 mM glucose/mKRBH and incubated for one hour at 37°C and 5% CO<sub>2</sub> without the lid. Afterwards, islets were transferred to a new well containing the same buffer and placed in the incubator for a further hour. Islets isolated from the same mouse and treated in the same way were always kept in the same well.

During the first of these two incubations, 1.5 ml reaction tubes with the desired treatments were prepared. For a basic GSIS experiment, tubes with each 500  $\mu$ l of 2 mM glucose/mKRBH (low glucose) and 20 mM glucose/mKRBH (high glucose) were pipetted, labeled and placed in the incubator with open lids to allow equilibration with the CO<sub>2</sub> pressure. Upon conclusion of the second incubation, 15 islets each were picked with a 20  $\mu$ l micropipette and pipetted in a tube containing the designed treatment. Tubes were then placed in the incubators for two hours with open lids. Afterwards, samples were mixed gently with a 200  $\mu$ l micropipette and allowed to settle for 5 minutes. 400  $\mu$ l supernatant were transferred to a new tube, while 500  $\mu$ l acid ethanol were added to the islets to lyse the cells and mobilize insulin. All samples were stored at -20°C until further use or measured immediately with a mouse insulin ELISA (MercoDia). Insulin secretion was expressed as percentage of total insulin content for any given sample. See 3.2.2.7 for details on the ELISA measurement.

For INS-1E cells, GSIS experiments were performed with attached monolayers in 24-well plates. All incubation steps were identical to islet GSIS.

### **3.2.3.6 Determination of islet oxygen consumption rate (OCR)**

Islets were hand-picked under a microscope and washed in 50 ml XF assay medium (Seahorse Bioscience) containing 3 mM glucose and 1% FCS. Islets were then seeded in a XF24 islet capture microplate (Seahorse bioscience) at a maximum density of 50 islets/well. The plate was the incubated for 1 hour at 37°C without CO<sub>2</sub> and without the lid. OCR measurement was then performed with an XF extracellular flux analyzer (Seahorse bioscience) according to the manufacturer's protocol. A final concentration of 3 mM glucose was added to stimulate the oxygen consumption, which was then blunted with 5  $\mu$ M oligomycin.

### **3.2.4 Immunohistochemistry**

#### **3.2.4.1 Immunohistochemistry on pancreatic cryosections**

Mice were euthanized by CO<sub>2</sub> and readily dissected to isolate the pancreas. After a quick wash in PBS, the organs were fixed in 4% PFA/PBS for 30 minutes at 4°C on a rocking platform. Specimens were washed twice in PBS and incubated at 4°C in 10% sucrose for 2 hours and then in 30% sucrose overnight, always under gentle rocking. The next day, tissues were transferred to a 2:1 OCT/30% sucrose solution for 2 h before being embedded in OCT on dry ice and stored at -80°C until further use.

Staining of the preparations was performed according to Watkins<sup>154</sup>. Briefly, sections with a thickness of 7-10 µm were cut with a cryostat at -30°C on the day of the staining, air-dried on a microscope slide (SuperFrost Plus®, Menzel-Gläser) and washed twice in PBST before blocking in 5% BSA/PBST for 2 hours at room temperature. Afterwards, primary antibodies diluted 1:200 in blocking solution were applied to the sections and incubated overnight at 4°C. Slides were then washed at least three times for 5 minutes with PBST, and adequate secondary antibodies were applied (diluted 1:500 in PBST) in combination with DAPI (1:1000) and incubated for 2 hours at room temperature. At least five washing steps in PBST for 10 minutes followed, after which slides were mounted with Vectashield® mounting medium (Biozol), sealed with nail polish and stored at 4°C before being analyzed with an Axioplan 2 epifluorescence microscope (Zeiss) combined to an AxioCam HRC camera (Zeiss) to obtain photographs.

#### **3.2.4.2 Whole mount staining of isolated islets**

The immunofluorescence whole staining of intact islets was performed according to a procedure modified from<sup>155</sup> and<sup>156</sup>. Isolated islets were cultured overnight and then transferred to a 1.5 ml reaction tube using a 200 µl micropipette. All incubation steps were performed with 10-15 islets per staining, with the islets free-floating at all times. In order to change the solution according to each staining step, islets were allowed to settle for at least 5 minutes and the solution carefully removed with a 200 µl micropipette.

Firstly, islets were fixed in PBS containing 2% PFA for 20 minutes at room temperature, washed once in PBS, and then permeabilized overnight at 4°C in a solution containing 0.3%

Triton X-100 (Sigma Aldrich), 1% BSA (Sigma Aldrich) and 5% goat serum (Invitrogen) to ensure blocking. Islets were then washed with PBS and incubated with primary antibodies diluted 1:200 in an identically composed permeabilization solution for 48 hours at 4°C. After three washing steps with PBS, adequate secondary antibodies were applied (diluted 1:500 in PBST) in combination with DAPI (1:1000) and again incubated for 48 hours at 4°C. Finally, islets were washed thoroughly with PBS and carefully transferred to a microscope slide (SuperFrost Plus®, Menzel-Gläser) where they were mounted with Vectashield® (Biozol), sealed with nail polish, and stored at 4°C until analysis.

To obtain images, samples were then subjected to optical sectioning at 5 µm intervals in the axial (z) dimension using a Zeiss LSM510 confocal laser scanning microscope (Zeiss) and the LSM 510 software.

### **3.2.5 Mouse methods**

#### **3.2.5.1 Animal housing**

Mice were kept in a specific-pathogen-free (SPF) environment, in compliance with the Federation of European Laboratory Animal Science Associations (FELASA) protocols. Unless otherwise specified for particular experimental conditions such as the high fat diet challenge, mice received standard rodent nutrition and water *ad libitum*. All animal experiments were performed under the approval of the responsible animal welfare authority.

#### **3.2.5.2 Generation of Dll1-βKO mice**

Dll1-βKO mice were generated by breeding the STOCK Tg(Ins2-cre/ERT)1Dam/J mouse line with the Dll1<tm1Mjo> line, that contains two loxP sites in the *Dll1* locus<sup>137,138</sup>. The STOCK Tg(Ins2-cre/ERT)1Dam/J line was on a B6CBAF1 mixed background, whereas the Dll1<tm1Mjo> line was on a pure C3HeB/FeJ background. Dll1-βKO mice used for this thesis are all the offspring of the original cross, and a backcross on the C3HeB/FeJ background is currently ongoing.

#### **3.2.5.3 Genotyping**

Genotyping of the Cre transgene in Dll1- $\beta$ KO mice was carried out with a standard PCR reaction (see 3.2.2.1) as described in the online JAX<sup>®</sup> protocols database (<http://jaxmice.jax.org/protocolsdb>, Stock number 008122). Genotyping was performed by Nina Schieven.

#### **3.2.5.4 Blood plasma collection**

The tail of the mice was slightly slit with a scalpel and massaged gently to enable the leakage of blood. Up to 50  $\mu$ l were collected in a lithium-heparin coated Microvette<sup>®</sup> CB 300 LH (Sarstedt) and centrifuged at 12,000 rpm and 4°C for two minutes. The plasma supernatant was transferred to a new reaction tube, frozen immediately in liquid nitrogen, and stored at -80°C until use.

#### **3.2.5.5 Blood glucose evaluation**

Blood glucose levels were analyzed in mice fasted for at least six hours. Leakage of a blood drop from the tail was achieved as described in 3.2.5.4. The measurement itself was performed in duplicates with the blood glucose analyzer Ascensia Elite (Bayer, Germany) using the supplied sensor strips.

#### **3.2.5.6 Intraperitoneal glucose tolerance test (ipGTT)**

The procedure was performed on conscious mice, fasted for six hours. Mice were weighed before the start of the procedure and a fasting glucose level was obtained via a small tail clip as described in 3.2.5.5. 1 ml/100 g body weight of a 20% glucose solution in sterile saline (corresponding to 2 g glucose/g body weight) was injected intraperitoneally at time 0. Blood glucose values and plasma samples were obtained as described above after 5, 15, 30, 60, and 120 minutes.

## 4. Results

### 4.1 *In vitro* analysis of *Dll1* and Notch signaling

#### 4.1.1 Isolated islets of Langerhans

Islets isolated from wild-type mice were analyzed to check the expression of Notch signaling components. As displayed in Figure 10, all four existing *Notch* genes are expressed in murine islets, and *Notch1* shows the highest expression. Expression could also be confirmed for the ligands *Dll1*, *Dll4*, *Jag1*, and *Jag2*, and for Notch targets from both the *Hes* and *Hey* gene families, with *Hes* genes displaying a markedly higher expression (see chapter 2.1.1 for details about Notch receptors, ligands, and targets).

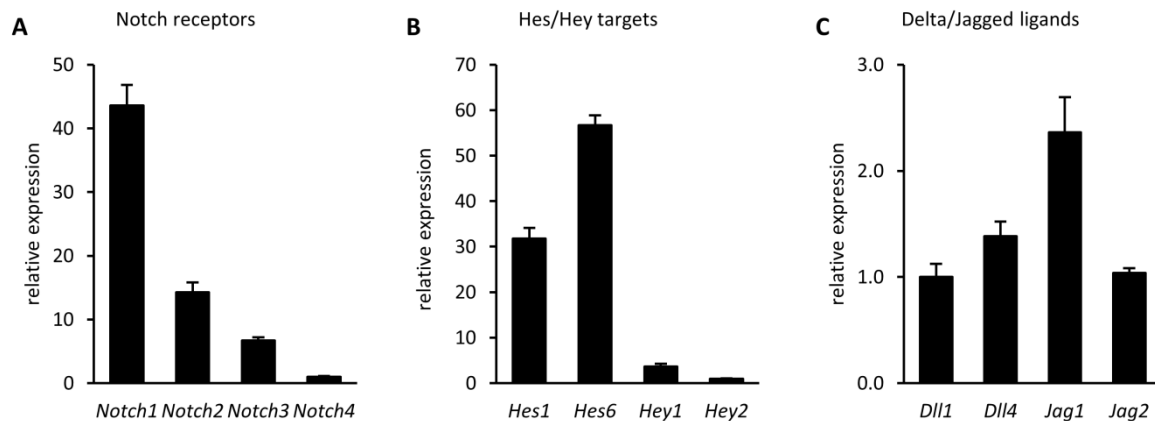


**Figure 10. Expression of Notch signaling genes in isolated primary C3HeB/FeJ islets.**

Islets were isolated from C3HeB/FeJ wild-type mice and the relative expression levels of Notch receptors (A), targets (B), and ligands (C) were analyzed via qRT-PCR. Expression was normalized to the housekeeping genes *Cyc1* and *Hmbs*. Error bars display the standard error of the mean (SEM) (n=8). Since the data refers to one single genotype, no statistical test was performed.

Furthermore, the same genes were analyzed in islets cultured for 24 or 72 hours. Consistent with previous reports, there is a general trend towards enhanced Delta/Notch gene expression with increasing culture duration. The receptor-encoding genes *Notch1* and *Notch3*, as well as the ligand-encoding *Dll1* and *Jag2*, were significantly upregulated in islets cultured for 72 hours compared to islets cultured overnight. The expression of analyzed target genes, however, remained unchanged (Figure 11).

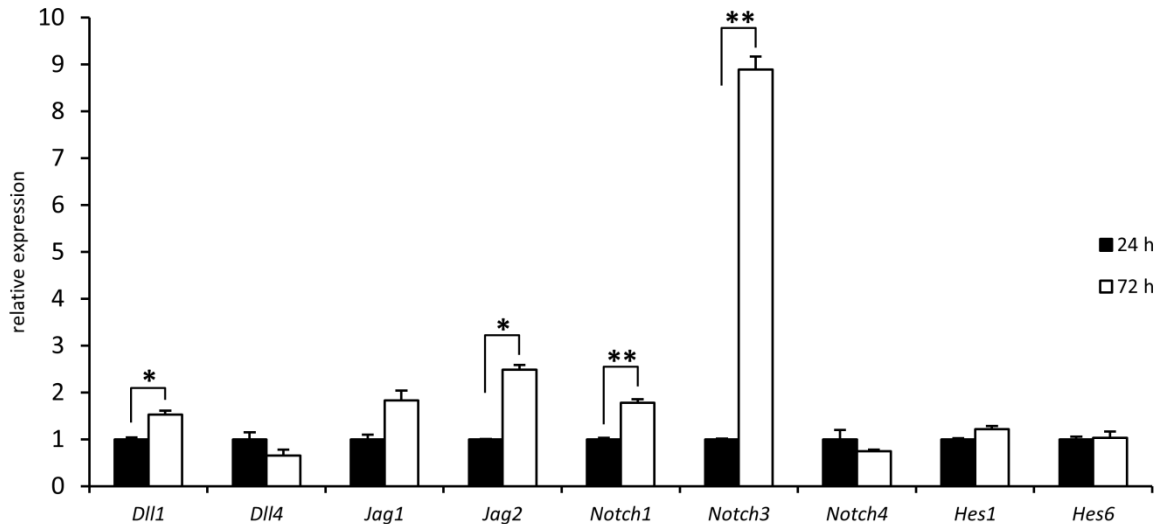


**Figure 11. Time-dependent regulation of Notch signaling genes in isolated primary C3HeB/FeJ islets.**

Islets were isolated from C3HeB/FeJ wild-type mice and cultivated as described (3.2.3.4) for either 24 or 72 hours. The relative mRNA levels of core Notch signaling components were then assessed by qRT-PCR. Expression was normalized to the housekeeping genes *Cyc1* and *Hmbs*. Error bars display the SEM (n=3). Differences were considered statistically significant at  $P < 0.05$  using a heteroscedastic two-tailed Student's t-test (\* $< 0.05$  and \*\* $< 0.01$ ).

#### 4.1.2 Insulinoma-derived cell line INS-1E

To gain additional insights in the role of DLL1 in adult pancreatic  $\beta$ -cells, further experiments were conducted in the insulinoma cell line INS-1E, a widely-used clonal  $\beta$ -cell model<sup>157</sup>.

Firstly, immunohistochemistry was performed to check whether the Notch signaling pathway is active in these cells. This could be confirmed by using an anti-NOTCH1 antibody that specifically recognizes the transcriptionally active intracellular domain NICD (see chapter 2.1.1 for details on NOTCH activation). NICD is present and localized to the nucleus of nearly all analyzed INS-1E cells (Figure 12 A). DLL1 is expressed as well and localized to the cytoplasm (Figure 12 B, C), likely reflecting the endosomal trafficking of the protein (2.1.1).

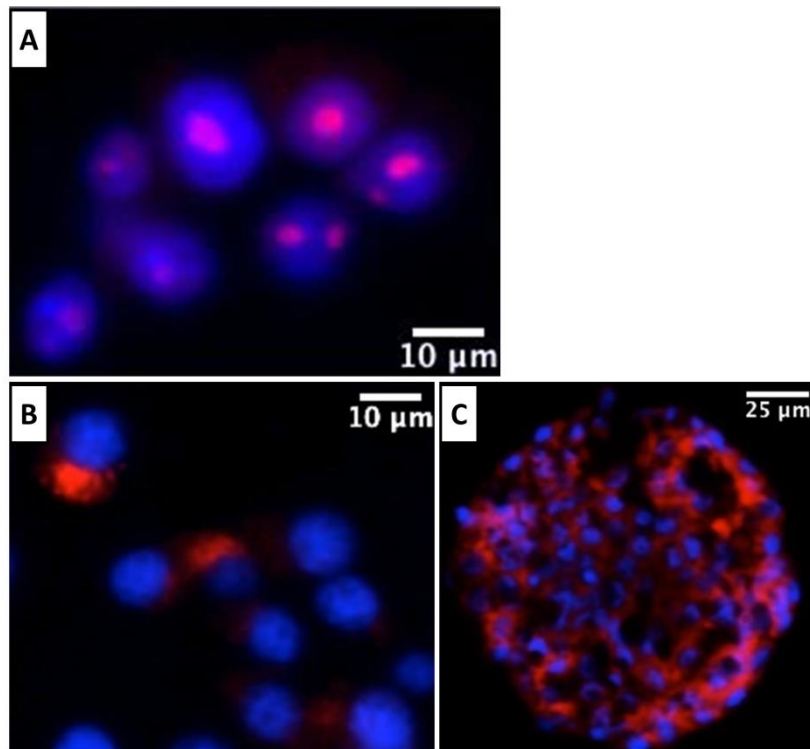


**Figure 12. Notch signaling activity in INS-1E cells.**

Immunohistochemical staining of NICD in INS-1E cells grown in a monolayer (**A**), and of DLL1 in both INS-1E monolayers (**B**) and pseudo-islets (**C**). Nuclei are always counterstained with DAPI.

Depending on the culture conditions, INS-1E cells can be cultivated either as a monolayer or as a collection of spheroid clusters comprising >1000 cells, commonly referred to as pseudo-islets. They closely resemble the shape of islets of Langerhans, despite being formed exclusively by  $\beta$ -cells<sup>157</sup>. Given that pseudo-islets display an improved functional responsiveness to glucose and secretagogues compared to the monolayer<sup>157</sup>, the relative expression of Delta/Notch pathway components was compared between these two states (Figure 13). While the expression of *Notch1* and its target *Hes1* is unchanged, the enhanced cell-cell contacts in pseudo-islets significantly affect the mRNA copy numbers of both *Dll1* and *Ins2*, which encodes for the insulin hormone.

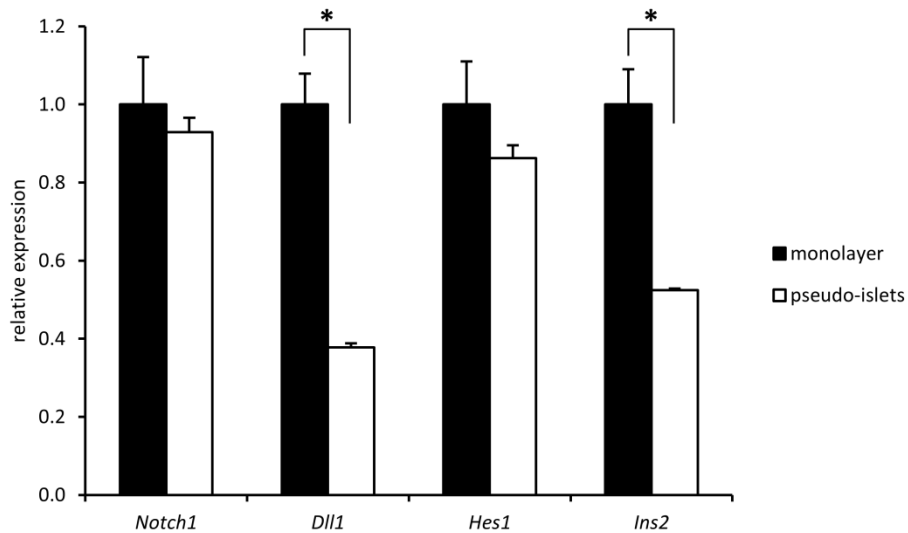


**Figure 13. qRT-PCR analysis of INS-1E cells grown in monolayers and as pseudo-islets.**

Relative expression levels of *Notch1*, *Dll1*, *Hes1*, and *Ins2*, assessed by qRT-PCR (n=3). Expression was normalized to the housekeeping genes *Sdha*, *Ppia*, and *Hprt*. Differences were considered statistically significant at  $P < 0.05$  using a heteroscedastic two-tailed Student's t-test ( $* < 0.05$ ). Error bars display the SEM.

Similarly, expression of *Ins2*, *Notch1*, *Dll1*, and *Hes1* was analyzed in INS-1E cells cultivated for 24 hours with Exendin-4 (Ex4) in varying concentrations. Exendin-4 is a GLP-1 agonist with important functions in  $\beta$ -cell biology (see chapter 2.2.2.2 for details) that has been shown by others to blunt *Ins2* expression in similar experiments<sup>158</sup>. Accordingly, both 5mM and 10 mM Exendin-4 were sufficient to induce a reduction of *Ins2* mRNA of about 40%. Interestingly, *Dll1* and *Hes1* exhibited an almost identical downregulation, whereas *Notch1* expression was not affected.

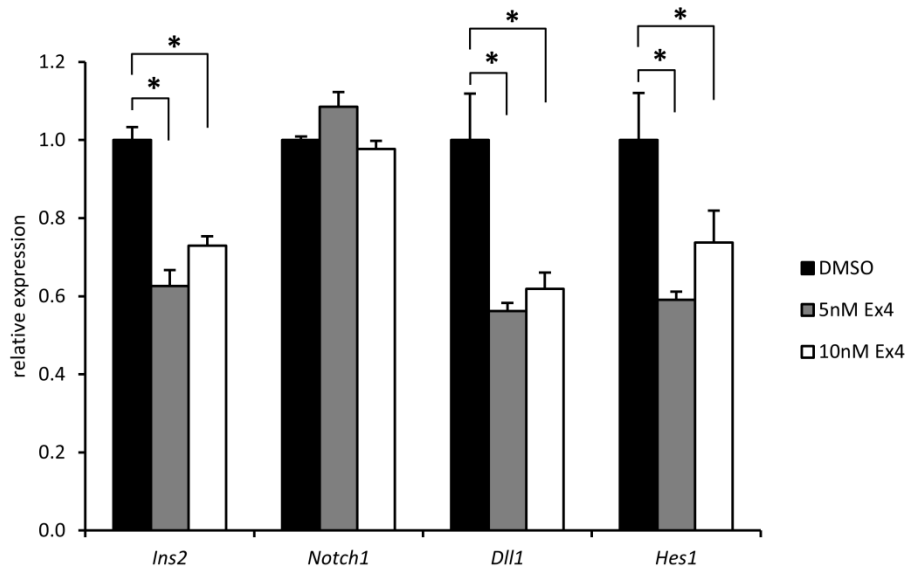


**Figure 14. qRT-PCR analysis of INS-1E cells incubated with the GLP-1 agonist Exendin-4 (Ex4).**

INS-1E monolayers were cultivated for 24 hours in medium supplemented with Exendin-4 in the specified concentrations. Relative expression levels of *Ins2*, *Notch1*, *Dll1*, and *Hes1* were assessed by qRT-PCR (n=3). Expression was normalized to the housekeeping genes *Sdha* and *Hprt*. Differences were considered statistically significant at  $P < 0.05$  using a heteroscedastic two-tailed Student's t-test ( $* < 0.05$ ). Error bars display the SEM.

Taken together, these results show that Notch signaling is active in INS-1E cells, and that both cell-cell contacts and Exendin-4 incubation regulate *Dll1* expression in a way almost identical to *Ins2* regulation.

In order to investigate its function in the INS-1E cell line more in depth, murine DLL1 was transiently overexpressed, either in its full length, wild-type form or without the intracellular PDZ-binding domain ATEV (*Dll1* $\Delta$ ATEV), which is known to mediate Notch-independent functions of DLL1 in other cell lines (see chapter 2.1.2). The corresponding experiments were performed by Benjamin Moritz as part of a master thesis that was planned and supervised within the framework of this PhD work. The expression vectors constructed and used for this purpose are summarized in Table 2.

Vector Name	Description
pDest26-Dll1-His	expression of his-tagged, full length DLL1
PDest26-Dll1 $\Delta$ ATEV	expression of his-tagged DLL1 without the intracellular PDZ-binding motif ATEV
pcDNA6.2-Dll1-EmGFP	co-cistronic expression of full length DLL1 and EmGFP
pcDNA6.2-Dll1 $\Delta$ ATEV-EmGFP	co-cistronic expression of DLL1 without the intracellular PDZ-binding motif ATEV and EmGFP
pDest26	pDest control vector
pcDNA6.2-EmGFP	EmGFP control vector

**Table 2. Dll1 overexpression constructs.**

Successful overexpression of DLL1 and DLL1 $\Delta$ A $\Delta$ EV was conformed by western blotting (Figure 15 A, B) and qRT-PCR (Figure 15 C). For all tested constructs, both full length DLL1 and the DLL1 extracellular and transmembrane domain (which is formed by ADAM-mediated proteolysis of DLL1, see chapter 2.1.2 for details) could be detected (Figure 15 A, B). This provides conclusive proof that, in addition to NICD, the DLL1 intracellular domain (DICD) is produced in pancreatic  $\beta$ -cells as well, an additional hint of Notch pathway activity in this context. Endogenous DLL1, on the other hand, could not be detected in protein lysates from INS-1E cells transfected with controls vector, likely a technical problem since endogenous expression had been confirmed both by immunohistochemistry and qRT-PCR (Figure 12 and Figure 13).

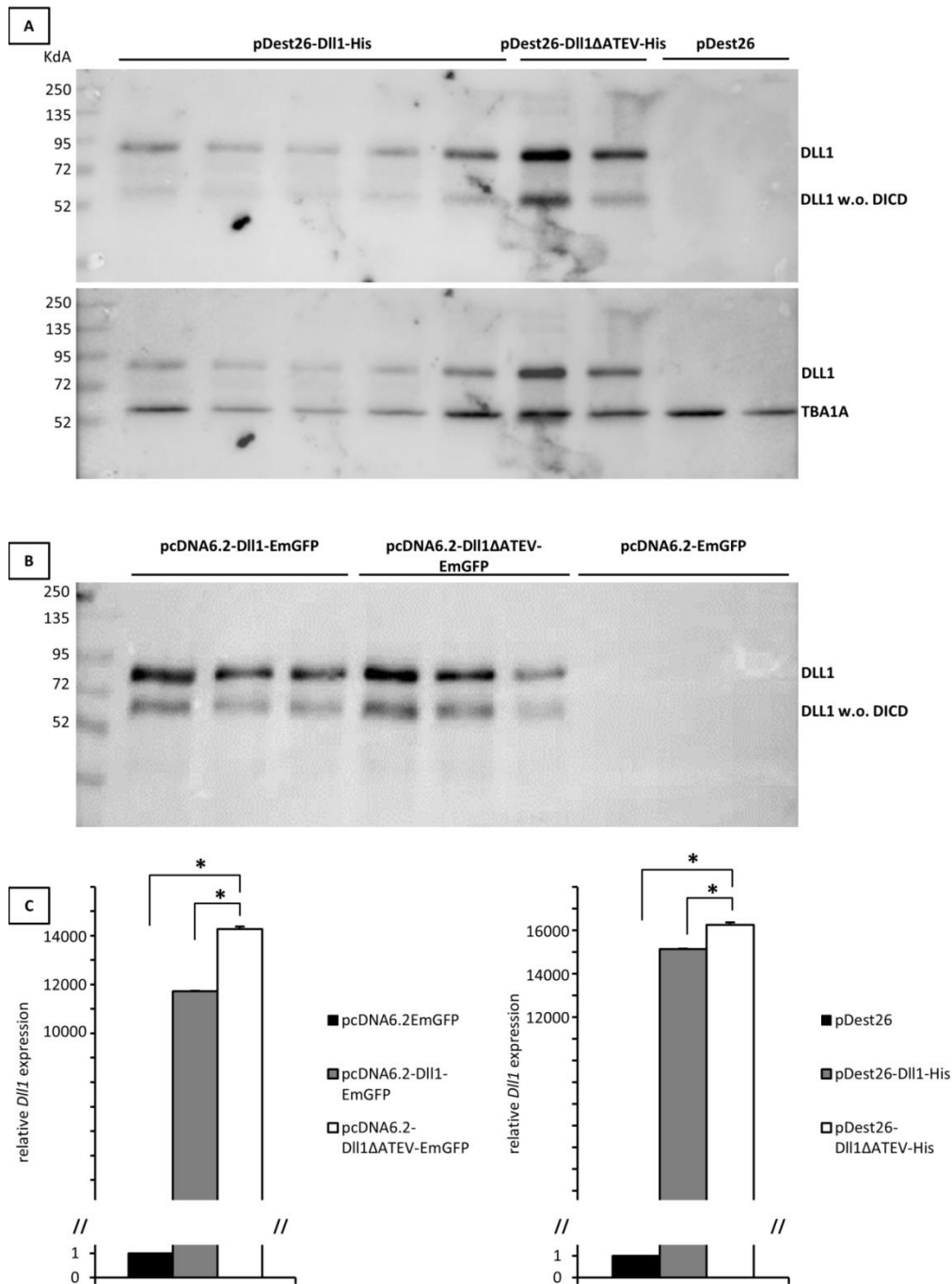


**Figure 15. DLL1 overexpression in INS-1E cells.**

**(A)** Western blot of DLL1 with INS-1E cell lysates after transient transfection with pDest-Dll1-His, pDest-Dll1ΔATEV-His, and pDest, using either the LS-C150273 anti-DLL1 antibody (LsBio) that detects both full length DLL1 and ADAM-digested DLL1 (top), or the DLL1-H265 antibody that only recognizes transmembrane DLL1 to allow for the concurrent detection of TBA1A1 (bottom). **(B)** Western blot of DLL1 with INS-1E cell lysates after transient transfection with pcDNA6.2-Dll1-EmGFP, pcDNA6.2-Dll1ΔATEV-EmGFP, and pcDNA6.2-EmGFP, using the LS-C150273 anti-DLL1 antibody (LsBio). In both **(A)** and **(B)**, every lane represent an independent transfection experiment. Both anti-DLL1 antibodies used are fully cross-reactive against rat DLL1, but the endogenous protein could nonetheless not be detected. **(C)** Relative expression of murine *Dll1* in INS-1E cells transiently transfected with the specified vectors, as measured by qRT-PCR (n=3). Expression was normalized to the housekeeping genes *B2m* and *Ppia*. Differences were considered statistically significant at  $P < 0.05$  using a heteroscedastic two-tailed Student's t-test ( $* < 0.05$ ). Error bars display the SEM.

INS-1E cells transiently overexpressing DLL1 were subjected to an *in vitro* glucose-stimulated insulin secretion (GSIS) test. Insulin secretion was unperturbed at both low and high glucose concentrations, suggesting that DLL1 is involved in neither glucose sensing nor the insulin secretory machinery (Figure 16).

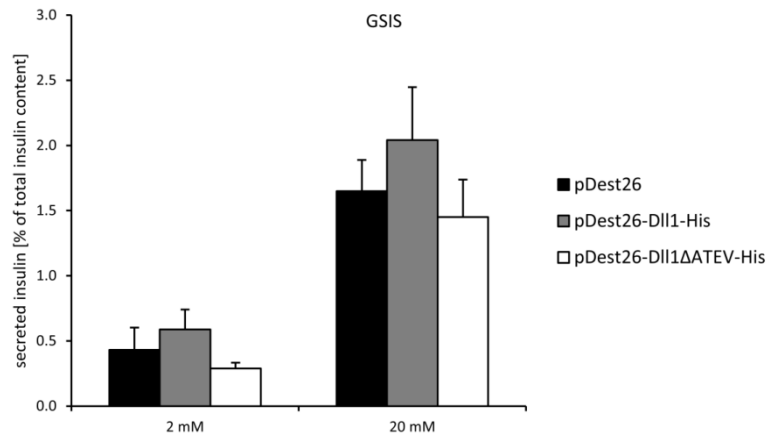


**Figure 16. *In vitro* GSIS in INS-1E cells transiently overexpressing DLL1 and DLL1ΔATEV.**

Secreted insulin of INS-1E cells transiently transfected with the specified vectors at 2 and 20 mM medium glucose, expressed as the percentage of total insulin content ( $n=3$ ). Samples were measured by ELISA. Error bars represent SEM values. Transfection with the EmGFP-based constructs led to very similar results (data not shown).

The complementary approach to the data presented above, namely the silencing of endogenous *Dll1* expression in INS-1E cells, was planned as an additional master thesis performed by Michael Sterr. Unfortunately, efficient *Dll1* knockdown could not be achieved. Summarizing, results presented here with both primary islets and the clonal  $\beta$ -line INS-1E suggest that the Delta/Notch pathway is active in adult  $\beta$ -cells, but exclude its implication in glucose-stimulated insulin secretion.

## 4.2 The Dll1-βKO

### 4.2.1 Conditional deletion of *Dll1* in adult pancreatic β-cells

Inducible, β-cell specific *Dll1* deletion was pursued by breeding the STOCK Tg(Ins2-cre/ERT)1Dam/J mouse line, which expresses a tamoxifen-inducible Cre recombinase under control of the *Ins2* promoter, with the *Dll1*<tm1Mjo> line, that contains two loxP sites in the *Dll1* locus<sup>137,138</sup>. The resulting *Cre*<sup>+</sup> *Dll1*<sup>fl/fl</sup> mice are hereinafter named Dll1-βKO.

Effectiveness and specificity of *Dll1* deletion was analyzed on islets isolated from Dll1-βKO mice and littermate controls. The Cre recombinase was activated by feeding the mice for four weeks with tamoxifen-containing chowder. Successful recombination leads to the excision of exons 3 and 4 from the *Dll1* gene and the generation of a stop codon that terminates transcription, and was examined by performing PCR on islet genomic DNA (gDNA) with primers designed to bind in the introns 2-3 and 4-5. This strategy yields two different PCR products depending on recombination: a longer product (2100 bp) in case of an intact locus and a shortened, recombination-dependent product (360 bp) (see Figure 17).

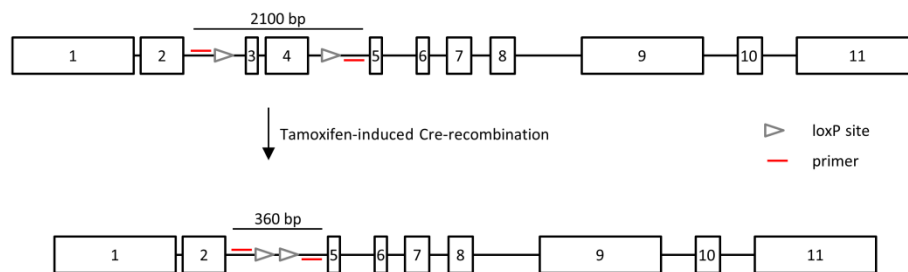


**Figure 17. Schematic representation of the *Dll1* locus and its recombination in β-cells of the Dll1-βKO mouse.** Upon activation of the Cre recombinase with tamoxifen, exon 3 and 4 are excised and a novel termination codon is generated. By designing specific primers in the intronic regions 2-3 and 4-5, the intact and recombined alleles can be distinguished by PCR.

The recombination-specific PCR product could only be produced with islet gDNA from Dll1-βKO mice (Figure 18 A), and was undetectable with spleen gDNA from the same animals and islet gDNA from both *Cre*<sup>-</sup> *Dll1*<sup>fl/fl</sup> (hereinafter named CreN for Cre-negative) and *Cre*<sup>+</sup> *Dll1*<sup>wt/wt</sup> (hereinafter CreY) controls, proving both Cre-dependency and tissue specificity of the deletion (Figure 18 A, B). The PCR product indicative of an intact locus was always present regardless of recombination; this was expected, considering that the gDNA was

isolated from whole islets that represent a mixture of different cell types, whereas the Ins2-cre/ERT transgene is only active in insulin-expressing  $\beta$ -cells.

Surprisingly, recombination could also be detected in islet gDNA from DII1- $\beta$ KO mice that did not receive any tamoxifen-containing chowder, suggesting that the Cre-recombinase is at least in part tamoxifen-independent (Figure 18 B).

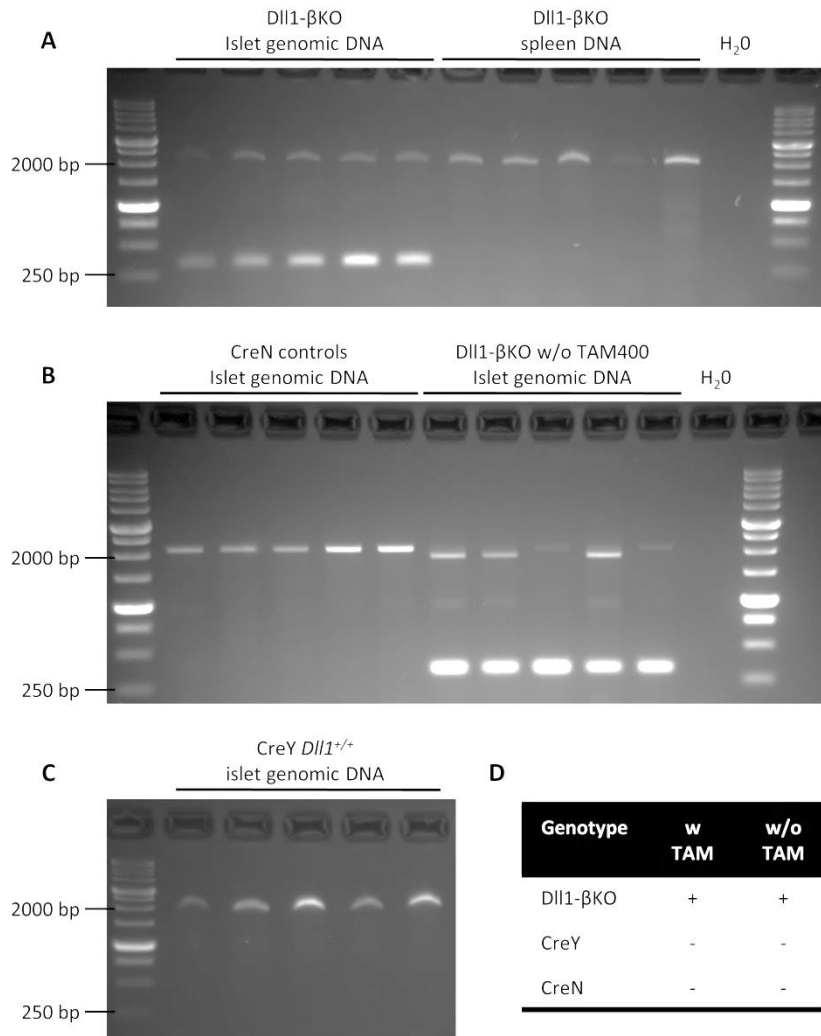


**Figure 18. Analysis of recombination in the *DII1* locus by PCR on genomic DNA.**

(A) The recombination-specific PCR product was clearly detectable with islet gDNA but not with spleen gDNA from the same DII1- $\beta$ KO mice, proving that recombination is islet-specific. Recombination is absent in CreN (B, left) and CreY controls (C) but could be detected with islet gDNA from DII1- $\beta$ KO that did not receive tamoxifen (TAM) (B, right). (D) Summary of recombination events in the analyzed genotypes. Recombination (+) takes place only in DII1- $\beta$ KO islets, but does so even in the absence of tamoxifen. All PCR reactions shown here were performed in parallel.

Downregulation of *Dll1* was further analyzed on the mRNA level by qRT-PCR on isolated islets. *Dll1* expression was found to be reduced to 40% in *Dll1*- $\beta$ KO islets compared to CreN and CreY controls. Downregulation was evident both in seven-weeks old animals (immediately after the tamoxifen-induction phase of four weeks) and thirty-seven weeks old mice (Figure 19).

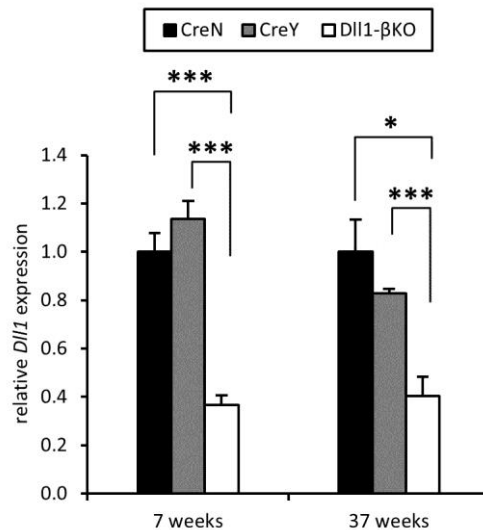


**Figure 19. Downregulation of *Dll1* expression in *Dll1*- $\beta$ KO islets.**

Relative *Dll1* expression in isolated islets from *Dll1*- $\beta$ KO, CreN, and CreY animals, as measured by qRT-PCR (n=5). Expression was normalized to the housekeeping genes *Sdha* and *Fbxw2*. Differences were considered statistically significant at  $P < 0.05$  using a heteroscedastic two-tailed Student's t-test (\* $< 0.05$ , \*\* $< 0.01$ , \*\*\* $< 0.001$ ). Error bars display the standard error of the mean (SEM).

Taken together, analyses on the gDNA and mRNA level found a persistent and specific *Dll1* knockdown in the pancreatic  $\beta$ -cells of the *Dll1*- $\beta$ KO.

#### 4.2.2 Expression analysis of Notch signaling components and targets

To ascertain the effect of *Dll1* downregulation on the Notch pathway as a whole, islets were isolated from 8-weeks old *Dll1*- $\beta$ KO and CreN mice and analyzed by qRT-PCR to assess the expression levels of core Notch signaling components. *Dll4* and *Hey2* were upregulated in *Dll1*- $\beta$ KO islets 1.6- and 1.8-fold, respectively. *Notch1* displayed a significant upregulation as well, but the magnitude of the effect was too small (less than 1.5 fold) to be considered relevant. All other measured ligands, receptors, and direct targets did not show any differential expression (Figure 20 A-C).

In addition to pathway genes,  $\beta$ -cell marker genes *Ins2*, *Pdx1*, *MafA*, *NeuroD1*, and *Nkx6.1* were assayed as well due to the involvement of *DLL1* in  $\beta$ -cell differentiation and

dedifferentiation. Their expression did not vary between Dll1- $\beta$ KO and control islets. The only exception was a slight upregulation of *Ins2* that, while significant, was lower than 1.5 fold (Figure 20 D).

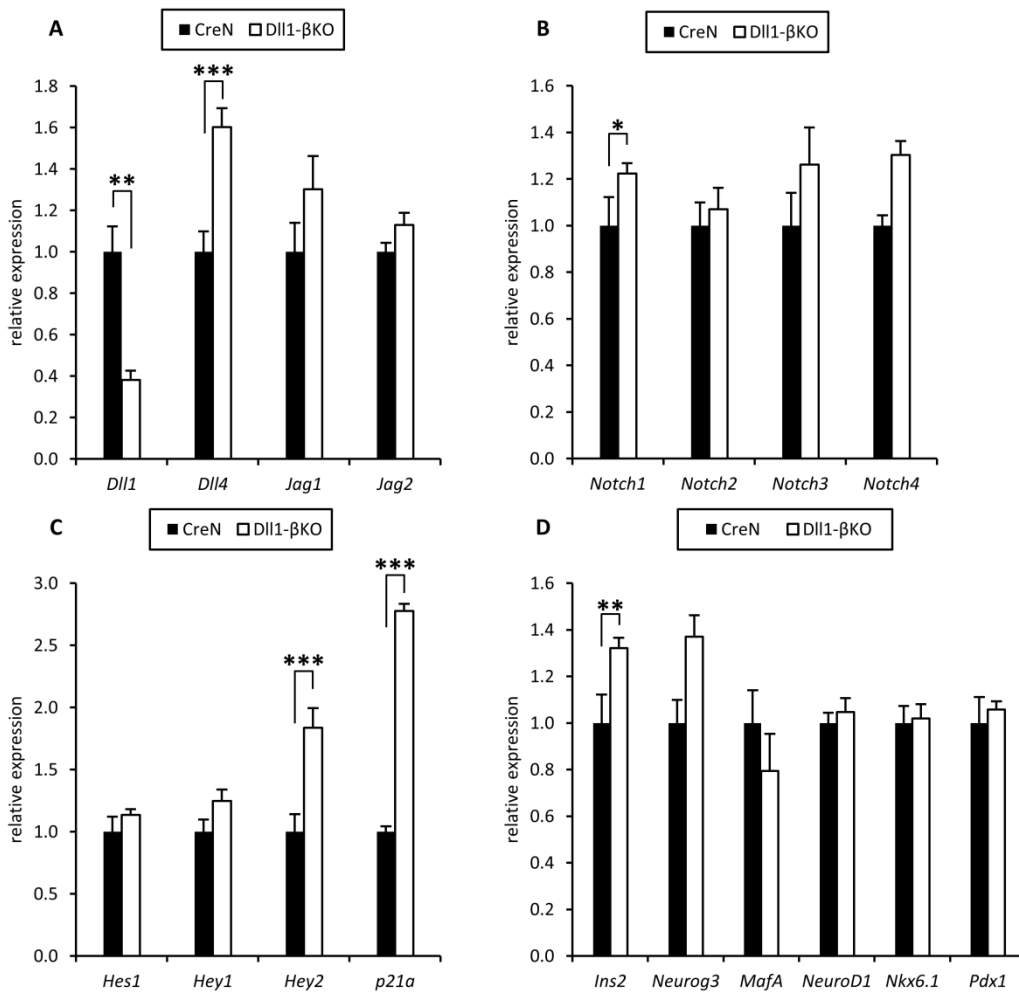


**Figure 20. qRT-PCR analysis of isolated islets from 8-weeks old Dll1- $\beta$ KO and CreN mice.**

Expression levels of DSL ligands (A), Notch receptors (B), selected Notch targets (C) and markers of  $\beta$ -cell phenotype (D) in isolated islets from Dll1- $\beta$ KO and CreN, assessed by qRT-PCR (n=6). Expression was normalized to the housekeeping genes *Sdha* and *Fbxw2*. Differences were considered statistically significant at  $P < 0.05$  using a heteroscedastic two-tailed Student's t-test (\* $< 0.05$ , \*\* $< 0.01$ , \*\*\* $< 0.001$ ). Error bars display the SEM.

Interestingly, the HES1 target *Cdkn1a* (*p21*), an indirect Notch signaling target, was upregulated even though *Hes1* itself was unchanged (Figure 20 C). To investigate whether this differential expression might be *Dll1*-independent, islets were isolated from CreY *Dll1*<sup>+/+</sup> animals and CreN *Dll1*<sup>+/+</sup> littermates. qRT-PCR showed that the upregulation of *p21* was

contingent to both Cre expression and its activation with tamoxifen, providing conclusive proof that its upregulation in *Dll1*- $\beta$ KO islets was an artifact independent of *Dll1* knockdown (Figure 21).

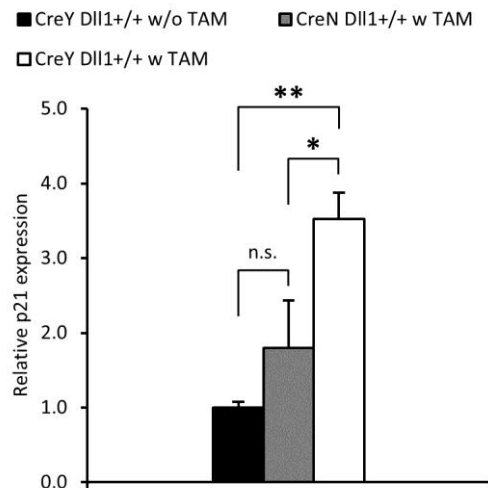


**Figure 21. Relative *p21* expression in islets of 8-weeks old CreY and CreN *Dll1*<sup>+/+</sup> mice.**

Expression levels of *p21* in CreY *Dll1*<sup>+/+</sup> and CreN *Dll1*<sup>+/+</sup> mice, determined by qRT-PCR (n=4). Mice were either fed with tamoxifen-containing chowder for four weeks (w TAM) or not (w/o TAM). Expression was normalized to the housekeeping genes *Sdha* and *Fbxw2*. Differences were considered statistically significant at  $P < 0.05$  using a heteroscedastic two-tailed Student's t-test (\* $< 0.05$ , \*\* $< 0.01$ ). Error bars display the SEM.

In conclusion, qRT-PCR analysis revealed Notch signaling modulations in 8-weeks old *Dll1*- $\beta$ KO islets, specifically upregulation of *Dll4* and *Hey2*, which are consistent with a compensation of the *Dll1* knockdown within the pathway. Furthermore, enhanced expression of *p21* in all *Cre*<sup>+</sup> animals suggests an effect of the Cre recombinase on islet cells.

#### 4.2.3 Islet physiology

Pancreatic and islet physiology was analyzed at 8 and 40 weeks of age by immunofluorescent antibody stainings of insulin and glucagon. For this purpose, the pancreata of 4 mice for each age and genotype were studied by staining 3 different frozen sections, each at least 300  $\mu$ m apart from the others (Figure 22 and Figure 23). Immunohistochemical experiments were performed by student Dennis Bleck as part of a practical internship supervised within the framework of this thesis.

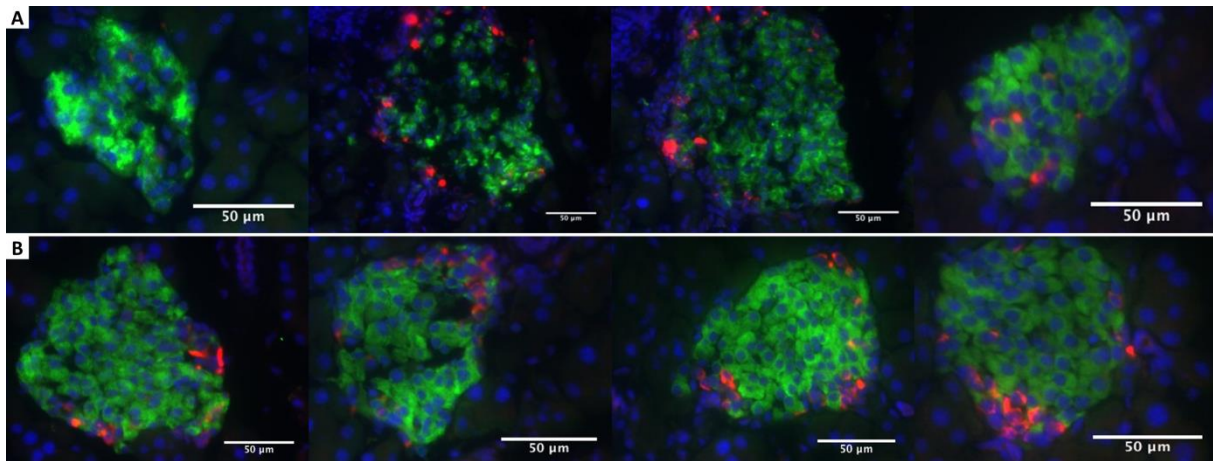


**Figure 22. Immunohistochemical analysis of pancreata in 8-weeks old Dll1- $\beta$ KO and CreN mice.**

Double staining of insulin (green) and glucagon (red) of frozen pancreatic sections from 8-weeks old Dll1- $\beta$ KO (A) and CreN (B) mice (n=4). Nuclei are counterstained with DAPI (blue). Every image presented here originated from a different mouse. In some instances, islets of Dll1- $\beta$ KO animals appeared to have disrupted insulin staining (see for example (A), second and third pictures), but subsequent repetitions could not confirm this finding, which was therefore likely dependent on the quality of the sections.

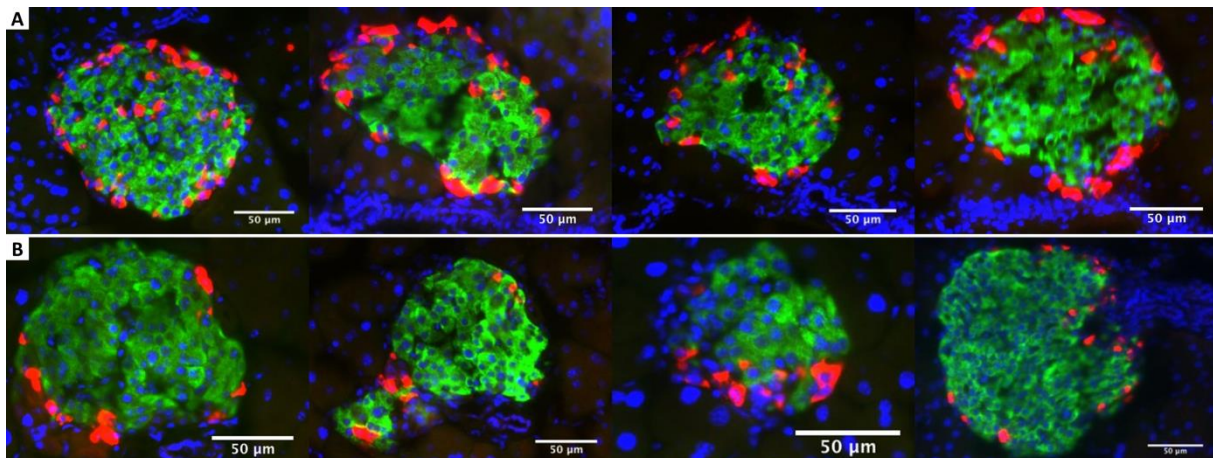


**Figure 23. Immunohistochemical analysis of pancreata in 40-weeks old Dll1- $\beta$ KO and CreN mice.**

Double staining of insulin (green) and glucagon (red) of frozen pancreatic sections from 40-weeks old Dll1- $\beta$ KO (A) and CreN (B) mice (n=4). Nuclei are counterstained with DAPI (blue). Every image displayed here originated from a different mouse.

The general morphology of the pancreas appeared unaltered in qualitative observations of islet distribution and islets size. Moreover, islet physiology, defined by the partitioning of  $\alpha$ - and  $\beta$ -cells, did not reveal any striking structural alterations between Dll1- $\beta$ KO and CreN mice.

Additionally, islet vascularization was analyzed by performing double stainings of insulin and laminin. Again, no differences between Dll1- $\beta$ KO mice and controls could be detected.

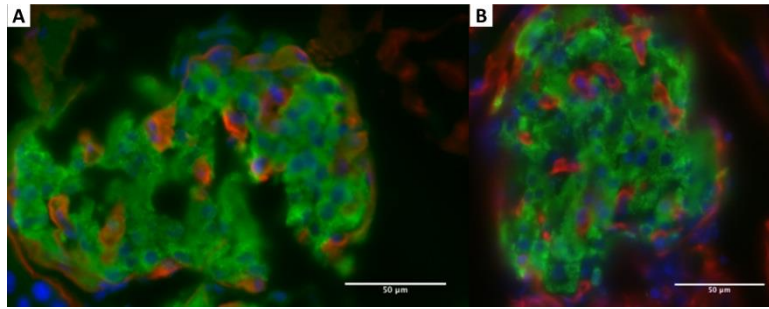


**Figure 24. Immunohistochemical analysis of islet vascularization in 12-weeks old Dll1- $\beta$ KO and CreN mice.** Double staining of insulin (green) and laminin (red) of frozen pancreatic sections from 12 weeks old Dll1  $\beta$ KO (A) and CreN (B) mice (representative images). Nuclei are counterstained with DAPI (blue).

#### 4.2.4 *In vitro* glucose-stimulated insulin secretion (GSIS)

Glucose-stimulated insulin secretion is the central role of  $\beta$ -cells, and was therefore analyzed in Dll1- $\beta$ KO mice. Islets were isolated from 11-weeks old Dll1- $\beta$ KO and CreN animals and tested *in vitro* with regard to insulin release under different glucose concentrations. No functional difference could be detected (Figure 25).

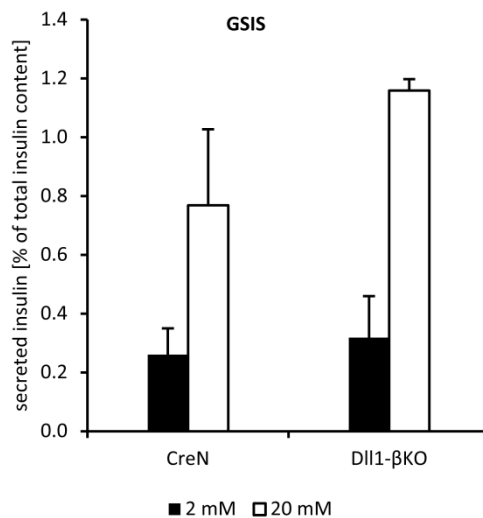


**Figure 25. *In vitro* GSIS in isolated islets from Dll1- $\beta$ KO and CreN mice.** Secreted insulin of Dll1- $\beta$ KO and CreN islets at 2 and 20 mM medium glucose, expressed as the percentage of total insulin content (n=2). Samples were measured by ELISA. Error bars represent SEM values.

#### 4.2.5 Transcriptomics analysis

##### 4.2.5.1 Expression profiling of Dll1- $\beta$ KO islets

To evaluate the effect of *Dll1* downregulation on the gene expression network of  $\beta$ -cells, genome-wide transcriptome analysis was performed with islets isolated from Dll1- $\beta$ KO animals and CreN littermate controls at the age of 37 weeks (n=5). The age of the animals

was selected to allow for possible dysregulations to develop despite the only slight modulation of Notch signaling activity at the age of 8 weeks (see 4.2.2). Data analysis was performed in collaboration with Barbara Fridrich.

105 genes were identified to be differentially regulated with a fold change of more than 2, while 486 genes were significantly regulated with a fold change of more than 1.5, using a false discovery rate (FDR) of <10% (Supplementary Table 1).

Among the Notch signaling genes, the ligand-encoding *Jag1* was upregulated 1.6 fold and the target *Hey1* showed a 2-fold upregulation in Dll1- $\beta$ KO islets. Neither *Dll4* nor *Hey2*, both upregulated in Dll1- $\beta$ KO islets from 8-weeks old animals (see 4.2.2), were significantly different between the two groups in this experiment, possibly due to the difference in age.

Characterization of the data set using the GeneRanker algorithm (Genomatix) revealed a strong overrepresentation of extracellular matrix (ECM) and connective tissue as well as a statistically relevant correlation with fibrosis, a pathological condition characterized by an excessive production of ECM (Supplementary Table 2). Accordingly, several of the most prominently upregulated genes, such as *Bgn*, *Dcn*, *Timp1*, *Tnc* and *, encoded for ECM components or, as in the case of the cytokine *Tgfb1* and the transcription factor *Ctgf*, for proteins known to drive their expression. To test the fibrosis association, qRT-PCR analysis was performed for selected genes on the same samples used for transcriptomics, with the addition of CreY controls not previously included. While the differential regulations between Dll1- $\beta$ KO and CreN islets revealed by the chip assays could be confirmed, they were found to be Cre-dependent and not an effect of *Dll1* downregulation, since expression did not vary between Dll1- $\beta$ KO and CreY samples for all the genes tested (Figure 26).*

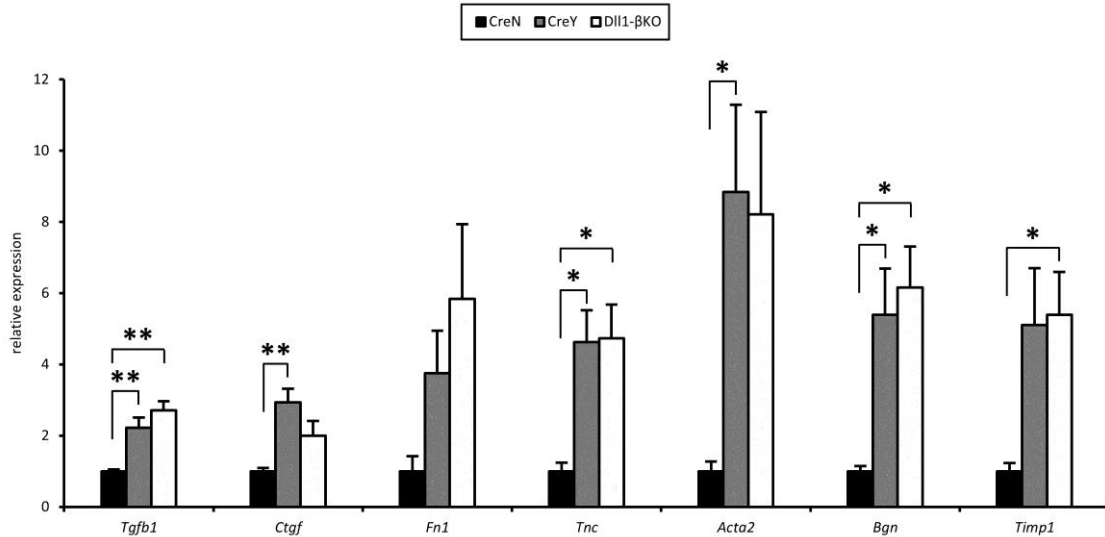


**Figure 26. qRT-PCR analysis of fibrosis-related genes in isolated islets from 37 weeks old mice.**

Expression levels of selected fibrosis-related genes in isolated islets from Dll1-βKO, CreN and CreY animals, assessed by qRT-PCR (n=5). Expression was normalized to the housekeeping genes *Sdha* and *Fbxw2*. Differences were considered statistically significant at  $P < 0.05$  using a heteroscedastic two-tailed Student's t-test (\* $< 0.05$ , \*\* $< 0.01$ ). Error bars display the SEM.

Combined with the findings described in 4.3, these results pointed to two different problems in the experimental setup:

- i. CreY controls should be included in the transcriptomic analysis, since Cre expression might have a large effect on the islet gene expression network, e.g. driving the upregulation of extracellular matrix components and stress-related genes like *Cdkn1a* (4.2.2);
- ii. Levels of acinar cell contamination may lead to unreproducible false positives and should therefore be monitored (see 4.3 for proof).

#### 4.2.5.2 Expression profiling of Dll1-βKO islets with a revised approach

In addition to the inclusion of CreY controls, a strategy was devised to match the purity of islets RNA samples, thereby minimizing the risk of false positives due to exocrine tissue contamination. Islets were isolated from 27-weeks old Dll1-βKO, CreN, and CreY mice (for a total of 30 animals) and samples were analyzed via qRT-PCR with regard to the expression of exocrine genes *Amy2a1* and *Ctrc*. Their relative expression was used as a marker for the amount of exocrine tissue included in the islet preparations. Those samples that showed an above-average amount of *Amy2a1* and *Ctrc* cDNA were discarded, and transcriptomic

analysis was performed only on selected samples with the lowest possible and most comparable levels of exocrine contamination (Figure 27).

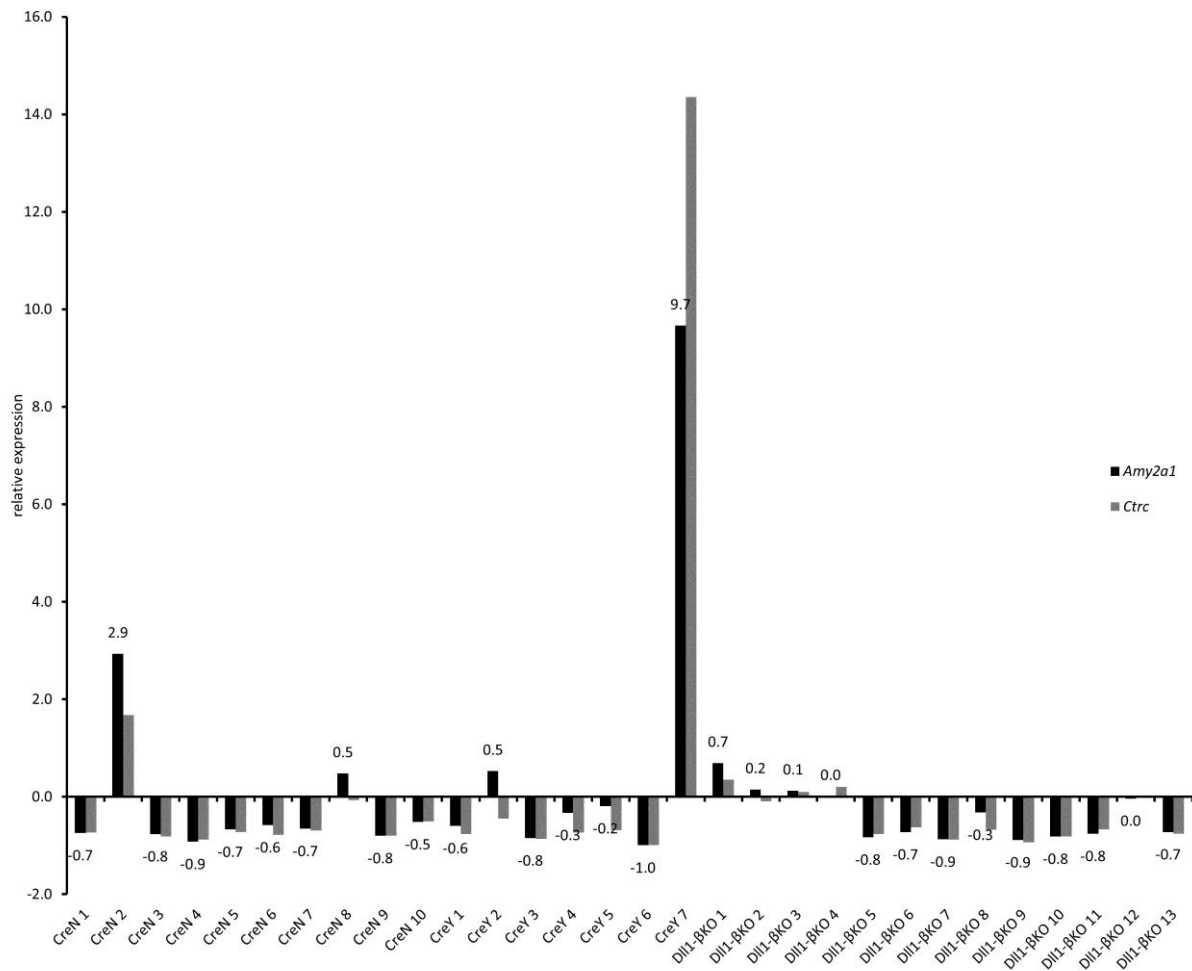


**Figure 27. Pre-selection of Dll1-βKO, CreN, and CreY samples for gene expression profiling.**

Relative expression of exocrine markers *Amy2a1* and *Ctrc* in Dll1-βKO, CreN, and CreY islet preparations, normalized to the housekeeping genes *Sdha* and *Fbxw2*. Expression of these genes is exclusive to acinar cells and was therefore used as an indicator of exocrine tissue contamination. The expression level of *Amy2a1* is indicated. Values were normalized to be distributed around the average of all samples (which is set to zero), meaning that samples showing a positive value had an above-average contamination and were discarded from subsequent experiments. Among the other samples, those with the lowest possible but still comparable amount of contamination were selected for transcriptomic analysis: CreN 1, 3, 5-7 and 9, CreY 1, 3, 4 and 6, and Dll1-βKO 5, 6, 8, 9, 10, 11 and 13.

The second round of expression profiling, executed thusly, resulted in 39 differentially regulated genes with a fold change of more than 2 between Dll1-βKO and CreN islets (FDR <10%), less than half of what had been the case in the first experiment without pre-selection of the samples. Expanding the analysis to include genes significantly regulated with a fold change of 1.5 produced 277 hits (Supplementary Table 3), still a vastly reduced number

compared to the first experiment. As displayed in Figure 28, the difference between the two experimental runs did not only regard the number of regulated genes but, to a great extent, their identity as well: only 157 hits were conserved. This divergence between the two data sets is likely explained by the different strategy pursued: the first run was performed without the aid of purity matching and is therefore liable to contain a larger number of false positives as well as false negatives. The age of the mice was also dissimilar (37-weeks in the first experiment and 27 in the second) and can be expected to partly account for the discrepancy as well.

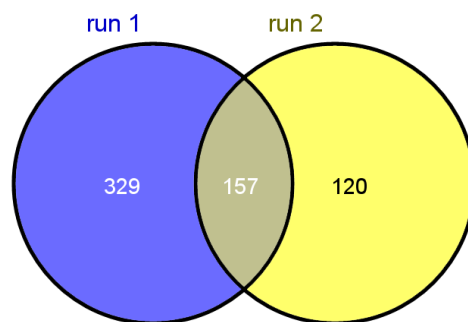


**Figure 28. Regulated genes between *Dll1*- $\beta$ KO and CreN islets in two different experimental runs.**

Crucially, of the 277 genes differentially regulated between *Dll1*- $\beta$ KO and CreN islets, only 16 could be conclusively proven to be dependent on the *Dll1* knockdown, meaning their expression was also regulated between *Dll1*- $\beta$ KO and CreY islets and unchanged between CreY and CreN samples. All other 261 hits were shown to be Cre-dependent, meaning that expression of the Cre recombinase had a vastly greater effect on the global gene expression network of the  $\beta$ -cell than the *Dll1* knockdown, producing approximately 94% of the differentially regulated genes. An indirect confirmation of this finding came from a cluster analysis that grouped the samples in accordance to the normalized intensity of all probe sets included on the chip assays, regardless of their statistical significance between groups. *Dll1*- $\beta$ KO and CreY samples tended, on the whole, to cluster together, underlining the global repercussions of the Cre transgene (Figure 29).

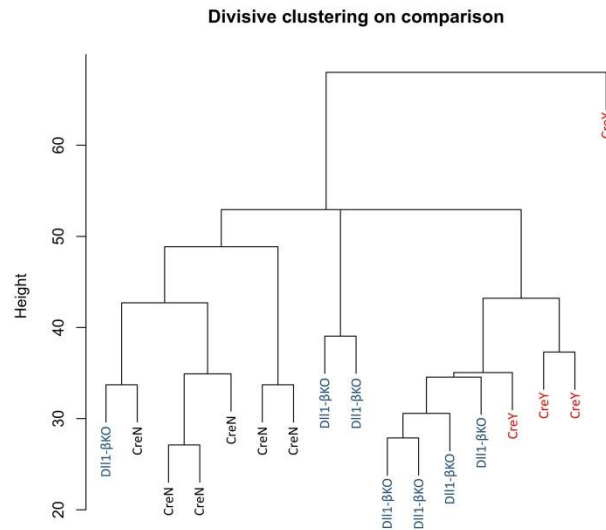


**Figure 29. Cluster analysis of *Dll1*- $\beta$ KO, CreN, and CreY islets samples in the second gene expression profiling experiment.**

An examination of the 261 certified Cre-dependent genes revealed that 144 of them were also regulated in the first transcriptomics experiment, meaning that they account for the majority of the 157 differentially regulated genes that turned up between CreN and *Dll1*- $\beta$ KO in both experimental runs (Figure 28). GeneRanker analysis with these 261 hits again indicated a significant correlation with the ECM, connective tissue, and fibrosis, providing conclusive evidence that this link is unrelated to *Dll1* and the Notch signaling pathway while confirming its validity (Supplementary Table 4). Moreover, even upregulation of *Cdkn1a*, already present in islets of 8-weeks old *Dll1*- $\beta$ KO and CreY mice, but not detectable in the first transcriptomics analysis, was confirmed as an effect of Cre expression. Less expectedly, upregulation of the Notch ligand *Jag1* and the target *Heyl* could be reproduced, but at the same time was proven to be Cre-related as well, meaning that both gene expression profiling assays failed to reveal any differential regulation of direct or indirect Notch signaling components or targets that was attributable to *Dll1*.

The 16 validated *Dll1*-dependent hits are shown in Table 3. 13 of these 16 genes were already found to be differentially regulated in the original chip assay, corroborating their validity. The concomitant upregulation of genes involved in the same pathway, such as *Aldh1a2* and *Aldh1a3*, both encoding for enzymes that regulate retinoic acid metabolism, is notable, as is the fact that several of the genes listed here have been described to be

expressed in the pancreatic  $\beta$ -cell. Selected genes were verified by qRT-PCR (Supplementary Figure 1).

Gene symbol	Gene name	Dll1- $\beta$ KO vs CreN	Dll1- $\beta$ KO vs CreY	regulated in both experiments
<b><i>Ptgs2</i></b>	Prostaglandin-endoperoxide synthase 2	2.6	2.3	y
<b><i>Spt1</i></b>	Salivary protein 1	2.2	2.0	
<b><i>Aldh1a2</i></b>	Aldehyde dehydrogenase family 1, subfamily A2	2.1	1.7	y
<b><i>Sfrp1</i></b>	Secreted frizzled-related protein 1	2.0	1.8	y
<b><i>H2-Aa</i></b>	Histocompatibility 2, class II antigen A, alpha	2.0	1.6	y
<b><i>Ly6a</i></b>	Lymphocyte antigen 6 complex, locus A	1.9	1.5	y
<b><i>Penk</i></b>	Preproenkephalin	1.8	1.4	y
<b><i>Gatm</i></b>	Glycine amidinotransferase (L-arginine:glycine amidinotransferase)	1.8	1.5	y
<b><i>Lum</i></b>	Lumican	1.8	1.4	y
<b><i>Pigr</i></b>	Polymeric immunoglobulin receptor	1.7	1.8	y
<b><i>Pros1</i></b>	Protein S (alpha)	1.7	1.8	y
<b><i>4930539E08Rik</i></b>	RIKEN cDNA 4930539E08 gene	1.7	1.5	y
<b><i>Wfdc17</i></b>	WAP four-disulfide core domain 17	1.6	1.8	y
<b><i>Aldh1a3</i></b>	Aldehyde dehydrogenase family 1, subfamily A3	1.6	1.7	y
<b><i>Syt13</i></b>	Synaptotagmin-like 3	-1.6	-2.5	
<b><i>Chi311</i></b>	Chitinase 3-like 1	-3.3	-1.6	

**Table 3. *Dll1*-dependent differentially regulated genes.**

The expression of *Ptgs2* was also analyzed in INS-1E cells incubated with N-[N-(3,5-Difluorophenacetyl)-L-alanyl]-S-phenylglycine t-butyl ester (DAPT), a strong inhibitor of  $\gamma$ -secretase and therefore Notch signaling<sup>159</sup> (see chapter 2.1.1). Despite efficient inhibition (as assessed by immunohistochemical staining of NICD, data not shown), no effect on *Ptgs2* expression was evident (Figure 30), possibly suggesting that the *Ptgs2* regulation in Dll1- $\beta$ KO islets is NOTCH-independent.

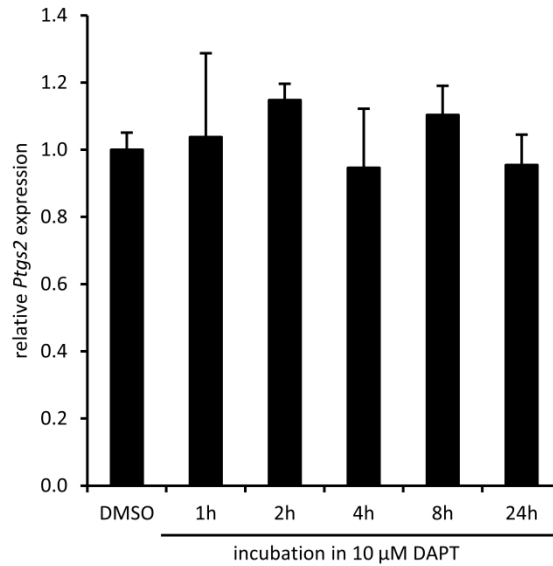


**Figure 30. *Ptgs2* expression in INS-1E cells incubated with DAPT.**

Relative expression of *Ptgs2* in INS-1E cells incubated in 10  $\mu$ M DAPT for the specified time, as assessed by qRT-PCR (n=3). Expression was normalized to the housekeeping genes *Gapdh* and *Sdha*. Error bars display the SEM.

Taken together, these results show that *Dll1* knockdown has a small but reproducible effect on the gene expression network of aged  $\beta$ -cells. At the same time, the data presented here underscores the importance of both purity matching in gene expression analyses of isolated islets and describes the effects of the Cre recombinase on pancreatic  $\beta$ -cells.

#### **4.2.6 Metabolic phenotyping**

Metabolic phenotyping of both male and female *Dll1*- $\beta$ KO animals was performed in parallel to both CreN and CreY controls in order to assess the effect of the *Dll1* knockdown *in vivo*. Immediately after the tamoxifen-induction period of four weeks, mice were characterized regarding weight, fasted blood glucose levels, plasma insulin levels, and body composition. Animals of each genotype and sex were then divided in two groups, one receiving a standard chow and the other receiving an experimental high fat diet in order to test if the *Dll1* knockdown had an effect on the ability of  $\beta$ -cells to react to a situation of increased physiological demand. Metabolic parameters of all animals were monitored regularly (Figure 31).

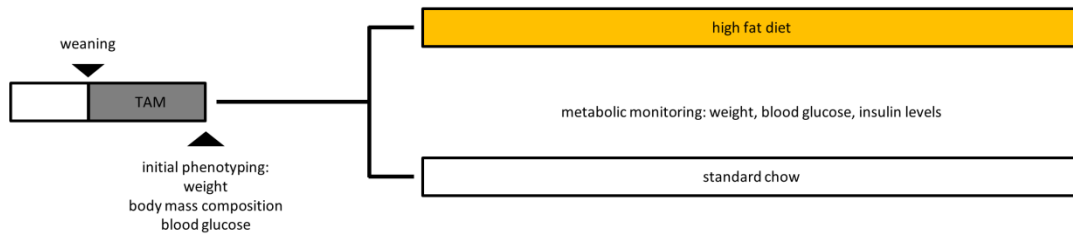


**Figure 31. Strategy for the metabolic phenotyping of the *Dll1*- $\beta$ KO.**

Body composition was measured with nuclear magnetic resonance (NMR) at the start of the experiment by Dr. Jan Rozman. As displayed in Figure 32, both fat and lean mass were unchanged between *Dll1*- $\beta$ KO and controls in both sexes. Even plotting the fat mass or the lean mass against the total weight for each individual animal did not reveal any altered distribution between the genotypes (Supplementary Figure 2), supporting the conclusion that the  $\beta$ -cell specific knockdown of *Dll1* had no effect on body composition at this age.

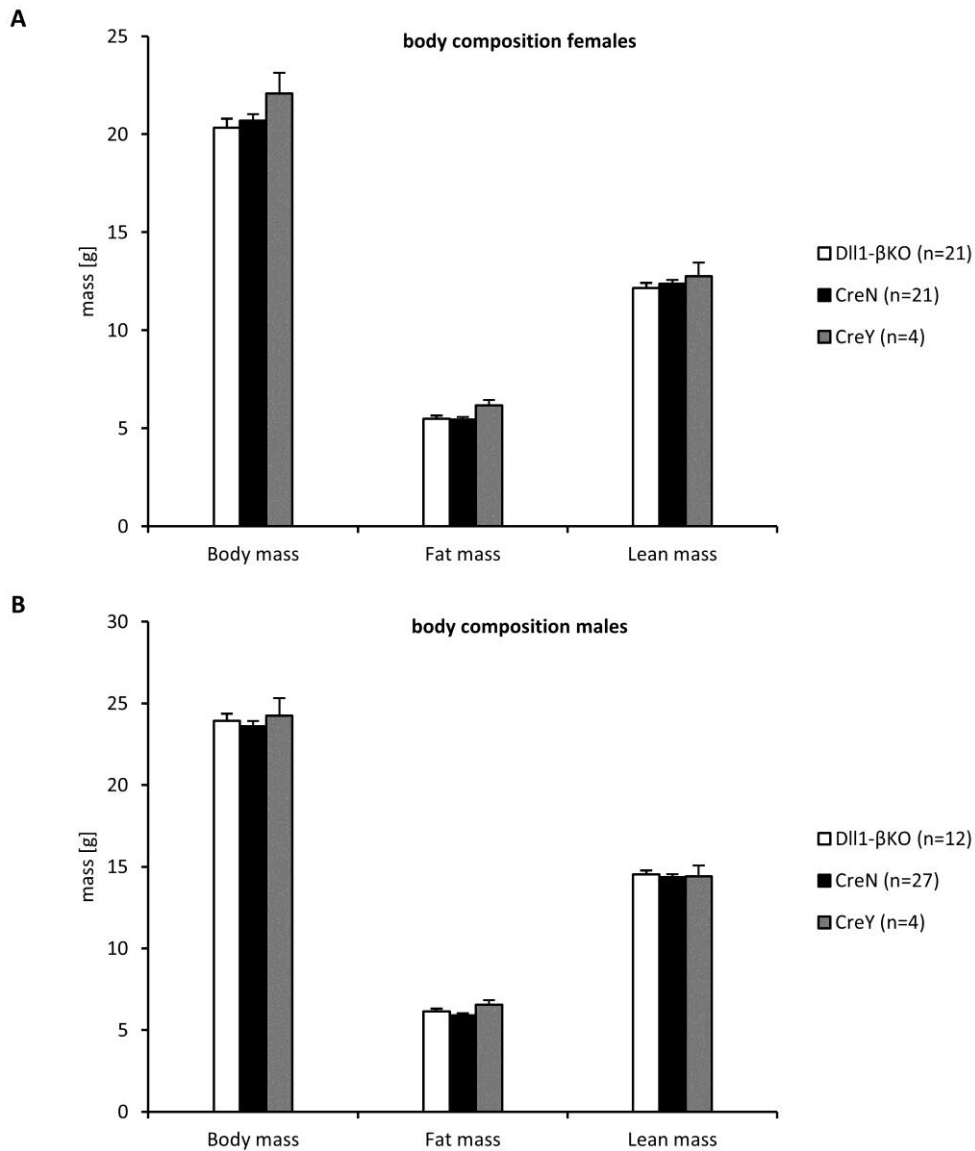


**Figure 32. Weight and body composition of 10-weeks old Dll1-βKO, CreN, and CreY mice at the onset of the experiment.**

Mice were weighed, fat and lean mass were determined with nuclear magnetic resonance (NMR). Error bars display the SEM.

Dll1-βKO and CreN mice were then divided in two diet groups (see Table 4), whereas all available CreY animals were assigned to a high fat diet due to their limited number.

females	high fat diet	standard diet	males	high fat diet	standard diet
Dll1-βKO	10	11	Dll1-βKO	6	6
CreN	12	9	CreN	15	12
CreY	4		CreY	4	

**Table 4. Number of animals involved in metabolic phenotyping by genotype, sex and diet.**

Figure 33 illustrates the weight development of the mice over the course of the experiment. No significant differences between genotypes are evident in both males and females, neither on the standard nor on the high fat diet. A slightly increased weight of *Dll1*- $\beta$ KO males compared to CreN controls on the standard chow was observed. However, this difference of approximately 4 grams, which first manifested after ten weeks of the experiment and remained stable thereafter, was statistically non-significant at all time points. A closer analysis of the weight of each individual mouse for both genotypes at the end of the experiment after 24 weeks (Supplementary Figure 3) further substantiates the null hypothesis of no real discrepancy in weight. Collectively, these data show that the *Dll1* knockdown had no consequences on body mass and body composition in both sexes and regardless of diet.

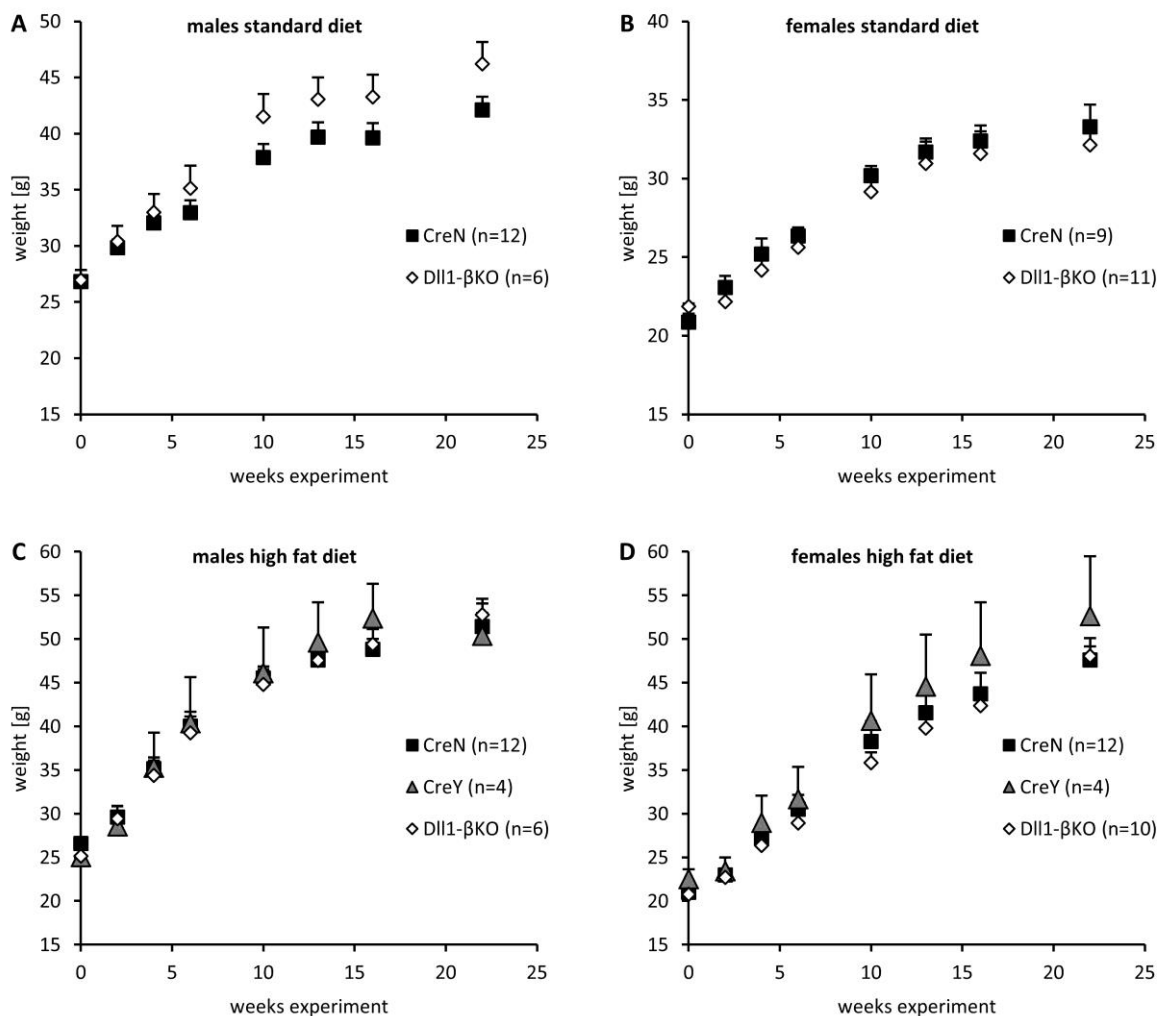


**Figure 33.** Body weight of *Dll1*- $\beta$ KO and control mice over the course of six months.

Dll1- $\beta$ KO, CreN, and CreY mice were fed either a standard chow (A, B) or a high fat diet (C, D) and their weight was measured on a regular basis. No statistically significant difference was found. Error bars represent SEM values.

Concomitantly to the body mass determination, mice were fasted for 6 hours prior to blood glucose measurement and plasma collection for the analysis of insulin levels. Fasted blood glucose levels are displayed in Figure 34. Dll1- $\beta$ KO males on the standard diet exhibited elevated blood glucose compared to CreN controls from the age of 11 weeks onwards, a small but stable and statistically significant elevation of about 30 mg/dl. The average blood glucose level of Dll1- $\beta$ KO males throughout the experiment (age 11-31 weeks) was 148-181 mg/dl, which can already be considered as mild hyperglycemia (Figure 34 A). When fed a high fat diet, the differences between Dll1- $\beta$ KO and CreN animals were always non-significant (Figure 34 C). This was likely explained by the fact that the high fat feeding induced an elevation of fasted blood glucose levels in both CreN and Dll1- $\beta$ KO males compared to the standard diet group of the same genotype, but this elevation was higher for CreN animals throughout the experiment (Figure 35). In females, on the other hand, Dll1- $\beta$ KO and CreN mice always showed comparable blood sugar values in both diet groups (Figure 34 B, D).

Surprisingly, the CreY controls behaved differently than both CreN and Dll1- $\beta$ KO animals. On the high fat diet, CreY animals exhibited distinct hyperglycemia in both males and females, with levels around and above 200 mg/dl, well above those displayed by the other genotypes (Figure 34 C, D).

Taken together, these results again point to a relevant effect of  $\beta$ -cell specific Cre expression. However, due to the lack of CreY animals in the standard diet group, this data cannot conclusively establish if the mild hyperglycemia of Dll1- $\beta$ KO male mice is attributable to the expression of Cre or the *Dll1* knockdown, or both.

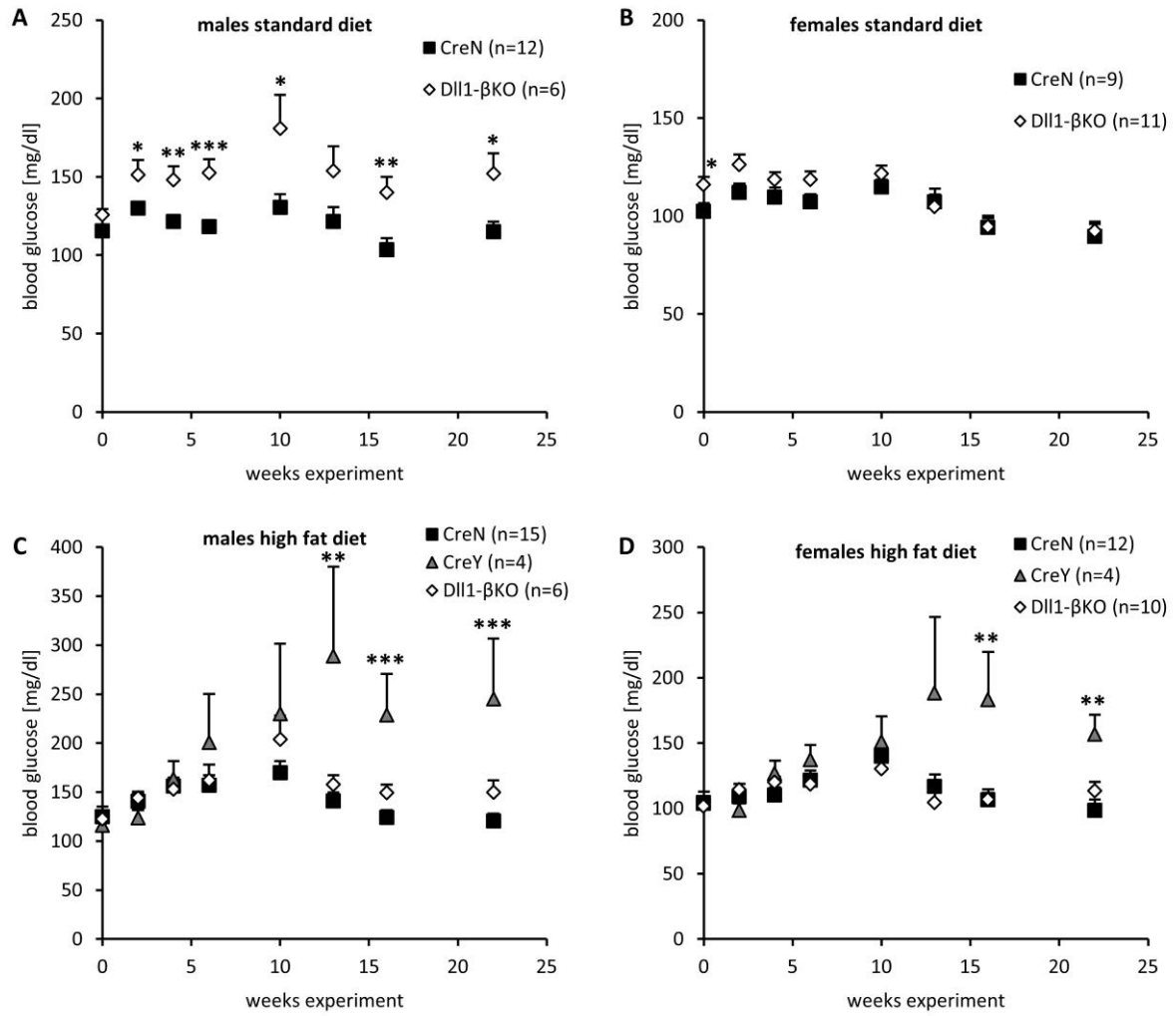


**Figure 34. Fasted blood glucose levels of Dll1-βKO and control mice over the course of six months.**

Dll1-βKO, CreN and CreY mice were fed either a standard chow (A, B) or a high fat diet (C, D) and their blood glucose was measured regularly after 6-hours fasting. Differences were considered statistically significant at  $P < 0.05$  using one way analysis of variance (ANOVA) (\* $< 0.05$ , \*\* $< 0.01$ , \*\*\* $< 0.001$ ). Error bars display SEM values.

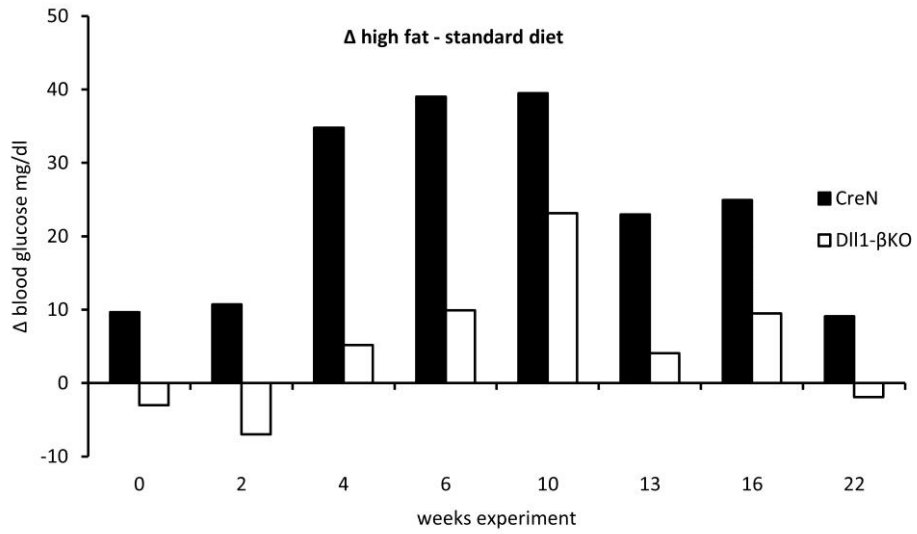


**Figure 35. Blood glucose increase between the high fat and standard diet groups of Dll1-βKO and CreN male mice.**

Despite these differences in blood glucose, plasma insulin levels were similar between Dll1-βKO and controls in both sexes and under all conditions (Figure 36).

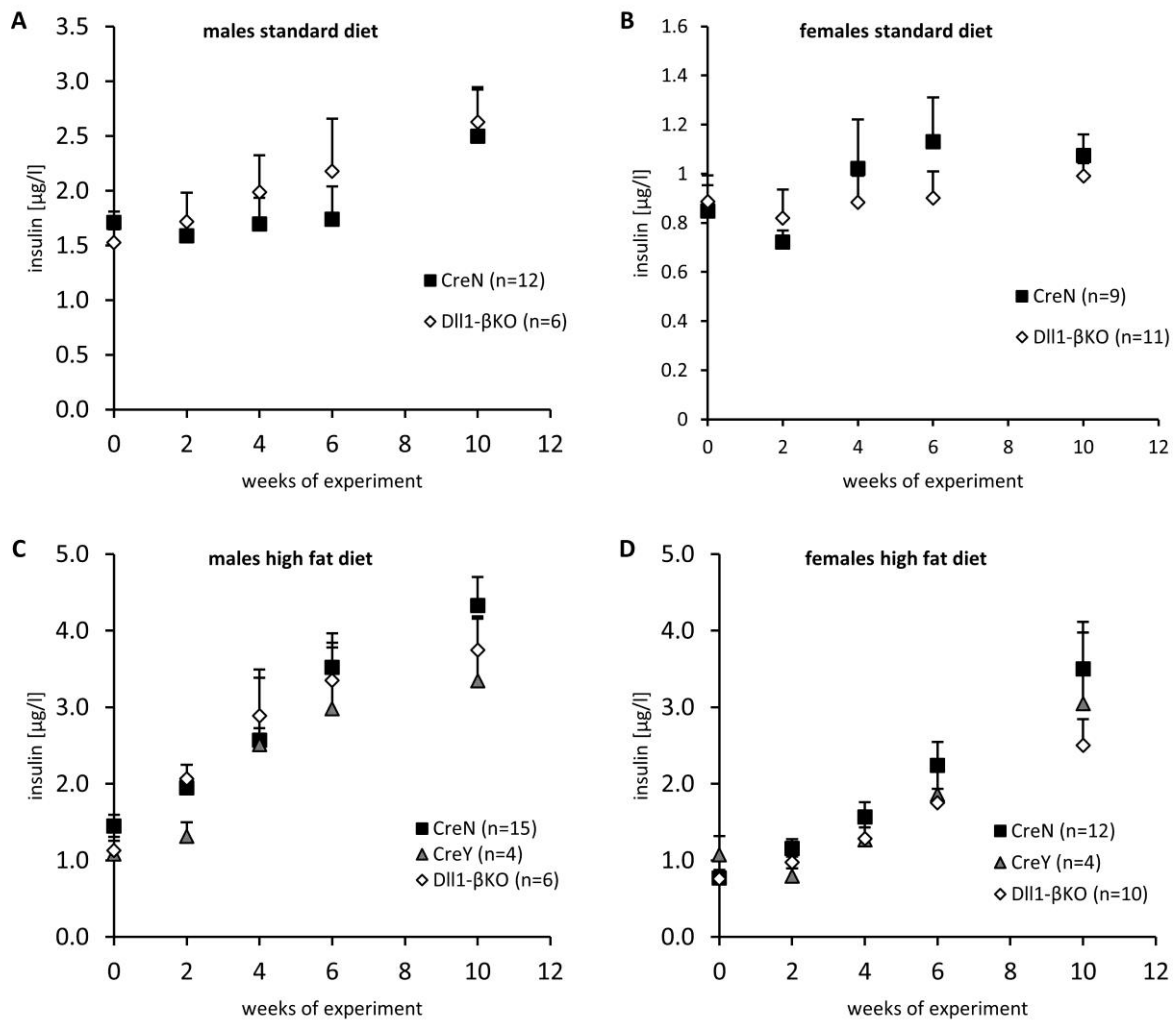


**Figure 36. Plasma insulin levels of Dll1-βKO and control mice.**

Dll1-βKO, CreN, and CreY mice were fed either a standard chow (A, B) or a high fat diet (C, D) and plasma was isolated regularly for ELISA insulin measurements. No statistically significant difference was found. Error bars display SEM values.

Likewise, no differences in either triglycerides or non-esterified fatty acids (NEFAs) levels could be found (Figure 37, measurements performed by Dr. Birgit Rathkolb).

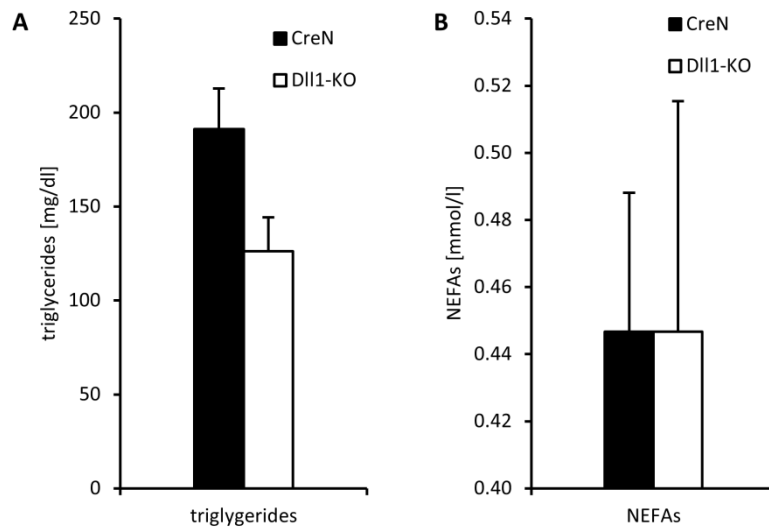


**Figure 37. Plasma levels of triglycerides and NEFAs in 34-weeks old Dll1- $\beta$ KO and CreN mice.**

Error bars display the SEM (n=6). Measurements were performed by Dr. Birgit Rathkolb.

Finally, an intraperitoneal glucose tolerance test was performed on male mice to better analyze  $\beta$ -cell function in the Dll1- $\beta$ KO. All analyzed animals were over 30 weeks of age, and had developed glucose intolerance by this point regardless of diet or genotype, complicating the interpretation of the results (Figure 38). Nevertheless, small statistically significant differences were observed between mice fed a standard diet, with the Dll1- $\beta$ KO animals exhibiting slightly more pronounced glucose intolerance, in accordance to their basal hyperglycemia described above.

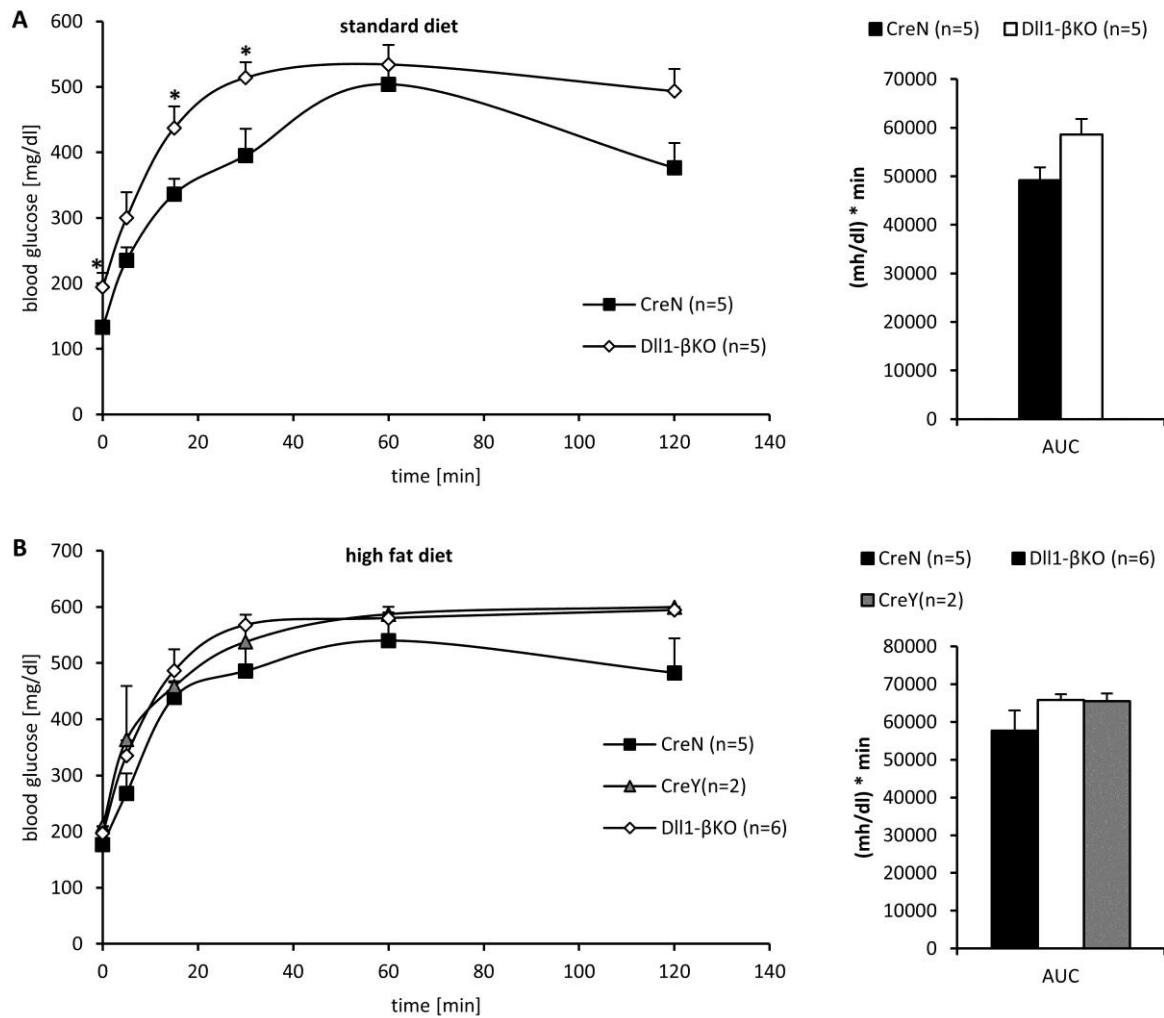


**Figure 38. Intra-peritoneal Glucose-tolerance test (GTT) on Dll1-βKO mice and controls.**

30-weeks old Dll1-βKO, CreN, and CreY mice, fed either a standard (A) or a high fat diet (B), were subjected to an intra-peritoneal GTT. Blood glucose levels over time (left) and the area under the curve (AUC, right) are shown. Statistical significance was measured by ANOVA (\*<0.05). Error bars represent SEM values.

### 4.3 Dll1\_T720A

The Dll1\_T720A line is an ENU-generated mouse line that harbors a point mutation leading to an amino acid exchange in the intracellular domain of DLL1. Given the importance of this domain for Notch signaling (see 2.1.2) and the results presented here showing that DICD is proteolytically released from the membrane-bound, full length DLL1 in  $\beta$ -cells (Figure 15), comparison of the Dll1\_T720A mouse with the Dll1- $\beta$ KO could be an important tool for the generation of mechanistic hypotheses.

Islets isolated from Dll1\_T720A mice and wild-type controls were analyzed by qRT-PCR with regard to the expression of islet markers and  $\beta$ -cell genes. No statistical differences could be ascertained between the two groups. The expression of *Dll1* and the Notch target *Hes1* were unchanged as well (Figure 39).

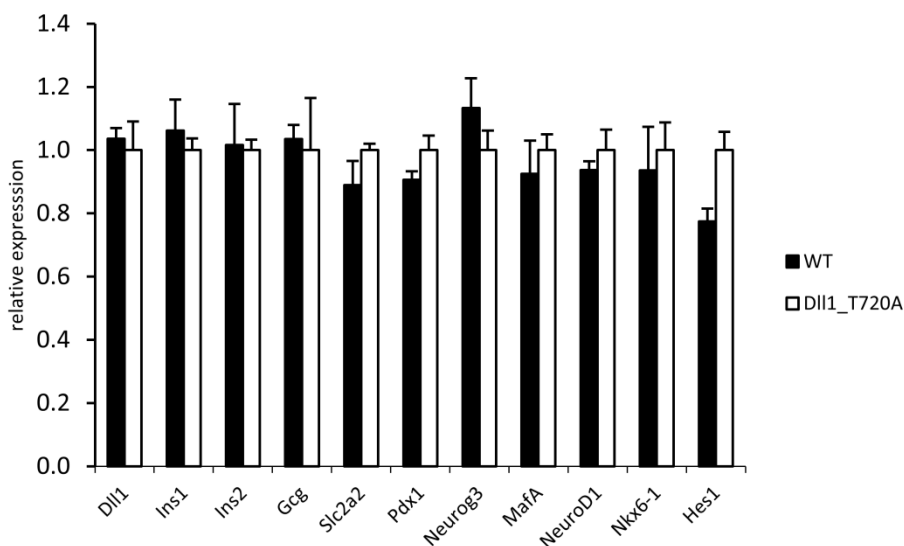


**Figure 39. qRT-PCR analysis of isolated islets from 16-weeks old Dll1\_T720A and wild type mice.**

Expression levels of *Dll1*, *Hes1* and islet genes in isolated islets from Dll1\_T720A and wild-type controls, assessed by qRT-PCR (n=3). Expression levels were normalized to the housekeeping genes *Actb*, *Gapdh*, and *Pgk1*. Error bars display the SEM.

To investigate the effects of the mutation on the islet gene expression program more in depth, islets were isolated from Dll1\_T720A mice and littermate controls aged 16 weeks (n=5) and analyzed with the same genome-wide transcriptome approach used for the Dll1- $\beta$ KO (4.2.5). Chip assay hybridization was performed by Barbara Fridrich, and data analysis was performed in collaboration with Barbara Fridrich and Martin Irmeler.

264 genes were identified to be differentially regulated with a fold change of more than 1.5 and a false discovery rate of <10%. Among the most prominently upregulated genes, however, were known acinar cell markers such as *Amy2a1*, *Cel*, *Cpa1*, and *Ctrc*, all encoding for enzymes secreted from the exocrine pancreas, suggesting that markedly different levels of acinar tissue may have contaminated the islet samples. A closer evaluation of the expression of said markers confirmed this supposition: in the case of *Amy2a1*, for example, even the wild-type sample with the highest relative expression exhibited a lower cDNA amount than almost every single Dll1\_T720A sample (Figure 40). Statistical significance of the upregulation was then inescapable, but simply reflected a random problem with the islet isolation technique and not an effect of the point mutation under study.

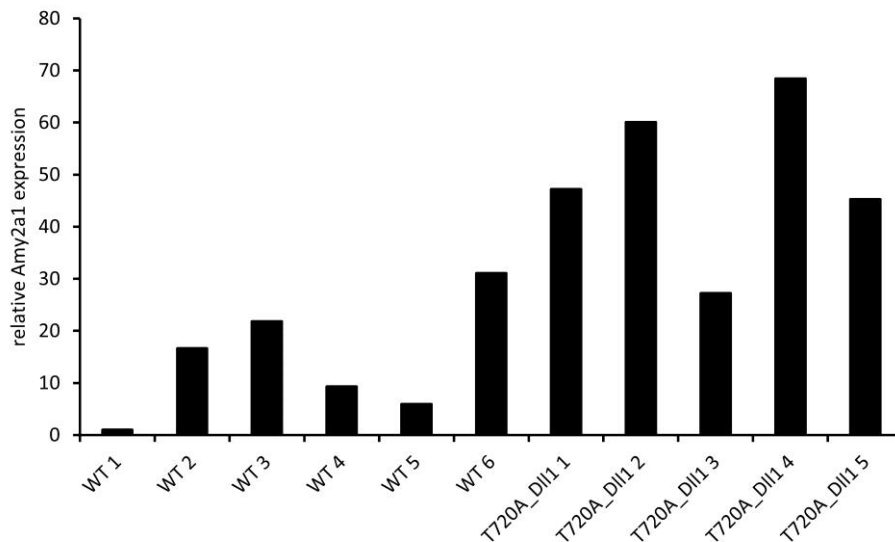


**Figure 40.** Relative *Amy2a1* expression in Dll1\_T720A and wild-type islet samples used for whole genome transcriptomics.

qRT-PCR analysis of new samples from mice of the same age confirmed the presence of false positives, given how selected hits from the whole genome transcriptomics could not be confirmed as dysregulated in Dll1\_T720A mutants (Figure 41).

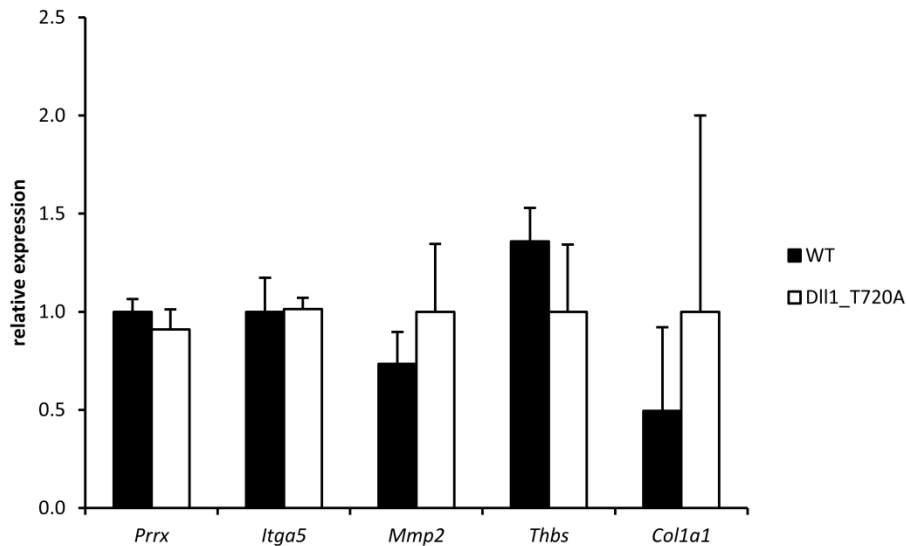


**Figure 41. qRT-PCR analysis of selected transcriptomics targets in 16-weeks old Dll1\_T720A and wild type mice.**

Expression levels of selected whole genome transcriptomics hits in new isolated islets from Dll1\_T720A and wild-type controls, assessed by qRT-PCR (n=4). Expression levels were normalized to the housekeeping genes *Actb*, *Gapdh*, and *Pgk1*. Error bars display the SEM.

A critical analysis of the data set, including comparisons with gene expression data banks and literature, revealed that at least 43 of the differentially regulated genes were expressed exclusively in the exocrine pancreas, and could therefore be discarded.

Supplementary Table 5 contains the remaining 221 differentially regulated genes, a set that is, however, still likely to contain further, less well-known acinar-dependent false positives.

Among the regulated genes is the Notch receptor *Notch2* as well as the Notch target *Heyl*, suggesting that Notch signaling is at least in part modulated by the Dll1\_T720A mutation. Given the presence of false positives in the data set, a comparison with the verified experiment performed with Dll1- $\beta$ KO mice and described in 4.2.5.2 is probably the best approach to avoid erroneous conclusions. Interestingly, of the 16 regulated genes in Dll1- $\beta$ KO islets (Table 3), 5 were also regulated in in Dll1\_T720A islets: *Ptgs2*, *Ly6a*, *Penk*, *Pigr*, and *Chi3l1*, further substantiating the validity and Dll1-dependency of these hits. The upregulation of *Ptgs2* may be particularly crucial, given how it is elicited by both *Dll1* knockdown (Table 3) and the T720A substitution in the intracellular domain of DLL1, but not by chemical inhibition of NOTCH1 (Figure 30). Taken together, these findings point to a possibly NOTCH-independent action of DLL1 in controlling *Ptgs2* expression in pancreatic  $\beta$ -cells.

For the generation of knowledge regarding exclusively the Dll1\_T720A mutation, a repetition of the experiment may be advisable.

#### 4.4 *Pax6*<sup>Leca2</sup>

The *Pax6*<sup>Leca2</sup> mouse line is characterized by a progressive  $\beta$ -cell loss in the adult pancreas, as previously demonstrated in our group by Daniel Gradinger<sup>136</sup>. With the intent of characterizing this phenotype in depth and discover the interacting genes that mediate PAX6 function in  $\beta$ -cell homeostasis, islets were isolated from *Pax6*<sup>Leca2</sup> mice and controls aged 4 and 20 weeks for whole genome transcriptomics. In total, 19 animals were analyzed: 4 homozygous *Pax6*<sup>Leca2</sup> mutant mice, 3 wild-type, and 4 heterozygous littermates aged 4 weeks; and 2 homozygous *Pax6*<sup>Leca2</sup> mutants with 3 wild-type controls aged 20 weeks. Notably, islets isolated from both homozygous and heterozygous *Pax6*<sup>Leca2</sup> mice were distinctly brighter than controls at both ages (data not shown). Group sizes were limited by the available number of homozygous mutants, which showed reduced penetrance in our animal cohort. Therefore, sample pre-selection following the strategy detailed in 4.2.5.2, while preferable, was not possible. The expression of the exocrine marker *Amy2a1* nevertheless proved to be comparable between all samples in the 4-weeks group (Supplementary Figure 4 B), while an increased exocrine contamination in mutant islets from the 20-weeks group was observed (Supplementary Figure 4 A). Unambiguously acinar-related genes were removed from the data sets.

In the 4-weeks group, 155 genes were differentially expressed between homozygous mutants and controls with a fold change of more than 2 (a strict parameter chosen due to both the small sample size and the impracticability to perform sample pre-selection) and an FDR of <10% (Supplementary Table 6). At this age, *Pax6*<sup>Leca2</sup> islets are still histologically indistinguishable from wild-type islets (Daniel Gradinger, personal communication). However, these extensive gene regulations may indicate that prospective changes, which will later result in  $\beta$ -cell loss, have already started. Applying the same filters, 52 genes were differentially regulated between heterozygous *Pax6*<sup>Leca2/wt</sup> and *Pax6*<sup>wt/wt</sup> samples (Supplementary Table 7), and 49 genes were differentially expressed between homozygous *Pax6*<sup>Leca2</sup> and heterozygous *Pax6*<sup>Leca2/wt</sup> islets (Supplementary Table 8) (see Figure 42 A for a qualitative comparison of the three data sets).

The differences between homozygous *Pax6*<sup>Leca2</sup> and wild-type controls were more pronounced in the 20-weeks age group, with 647 differentially regulated genes

(Supplementary Table 9). 107 genes were regulated at both analyzed ages, whereas 48 genes were specific to the 4-weeks and 540 to the 20-weeks age (Figure 42 B). The enhanced number of differentially regulated genes in the 20-weeks group was likely due to both the progressive deterioration of  $\beta$ -cell maintenance and a greater effect of exocrine contamination on this data set (see Supplementary Figure 4).

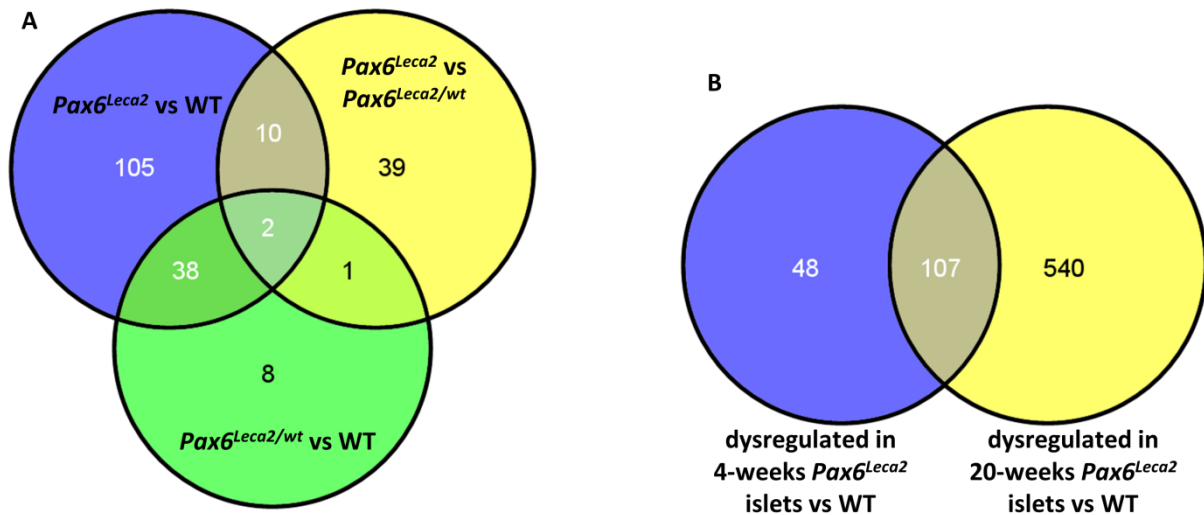


**Figure 42. Genome-wide expression analysis of *Pax6*<sup>Leca2</sup> mutant islets.**

Data sets of differentially expressed genes in the *Pax6*<sup>Leca2</sup> experiments, displayed as intersecting sets between the different genotypes measured in the 4-weeks age group (A) and between the 4 and 20-weeks age groups (B).

The 540 genes differentially regulated exclusively in the 20-weeks animals might also be secondary to the  $\beta$ -cell loss phenotype, which is already very pronounced at this age and accompanied by a change in islet composition, whereas the 107 genes differentially regulated at both ages and the 48 genes that were specifically regulated in the 4-weeks old mutant islets may represent more immediate PAX6 targets.

Since *Amy2a1* expression levels suggested that the 4-weeks group data set may be more accurate, only these genes were utilized for further bioinformatic analysis. The data set was examined to discover overrepresented transcription factor (TF) binding sites in the promoter regions of the 155 genes differentially regulated in the 4-weeks old mutants, using the FrameWorker software (Genomatix). More than 75% of promoters contained a consensus sequence for the E-twenty-six (ETS) TF family and the homeodomain TF family. PAX6, while not a member of either of these families, has been shown to bind to both consensus sequences (see 5.2.1 and 5.2.2 for an in-depth discussion). This suggests that a large number

of differentially regulated genes in the 4-weeks old islets of homozygous *Pax6*<sup>Leca2</sup> mice may be direct targets of PAX6, therefore validating the experimental results. FrameWorker analysis of the 48 genes regulated only in 4-weeks old homozygous *Pax6*<sup>Leca2</sup> islets, and therefore hypothesized to be the most immediate PAX6 targets in the data set, produced the same qualitative conclusion, with binding sites for the ETS and homeodomain TF families found in more than 80% of the promoters. In addition, the SOX/SRY and the HOX TF families were found to be overrepresented as well.

Moreover, literature mining with the 155 genes differentially regulated in 4-weeks old *Pax6* mutants using the GeneRanker software revealed significant co-citations with genes relevant to islet function. Among them are master regulators of  $\beta$ -cell homeostasis and maintenance of  $\beta$ -cell identity, such as *Pdx1*, *Neurod2*, *Mafa*, *Hnf1a*, and *ChgA*. Furthermore, the glucose transporter *Slc2a2*, the glucose-metabolizing enzymes *Gck* and *G6pc*, and the voltage-gated Ca<sup>2+</sup>-channel *Cacng2*, all essential for proper  $\beta$ -cell function (see 2.2.2.2), were found to be co-cited as well, as was the glucagon-encoding *Gcg* (Table 5).

Co-cited genes	P-value	Differentially regulated genes
<b><i>Pdx1</i></b>	1.08E-03	<i>Ffar1, Mlxipl, Pcx, G6pc2, Dlk1, Neurog3</i>
<b><i>Neurod2</i></b>	2.23E-03	<i>Pgf, Itpr1, Neurog3</i>
<b><i>Hnf1a</i></b>	2.97E-03	<i>Fmo1, Mlxipl, Muc4, B3galt5, Adh1, Neurog3, Pgf, Ddc</i>
<b><i>Zfp146</i></b>	5.29E-03	<i>Prlr, Lgi1</i>
<b><i>Egr1</i></b>	5.39E-03	<i>Camk1g, Hpse, Edn3, Grin1, Ptprz1, Pgf, Clec7a, Eapp, Cnr1</i>
<b><i>Fos</i></b>	8.19E-03	<i>Camk1g, Ucn3, Grin1, Ccl28, Adora1, Cnr1, Ddc, Oprl1, Tacr3</i>
<b><i>Mafa</i></b>	9.95E-03	<i>Mlxipl, G6pc2, Neurog3</i>
<b><i>Gcg</i></b>	3.48E-04	<i>Ffar1, Pcx, Gcgr, Ffar3, Neurog3, O3far1</i>
<b><i>Cacng2</i></b>	1.55E-03	<i>Grin1, Magi2, Rasd2</i>
<b><i>Gck</i></b>	1.64E-03	<i>Ffar1, Pcx, Gcgr, G6pc2, Neurog3</i>
<b><i>G6pc</i></b>	2.54E-03	<i>Mlxipl, Pcx, Gcgr, G6pc2</i>
<b><i>Slc2a2</i></b>	2.55E-03	<i>Ffar1, Mlxipl, Pcx, G6pc2, Neurog3</i>
<b><i>ChgA</i></b>	4.06E-03	<i>Nrcam, G6pc2, Itpr1, Neurog3, Ddc</i>

**Table 5. GeneRanker analysis of genes co-cited with the differentially regulated genes between 4-weeks old homozygous *Pax6*<sup>Leca2</sup> and wild-type mice.**

Further strengthening the association of the data set with both PAX6 function and islets, GO-term analysis revealed mainly neuronal and endocrine tissues to be overrepresented (Table 6), including islets and  $\beta$ -cells. A breakdown of correlated diseases produced a similar result, with several genes found to be annotated with insulinoma, islet cell adenoma, pancreatitis, hyperinsulinism, and diabetes, among others (Table 7).

Tissue	P-value	List of observed genes
BRAIN	4.13E-06	<i>Tnr, Tacr3, Camk1g, Ankrd34b, Rasgrf2, Ffar1, Ucn3, Prlr, Hspa12a, Pcx, Ddc, Rasd2, Grin1, Dpp10, Slc38a1, Oprl1, Rab3c, Ppp1r1a, Trim9, Nrcam, Magi2, Adora1, L1cam, Slc4a10, Jph3, Itgb8, Kcnh5, Enpep, Dmrta1, Iqsec3, Ust, Trpm3, Lrrn3, Cnr1, Cdh8, Ttyh1, Dock3, Lgi1, Itpr1, Slco1a5, Ptprz1</i>
CENTRAL NERVOUS SYSTEM	6.93E-06	<i>Tnr, Tacr3, Cntfr, Ffar1, Crim1, C1ql3, Ddc, Grin1, Dpp10, Oprl1, Gpm6a, Adora1, L1cam, Cnr1, Cdh8, Robo1, Lgi1, Slitrk6, Ptprz1</i>
CEREBRAL CORTEX	1.10E-05	<i>Tnr, Tacr3, Ffar1, Ddc, Edn3, Grin1, Oprl1, Adora1, L1cam, Slc4a10, Kcnh5, Lrrn3, Cnr1, Cdh8, Itpr1, Ptprz1</i>
SOLITARY NUCLEUS	3.53E-05	<i>Tacr3, Ucn3, Ddc, Grin1, Oprl1, Adora1, Cnr1</i>
CEREBELLUM	1.02E-04	<i>Tnr, Tacr3, Ddc, Rasd2, Edn3, Grin1, Fgf14, Nrcam, Gpm6a, Adora1, L1cam, Slc4a10, Ust, Lrrn3, Cnr1, Cdh8, Itpr1, Ptprz1</i>
INSULIN SECRETING CELLS	1.52E-04	<i>Ffar1, O3far1, Ucn3, Mlxipl, Pcx, Rasd2, Gcgr, Trpm3, Neurog3, G6pc2</i>
STOMACH	3.37E-04	<i>Tacr3, Gucy2c, Edn3, Gcgr, Ccl28, Dlk1, Muc4, Lyz2, Adh1, Neurog3, Sult1c2</i>
ADIPOSE TISSUE	3.46E-04	<i>O3far1, Mlxipl, Prlr, Pcx, Gcgr, Dlk1, Rab3c, Ppp1r1a, Ffar3, Ly86, Cnr1</i>
ARCUATE NUCLEUS	5.68E-04	<i>Tacr3, Prlr, Ddc, Grin1, Oprl1, Neurog3</i>
ISLETS OF LANGERHANS	6.44E-04	<i>Ffar1, Mlxipl, Pcx, Ddc, Gcgr, Dlk1, Lyve1, Neurog3, G6pc2</i>

**Table 6. GeneRanker analysis of tissues associated with the differentially regulated genes between 4-weeks old homozygous *Pax6*<sup>Leca2</sup> and wild-type mice.**

Disease	P-value	List of observed genes
Brain Injuries	3.61E-05	<i>Tnr, Cybb, Gucy2c, Cntfr, Prlr, Pcx, Ddc, Edn3, Grin1, Oprl1, Cd55, Adora1, L1cam, Ly86, Serpina3n, Trpm3, Lrrn3, Cnr1, Lgi1, Itpr1, Chi3l1, Serpina7, Ptprz1</i>
Nervous System Diseases	3.72E-05	<i>Tnr, Cer1, Cybb, Tacr3, Camk1g, Defb1, Egflam, Expi, Gucy2c, Cntfr, Rasgrf2, Slc26a1, Ffar1, Hpse, Nxph1, Fmo1, Ttc28, Cecr2, Ucn3, Blnk, Mlxipl, Prlr, Il17re, Hspa12a, Mlph, Jam2, Msln, Pcx, Pgf, P2ry13, Ddc, Rasd2, Clec7a, Edn3, Grin1, Rerg, Gcgr, Fhl2, Dapl1, Ccl28, Dlk1, Dpp10, Fgf14, Slc38a1, Cd53, Eapp, Oprl1, Prrg3, Cd55, Trim9, Nrcam, Lyve1, Arhgap36, Magi2, Gpm6a, Adora1, L1cam, Slc4a10, Csn3, Jph3, Ly86, Lyz2, Crybb3, Ipcef1, Itgb8, Kcnh5, Enpep, Stc2, Serpina3n, Dbc1, Rnf182, Trpm3, Lrrn3, Arap2, Abcb4, C1qc, Cnr1, Cdh8, Adh1, Robo1, Mpp3, Gabra3, Ttyh1, Dock3, Lgi1, Itpr1, Neurog3, Chi3l1, Itpkb, Serpina7, Cdh9, Sult1c2, Chst8, Slitrk6, Nell1, Elmod1, Ptprz1, Fgb</i>
Adenoma, Islet Cell	6.54E-05	<i>Ffar1, Ucn3, Mlxipl, Prlr, Pcx, Ddc, Grin1, Gcgr, Dlk1, Cd55, Lyve1, Trpm3, Cnr1, Robo1, Itpr1, Neurog3, Serpina7, G6pc2</i>

<b>Insulinoma</b>	7.01E-05	<i>Ffar1, Ucn3, Mlxipl, Prlr, Pcx, Ddc, Grin1, Gcgr, Dlk1, Cd55, Lyve1, Trpm3, Cnr1, Robo1, Itpr1, Neurog3, G6pc2</i>
<b>Gastroenteritis</b>	8.78E-05	<i>Tnr, Cybb, Tacr3, Defb1, Expi, Gucy2c, Cntfr, Hpse, Ucn3, Prlr, Il17re, Jam2, Msln, Pgf, P2ry13, Ddc, Clec7a, Edn3, Grin1, Ccl28, Dlk1, Muc4, Cd53, Oprl1, Cd55, Magi2, Adora1, Csn3, Ly86, Lyz2, Enpep, Abcb4, Cnr1, Itpr1, Chi3l1, Serpina7, Nell1, Ptprz1</i>
<b>Pancreatic Diseases</b>	8.83E-05	<i>Cybb, Tacr3, Defb1, Gucy2c, Rasgrf2, Ffar1, Hpse, Nxph1, Gm5771, Ucn3, Mlxipl, 1810009J06Rik, Prlr, Msln, Pcx, Pgf, Ddc, Edn3, Grin1, Gcgr, Ccl28, Dlk1, Dpp10, Muc4, B3galt5, Rab3c, Cd55, Nrcam, Lyve1, Adora1, L1cam, Slc4a10, Ly86, Lyz2, Enpep, Stc2, Trpm3, Abcb4, Cnr1, Adh1, Robo1, Itpr1, Neurog3, Chi3l1, Serpina7, G6pc2</i>
<b>Digestive System Diseases</b>	1.03E-04	<i>Spc25, Tnr, Cybb, Tacr3, Defb1, Expi, Gucy2c, Cntfr, Rasgrf2, Slc26a1, Ffar1, O3far1, Hpse, Nxph1, Fmo1, Gm5771, Angptl7, Cecr2, Ucn3, Blnk, Mlxipl, 1810009J06Rik, Prlr, Il17re, Jam2, Msln, Pcx, Pgf, P2ry13, Ddc, Rasd2, Clec7a, Edn3, Grin1, Rerg, Enpp3, Gcgr, Fhl2, Ccl28, Dlk1, Dpp10, Calml4, Fgf14, Gpr158, Slc38a1, Nostrin, Muc4, Cd53, B3galt5, Oprl1, Rab3c, Ppp1r1a, Cd55, Nrcam, Lyve1, Arhgap36, Magi2, Adora1, L1cam, Slc4a10, Csn3, Ly86, Lyz2, Gcnt3, Itgb8, Enpep, Stc2, Dbc1, Trpm3, Abcb4, C1qc, Cnr1, Adh1, Parm1, Robo1, Gabra3, Lgi1, Itpr1, Rab17, Neurog3, Chi3l1, Slco1a5, Serpina7, Hs6st2, Sult1c2, Nell1, G6pc2, Ptprz1, Fgb</i>
<b>Pancreatic Neoplasms</b>	9.21E-04	<i>Gucy2c, Rasgrf2, Ffar1, Hpse, Nxph1, Gm5771, Ucn3, Mlxipl, Prlr, Msln, Pcx, Pgf, Ddc, Edn3, Grin1, Gcgr, Ccl28, Dlk1, Muc4, B3galt5, Rab3c, Cd55, Nrcam, Lyve1, Adora1, L1cam, Lyz2, Enpep, Trpm3, Cnr1, Adh1, Robo1, Itpr1, Neurog3, Chi3l1, Serpina7, G6pc2</i>
<b>Pancreatitis</b>	1.30E-03	<i>Cybb, Tacr3, Defb1, Gucy2c, Hpse, 1810009J06Rik, Msln, Edn3, Ccl28, Dpp10, Muc4, Cd55, Adora1, L1cam, Enpep, Stc2, Cnr1, Neurog3, Serpina7, G6pc2</i>
<b>Glucose Intolerance</b>	1.60E-03	<i>Cybb, Ffar1, O3far1, Mlxipl, Prlr, Pcx, Gcgr, Dlk1, Ffar3, Adora1, Cnr1, Itpr1, Neurog3, G6pc2</i>
<b>Diabetes Mellitus, Experimental</b>	2.85E-03	<i>Cybb, Tacr3, Defb1, Cntfr, Ffar1, Hpse, Fmo1, Mlxipl, Prlr, Pcx, Pgf, Ddc, Edn3, Grin1, Gcgr, Fhl2, Dlk1, Oprl1, Ppp1r1a, Cd55, Lyve1, Adora1, Abcb4, Cnr1, Itpr1, Neurog3, Chi3l1, Serpina7, G6pc2</i>
<b>Hyperinsulinism</b>	3.75E-03	<i>Cybb, Cntfr, Ffar1, O3far1, Hpse, Ucn3, Mlxipl, Prlr, Msln, Pcx, Pgf, Ddc, Clec7a, Grin1, Gcgr, Ccl28, Dlk1, Ffar3, Adora1, Ly86, Gcnt3, Cnr1, Itpr1, Neurog3, Chi3l1, Serpina7, G6pc2, Fgb</i>

**Table 7. GeneRanker analysis of disease annotated with the differentially regulated genes between 4-weeks old homozygous *Pax6<sup>Leca2</sup>* and wild-type mice.**

Analysis of the genes correlated by the GeneRanker software with islet tissue, islet function, and pancreatic diseases, unsurprisingly uncovers many interesting targets. *Neurog3*, for example, the marker of all endocrine progenitors whose expression is almost undetectable in adult islets (see 2.2.1.1), was upregulated in homozygous *Pax6<sup>Leca2</sup>* islets at both analyzed ages, as was *Msln*, another gene associated with undifferentiated  $\beta$ -cells. *Ucn3*, on the other

hand, a marker of mature  $\beta$ -cells, was downregulated together with other genes central to  $\beta$ -cell function such as *Ffar1*, *G6pc2*, *Gcgr* (encoding for the glucagon receptor), *Mlxipl*, *Pcx*, and others, while neuronal markers like *Tacr3* were upregulated (see 5.2.4 for discussion and specific references).

The differential regulation of selected genes was further analyzed and confirmed by qRT-PCR. Figure 43 display the results with islets from 4-weeks old *Pax6<sup>Leca2</sup>*, heterozygous, and WT mice for a downregulated  $\beta$ -cell marker (*Gcgr*), an upregulated neuronal marker (*Tacr3*) and the upregulated developmental gene *Neurog3*. Similarly, their regulation could be confirmed in the 20-weeks old group as well (see Supplementary Figure 5).

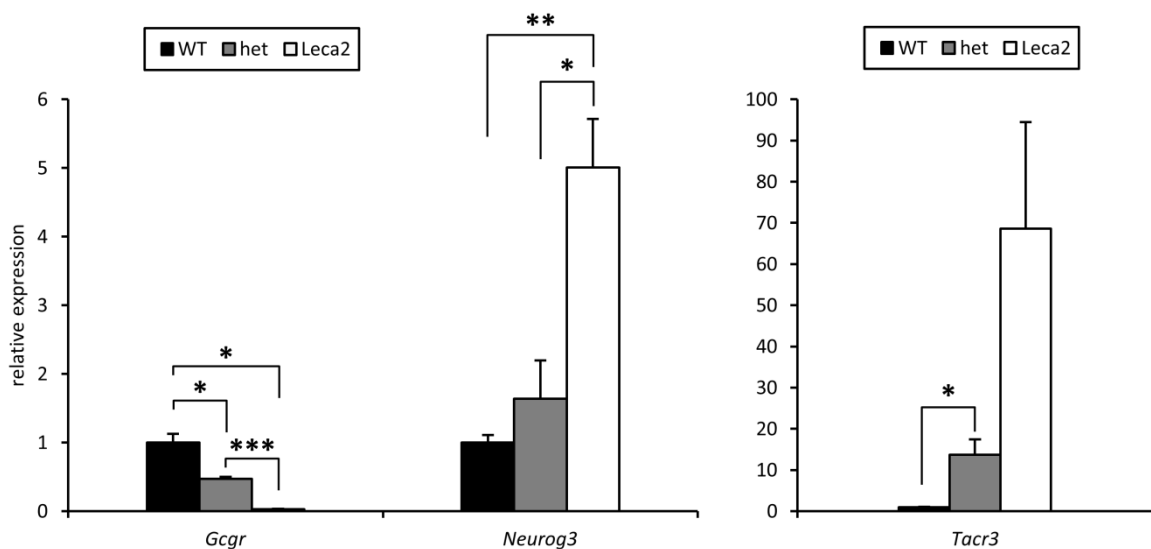


**Figure 43.** qRT-PCR analysis of selected genes in islets from 4-weeks old *Pax6<sup>Leca2</sup>* (n=5), heterozygous (n=6), and WT (n=3) mice.

Differences were considered statistically significant at  $P < 0.05$  using a heteroscedastic two-tailed Student's t-test (\* $<0.05$ , \*\* $<0.01$ , \*\*\* $<0.001$ ). Error bars display the SEM.

Taken together, these results describe the genetic expression pattern that underlies the progressive  $\beta$ -cell loss of *Pax6<sup>Leca2</sup>* mice. The data set is most consistent with an attenuation of  $\beta$ -cell function due not to  $\beta$ -cell death but rather dedifferentiation, as discussed in detail in 5.2.4.

Finally, preliminary results with islets isolated from 13-weeks old *Pax6<sup>Leca2</sup>* mice and wild-type littermates showed that the mutants had reduced insulin content (Figure 44), in accordance with previous histological results<sup>136</sup> and the gene expression analyses presented here.

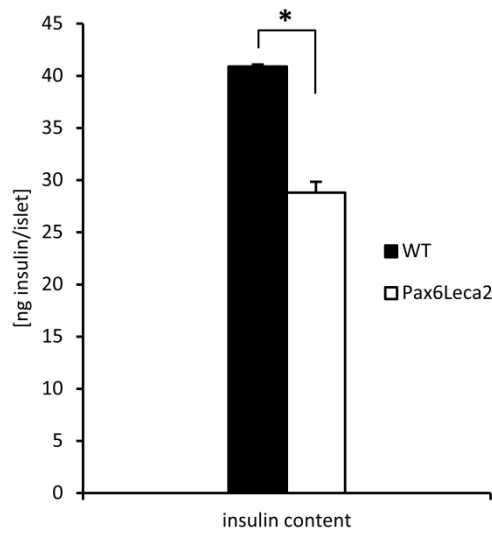


**Figure 44. Insulin content of islets isolated from 13-weeks old *Pax6<sup>Leca2</sup>* mice and wild-type littermates.** Samples were measured by ELISA (n=2). Error bars represent SEM values. Differences were considered statistically significant at  $P < 0.05$  using a heteroscedastic two-tailed Student's t-test (\* $< 0.05$ ).

## 4.5 Islet cell culture: general findings

Several technical experiments were performed with islets isolated from wild-type mice as an ongoing effort to implement *in vitro* techniques for the standardized analysis of  $\beta$ -cells in our laboratories.

The contamination of islet samples described in chapters 4.2.5.2 and 4.3 was monitored more closely by culturing islets for an increasing amount of time and assessing *Amy2a1* and *Ins2* expression via qRT-PCR. *Amy2a1* levels are dramatically reduced by approximately 50 fold after 72 hours, while *Ins2* expression remains constant and even shows a small, non-significant upward trend (Figure 45). This data strongly suggests that, under the culture conditions employed here (see chapter 3.2.3.4), acinar cells, marked by *Amy2a1*, die off after a short period of time and only islets remain viable, thereby increasing sample purity.

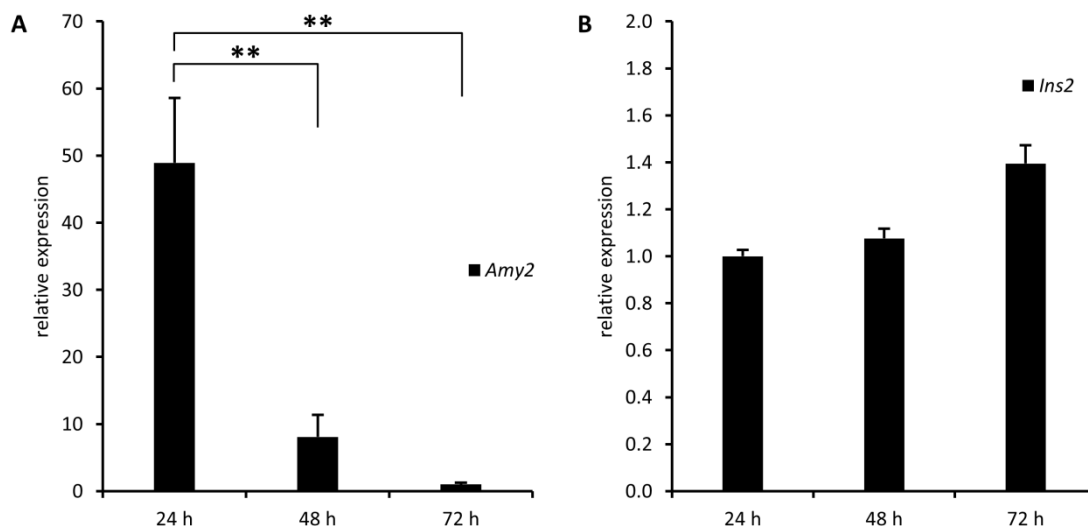


**Figure 45. Relative expression of *Amy2a1* (A) and *Ins2* (B) in isolated C3HeB/FeJ islets after 24, 48, and 72 hours culture, as measured by qRT-PCR.**

Expression was normalized to the housekeeping genes *Cyc1* and *Rpl13a*. Error bars display the SEM (n=7). Differences were considered statistically significant at  $P < 0.05$  using a heteroscedastic two-tailed Student's t-test (\*\* $< 0.01$ ).

An additional technical effort, pursued in close collaboration with Dr. Andras Franko, was the establishment of a protocol for measuring islet oxygen consumption *in vitro*. While the measurement can be achieved with the standardized procedure described in detail in 3.2.3.6, islet size proved to be a decisive factor, since even a difference of 50  $\mu\text{m}$  in diameter has an effect of factor 2 on oxygen consumption (Figure 46). Bigger islets respond to glucose

with only a slight metabolic increase, a sign of poor oxygen utilization. This likely reflects the fact that *in vitro* oxygen is exclusively provided by diffusion, which is naturally slower in bigger islets. Our data shows that metabolic experiments with primary islets should be performed exclusively on those with a diameter <150  $\mu\text{m}$ .

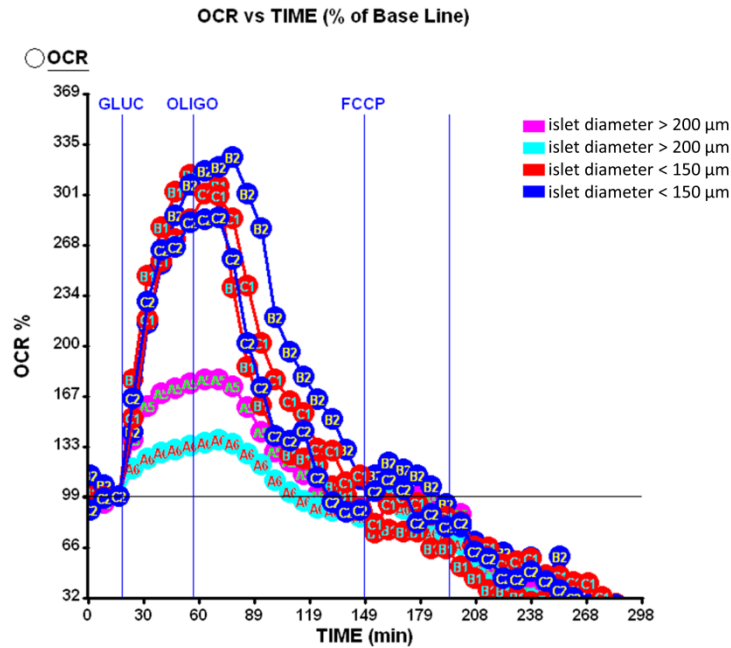


**Figure 46. Oxygen consumption rate (OCR) of islets isolated from BL6J wild-type mice.**

Islets size was discriminated by eye and measured later by photographing the islet wells. The OCR is represented as a percentage of the basal level, which is set to 100%. Blue lines indicate the time point of injection of glucose (GLUC, 20 mM), oligomycin (OLIGO, 5  $\mu\text{M}$ ), and carbonyl cyanide 4-trifluoromethoxyphenylhydrazone (FCCP, 1  $\mu\text{M}$ ). Isolated islets are responsive to glucose as expected, but smaller islets display an OCR enhanced by factor 2, likely reflecting an oxygen diffusion limit in bigger islets. The measurement was performed in collaboration with Dr. Andras Franko.

Finally, a protocol for the analysis of the architecture of isolated, intact islets was established (see 3.2.4.2 for the detailed procedure). By performing a whole mount immunohistochemical double staining of insulin and glucagon, the distribution of  $\alpha$ - and  $\beta$ -cells can be analyzed via optical slices through the z-dimensional axis, using a laser scanning microscope (Figure 47). While not suitable for high throughput analysis, this technique gives a complete, three-dimensional overview on the composition of an islet.

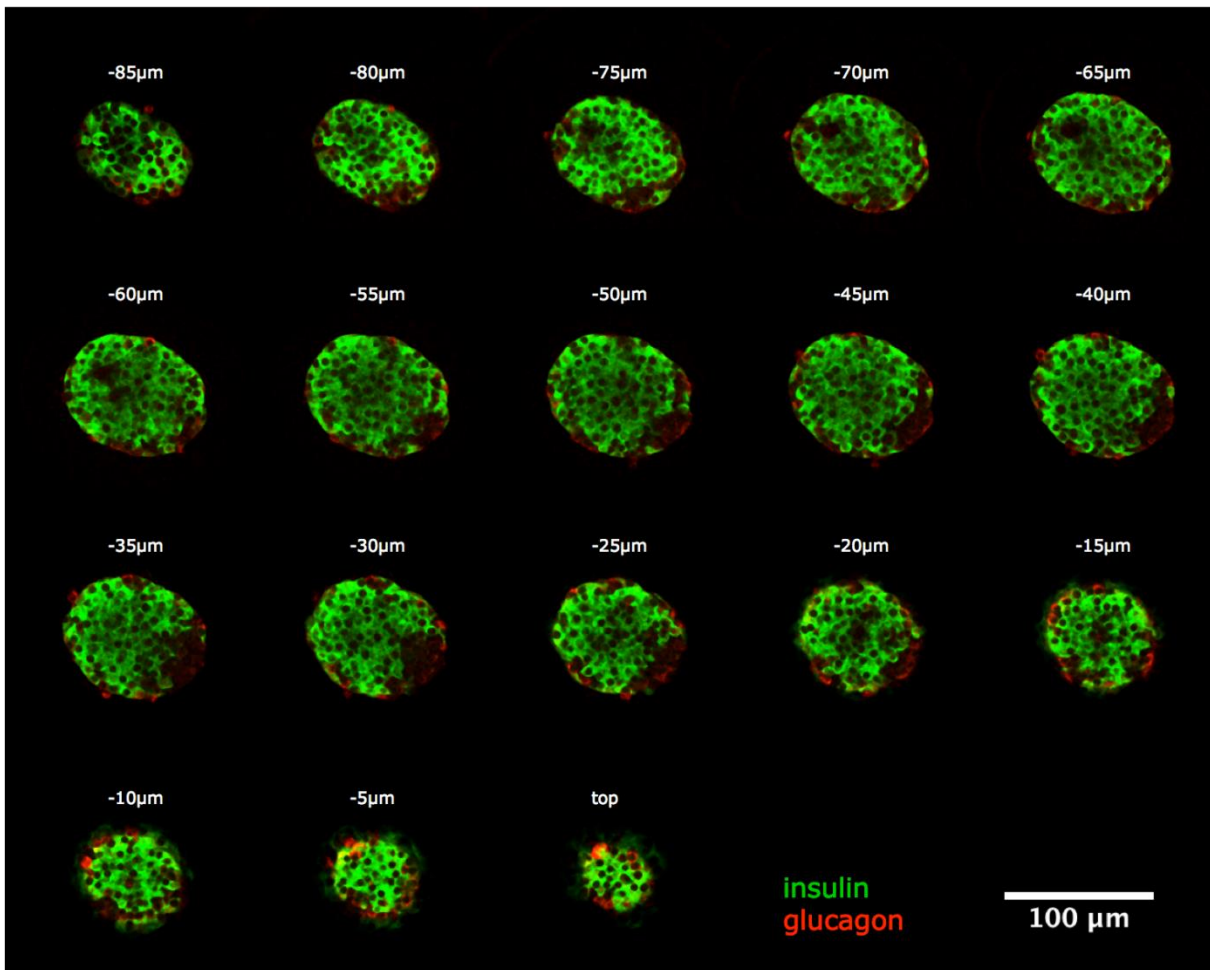


**Figure 47. Architecture of an isolated, intact C3HeB/FeJ islet, assessed with a laser scanning microscope.**

A whole mount immunohistochemical double staining of insulin (green) and glucagon (red) was performed. Images of one single islet were then taken with a laser scanning microscope performing optical sectioning at 5 µm intervals in the axial (z) dimension.

## 5. Discussion

### 5.1 Dll1

#### 5.1.1 *In vitro* analysis of Dll1

The *in vitro* data collected both with primary wild-type islets and with the clonal  $\beta$ -cell line INS-1E provides evidence that Notch signaling is active in adult  $\beta$ -cells. The expression of NICD and its localization to INS-1E cell nuclei is, in itself, sufficient to prove this activity (see Figure 12). Moreover, transient overexpression of DLL1 demonstrated that the ADAM-mediated release of D1CD takes place in  $\beta$ -cells (Figure 15). Considering how D1CD has been described in some contexts to mediate Notch-independent functions<sup>36,37,41</sup> (see chapter 2.1.2 for details), a more specific, in depth analysis of its role in  $\beta$ -cells may be of interest. This line of investigation is currently being pursued by other members of our group. Overexpression of DLL1 in INS-1E cells does not have any effects on glucose-stimulated insulin secretion (Figure 16). Combined with the findings that *in vitro* GSIS is also unaltered in islets isolated from Dll1- $\beta$ KO mice (Figure 25), and that *in vivo* plasma insulin levels of these mice are indistinguishable from controls (Figure 36), this provides evidence that DLL1 does not play any role in GSIS, in accordance with experiments published by Dror *et al.*<sup>116</sup>. Interestingly, *Dll1* expression is co-regulated with *Ins2* expression in two independent instances, namely through enhanced cell-cell contacts in the formation of INS-1E pseudo-islets and through incubation with the GLP-1 agonist Exendin-4. In both cases, *Dll1* and *Ins2* are downregulated to approximately half of their basal expression. The importance of these findings, if any, is yet to be established.

#### 5.1.2 Dll1- $\beta$ KO

##### 5.1.2.1 Effects of *Ins2*-controlled expression of Cre in pancreatic $\beta$ -cells

The Cre-mediated excision of loxP-flanked regions of genomic DNA is a widely deployed tool for the targeted deletion of genes<sup>160,161</sup>. The generation of the Dll1- $\beta$ KO mouse line reported in this dissertation made use of inducible Cre-lox technology, a variant in which the Cre protein is fused to a modified estrogen receptor (ER) that confines Cre to the cytoplasm through binding of HSP90 and allows nuclear translocation and therefore recombinase activity exclusively in the presence of 4-hydroxytamoxifen<sup>162,163</sup>.

In order to target the deletion of *Dll1* to pancreatic  $\beta$ -cells, we utilized the STOCK Tg(*Ins2-cre/ERT*)1Dam/J Cre-driver line (commonly and hereinafter called RIP-CreER) that expresses the CreER transgene under control of the *Ins2* promoter<sup>137</sup>. Remarkably, results from both gene expression analyses (4.2.2 and 4.2.5) and metabolic phenotyping (4.2.6) conclusively demonstrate that the effect of the RIP-CreER transgene on  $\beta$ -cells is neither neutral nor benign. Both male and female Cre-expressing controls (CreY) that lacked loxP sites in the *Dll1* locus nevertheless displayed significantly elevated blood glucose when fed a high fat diet compared to *Dll1*- $\beta$ KO and CreN mice (Figure 34). Moreover, the direct comparison of CreY and CreN islets with whole genome transcriptomics showed vast repercussions of Cre on the global gene expression pattern of  $\beta$ -cells.

In the light of previous reports on the RIP-Cre line<sup>164</sup>, which utilizes the same *Ins2* promoter fragment as the RIP-CreER line to drive expression of a non-inducible Cre, these findings may not be surprising. RIP-Cre mice have been known for almost a decade to develop glucose intolerance due to reduced insulin secretion, even in the absence of loxP sites<sup>165</sup>. Moreover, young RIP-Cre mice display reduced  $\beta$ -cell mass due to islet hypoplasia<sup>166</sup>. While the mechanism of this impairment of  $\beta$ -cell function is yet to be elucidated, more general negative effects of Cre on mammalian cells have been described that may explain it. The mouse genome contains endogenous “pseudo-loxP” sites that are highly susceptible to Cre-mediated recombination<sup>167</sup>, and their manipulation, though not studied in detail, cannot be considered physiological. Moreover, several *in vitro* studies showed directly that Cre can be cytotoxic for mammalian cells<sup>168,169</sup>, most likely due to chromosomal aberrations caused by the formation of both single- and double-strand DNA breaks<sup>170,171</sup>.

The RIP-CreER line used in this study should be a viable strategy to overcome these very problems, in that it allows, at least in theory, temporal control of Cre activity, limiting it to the period of tamoxifen induction<sup>172</sup>. The exposure of the genome to Cre is hereby shortened, which should reduce the adverse effects described above. However, a recent targeted study of RIP-CreER mice convincingly proved that this system is leaky: nuclear translocation and recombination of floxed alleles occur even in the absence of tamoxifen, to an extent in some cases similar to tamoxifen-treated mice<sup>173</sup>. This finding is mirrored by the data presented in Figure 18, showing that recombination in the *Dll1* locus of *Dll1*- $\beta$ KO mice is at least in part tamoxifen-independent.

If the CreER fusion protein is able to localize to the nucleus even without induction by tamoxifen, the exposure of the nucleus to the Cre recombinase enzyme is not limited to the planned induction period, and RIP-CreER and Dll1- $\beta$ KO animals are not protected from the same  $\beta$ -cell impairment reported by Lee *et al.*<sup>165</sup> for RIP-Cre mice. The results presented here, showing that CreY controls are much more susceptible to high fat diet-induced hyperglycemia, clearly corroborate this view. Furthermore, the data collected in whole genome transcriptomics and qRT-PCR experiments with isolated islets allows for the molecular dissection of such an effect.

As detailed in 4.2.2 and 4.2.5, the majority of Cre-dependent upregulated genes in both Dll1- $\beta$ KO and CreY islets encoded for ECM components, such as *Bgn*, *Dcn*, *Timp1*, *Tnc* and *Fn1*, whose enhanced expression was confirmed by qRT-PCR as well (Figure 26). Fittingly, GeneRanker<sup>TM</sup> analysis of certified Cre-targets found an association of the data set with the extracellular matrix and connective tissue, as well as a co-annotation with fibrosis, a pathology precisely characterized by an excessive production of ECM. Islet fibrosis was described in different rodent models of T2DM<sup>174-176</sup>, and, while it has been specifically proposed as an event secondary to hyperglycemia and  $\beta$ -cell impairment in some of those studies<sup>175</sup>, its correlation to the gene expression pattern of Cre-positive isolated islets is nevertheless intriguing. Homo-Delarche *et al.*<sup>177</sup> performed a whole genome transcriptomics analysis of islets isolated from one such T2DM model, the GK rat, and found overexpression of several of the same genes upregulated in a Cre-dependent manner in the experiments reported here, such as *Timp1*, *Fn1*, *Col1a1*, *Dcn*, *Lox*, and *Mmp14*, as well as a strong association to the ECM. In a different model, the OLETF rat, pancreatic fibrosis was again found to be correlated to the overexpression of *Fn1* and *Col1a1*, but also, interestingly, to the cytokine-encoding gene *Tgfb1*<sup>178</sup>. Yoshikawa *et al.*<sup>178</sup> advanced a causal role for TGF $\beta$ 1 in the development of islet fibrosis, reasoning that its expression paralleled the appearance of the fibrotic phenotype. Given that *Tgfb1* was found to be overexpressed in CreY islets both by whole genome transcriptomics and qRT-PCR (see Figure 26), this is of relevance to the data discussed here. *In vitro* experiments in a human pancreatic adenocarcinoma cell line showed that *Tgfb1* overexpression was sufficient to increase the cellular amount of COL1 and FN1<sup>179</sup>. The expression of the connective tissue growth factor gene (*Ctgf*), another target significantly upregulated in CreY islets and tightly linked to fibrosis in other contexts<sup>180,181</sup>,

was reported to be enhanced as well<sup>179</sup>. Crucially, *in vivo* overexpression of *Tgfb1* in mice was confirmed by different studies to induce pancreatic fibrosis<sup>182,183</sup>. Taken together, the gene expression pattern of Cre-expressing islets closely resembles that of TGF $\beta$ 1-induced fibrosis. This allows hypothesizing that Cre-related cellular stress of the type discussed above is responsible for *Tgfb1* upregulation.

The presence of Cre-induced stress in islets isolated from RIP-CreER mice is conclusively proven by the upregulation of *Cdkn1a* as measured by qRT-PCR and transcriptomics. *Cdkn1a* encodes for a strong inhibitor of cyclin-dependent kinases, and is hereby a negative controller of cell cycle progression and proliferation<sup>184</sup>. Its protein product acts downstream of p53 in the cellular response to stress<sup>185</sup> and plays a major role in the DNA damage response, not only by inducing cell cycle arrest but also by participating directly in DNA repair<sup>186</sup>. Considering these roles of *Cdkn1a* and the ability of the Cre enzyme to cause DNA damages as mentioned, upregulation of its mRNA may be a direct effect of Cre expression. While this direct link is novel, other genes involved in the DNA damage response were reported to be upregulated by Cre in another context<sup>169</sup>. Crucially, TGF $\beta$ 1 and CDKN1A have been shown to cooperate in the negative control of cell proliferation<sup>187</sup>, and TGF $\beta$ 1 can increase the expression of *Cdkn1a*, at least *in vitro*<sup>188</sup>, meaning that the *Cdkn1a* upregulation shown here might be *Tgfb1*-dependent as well.

This finding seems consistent with a model in which the RIP-CreER transgene causes unspecific single- and double-strand DNA breaks in pancreatic  $\beta$ -cells, leading to upregulation of *Tgfb1*, *Cdkn1a* and ultimately of fibrotic markers. The cellular stress hereby caused is reflected in the higher susceptibility of CreY mice to high fat diet-induced hyperglycemia. While Cre-induced  $\beta$ -cell impairment has been described, this data provide for the first time the chance to study its underlying molecular mechanism. However, since the experiments reported here were originally devised to analyze *Dll1* deletion and not Cre-dependent effects, different study designs will be needed to reach incontrovertible conclusions about the RIP-CreER line. *Cre*<sup>+</sup> mice should be more stringently compared to *Cre*<sup>-</sup> animals that lack any transgenic loxP sites, instead of the *Cre*<sup>-</sup> *Dll1*<sup>fl/fl</sup> and *Dll1*- $\beta$ KO mice used here.

More generally, these results underscore the importance of including Cre-expressing controls in every experiment that makes use of Cre/loxP technology for the manipulation of pancreatic  $\beta$ -cells .

### **5.1.2.2 Metabolic phenotyping**

The described Cre-related effects are of great importance for the interpretation of the Dll1- $\beta$ KO results, particularly with regard to the metabolic phenotyping experiments.

While it could be convincingly shown that  $\beta$ -cell-specific knockdown of *Dll1* has no effect on either weight development (Figure 33) or body composition (Figure 32), the interpretation of blood glucose levels in Dll1- $\beta$ KO and control mice presents more challenges. Dll1- $\beta$ KO males displayed a mild hyperglycemia compared to CreN controls when fed a standard diet (Figure 34 A), but there was no significant difference between these two groups under the high-fat diet feeding regimen.

Due to the limited number of animals available at the time, CreY controls were included only in the high-fat diet experiment, where they exhibited pronounced hyperglycemia compared to both Dll1- $\beta$ KO and CreN mice in males as well as females (Figure 34 C, D). Due to the lack of CreY controls in the standard diet group, this data is currently insufficient to determine whether the mild hyperglycemia of Dll1- $\beta$ KO males is attributable to Cre-expression or *Dll1* knockdown, or both. Interestingly, however, the results of the high-fat diet experiment show a stark contrast between CreY and Dll1- $\beta$ KO animals. The hyperglycemia of CreY mice has been discussed in 5.1.2.1 and is very likely caused by known adverse effects of the Cre enzyme in mammalian cells in general and in  $\beta$ -cells in particular. Nevertheless, the lack of an identical effect in Dll1- $\beta$ KO mice is somewhat surprising, given that both groups hold the same RIP-CreER transgene and were subjected to the same period of tamoxifen induction. The Cre-dosage can then be assumed to be identical, as should be the adverse effects on  $\beta$ -cells. The latter, contrary to expectations, is not the case. There are at least two different possible mechanisms underlying this finding:

- (a) the *Dll1* knockdown in Dll1- $\beta$ KO animals might have a protective effect on the  $\beta$ -cells, mitigating the Cre-induced impairment;
- (b) another possibility is that the presence of specific, transgenic loxP sites in the genome of Dll1- $\beta$ KO mice reduces the unspecific single- and double-strand DNA

breaks caused by the interaction of Cre with endogenous “pseudo-loxP” sites, and therefore minimizes cellular stress, simply through the higher binding affinity of the genuine loxP sites to the recombinase.

A definitive prove of hypothesis (a), a positive effect of the *Dll1* knockdown on  $\beta$ -cells, would be the measurable presence of said effect in the comparison between *Dll1*- $\beta$ KO and CreN mice as well. This, however, was not the case in the vast majority of the experiments performed, including the immunohistochemical analysis of islet physiology in young and old animals and the *in vitro* GSIS experiments with isolated islets, where no differences could be ascertained (Figure 22-Figure 25). Indeed, the only phenotypical difference between *Dll1*- $\beta$ KO and CreN mice was the mild hyperglycemia of *Dll1*- $\beta$ KO males when fed a standard diet, a finding that, as discussed above, cannot be attributed to *Dll1* knockdown beyond any doubt, and in any case does not point to any beneficial effects. Hypothesis (b), on the other hand, pertains to the biochemical properties of the Cre recombinase reaction, and cannot be either proven or disproven by the physiological experiments presented here.

Taken together, this data again points to the importance of CreY controls for the correct interpretation of results. Ideally, *Dll1*- $\beta$ KO mice should exhibit a phenotype compared to both CreY and CreN controls in the same experiment, in order for the effect to be truly reliable. Accordingly, repetition of blood glucose monitoring with inclusion of CreY controls will be interesting.

### **5.1.2.3 Gene expression analyses**

Careful planning of the whole genome transcriptomics experiment allowed the identification of a small set of 16 genes that are differentially regulated in isolated islets from aged *Dll1*- $\beta$ KO mice in comparison to both CreY and CreN controls (Table 3). Crucially, 5 of these genes (*Ptgs2*, *Ly6a*, *Penk*, *Pigr*, and *Chi3l1*) displayed the same differential regulation in an analogous experiment with *Dll1*\_T720A islets, corroborating the finding that their expression is in some way under the control of *Dll1* in islets.

Among them, *Ptgs2* (previously known as *Cox-2* for cyclooxygenase-2) is of particular interest, given previous reports about its function in  $\beta$ -cells. It encodes for one of two cyclooxygenases that catalyze the conversion of arachidonic acid into endoperoxide intermediates, the rate-limiting step in the production of prostaglandins<sup>189</sup>. In most tissues,

the constitutively expressed prostaglandin synthase is PTGS1, while PTGS2 is turned on by inflammation. Pancreatic islets, however, are one exception to this rule: there, the normally inducible *Ptgs2* is dominantly expressed, both constitutively and under interleukin-1 (IL-1) stimulation<sup>190,191</sup>. The main enzymatic product of PTGS2 is prostaglandin E<sub>2</sub> (PGE<sub>2</sub>), a lipid inflammatory messenger that, if overproduced in islets through IL-1-stimulated *Ptgs2* overexpression, blunts insulin secretion by reducing adenylyl cyclase activity<sup>192</sup>. This suggests that excessive PTGS2 activity may be mediating the impairment of  $\beta$ -cell function caused by inflammatory pathways. Accordingly, its specific inhibition in mice prevents streptozotocin-mediated destruction of  $\beta$ -cells and the onset of diabetes *in vivo*<sup>193</sup>. However, a subsequent *in vitro* study using isolated islets of rodent and human origin found that PTGS2 inhibitors failed to prevent  $\beta$ -cell dysfunction and damage initiated by a cytokine cocktail containing IL-1<sup>194</sup>, meaning this point is still debated. Regardless of these inconsistencies, *Ptgs2* expression in islets was found to be upregulated in the aftermath of high glucose concentrations both *in vivo* and *in vitro*<sup>195</sup>, another sign that the link to a role in  $\beta$ -cell impairment is real.

A link between Notch signaling and *Ptgs2* has been established for other cellular contexts. Both NOTCH1 (the regular binding partner of DLL1 within the pathway) and NOTCH2 promote gastric cancer progression in a PTGS2-dependent fashion and, crucially, their activated intracellular domains can bind to the *Ptgs2* promoter and induce its expression<sup>196,197</sup>. The upregulation of *Ptgs2* in Dll1- $\beta$ KO and Dll1\_T720A islets could therefore conceivably be ascribed to direct control by the DLL1-NOTCH1 axis. However, since whole genome transcriptomics of the selected time points (27-weeks and 37-weeks old animals) failed to reveal any differential regulation of direct or indirect Notch signaling components or targets, the possibility remains that the DLL1-mediated upregulation of *Ptgs2* is NOTCH-independent. This is further suggested by the absence of a similar effect in DAPT-treated INS-1E cells (Figure 30) (DAPT chemically inhibits NOTCH activation).

Also notable is the upregulation of *Aldh1a2* and *Aldh1a3* (often known as *Raldh2* and *Raldh3* for retinaldehyde dehydrogenase) in Dll1- $\beta$ KO islets, both encoding for enzymes that regulate retinoic acid (RA) metabolism. RA is a metabolite of vitamin A that during pancreatic endocrine development stimulates both the appearance of NEUROG3<sup>+</sup> pancreatic progenitors and their further differentiation into  $\beta$ -cells through an ALDH1A1-mediated

process that involves attenuated expression of the Notch target gene *Hes1*<sup>198</sup>. Interestingly, the expression of *Aldh1a3* is increased in islets isolated from a mouse model of high fat diet-induced diabetes<sup>199</sup>. Further experiments showed that *Aldh1a3* expression was enhanced *in vitro* by high glucose concentrations in  $\alpha$ - and  $\beta$ -cell lines alike, and its overexpression decreased GSIS<sup>199,200</sup>. The overexpression of *Aldh1a2* and *Aldh1a3* in Dll1- $\beta$ KO islets, then, matches the upregulation of *Ptgs2* and is reminiscent of hyperglycemia-induced  $\beta$ -cell impairment.

Paschaki *et al.*<sup>201</sup> recently reported that *Dll1* transcripts were markedly reduced in the spinal cord and neural tube of *Aldh1a2*<sup>-/-</sup> mutants. This finding, while insufficient to explain the *Dll1*-dependent *Aldh1a2* regulation presented here, at least establishes a clear connection between the two genes, and more generally, between *Dll1* and retinoic acid metabolism, as already suggested elsewhere<sup>202</sup>.

Other *Dll1*-regulated genes described in Table 3 have been linked to islet function but are less well characterized. *Chi3l1*, downregulated in both Dll1- $\beta$ KO and Dll1\_T720A islet, is an inflammation marker whose protein product (YKL-40) is elevated in the plasma of T2DM<sup>203</sup> and T1DM patients<sup>204</sup>, though its role in  $\beta$ -cells is unknown. *Sfrp1* encodes for an antagonist of Wnt signaling and can, at least *in vitro*, nullify the positive effect of Wnt molecules on  $\beta$ -cell proliferation and insulin secretion<sup>205</sup>. The involvement of Wnt signaling is intriguing, since the intracellular domain of DLL1 has been implicated in the integration and cross-talk of the Notch and Wnt pathways<sup>206</sup>, but no relationship between SFRP1 and DLL1 are described to date. *H2-Aa* is the murine ortholog of human *HLA-DQA1*, a gene located in the major histocompatibility complex (MHC) region and strongly associated to T1DM<sup>207</sup>.

Taken together, the gene expression pattern of islets isolated from Dll1- $\beta$ KO mice presents some features resembling  $\beta$ -cell impairment, and may be the molecular explanation of the hyperglycemia displayed by Dll1- $\beta$ KO males. However, only a small set of genes could be found to be differentially regulated, and strikingly, no direct target of Notch signaling was perturbed. This points to a relatively small effect of *Dll1* on adult  $\beta$ -cells or to some sort of compensation, as suggested by the upregulation of *Dll4* measured by qRT-PCR in younger animals (8-weeks old, see Figure 20). *Dll4* encodes for another Notch ligand that, when expressed, has the ability to bind the same preferred receptor as DLL1, NOTCH1<sup>208,209</sup>, and could therefore conceivably attenuate the effects of the *Dll1* knockdown. Partial functional

redundancy between *Dll1* and *Dll4* has been proposed before, albeit in a very different context<sup>210</sup>. Pellegrinet *et al.*<sup>210</sup> showed that in intestinal progenitor cells, loss of DLL4 is completely counterbalanced by DLL1. While loss of DLL1 is only partially compensated by DLL4, the double knockout exhibits the most pronounced phenotype and a total abrogation of NOTCH1 activation.

Compensation through other Notch ligands in Dll1- $\beta$ KO mice is unlikely, given that they do not localize to  $\beta$ -cells<sup>211</sup>.

### **5.1.3 Conclusion and future perspective**

As mentioned in 2.3.3, a role for Notch signaling in adult metabolism is emerging from the literature. A recent example is the report from Pajvani *et al.*<sup>212</sup> that *Notch1* plays a major role in hepatic glucose production, with gain-of-function promoting insulin resistance and loss-of-function improving insulin sensitivity. More to the point for the experiments discussed here, Rubio-Aliaga *et al.*<sup>213</sup> reported that global *Dll1* haploinsufficiency has metabolic consequences such as reduced body weight and size, altered fat and lean mass ratio and higher energy uptake. The study of Dll1- $\beta$ KO mice was aimed to determine whether the metabolic role of the DLL1-NOTCH1 axis is mediated, at least in part, by cell-autonomous effects in the pancreatic  $\beta$ -cell. Little research has been performed in this area to date, but Murtaugh *et al.*<sup>66</sup> described the transgenic overexpression of the constitutively active NOTCH1<sup>ICD</sup> in adult murine  $\beta$ -cells and found no perturbation of islet physiology. In this respect, their data matches the finding that *Dll1* knockdown has no effect on pancreas and islet morphology. Accordingly, no dramatic phenotype could be ascertained in either metabolic experiments or gene expression analyses. Nevertheless, Dll1- $\beta$ KO mice displayed mild hyperglycemia, and a small network of genes with known functions in  $\beta$ -cell biology was differentially regulated in isolated islets. To investigate this network further, and to conclusively prove whether some of these regulations are NOTCH-independent, the *in vitro* knockdown of Dll1 in clonal  $\beta$ -cell lines would be of interest. Given that this approach proved to be unsuccessful in the rat insulinoma INS-1E cell line used here (4.1.2), it is advisable to switch to the murine cell line MIN6<sup>214</sup> or even the recently reported human pancreatic  $\beta$ -cell line EndoC- $\beta$ H1<sup>215</sup>.

A crucial future experiment will be the repetition of metabolic phenotyping on a standard diet feeding regimen, this time with the inclusion of CreY controls in order to conclusively demonstrate whether the hyperglycemia is *Dll1*-dependent. More generally, since the whole genome transcriptomics points to a small effect of the *Dll1* knockdown and a compensation through *Dll4*-upregulation was hypothesized, it might be interesting to generate and phenotype a *Dll1/Dll4*  $\beta$ -cell specific double knockout, a strategy that already proved successful in other contexts<sup>210</sup>.

## 5.2 $Pax6^{Leca2}$

### 5.2.1 $PAX6^{R128C}$ has direct effects on the global gene expression pattern of adult islets

The data sets presented in 4.4 describe 155 genes that are differentially regulated in 4-weeks old  $Pax6^{Leca2}$  islets compared to wild types, and 647 genes in 20-weeks old islets. In order to integrate these emerging candidates with available knowledge about PAX6 transcriptional control, it is useful to compare them to a recent publication that listed direct interactions of PAX6 with genomic DNA. Xie *et al.*<sup>216</sup> made use of ChIP-on-chip technology (the combination of chromatin immunoprecipitation with DNA microarrays) to describe a total of nearly 5000 gene promoters occupied by PAX6 in the mouse. Only approximately 25% of dysregulated genes in both 4 and 20-weeks old  $Pax6^{Leca2}$  islets from the experiments described here were also directly bound by PAX6 according to the data reported by Xie *et al.*<sup>216</sup>: 38 and 152 genes, respectively (see Supplementary Table 10, Supplementary Table 11 and Figure 48).

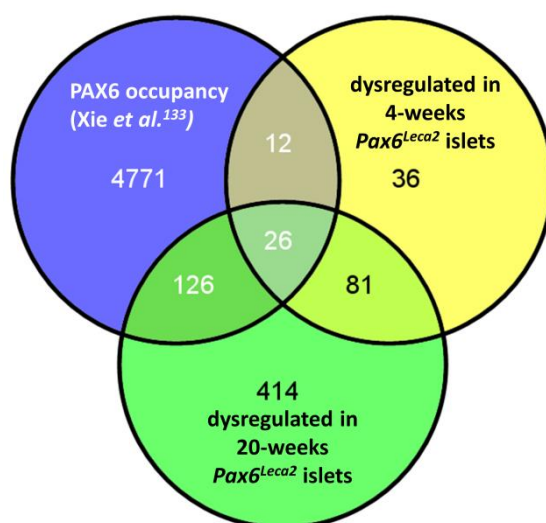


**Figure 48.** Venn diagram depicting the overlap between the dysregulated genes in  $Pax6^{Leca2}$  islets and those genes reported by Xie *et al.*<sup>216</sup> to be directly bound by PAX6.

Xie *et al.*<sup>216</sup> used chromatin from three different sources for their experiments, namely newborn lens, embryonic forebrain and the pancreatic  $\beta$ -cell line  $\beta$ -TC3. Analyzing in which of these tissues the genes comprising the overlap between the two studies were reported to bind yields a surprising result: only a minority were occupied by PAX6 in the  $\beta$ -TC3 cell line, whereas most were identified to be targets exclusively in lens and forebrain<sup>216</sup>, and as such

should not be expected to be targets in isolated islets (see Supplementary Table 10 and Supplementary Table 11 for details). This apparent discrepancy is most likely dependent on the use of very different pancreatic source materials for the experiments detailed here and those performed by Xie *et al.*<sup>216</sup>. The  $\beta$ -TC3 cell line was established by transgenic expression of an oncogene under the control of the *Ins2* promoter and derived from the resulting insulinomas<sup>217,218</sup>, and can therefore be considered a more artificial model than primary isolated islets. Furthermore, islets are composed of five different cell types, meaning that the whole genome transcriptomics results detailed in 4.4 necessarily include genes that are PAX6 targets in  $\alpha$ -,  $\delta$ -, PP- and  $\epsilon$ -cells and would remain undetected in an analysis carried out exclusively with  $\beta$ -TC3 cells. Finally, the two juxtaposed data sets, ours and from Xie *et al.*<sup>216</sup>, measured different attributes, i.e. mRNA levels that are under the control of a PAX6 mutant and gene promoters that are directly bound by PAX6, meaning technical differences are also likely to contribute to the discrepancy described above.

Similarly to the whole genome transcriptomics experiments discussed here, an analysis of *Pax6*<sup>Leca2</sup> cerebral cortices was recently reported<sup>219</sup>. Strikingly, despite the fact that a large number of neuronal genes were found to be differentially regulated in islets (Supplementary Table 6-10), there is no overlap between genes differentially regulated in islets or cortices. These differences to previous studies probably collectively underline the dependency of PAX6 action, and more generally of transcription factors, on the cellular context, something that has been widely reported to be the case<sup>131,220</sup>.

Summarizing, the comparison with the ChIP-on-chip experiment from Xie *et al.*<sup>216</sup> offers a first important validation of our transcriptomics data as descriptive of a large PAX6-dependent change in islet global gene expression. This is in accordance with a model in which PAX6<sup>R128C</sup> modulates the expression of a large number of direct PAX6<sup>WT</sup> targets, conceivably through modified DNA-binding affinities of the mutated RED domain, and those initial changes then lead to more broad perturbations, i.e. the differential regulation of genes not directly bound by PAX6 itself.

The crystal structure of the paired domain of human PAX6, whose amino acid sequence is identical to the murine homologue, substantiates the view that R128C changes the DNA-binding properties of PAX6. Xu *et al.*<sup>221</sup> solved the structure of the paired domain in complex with its optimal DNA-binding site and determined that R128, precisely the arginine

substituted in the *Pax6*<sup>Leca2</sup> mouse, is responsible for direct van der Waals contacts as well as hydrogen bonds with the DNA<sup>221,†</sup>. The substitution of an arginine, a large polar amino acid, with the much smaller and nonpolar cysteine, is likely to disrupt both van der Waals and hydrogen bonds. Preliminary *in silico* analyses, recently performed by Walcher *et al.*<sup>219</sup>, support the model proposed here by showing a diminished DNA-binding affinity for the R128C RED subdomain compared to the wild type. This is in agreement with previous biochemical studies<sup>220,222,223</sup>. Interestingly, R128C is a naturally occurring PAX6 missense mutation in human patients of foveal hypoplasia<sup>224</sup>, leading to multiple studies of its properties. Although the exact effects of the R128C substitution seemed to be dependent on the cell line used, all these studies reported decreased or abolished DNA binding for both isoform 1 and 5a (but with sometimes differing effects on the two variants)<sup>220,222,223</sup>, in accordance with the structural data. Altogether, the properties of PAX6<sup>R128C</sup> explain at least in part the measured dysregulation of a large number of direct PAX6 targets in *Pax6*<sup>Leca2</sup> islets.

PAX6 has been shown to bind to promoter regions through a highly cooperative interaction of its domains<sup>131,220,225</sup>. The three different DNA-binding domains of PAX6, PAI, RED and HD, all bind to different, specific DNA-sequences when singularly analyzed *in vitro*, but synergistic action between them has long been known as an important mode of action of PAX proteins that broadens the number of recognized sequences<sup>131</sup>, meaning the effects of the R128C substitution on the DNA-binding properties of PAX6 are not necessarily limited to those described above and pertaining the direct involvement of this residue in sequence recognition.

Naturally occurring missense mutations in the human PAX6 protein were extensively analyzed and found not only to influence the binding of the altered domain, but to have more pleiotropic effects on the properties of the whole protein that further depended on the specific cellular environment<sup>220,222,223</sup>. Singh *et al.*<sup>226</sup>, for instance, performed a systematic study of mutations in both PAI and RED, demonstrating an effect on the binding

---

<sup>†</sup>Note that the PAX6 nomenclature used by Xu *et al.*<sup>221</sup> is off by three residues from the canonical nomenclature used in this dissertation. The authors do not count the first three residues of PAX6 because they are not part of the paired domain, and therefore call the arginine substituted in *Pax6*<sup>Leca2</sup> R125 instead of the correct R128, referring nevertheless to the same residue.

of homeodomain targets. The FrameWorker<sup>TM</sup> analysis detailed in 4.4 suggests that a similar effect is at work in *Pax6*<sup>Leca2</sup> islets: the promoters of more than 75% of differentially regulated genes at the 4-week time point contained a consensus sequence for the homeodomain TF family. The R128C substitution, then, has wide effects on the transcriptional activity of PAX6 that are not limited to the RED subdomain.

### **5.2.2 PAX6<sup>R128C</sup> modulates the interaction of the RED subdomain with ETS transcription factors**

FrameWorker<sup>TM</sup> analysis also identified consensus sequences for the ETS transcription factor family<sup>227</sup> to be overrepresented in the data sets discussed here. A connection between PAX and ETS proteins has already been described in other contexts. The *Drosophila* homologue of murine PAX6, termed PAX-QNR, has been shown to specifically recognize numerous ETS binding sites<sup>228</sup>, allowing to speculate that the observed correlation to this family may actually depend on the modulated DNA-binding affinities of PAX6<sup>R128C</sup> described above. Besides, there is at least one instance in which a member of the ETS family was found to be a direct target of PAX6<sup>229</sup>, opening up the possibility that the link might also be a downstream effect of the mutation. Most intriguingly, a direct protein-protein interaction between paired-box and ETS transcription factors has been proposed and showed for human PAX5, whose binding to ETS family members forms functional complexes that are important in the regulation of B-cell-specific promoters<sup>230</sup>. Such an interaction has never been demonstrated for PAX6, but Xu *et al.*<sup>221</sup> proposed it, reasoning that the paired domain is largely conserved between PAX5 and PAX6 and that the residues making up the PAX5 docking site with the ETS domain are nearly identical in the two proteins. Crucially, this docking site is located in the RED subdomain<sup>221,230</sup>, and while R128 is not one of the residues proposed to be directly involved, it is definitely conceivable, albeit speculative, that the insertion of a cysteine in place of a chemically very different arginine might induce a conformational change in the entire RED domain sufficient to dampen the interaction with ETS proteins. Taken together, the transcriptomics data detailed in 4.4 propose for the first time an important role for PAX6-ETS domain interaction in islet cell homeostasis. The distortion of this interaction through the R128C substitution, either directly or via reduced binding to shared DNA

consensus sequences, affects a large number of dysregulated genes in *Pax6<sup>Leca2</sup>* islets, as determined via the FrameWorker™ software tool.

### 5.2.3 PAX6-regulated islet marker genes in *Pax6<sup>Leca2</sup>* islets

*Pax6<sup>Leca2</sup>* mice show a novel islet phenotype that differs from that displayed by other *Pax6* mouse models. Most notably, the *Pax6<sup>Leca2</sup>* line is almost unique in that it does not display a pancreatic developmental phenotype, as determined by our group<sup>136</sup> (see also 2.4).

To explore the distinctiveness of the *Pax6<sup>Leca2</sup>* model further, the whole genome transcriptomics results presented in this dissertation were compared to literature knowledge about several crucial islet genes whose mRNA levels are controlled by PAX6, either directly or indirectly. Selected genes are listed in Table 8 together with the expression ratios between *Pax6<sup>Leca2</sup>* and wild-type islets.

PAX6-regulated (literature)	<i>Pax6<sup>Leca2</sup></i> /WT (4 weeks)	<i>Pax6<sup>Leca2</sup></i> /WT (20 weeks)	co-cited with differentially regulated genes
<i>Ins2</i> <sup>61,134,231,232</sup>	1.0	1.0	
<i>Ins1</i> <sup>61,134,231-233</sup>	0.9	0.9	
<i>Gcg</i> <sup>61,134,233-235</sup>	1.0	1.0	✓
<i>Sst</i> <sup>61,233</sup>	0.9	0.9	
<i>Pcsk1</i> <sup>134,231,236</sup>	1.2	1.2	
<i>Pcsk2</i> <sup>231,237</sup>	1.0	0.9	
<i>Pdx1</i> <sup>133,134,231,238</sup>	0.8	0.7	✓
<i>Mafa</i> <sup>231,239</sup>	0.7	0.5	✓
<i>Slc2a2</i> <sup>133,134,231</sup>	0.8	0.4*	✓
<i>Gck</i> <sup>231</sup>	1.1	1.1	✓
<i>Gipr</i> <sup>231</sup>	1.1	0.8	
<i>Glp1r</i> <sup>231</sup>	0.8	0.8	
<i>Nkx6-1</i> <sup>134,231</sup>	1.0	0.9	

**Table 8.** List of genes whose expression is controlled by PAX6 in pancreatic islet cells of rat, mouse, or human origin.

Along with the gene symbol and the literature source about PAX6 control, the expression ratios between *Pax6<sup>Leca2</sup>* and wild-type islets from either 4 or 20-weeks old mice are displayed. All differences were statistically non-significant, with the exception of *Slc2a2* in islets from the older group (\*). The last column indicates if GeneRanker™ analysis found the respective gene to be co-cited with the differentially regulated genes in a significant manner.

Strikingly, almost none of the islet and  $\beta$ -cell markers displayed in Table 8 were differentially regulated in *Pax6<sup>Leca2</sup>* islets from mice of either 4 or 20-weeks of age in a statistically significant manner, with the exception of the glucose transporter *Slc2a2*. Most notably, the expression levels of *Gcg*, *Ins1*, *Ins2*, and *Sst*, the genes encoding for the endocrine hormones

glucagon, insulin, and somatostatin, were unchanged. Their direct and indirect regulation through PAX6 is a well-established fact, resulting from the study of *Pax6* knockouts<sup>60,134</sup>, mutants<sup>61,240</sup> and biochemical experiments<sup>231,234,235,241</sup>. In rats, PAX6 binds to a promoter sequence shared by *Gcg*, *Ins2*, and *Sst* called pancreatic islet cell enhancer sequence (PISCES)<sup>233</sup> and positively regulates their expression<sup>234,235,241</sup>. Moreover, the rodent insulin genes are under the control of PDX1<sup>242,243</sup> and MAFA<sup>243–246</sup> both during development as well as in adult  $\beta$ -cells. Since PAX6 drives the expression of *Pdx1*<sup>231,238</sup> and *Mafa*<sup>231,239</sup>, its effect on *Ins1* and *Ins2* is even greater, making the lack of their downregulation all the more surprising. This is particularly the case for islets from 20-weeks old *Pax6*<sup>Leca2</sup> mice: at this age, *Pax6*<sup>Leca2</sup> animals exhibit reduced  $\beta$ -cell area and advanced islet degeneration<sup>136</sup>, and preliminary studies on isolated islets seemingly confirmed such a trend by pointing to reduced insulin content. Collectively, these findings could be expected to be mirrored in the transcriptomics data by differentially reduced expression of *Ins1* and *Ins2*.

It is plausible that at least two causes contributed to the absence of such an outcome. Firstly, the islet isolation technique might favor islets that retain a more normal structure over the more degenerated ones. Considering, however, that isolated islets from *Pax6*<sup>Leca2</sup> mice do contain less insulin protein, the isolation bias, if present, cannot fully explain the unchanged expression of the insulin genes. Furthermore, due to breeding difficulties with the *Pax6*<sup>Leca2</sup> line, only a small number of mutants could be included in the experiment. Combined to the fact that the microarray analysis can underestimate the extent of differential regulations compared to other methods, this may have led to false negatives and to some differential regulations that were statistically non-significant despite showing a clear trend. An attractive way to integrate the data is the careful consideration of the GeneRanker<sup>TM</sup> analysis depicted in Table 5, containing genes that were found to be co-cited with the data set of differentially regulated genes. Among them are *Pdx1* (with the strongest statistical correlation), *Mafa*, *Gcg*, and *Gck*, all of them known to be downstream of PAX6 and yet not differentially regulated in the transcriptomics experiments reported here (Table 8). Their correlation to the data set, based on literature mining, suggests that at least the pathways they are part of are perturbed in *Pax6*<sup>Leca2</sup> islets, allowing the speculation that their lack of differential regulation may be the outcome of the technical issues mentioned above, most notably the small number of samples. This is particularly relevant for *Pdx1* and *Mafa*,

whose expression levels, despite being statistically non-significant, show a clear trend towards a reduction in *Pax6*<sup>Leca2</sup> islets that worsens with age.

The qRT-PCR run depicted in Supplementary Figure 5 additionally confirms at least the possibility that the microarray analysis missed some differential regulations by proving a tendency towards reduced *Ins2* expression in *Pax6*<sup>Leca2</sup> samples.

The expression of other described PAX6 targets remained unchanged as well. PAX6 is known to regulate the expression of *Pcsk2*<sup>237</sup>, a gene encoding for the main processing enzyme of glucagon biosynthesis. The expression of *Pcsk2* was nearly absent in *Pax6*<sup>Aey18</sup> embryos<sup>240</sup>. Similarly, PAX6 has further been shown to bind to the promoter of *Pcsk1*, which fulfills the same role in proinsulin processing. Human patients with a truncated PAX6 homeodomain indeed show defects in insulin biosynthesis and blood glucose homeostasis, corresponding to similar findings in mice with an analogous mutation<sup>236</sup>. According to its function, *in vitro* experiments showed that *Pcsk1* downregulation induced by PAX6 deficiency leads to a higher proinsulin/insulin ratio<sup>231</sup>. However, both *Pcsk1* and *Pcsk2* expression are unaffected in *Pax6*<sup>Leca2</sup> islets under the conditions tested here.

Taken together, the reason for the difference between genes known in literature to be under direct or indirect transcriptional control of PAX6 in islet cells and the results shown in section 4.4 is most likely twofold:

- i. the studies cited in Table 8 are loss-of-function analyses or involve mutations in other PAX6 domains. Therefore, the overlap with the single amino acid substitution in the RED subdomain of *Pax6*<sup>Leca2</sup> mice cannot be expected to be total, especially given the novel islet phenotype of these mice;
- ii. indirect evidence discussed above introduces the possibility that some differential regulations were missed by the implemented approach.

Further qRT-PCR analyses of candidate genes in *Pax6*<sup>Leca2</sup> islets will be needed to discriminate case by case between the two.

#### **5.2.4 $\beta$ -cell dedifferentiation in *Pax6*<sup>Leca2</sup> islets**

Despite the differences to previous studies discussed above, the data presented here demonstrate a conspicuous reduction of  $\beta$ -cell-specific genes in *Pax6*<sup>Leca2</sup> islets. The most prominently downregulated gene is, at both ages tested, *Ffar1* (previously *Gpr40*), whose

expression is diminished almost 20-fold. The extent of the dysregulation likely reflects the fact that *Ffar1* is expressed at exceptionally high levels in  $\beta$ -cells<sup>247</sup>. It encodes for a free fatty acid receptor and mediates the amplification of GSIS by non-esterified fatty acids (NEFAs)<sup>247,248</sup>, meaning it is involved in the insulin secretory response. *Ffar3*, which belongs to the same family of receptors, was downregulated as well.

Other receptors relevant to the control of metabolism by  $\beta$ -cells also showed diminished expression. *Gcgr*, encoding for the glucagon receptor, was downregulated more than 4-fold in young and old *Pax6<sup>Leca2</sup>* islets. Sorensen *et al.*<sup>249</sup> previously reported that islets isolated from *Gcgr<sup>-/-</sup>* mice displayed a blunted GSIS, implicating *Gcgr* in  $\beta$ -cell function. Fittingly,  $\beta$ -cell-specific overexpression of *Gcgr* causes the reverse phenotype, with enhanced GSIS and an increase in  $\beta$ -cell mass<sup>250</sup>. *Adora1*, the adenosine A1 receptor, is relevant for the amplitude and pulsatile nature of insulin, glucagon, and somatostatin secretion<sup>251,252</sup>. Its expression is progressively reduced by 2.5 and 3.8-fold in *Pax6<sup>Leca2</sup>* islets. The receptor for prolactin, *Prlr*, which regulates  $\beta$ -cell expansion during pregnancy<sup>253</sup>, likewise displayed a diminished expression.

As illustrated in 2.2.2.2,  $\beta$ -cell function depends not only on receptors that integrate outside signals, among those the ones discussed above, but also on the activity of metabolic enzymes within the  $\beta$ -cells themselves. It is therefore of note that  $\beta$ -cell-enriched enzymes involved in carbohydrate metabolism are downregulated as well by the *Leca2* mutation. Specifically, the expression levels of *Pcx* and *G6pc2* are diminished. PCX is an enzyme that catalyzes the conversion of pyruvate to oxaloacetate as a part of the citric acid cycle<sup>254</sup>. Interestingly, reduced PCX enzymatic activity has been found in the islets of both rodent and human diabetic subjects<sup>255,256</sup>. Moreover, *Pcx* deficiency in rat insulinoma cells reduces insulin secretion<sup>257,258</sup>, implicating pyruvate cycling in GSIS<sup>259</sup>. *G6pc2* (formerly *Igrp* for islet-specific glucose-6-phosphatase related protein) is expressed specifically in  $\beta$ -cells<sup>260</sup> and, while its precise function remains debated, its protein product possesses glucose-6-phosphatase activity<sup>261</sup>, suggesting a role in glucose sensing and thereby GSIS control. Accordingly, the human *G6PC2* gene is associated with increased plasma glucose levels in human population studies<sup>262,263</sup>. Its downregulation in *Pax6<sup>Leca2</sup>* islets is not unexpected, since its expression has been found to be dependent on direct PAX6 binding through synergistic action of the PD and HD domains<sup>264</sup>.

In addition to transmembrane receptors and enzymes, other master regulators of GSIS display diminished expression in *Pax6*<sup>Leca2</sup> islets. Of particular interest among them is *Ucn3*, a gene encoding for a member of the corticotropin-releasing factor (CRF) family of peptides. *Ucn3* is strongly expressed in pancreatic  $\beta$ -cells. Its protein product is secreted in response to glucose and was shown to increase insulin and glucagon secretion when injected intravenously in rats, an action mediated by its specific receptor CRHR2<sup>265</sup>. Accordingly, insulin secretion in response to high glucose in mice was attenuated by either *Ucn3* deficiency or administration of a selective CRHR2 antagonist both *in vitro* and *in vivo*, whereas basal insulin secretion was not affected<sup>266</sup>. *Ucn3* deletion also protected mice from aging- or high fat diet-induced hyperinsulinemia, leading Li *et al.*<sup>266</sup> to propose a role for UCN3 in augmenting insulin secretion specifically under conditions of excessive caloric intake. In addition to these mechanistic studies, an effort to provide an operational definition of  $\beta$ -cell maturation identified *Ucn3* as a marker of functional  $\beta$ -cells that is not expressed in neonatal islets but turned on selectively in mature  $\beta$ -cells<sup>267</sup>. *Ucn3* is significantly downregulated in *Pax6*<sup>Leca2</sup> islets, 2.0-fold in 4-weeks old animals and 4.0-fold in 20-weeks old animals, meaning its diminishing expression mirrors the progressive islet degradation of these animals.

Taken together, the R128C substitution in PAX6 causes downregulation of genes relevant at different junctions of GSIS control, namely receptors, metabolic enzymes, and secreted enhancers. This explains the GeneRanker<sup>TM</sup> analysis that found insulinoma, pancreatic diseases, and glucose intolerance, among others, to be co-annotated diseases with the data set of differentially regulated genes (see Table 7). Considering also that genes co-cited with the data set included *Pdx1*, *MafA*, *Gck*, *Neurod2*, and *Hnf1a* (see Table 5), the data presented here point to a generalized impairment of  $\beta$ -cell function and  $\beta$ -cell identity. Such a result can be explained in two possible ways:

- (a) the measured loss of  $\beta$ -cell identity might simply reflect a diminished  $\beta$ -cell mass due to apoptosis;
- (b) alternatively, it might reflect a cell-autonomous effect of the mutation on  $\beta$ -cell maintenance and a reversion of the  $\beta$ -cells to an immature state, as suggested by the progressive loss of *Ucn3* expression.

Firstly, it is important to note that while many markers of functional  $\beta$ -cells were downregulated, *Ins1*, *Ins2*, *Pcsk1*, and *Pdx1* were not. Even allowing for the possibility that these may be false negatives (see 5.2.3), if the phenotype was merely a cause of  $\beta$ -cell death within the islets, expression levels of these genes should be the most prominently blunted, since they have the highest mRNA levels to begin with (personal experience, data not shown). The fact that this is not the case, combined with the downregulation of factors like *Ucn3* or *Ffar1*, which specifically mark mature  $\beta$ -cells, offers a first hint that  $\beta$ -cell death is at least not the only explanation. Secondly, while this discussion concentrated thus far on the downregulated genes, those whose expression was elevated in *Pax6*<sup>Leca2</sup> islets may offer the best way to discriminate between those two hypotheses. In this respect, the upregulation of *Neurog3* and *Msln* is of particular relevance.

*Neurog3* expression peaks during embryonic development, but fades rapidly after birth and is almost undetectable in the adult islet<sup>54,57</sup>. Recently, Talchai et al.<sup>55</sup> proposed  $\beta$ -cell dedifferentiation as an important diabetogenic mechanism, and identified an increase in NEUROG3, among other factors, as indicative of the reversion of  $\beta$ -cells to a progenitor-like state. In the different mouse models they examined, high expression and nuclear localization of NEUROG3 always accompanied the loss of  $\beta$ -cell phenotype. While the data presented here is based exclusively on gene expression analyses, and nuclear localization could not be determined, *Neurog3* upregulation in young and old *Pax6*<sup>Leca2</sup> islets (2.3 and 2.2-fold, respectively) is highly suggestive. If  $\beta$ -cell death were the sole cause of the dysregulations mentioned above, there would be no real explanation for the enhanced expression of *Neurog3*.

The role of *Msln* (mesothelin) in pancreatic endocrine development is much less investigated, but its expression peaks in postnatal  $\beta$ -cells during their maturation, and then fades in the adult islet<sup>268</sup>. Similar to *Neurog3*, *Msln* was upregulated by 5.1-fold in 4-weeks old and 1.8-fold, albeit non-significantly, in 20-weeks old *Pax6*<sup>Leca2</sup> islets. Again, this seems to suggest that  $\beta$ -cells are cell-autonomously reverting to an immature state, rather than dying. Other findings further corroborated hypothesis (b). In addition to the downregulation of several  $\beta$ -cell genes mentioned above, GeneRanker<sup>TM</sup> analysis revealed the significant upregulation of many genes involved in neuronal function, especially at the 4-weeks stage, such as *Tacr3*, *Cnr1*, *Ddc*, *Ust*, *Tnr*, and others (see Table 6). At a first glance, the modulation

of neuronal genes is not surprising, given the known roles of PAX6 in this tissue<sup>123</sup>. Some of the regulated genes may even be partially involved in  $\beta$ -cell function. *Tacr3*, for example, encodes for the tachykinin receptor 3 and is involved in the reaction to dopaminergic stimuli<sup>269</sup>, relevant since dopamine is a negative regulator of GSIS<sup>270</sup>. *Cnr1*, the cannabinoid receptor 1, is a hypothalamic gene that is also physiologically active in islets, where its expression is decreased in response to glucose<sup>271</sup>. Reports about its function in  $\beta$ -cells differ somewhat, but involvement in GSIS is an established fact<sup>272–274</sup>. Moreover, *Ddc*, which encodes for the enzyme dopa decarboxylase, does not have any identified function in islets but is reported as a rodent  $\beta$ -cell autoantigen<sup>275</sup>, meaning it is naturally expressed there. More generally, it has been known for a long time that  $\beta$ -cells and neurons share important phenotypic traits, most notably the ability to generate and respond to action potentials with regulated exocytosis, as well as the expression of several markers<sup>276–278</sup>. Nevertheless, these similarities do not necessarily explain the upregulation of neuronal genes in *Pax6*<sup>Leca2</sup> islets, especially since it takes place in temporal coincidence with the downregulation of *bona fide*  $\beta$ -cell markers. An important hint for the correct interpretation of this finding comes from an investigation of *Foxa1/Foxa2* double knockout mice performed by Gao *et al.*<sup>279</sup>. The whole genome transcriptomic analysis of islets isolated from these animals shares some critical similarities with the results presented here, in that it entails the concurrent reduction of  $\beta$ -cell markers and activation of neuronal genes, some of them the very same reported here to be upregulated in *Pax6*<sup>Leca2</sup> islets, namely *Tacr3* (the gene with the highest fold of induction in young *Pax6*<sup>Leca2</sup> islets as well as islets from *Foxa1/Foxa2* double knockouts), *Penk*, and *Ust*. Similarly to PAX6, FOXA1 and FOXA2 are crucial for pancreatic endocrine development<sup>57,58</sup>, and Gao *et al.*<sup>279</sup> propose a role for them in the maintenance of  $\beta$ -cell maturity and functionality. Our results advance an analogous role for PAX6: as is the case with the upregulation of *Neurog3* and *Msln*, enhanced expression of neuronal genes cannot be easily explained by  $\beta$ -cell death, but rather points to a loss of  $\beta$ -cell phenotype. The comparison of our results with the transcriptomic data from *Foxa1/Foxa2* double knockouts<sup>279</sup> allows to speculate that upregulation of neuronal factors may be a common feature of  $\beta$ -cells that are either reverting to a previous developmental state or in any case losing their phenotype. In this respect, those neuronal genes that are already expressed in

$\beta$ -cells, like the aforementioned *Tacr3*, *Cnr1*, and *Ddc*, may be the first whose expression is augmented.

Analysis of genes differentially upregulated only in 20-weeks old *Pax6<sup>Leca2</sup>* islets mirrors the fact that the islet degeneration in these mice worsens with age<sup>136</sup>. Quintens *et al.*<sup>280</sup> were among the first to advance the concept of “forbidden”  $\beta$ -cell genes, meaning genes whose transcription can be as detrimental to  $\beta$ -cell function as loss of crucial components, and are specifically repressed in healthy  $\beta$ -cells. *Ldha*, encoding for one of those factors, namely a lactate dehydrogenase subunit<sup>280,281</sup>, is significantly upregulated 2.4-fold in 20-weeks old *Pax6<sup>Leca2</sup>* islets, but not in the younger animals. Furthermore *Rest* (RE-1 silencing transcription factor), whose transcription is normally absent from  $\beta$ -cells as well<sup>278,282</sup>, is induced 2.1-fold. *Rest* is a transcriptional repressor that prevents the expression of neuronal genes and, as such, is largely absent from neurons and  $\beta$ -cells<sup>278</sup>, an instance that contributes to the similarity between these two tissues discussed above. Martin *et al.*<sup>283</sup> used transgenic mice to overexpress *Rest* specifically in  $\beta$ -cells, and showed that the resulting islets contained less insulin and had a blunted GSIS under high glucose conditions, leading to reduced plasma insulin and glucose intolerance *in vivo*. Their study demonstrates that *Rest* expression in  $\beta$ -cells is sufficient to cause loss of phenotype, meaning its induction in 20-weeks old *Pax6<sup>Leca2</sup>* islets is suggestive of an even more advanced dedifferentiation than in younger animals of the same genotype. This interpretation is corroborated by the fact that *Slc2a2*, a gene absolutely central to GSIS as described in 2.2.2.2, is downregulated in the older but not in the younger mutant islets.

Additional indirect evidence for the link to  $\beta$ -cell dedifferentiation comes from the overrepresentation of binding sequences for the SOX/SRY and HOX transcription factor families in the promoters of the 48 genes regulated only in 4-weeks old *Pax6<sup>Leca2</sup>* islets, and therefore hypothesized to be the most immediate PAX6 targets in the data set. These TF families, and particularly their members NANOG and SOX9, were among the regulators of *in vivo*  $\beta$ -cell dedifferentiation in the experiments of Talchai *et al.*<sup>55</sup>. While they are not dysregulated themselves, differential regulation of their targets may be indicative of dedifferentiation. The progenitor-like ex- $\beta$ -cells found by Talchai *et al.*<sup>55</sup> also expressed higher levels of *ChgA*, which was linked to the *Pax6<sup>Leca2</sup>* transcriptome by GeneRanker<sup>TM</sup>

analysis. These instances, while not particularly conclusive on their own, neatly fit into the emerging picture.

While further experiments will be needed to confirm or falsify the hypothesis advanced here (see 5.2.5 for proposed studies), the global gene expression network of *Pax6*<sup>Leca2</sup> islets is most consistent with  $\beta$ -cell dedifferentiation.

### **5.2.5 Conclusion and future perspective**

In conclusion, the whole genome transcriptomics experiments presented here serve to qualify the islet degradation phenotype of *Pax6*<sup>Leca2</sup> mice. At both ages tested, the mutation led to the significant downregulation of several markers of functional and mature  $\beta$ -cells, an instance that is consistent with either  $\beta$ -cell death or dedifferentiation. The concomitant upregulation of the developmental gene *Neurog3*, among others, as well as the enhanced expression of neuronal markers and “forbidden”  $\beta$ -cell genes, however, is inconsistent with  $\beta$ -cell death and rather points to a cell-autonomous loss of  $\beta$ -cell phenotype. A role for PAX6 in  $\beta$ -cell maintenance is, as such, not novel. A recent study by Hart *et al.*<sup>134</sup> reported that conditional deletion of *Pax6* in the adult mouse leads to diabetes and to loss of expression of many islet- and  $\beta$ -cell markers, but the mechanism for the  $\beta$ -cell loss was not investigated. Here,  $\beta$ -cell dedifferentiation is advanced as the cause for the pancreatic phenotype of *Pax6*<sup>Leca2</sup> mice.

Several future experiments are needed to corroborate this intriguing hypothesis. First of all, while these results seem to exclude  $\beta$ -cell death as the sole cause for the phenotype, it is indispensable to measure apoptosis directly in *Pax6*<sup>Leca2</sup> pancreata in order to disprove this possibility conclusively. Interestingly, experiments performed by Daniel Gradinger in our group found enhanced proliferation in *Pax6*<sup>Leca2</sup> islets<sup>136</sup>, an instance that fits to the hypothesis advanced here: adult, mature  $\beta$ -cells are largely post-mitotic, meaning dedifferentiation and proliferation are tightly linked<sup>117,119</sup>. Determining the identity of the proliferating cells in *Pax6*<sup>Leca2</sup> islets by analyzing their expression of insulin, UCN3 or NEUROG3, will strengthen our understanding of the phenotype.

Likewise, the differential regulations most crucial to the hypothesis will have to be confirmed on the protein level, either by western blotting with isolated islets or immunohistochemical stainings. Of particular importance, in this respect, will be to confirm the upregulation of NEUROG3, to check for its nuclear localization, and to perform NEUROG3/UCN3 or NEUROG3/INS double stainings that would convincingly show *in vivo* dedifferentiation of  $\beta$ -cells in *Pax6<sup>Leca2</sup>* mice.

While the future studies detailed so far will serve to determine whether the interpretation laid out in this discussion is correct, it might also be interesting to examine which direct targets of PAX6 in the pancreatic islet are primarily responsible for the global phenotype. In this respect, the interaction of PAX6 with ETS transcription factors is probably the most interesting approach, since ETS proteins do not have reported functions in the endocrine pancreas and may represent novel targets. Starting from the model proposed by Xu *et al.*<sup>221</sup>, protein modeling could be used to analyze if the R128C substitution really affects the interaction, as speculated here. Furthermore, co-immunoprecipitation of PAX6 in islets isolated from wild-type mice can be used to determine which ETS factors, if any, forms functional complexes with PAX6 in adult islets. ChIP-on-chip experiments with isolated islets, targeted either to PAX6 or the ETS binding partners, would ultimately be necessary to compare with the transcriptomics data presented here and help unravel novel regulators of  $\beta$ -cell identity.

Given the large number of GSIS-relevant genes that are differentially regulated in *Pax6<sup>Leca2</sup>* islets, *in vitro* GSIS is another logical next step. Finally, metabolic phenotyping of *Pax6<sup>Leca2</sup>* mice, with techniques and experiments similar to those reported in 4.2.6, will be needed to determine the relevance of the molecular data reported here.

As mentioned above, the R128C missense mutation is naturally occurring in the human population<sup>224</sup>. While this particular allele has not yet been reported to be associated with glucose intolerance or diabetes, several PAX6 mutations have been recognized as factors contributing to  $\beta$ -cell dysfunction in diabetic patients<sup>236,284</sup>. Examination of a human pedigree with a PAX6<sup>R128C</sup> mutation might therefore be interesting.

### 5.3 General comments about islet isolation

In addition to the generation of the scientific hypotheses discussed above, the data presented in this thesis also highlights some challenges and caveats regarding the islet isolation technique.

Most importantly, the presence of small amounts of remaining exocrine tissue in virtually every islet sample (see Figure 9) can be a confounding factor when performing gene expression analyses. Even slight differences in purity between individual separations can lead to problems, as known from literature<sup>285</sup> as well as exemplified by the experiments displayed in 4.3 and 4.2.5.1. The strategy of purity matching and sample selection reported in 4.2.5.2 consists of determining the expression of exocrine markers *Amy2a1* and *Ctrc* by qRT-PCR and then choose the samples with the lowest possible and most comparable acinar contamination. This is essentially the same approach first reported by White and Kaestner<sup>285</sup>, and subsequently employed by others<sup>286</sup>. The possible pitfalls of not using this strategy are exemplified by the data comparing islets isolated from *Dll1\_T720A* mice and littermate controls (4.3). As shown in Figure 40, differences in sample purity between the two genotype groups were large, and produced statistically significant differential regulations in genes that are not expressed in islet cells, such as *Amy2a1*, *Cel*, *Cpa1*, and *Ctrc*. These differences have to be considered the consequence of the islet preparation technique rather than an experimental result<sup>285,286</sup>.

Purity matching and sample selection should be performed whenever possible, as emphasized by these findings. There are instances, however, when discarding a large percentage of the samples is impractical, as was the case for the *Pax6<sup>Leca2</sup>* experiments of this thesis due to the limited amount of animals available. The expression of exocrine markers should nevertheless be monitored to estimate the extent of the problem (see 4.4), and differentially regulated genes unambiguously proven to be acinar-dependent should be removed from the data set, as was done here. The work of Dreja *et al.*<sup>287</sup>, containing an explicit comparison of islet and acinar transcripts, was used as a primary reference for filtering acinar-expressed genes.

Finally, it should be noted that with the culture conditions used here, exocrine contamination in islet cell cultures decreases with time (see Figure 45), most likely due to

acinar cell death. This instance suggests that keeping islets in culture for more than 24 hours, used here for all experiments, might represent an additional, viable strategy to overcome problems deriving from exocrine contaminations.

Whichever strategy is pursued, accurate islet gene expression profiles can only be determined by taking this caveat into account.

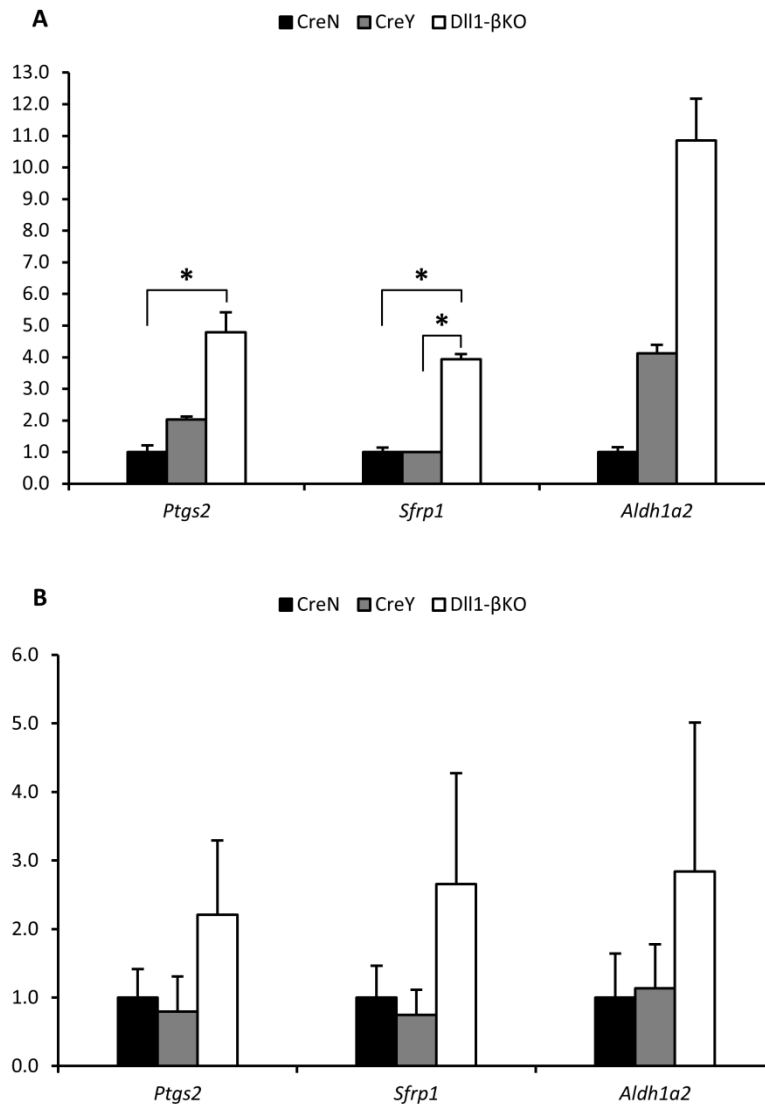
Moreover, measurements of the oxygen consumption rate (OCR) with wild-type islets proved a fundamental role for islet size in *in vitro* functional assays. This is in accordance with multiple reports about rodent islets showing that bigger islets, on average, have poor oxygen utilization and secrete less insulin than small islets<sup>288-290</sup>. Functional assays should therefore be performed exclusively with islets smaller than 150  $\mu\text{m}$  in diameter, as was done here.

## 5.4 Closing remarks

The analysis of Dll1- $\beta$ KO and *Pax6*<sup>Leca2</sup> mice during this thesis confirmed a role for these endocrine developmental genes in the adult islet of Langerhans. While the data regarding the Dll1- $\beta$ KO line showed a mild phenotype involving the dysregulation of a small number of genes, analysis of islets isolated from *Pax6*<sup>Leca2</sup> animals helped to establish that the mechanism of  $\beta$ -cell loss in these mice involves  $\beta$ -cell dedifferentiation. These data can support the future identification of novel targets in the fight against diabetes.

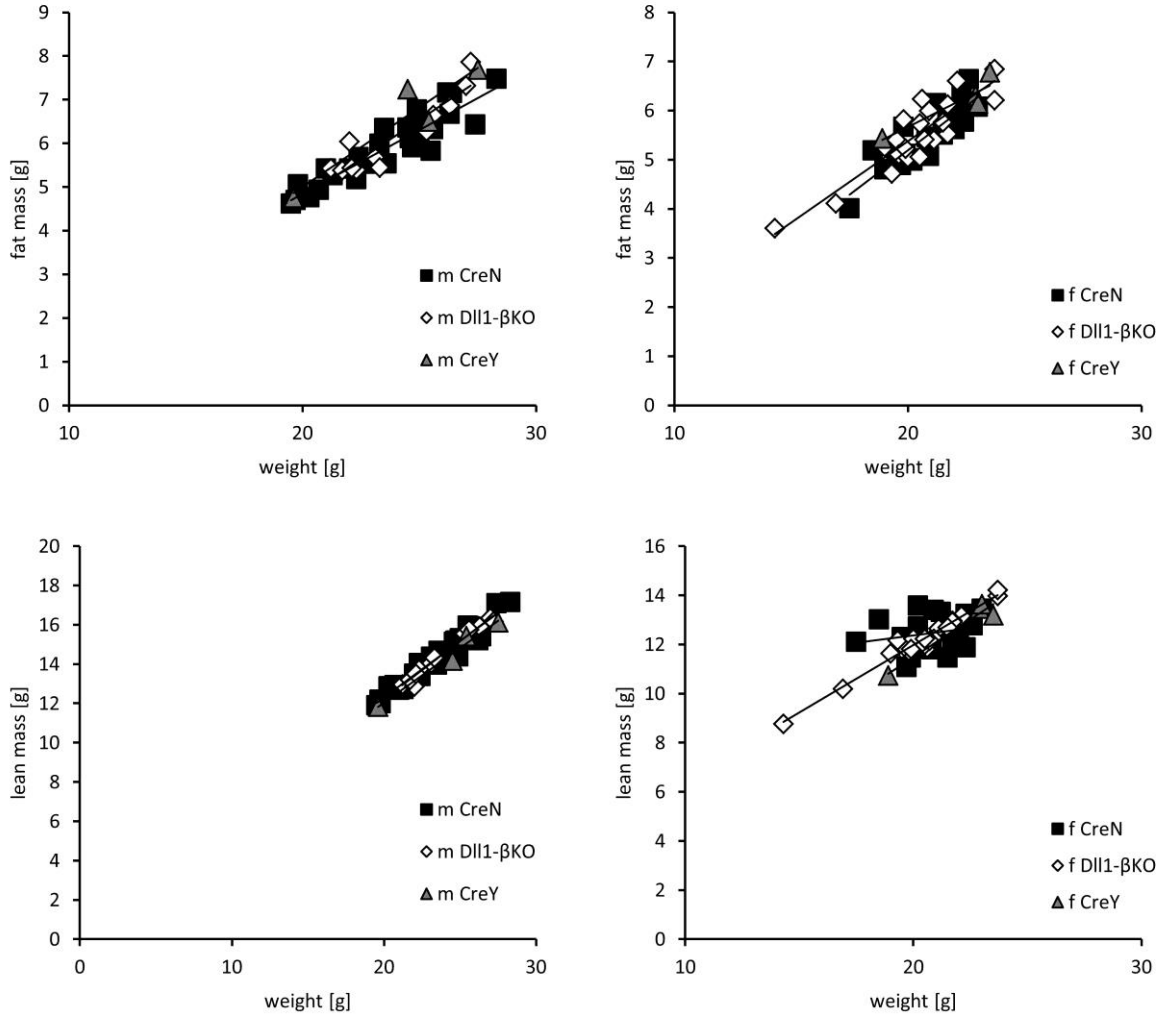
## 6. Appendix

### 6.1 Supplementary Figures

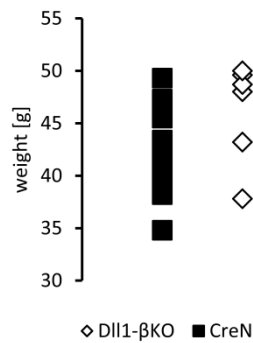


**Supplementary Figure 1. qRT-PCR analysis of selected genes in islets from Dll1-βKO, CreY, and CreN mice.**

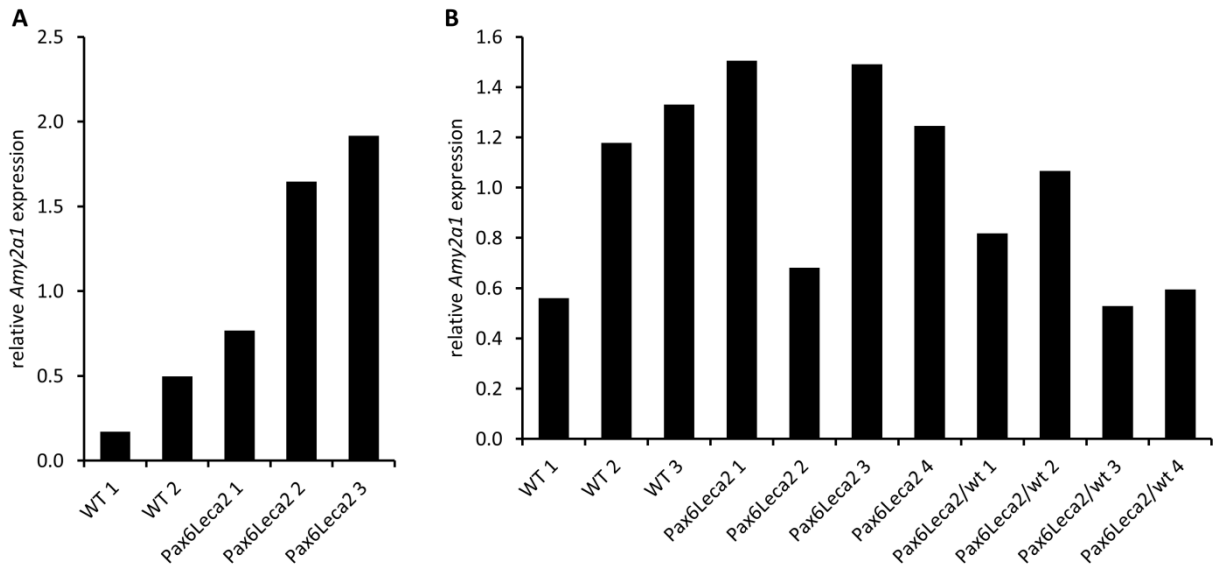
Differences were considered statistically significant at  $P < 0.05$  using a heteroscedastic two-tailed Student's t-test ( $* < 0.05$ ). Error bars display the SEM. **(A)** qRT-PCR with the same islet samples selected for transcriptomics due to their low and comparable exocrine contamination (see **Figure 27**) ( $n=5, 2,$  and  $6$  for Dll1-βKO, CreY, and CreN, respectively). **(B)** qRT-PCR with those islet samples that were discarded due to exocrine contamination ( $n=6, 6,$  and  $4$  for Dll1-βKO, CreY, and CreN, respectively). While the trend is the same in **(A)** and **(B)**, the SEM is much lower in the pre-selected samples, confirming the importance and validity of the strategy.



**Supplementary Figure 2. Fat and lean mass of 10-weeks old Dll1-βKO, CreN, and CreY mice, both males (m) and females (f), plotted against their weight (4.2.6).**

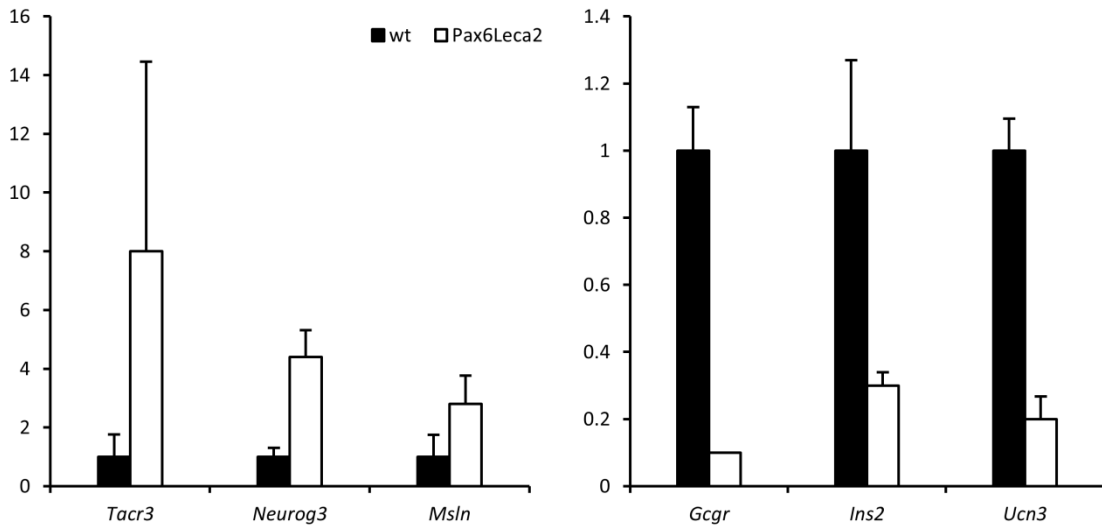


**Supplementary Figure 3. Weight of Dll1-βKO and CreN male mice fed with a standard chow and aged 31 weeks.**



**Supplementary Figure 4. Relative *Amy2a1* expression in homozygous *Pax6<sup>Leca2</sup>*, heterozygous *Pax6<sup>Leca2/wt</sup>* and wild-type islets.**

Expression was determined by whole genome transcriptomics in samples from 4-weeks old (A) and 20-weeks old (B) mice.



**Supplementary Figure 5. qRT-PCR analysis of selected genes in islets from 20-weeks old homozygous *Pax6<sup>Leca2</sup>* and WT mice.**

Error bars display the SEM (n=3).

## 6.2 Supplementary Tables

**Supplementary Table 1. Differentially expressed genes in isolated islets from Dll1- $\beta$ KO and CreN mice (4.2.5.1) filtered for a fold change of at least 1.5 and (FDR <10%).**

Gene Symbol	Dll1- $\beta$ KO/CreN	Biglycan
<i>Bgn</i>	5.1	Biglycan
<i>Dcn</i>	4.9	Decorin
<i>Timp1</i>	4.4	Tissue inhibitor of metalloproteinase 1
<i>Tnc</i>	4.2	Tenascin C
<i>Acta2</i>	3.7	Actin, alpha 2, smooth muscle, aorta
<i>Postn</i>	3.5	Periostin, osteoblast specific factor
<i>Lyz2</i>	3.5	Lysozyme
<i>Fgb</i>	3.5	Fibrinogen, B beta polypeptide
<i>Vim</i>	3.5	Vimentin
<i>Fn1</i>	3.3	Fibronectin 1
<i>Lgals1</i>	3.3	Lectin, galactose binding, soluble 1
<i>Ptgs2</i>	3.2	Prostaglandin-endoperoxide synthase 2
<i>Aldh1a3</i>	3.2	Aldehyde dehydrogenase family 1, subfamily A3
<i>Mfap5</i>	3.1	Microfibrillar associated protein 5
<i>Lrg1</i>	3.1	Leucine-rich alpha-2-glycoprotein 1
<i>Esr1</i>	3.1	Estrogen receptor 1 (alpha)
<i>Ctsc</i>	3.0	Cathepsin C
<i>Serpina3n</i>	3.0	Serine (or cysteine) peptidase inhibitor, clade A, member 3N
<i>Fgg</i>	3.0	Fibrinogen, gamma polypeptide
<i>Col8a1</i>	3.0	Collagen, type VIII, alpha 1
<i>Lox</i>	2.9	Lysyl oxidase
<i>Pdgfrb</i>	2.9	Platelet derived growth factor receptor, beta polypeptide
<i>Dpt</i>	2.9	Dermatopontin
<i>Pigr</i>	2.9	Polymeric immunoglobulin receptor
<i>Fbn1</i>	2.9	Fibrillin 1
<i>Cpb2</i>	2.8	Carboxypeptidase B2 (plasma)
<i>Fstl1</i>	2.8	Follistatin-like 1
<i>4930539E08Rik</i>	2.6	RIKEN cDNA 4930539E08 gene
<i>Col1a1</i>	2.6	Collagen, type I, alpha 1
<i>Penk</i>	2.6	Preproenkephalin 1
<i>Aebp1</i>	2.6	AE binding protein 1
<i>Mmp14</i>	2.5	Matrix metalloproteinase 14 (membrane-inserted)
<i>Il11</i>	2.5	Interleukin 11
<i>Aqp4</i>	2.5	Aquaporin 4
<i>Scd1</i>	2.5	Stearoyl-Coenzyme A desaturase 1
<i>Igkv4-74</i>	2.5	immunoglobulin kappa variable 4-74
<i>Cd44</i>	2.4	CD44 antigen
<i>Cdh11</i>	2.4	Cadherin 11
<i>Inhba</i>	2.4	Inhibin beta-A
<i>Olfml3</i>	2.4	Olfactomedin-like 3
<i>Lbp</i>	2.4	Lipopolysaccharide binding protein
<i>Cygb</i>	2.4	Cytoglobin
<i>Itga5</i>	2.3	Integrin alpha 5 (fibronectin receptor alpha)
<i>Il2rg</i>	2.3	Interleukin 2 receptor, gamma chain
<i>Cryab</i>	2.3	Crystallin, alpha B
<i>Il6</i>	2.3	Interleukin 6
<i>Anxa2</i>	2.2	Annexin A2

## Appendix

<b>6330403K07Rik</b>	2.2	RIKEN cDNA 6330403K07 gene
<b>Ascl1</b>	2.2	Achaete-scute complex homolog-like 1 (Drosophila)
<b>Gatm</b>	2.2	Glycine amidinotransferase (L-arginine:glycine amidinotransferase)
<b>Cxcl14</b>	2.2	Chemokine (C-X-C motif) ligand 14
<b>Cnn2</b>	2.2	Calponin 2
<b>C4b</b>	2.2	Complement component 4B (Childo blood group)
<b>Cd53</b>	2.2	CD53 antigen
<b>Ly86</b>	2.2	Lymphocyte antigen 86
<b>Plekhhb1</b>	2.2	Pleckstrin homology domain containing, family B (evectins) member 1
<b>Layn</b>	2.2	Layilin
<b>Mmp2</b>	2.2	Matrix metalloproteinase 2
<b>Laptm5</b>	2.2	Lysosomal-associated protein transmembrane 5
<b>Srpx2</b>	2.2	Sushi-repeat-containing protein, X-linked 2
<b>Axl</b>	2.1	AXL receptor tyrosine kinase
<b>Col1a2</b>	2.1	Collagen, type I, alpha 2
<b>Fkbp10</b>	2.1	FK506 binding protein 10
<b>Sfrp1</b>	2.1	Secreted frizzled-related protein 1
<b>Mpeg1</b>	2.1	Macrophage expressed gene 1
<b>Wfjkn2</b>	2.1	WAP, follistatin/kazal, immunoglobulin, kunitz and netrin domain containing 2
<b>Sparc</b>	2.1	Secreted acidic cysteine rich glycoprotein
<b>Lum</b>	2.1	Lumican
<b>C1qb</b>	2.1	Complement component 1, q subcomponent, beta polypeptide
<b>Large</b>	2.1	Like-glycosyltransferase
<b>Heyl</b>	2.1	Hairy/enhancer-of-split related with YRPW motif-like
<b>C1qc</b>	2.1	Complement component 1, q subcomponent, C chain
<b>Cd74</b>	2.1	CD74 antigen (invariant polypeptide of major histocompatibility complex, class II antigen-associated)
<b>4932431H17Rik</b>	2.1	RIKEN cDNA 4932431H17 gene
<b>Col6a3</b>	2.0	Collagen, type VI, alpha 3
<b>Vcam1</b>	2.0	Vascular cell adhesion molecule 1
<b>Ndr2</b>	2.0	N-myc downstream regulated gene 2
<b>St8sia1</b>	2.0	ST8 alpha-N-acetyl-neuraminide alpha-2,8-sialyltransferase 1
<b>Serpinf1</b>	2.0	Serine (or cysteine) peptidase inhibitor, clade F, member 1
<b>Des</b>	2.0	Desmin
<b>Gsta4</b>	2.0	Glutathione S-transferase, alpha 4
<b>Pdpr</b>	2.0	Podoplanin
<b>Reg3b</b>	2.0	Pancreatitis-associated protein
<b>Gnai1</b>	2.0	Guanine nucleotide binding protein, alpha inhibiting 1
<b>Tgfb1</b>	2.0	Transforming growth factor, beta 1
<b>Angptl2</b>	2.0	Angiopietin-like 2
<b>Csf2rb</b>	2.0	Colony stimulating factor 2 receptor, beta, low-affinity (granulocyte-macrophage)
<b>Tfpi2</b>	2.0	Tissue factor pathway inhibitor 2
<b>Sdc1</b>	2.0	Syndecan 1
<b>Aass</b>	2.0	Amino adipate-semialdehyde synthase
<b>Eda2r</b>	2.0	Ectodysplasin A2 isoform receptor
<b>Gm11428</b>	2.0	Predicted gene, OTTMUSG00000000971
<b>Cyp1b1</b>	2.0	Cytochrome P450, family 1, subfamily b, polypeptide 1
<b>9030420J04Rik</b>	2.0	RIKEN cDNA 9030420J04 gene
<b>Spsb1</b>	2.0	SplA/ryanodine receptor domain and SOCS box containing 1
<b>Pla2g7</b>	1.9	Phospholipase A2, group VII (platelet-activating factor acetylhydrolase, plasma)
<b>Plod2</b>	1.9	Procollagen lysine, 2-oxoglutarate 5-dioxygenase 2

Appendix

<i>Cfb</i>	1.9	Complement factor B
<i>Serping1</i>	1.9	Serine (or cysteine) peptidase inhibitor, clade G, member 1
<i>Olfml2b</i>	1.9	Olfactomedin-like 2B
<i>Sulf2</i>	1.9	Sulfatase 2
<i>Car15</i>	1.9	Carbonic anhydrase 15
<i>Runx1</i>	1.9	Runt related transcription factor 1
<i>C3</i>	1.9	Complement component 3
<i>Prrx1</i>	1.9	Paired related homeobox 1
<i>ApoE</i>	1.9	Apolipoprotein E
<i>Dio1</i>	1.9	Deiodinase, iodothyronine, type I
<i>Fscn1</i>	1.9	Fascin homolog 1, actin bundling protein ( <i>Strongylocentrotus purpuratus</i> )
<i>Fam38a</i>	1.9	CDNA sequence BC039210
<i>Gstp1</i>	1.9	Glutathione S-transferase, pi 1
<i>Rcn3</i>	1.9	Reticulocalbin 3, EF-hand calcium binding domain
<i>Pik3c2g</i>	1.9	Phosphatidylinositol 3-kinase, C2 domain containing, gamma polypeptide
<i>Mustn1</i>	1.9	Musculoskeletal, embryonic nuclear protein 1
<i>Fetub</i>	1.9	Fetuin beta
<i>Elmod1</i>	1.9	ELMO domain containing 1
<i>Tgfb3</i>	1.9	Transforming growth factor, beta 3
<i>Ctgf</i>	1.9	Connective tissue growth factor
<i>Fbp1</i>	1.9	Fructose biphosphatase 1
<i>Egln3</i>	1.9	EGL nine homolog 3 ( <i>C. elegans</i> )
<i>Fgf2</i>	1.9	Fibroblast growth factor 2
<i>Lrrc32</i>	1.9	leucine rich repeat containing 32
<i>Asb4</i>	1.9	Ankyrin repeat and SOCS box-containing protein 4
<i>Fcgr1g</i>	1.8	Fc receptor, IgE, high affinity I, gamma polypeptide
<i>Acp5</i>	1.8	Acid phosphatase 5, tartrate resistant
<i>Lsp1</i>	1.8	Lymphocyte specific 1
<i>Ambp</i>	1.8	Alpha 1 microglobulin/bikunin
<i>Pla2g4a</i>	1.8	Phospholipase A2, group IVA (cytosolic, calcium-dependent)
<i>Ldha</i>	1.8	Lactate dehydrogenase A
<i>Ccdc80</i>	1.8	Coiled-coil domain containing 80
<i>Pamr1</i>	1.8	peptidase domain containing associated with muscle regeneration 1
<i>Ebf1</i>	1.8	Early B-cell factor 1
<i>Gria3</i>	1.8	Glutamate receptor, ionotropic, AMPA3 (alpha 3)
<i>Uchl1</i>	1.8	Ubiquitin carboxy-terminal hydrolase L1
<i>Nckap1l</i>	1.8	NCK associated protein 1 like
<i>Tgm2</i>	1.8	Transglutaminase 2, C polypeptide
<i>Avpr1b</i>	1.8	Arginine vasopressin receptor 1B
<i>Csf2rb2</i>	1.8	Colony stimulating factor 2 receptor, beta 2, low-affinity (granulocyte-macrophage)
<i>Tgfb1</i>	1.8	Transforming growth factor, beta induced
<i>Ednra</i>	1.8	Endothelin receptor type A
<i>Vcan</i>	1.8	Versican
<i>C1rb</i>	1.8	Complement component 1, r subcomponent
<i>Tnfaip6</i>	1.8	Tumor necrosis factor alpha induced protein 6
<i>Serpinb6b</i>	1.8	Serine (or cysteine) peptidase inhibitor, clade B, member 6b
<i>Ankrd34c</i>	1.8	RIKEN cDNA B230218L05 gene
<i>Col10a1</i>	1.8	Collagen, type X, alpha 1
<i>Slc40a1</i>	1.8	Solute carrier family 40 (iron-regulated transporter), member 1
<i>Pcolce</i>	1.8	Procollagen C-endopeptidase enhancer protein
<i>Tspan4</i>	1.8	Tetraspanin 4
<i>Cd81</i>	1.8	CD 81 antigen

Appendix

<i>Ache</i>	1.8	Acetylcholinesterase
<i>Tmem173</i>	1.8	Transmembrane protein 173
<i>1700007K13Rik</i>	1.8	RIKEN cDNA 1700007K13 gene
<i>Osmr</i>	1.8	Oncostatin M receptor
<i>Gpx8</i>	1.8	RIKEN cDNA 2310016C16 gene
<i>Dhrs3</i>	1.8	Dehydrogenase/reductase (SDR family) member 3
<i>Dusp26</i>	1.8	Dual specificity phosphatase 26 (putative)
<i>Arg1</i>	1.8	Arginase 1, liver
<i>Igh</i>	1.8	Immunoglobulin heavy chain complex
<i>Fam70a</i>	1.8	family with sequence similarity 70, member A
<i>Msn</i>	1.8	Moesin
<i>Cybb</i>	1.8	Cytochrome b-245, beta polypeptide
<i>Qsox1</i>	1.8	Quiescin Q6 sulfhydryl oxidase 1
<i>Jam2</i>	1.8	Junction adhesion molecule 2
<i>C2</i>	1.8	Complement component 2 (within H-2S)
<i>Ly6a</i>	1.8	Lymphocyte antigen 6 complex, locus A
<i>Lhfp</i>	1.8	Lipoma HMGIC fusion partner
<i>Abcg2</i>	1.8	ATP-binding cassette, sub-family G (WHITE), member 2
<i>Pla2g2d</i>	1.8	Phospholipase A2, group IID
<i>Gstp2</i>	1.8	Glutathione S-transferase, pi 2
<i>IghmAC38.205.12</i>	1.8	Ig mu chain V region AC38 205.12
<i>Fam84a</i>	1.7	Expressed sequence AW125753
<i>Clec7a</i>	1.7	C-type lectin domain family 7, member a
<i>Pdzrn3</i>	1.7	PDZ domain containing RING finger 3
<i>Msr1</i>	1.7	Macrophage scavenger receptor 1
<i>C1rl</i>	1.7	Complement component 1, r subcomponent-like
<i>Serpine1</i>	1.7	Serine (or cysteine) peptidase inhibitor, clade E, member 1
<i>Capg</i>	1.7	Capping protein (actin filament), gelsolin-like
<i>Crybb3</i>	1.7	Crystallin, beta B3
<i>Sez6l</i>	1.7	Seizure related 6 homolog like
<i>Ms4a6c</i>	1.7	Membrane-spanning 4-domains, subfamily A, member 6C
<i>Enpp1</i>	1.7	Ectonucleotide pyrophosphatase/phosphodiesterase 1
<i>9130213B05Rik</i>	1.7	RIKEN cDNA 9130213B05 gene
<i>Tmem179</i>	1.7	Transmembrane protein 179
<i>Sorcs2</i>	1.7	Sortilin-related VPS10 domain containing receptor 2
<i>Aldh1l1</i>	1.7	Aldehyde dehydrogenase 1 family, member L1
<i>Antxr1</i>	1.7	Anthrax toxin receptor 1
<i>Cyba</i>	1.7	Cytochrome b-245, alpha polypeptide
<i>Cmklr1</i>	1.7	Chemokine-like receptor 1
<i>Pxdn</i>	1.7	Peroxidasin homolog (Drosophila)
<i>Phlda3</i>	1.7	Pleckstrin homology-like domain, family A, member 3
<i>Fads2</i>	1.7	Fatty acid desaturase 2
<i>Lrp1</i>	1.7	Low density lipoprotein receptor-related protein 1
<i>Antxr2</i>	1.7	Anthrax toxin receptor 2
<i>Gm10021</i>	1.7	Predicted gene, ENSMUSG00000057445
<i>Socs3</i>	1.7	Suppressor of cytokine signaling 3
<i>Cd38</i>	1.7	CD38 antigen
<i>Pmp22</i>	1.7	Peripheral myelin protein
<i>Pltp</i>	1.7	Phospholipid transfer protein
<i>Dhcr24</i>	1.7	24-dehydrocholesterol reductase
<i>Wbscr27</i>	1.7	Williams Beuren syndrome chromosome region 27 (human)
<i>Ehd2</i>	1.7	EH-domain containing 2
<i>Vtn</i>	1.7	Vitronectin

<b>Rbms3</b>	1.7	RNA binding motif, single stranded interacting protein
<b>Renbp</b>	1.7	Renin binding protein
<b>Ctse</b>	1.7	Cathepsin E
<b>Gpm6a</b>	1.7	Glycoprotein m6a
<b>Ptprc</b>	1.7	Protein tyrosine phosphatase, receptor type, C
<b>Serpinh1</b>	1.7	Serine (or cysteine) peptidase inhibitor, clade H, member 1
<b>Bcl3</b>	1.7	B-cell leukemia/lymphoma 3
<b>Adamts2</b>	1.7	A disintegrin-like and metallopeptidase (reprolysin type) with thrombospondin type 1 motif, 2
<b>Ddr2</b>	1.7	Discoidin domain receptor family, member 2
<b>Sla</b>	1.7	Src-like adaptor
<b>Tgfbr3</b>	1.7	Transforming growth factor, beta receptor III
<b>Rab37</b>	1.7	RAB37, member of RAS oncogene family
<b>Il33</b>	1.7	Interleukin 33
<b>Wnt4</b>	1.7	Wingless-related MMTV integration site 4
<b>Ecm1</b>	1.7	Extracellular matrix protein 1
<b>Ldlr</b>	1.7	Low density lipoprotein receptor
<b>Bnc2</b>	1.7	Basonuclin 2
<b>Cspg4</b>	1.7	Chondroitin sulfate proteoglycan 4
<b>Timp2</b>	1.7	Tissue inhibitor of metalloproteinase 2
<b>Dpysl3</b>	1.7	Dihydropyrimidinase-like 3
<b>Gfra3</b>	1.7	Glial cell line derived neurotrophic factor family receptor alpha 3
<b>Slc38a5</b>	1.7	Solute carrier family 38, member 5
<b>Ngf</b>	1.6	Nerve growth factor, beta
<b>H6pd</b>	1.6	Hexose-6-phosphate dehydrogenase (glucose 1-dehydrogenase)
<b>Sema4a</b>	1.6	Sema domain, immunoglobulin domain (Ig), transmembrane domain (TM) and short cytoplasmic domain, (semaphorin) 4A
<b>Insig1</b>	1.6	Insulin induced gene 1
<b>Tfpi</b>	1.6	Tissue factor pathway inhibitor
<b>Tmem98</b>	1.6	Transmembrane protein 98
<b>Ms4a6d</b>	1.6	Membrane-spanning 4-domains, subfamily A, member 6D
<b>Pld4</b>	1.6	Phospholipase D family, member 4
<b>Ldlrad3</b>	1.6	Low density lipoprotein receptor class A domain containing 3
<b>A930017M01Rik</b>	1.6	RIKEN cDNA A930017M01 gene
<b>Fmo5</b>	1.6	Flavin containing monooxygenase 5
<b>Arhgdib</b>	1.6	Rho, GDP dissociation inhibitor (GDI) beta
<b>Gfra2</b>	1.6	Glial cell line derived neurotrophic factor family receptor alpha 2
<b>Oat</b>	1.6	Ornithine aminotransferase
<b>Pros1</b>	1.6	Protein S (alpha)
<b>Cp</b>	1.6	Ceruloplasmin
<b>Thy1</b>	1.6	Thymus cell antigen 1, theta
<b>Pde3a</b>	1.6	Phosphodiesterase 3A, cGMP inhibited
<b>Ugt1a9</b>	1.6	UDP glucuronosyltransferase 1 family, polypeptide A9
<b>Gstm1</b>	1.6	Glutathione S-transferase, mu 1
<b>Clip4</b>	1.6	CAP-GLY domain containing linker protein family, member 4
<b>Ceacam10</b>	1.6	CEA-related cell adhesion molecule 10
<b>Egr2</b>	1.6	Early growth response 2
<b>Tyrobp</b>	1.6	TYRO protein tyrosine kinase binding protein
<b>Hspb1</b>	1.6	Heat shock protein 1
<b>Tm4sf1</b>	1.6	Transmembrane 4 superfamily member 1
<b>Ctss</b>	1.6	Cathepsin S
<b>Cd52</b>	1.6	CD52 antigen
<b>Lgals3</b>	1.6	Lectin, galactose binding, soluble 3

Appendix

<i>Has2</i>	1.6	Hyaluronan synthase 2
<i>Arid5b</i>	1.6	AT rich interactive domain 5B (Mrf1 like)
<i>Aldh1a2</i>	1.6	Aldehyde dehydrogenase family 1, subfamily A2
<i>Gucy1a3</i>	1.6	Guanylate cyclase 1, soluble, alpha 3
<i>Loxl1</i>	1.6	Lysyl oxidase-like 1
<i>Slc2a3</i>	1.6	Solute carrier family 2 (facilitated glucose transporter), member 3
<i>Gm609</i>	1.6	Gene model 609, (NCBI)
<i>Lcp1</i>	1.6	Lymphocyte cytosolic protein 1
<i>Npl</i>	1.6	N-acetylneuraminate pyruvate lyase
<i>Ltbp4</i>	1.6	Latent transforming growth factor beta binding protein 4
<i>Ctsh</i>	1.6	Cathepsin H
<i>Serpine2</i>	1.6	Serine (or cysteine) peptidase inhibitor, clade E, member 2
<i>Jag1</i>	1.6	Jagged 1
<i>Tmem47</i>	1.6	Transmembrane protein 47
<i>9430031J16Rik</i>	1.6	RIKEN cDNA 9430031J16 gene
<i>Fgl1</i>	1.6	Fibrinogen-like protein 1
<i>Igfbp5</i>	1.6	Insulin-like growth factor binding protein 5
<i>Gfra1</i>	1.6	Glial cell line derived neurotrophic factor family receptor alpha 1
<i>H2-Ab1</i>	1.6	Histocompatibility 2, class II antigen A, beta 1
<i>Zeb2</i>	1.6	Zinc finger E-box binding homeobox 2
<i>Anpep</i>	1.6	Alanyl (membrane) aminopeptidase
<i>Rgs1</i>	1.6	Regulator of G-protein signaling 1
<i>Alox5ap</i>	1.6	Arachidonate 5-lipoxygenase activating protein
<i>Wisp1</i>	1.6	WNT1 inducible signaling pathway protein 1
<i>AW551984</i>	1.6	Expressed sequence AW551984
<i>Dnm3</i>	1.6	Dynamin 3
<i>Pfkfb3</i>	1.6	6-phosphofructo-2-kinase/fructose-2,6-biphosphatase 3
<i>Crlf1</i>	1.6	Cytokine receptor-like factor 1
<i>Lcp2</i>	1.6	Lymphocyte cytosolic protein 2
<i>Grik3</i>	1.6	Glutamate receptor, ionotropic, kainate 3
<i>Serpina1a</i>	1.6	Serine (or cysteine) peptidase inhibitor, clade B, member 1a
<i>Kcnk16</i>	1.6	Potassium channel, subfamily K, member 16
<i>Dscam</i>	1.6	Down syndrome cell adhesion molecule
<i>Scnn1g</i>	1.6	Sodium channel, nonvoltage-gated 1 gamma
<i>Il18bp</i>	1.6	Interleukin 18 binding protein
<i>Fxyd3</i>	1.6	FXYD domain-containing ion transport regulator 3
<i>Fxyd6</i>	1.6	FXYD domain-containing ion transport regulator 6
<i>Plxnd1</i>	1.6	Plexin D1
<i>Dab2</i>	1.6	Disabled homolog 2 (Drosophila)
<i>Nes</i>	1.6	Nestin
<i>Akr1b8</i>	1.6	Aldo-keto reductase family 1, member B8
<i>GpnmB</i>	1.6	Glycoprotein (transmembrane) nmb
<i>B4galnt1</i>	1.6	Beta-1,4-N-acetyl-galactosaminyl transferase 1
<i>Cldn3</i>	1.6	Claudin 3
<i>Col6a2</i>	1.6	Collagen, type VI, alpha 2
<i>1600029D21Rik</i>	1.6	RIKEN cDNA 1600029D21 gene
<i>9030425E11Rik</i>	1.6	RIKEN cDNA 9030425E11 gene
<i>S100a6</i>	1.6	S100 calcium binding protein A6 (calcyclin)
<i>Sfpi1</i>	1.6	SFFV proviral integration 1
<i>Rit2</i>	1.6	Ras-like without CAAX 2
<i>Dcdc2a</i>	1.6	Doublecortin domain containing 2a
<i>Smarca1</i>	1.6	SWI/SNF related, matrix associated, actin dependent regulator of chromatin, subfamily a, member 1

Appendix

<b>H2-Aa</b>	1.6	Histocompatibility 2, class II antigen A, alpha
<b>Cacnb3</b>	1.5	Calcium channel, voltage-dependent, beta 3 subunit
<b>Mpp2</b>	1.5	Membrane protein, palmitoylated 2 (MAGUK p55 subfamily member 2)
<b>Abhd14b</b>	1.5	Abhydrolase domain containing 14b
<b>Bambi</b>	1.5	BMP and activin membrane-bound inhibitor, homolog (Xenopus laevis)
<b>Rnf122</b>	1.5	Ring finger protein 122
<b>Pgf</b>	1.5	Placental growth factor
<b>Tmprss2</b>	1.5	Transmembrane protease, serine 2
<b>Gpr165</b>	1.5	G protein-coupled receptor 165
<b>5330437I02Rik</b>	1.5	RIKEN cDNA 5330437I02 gene
<b>Car8</b>	1.5	Carbonic anhydrase 8
<b>Crip2</b>	1.5	Cysteine rich protein 2
<b>Pi15</b>	1.5	Peptidase inhibitor 15
<b>Sp140</b>	1.5	Sp140 nuclear body protein
<b>Gm2a</b>	1.5	GM2 ganglioside activator protein
<b>Pknox2</b>	1.5	Pbx/knotted 1 homeobox 2
<b>Mkx</b>	1.5	Mohawk
<b>Blvrb</b>	1.5	Biliverdin reductase B (flavin reductase (NADPH))
<b>Cd180</b>	1.5	CD180 antigen
<b>Nlgn1</b>	1.5	Neuroigin 1
<b>Mgp</b>	1.5	Matrix Gla protein
<b>Htra1</b>	1.5	HtrA serine peptidase 1
<b>Sult1d1</b>	1.5	Sulfotransferase family 1D, member 1
<b>Zdhhc14</b>	1.5	Zinc finger, DHHC domain containing 14
<b>Slc7a7</b>	1.5	Solute carrier family 7 (cationic amino acid transporter, y+ system), member 7
<b>Tmsb4x</b>	1.5	Thymosin, beta 4, X chromosome
<b>Ctsz</b>	1.5	Cathepsin Z
<b>Clmn</b>	1.5	Calmin
<b>Sulf1</b>	1.5	Sulfatase 1
<b>Agap2</b>	1.5	Centaurin, gamma 1
<b>Dock1</b>	1.5	Dedicator of cyto-kinesis 1
<b>Gja1</b>	1.5	Gap junction protein, alpha 1
<b>Ccnd1</b>	1.5	Cyclin D1
<b>A4galt</b>	1.5	Alpha 1,4-galactosyltransferase
<b>St6gal1</b>	1.5	Beta galactoside alpha 2,6 sialyltransferase 1
<b>Pmepa1</b>	1.5	Transmembrane, prostate androgen induced RNA
<b>Mef2c</b>	1.5	Myocyte enhancer factor 2C
<b>Gfpt2</b>	1.5	Glutamine fructose-6-phosphate transaminase 2
<b>Cald1</b>	1.5	Caldesmon 1
<b>H2-Eb1</b>	1.5	Histocompatibility 2, class II antigen E beta
<b>Ralgds</b>	1.5	Ral guanine nucleotide dissociation stimulator
<b>Edn3</b>	1.5	Endothelin 3
<b>Ccl7</b>	1.5	Chemokine (C-C motif) ligand 7
<b>Smo</b>	1.5	Smoothed homolog (Drosophila)
<b>Col15a1</b>	1.5	Collagen, type XV
<b>Serpina10</b>	1.5	Serine (or cysteine) peptidase inhibitor, clade A (alpha-1 antiproteinase, antitrypsin), member 10
<b>Serpina9</b>	1.5	Serine (or cysteine) peptidase inhibitor, clade B, member 9
<b>Camk1g</b>	1.5	Calcium/calmodulin-dependent protein kinase I gamma
<b>Emp1</b>	1.5	Epithelial membrane protein 1
<b>Fgl2</b>	1.5	Fibrinogen-like protein 2
<b>Tlr13</b>	1.5	Toll-like receptor 13
<b>Kcnj3</b>	1.5	Potassium inwardly-rectifying channel, subfamily J, member 3

<i>Gprasp2</i>	1.5	G protein-coupled receptor associated sorting protein 2
<i>Dock2</i>	1.5	Dedicator of cyto-kinesis 2
<i>Man2a1</i>	1.5	Mannosidase 2, alpha 1
<i>5330426P16Rik</i>	-1.5	RIKEN cDNA 5330426P16 gene
<i>2700007P21Rik</i>	-1.5	RIKEN cDNA 2700007P21 gene
<i>Gpr98</i>	-1.5	G protein-coupled receptor 98
<i>Plk3</i>	-1.5	Polo-like kinase 3 (Drosophila)
<i>Tmem97</i>	-1.5	Transmembrane protein 97
<i>Hax1</i>	-1.5	HCLS1 associated X-1
<i>Mpp6</i>	-1.5	Membrane protein, palmitoylated 6 (MAGUK p55 subfamily member 6)
<i>Gpt2</i>	-1.5	Glutamic pyruvate transaminase (alanine aminotransferase) 2
<i>Ascc2</i>	-1.5	Activating signal cointegrator 1 complex subunit 2
<i>Dennd4a</i>	-1.5	DENN/MADD domain containing 4A
<i>BC003331</i>	-1.5	CDNA sequence BC003331
<i>Tat</i>	-1.5	Tyrosine aminotransferase
<i>Fhdc1</i>	-1.5	FH2 domain containing 1
<i>Hspa9</i>	-1.5	Heat shock protein 9
<i>Raph1</i>	-1.5	Ras association (RalGDS/AF-6) and pleckstrin homology domains 1
<i>Rian</i>	-1.5	RNA imprinted and accumulated in nucleus
<i>Crhr1</i>	-1.5	Corticotropin releasing hormone receptor 1
<i>Crybg3</i>	-1.5	CDNA sequence BC043118
<i>AK220484</i>	-1.5	CDNA sequence AK220484
<i>6820431F20Rik</i>	-1.5	RIKEN cDNA 6820431F20 gene
<i>6720457D02Rik</i>	-1.5	RIKEN cDNA 6720457D02 gene
<i>Eif1ad</i>	-1.5	eukaryotic translation initiation factor 1A domain containing
<i>Nfu1</i>	-1.5	NFU1 iron-sulfur cluster scaffold homolog ( <i>S. cerevisiae</i> )
<i>Ifi2711</i>	-1.5	DNA segment, Chr 12, ERATO Doi 647, expressed
<i>Mtbp</i>	-1.5	Mdm2, transformed 3T3 cell double minute p53 binding protein
<i>Tmem144</i>	-1.5	Transmembrane protein 144
<i>Asb11</i>	-1.5	Ankyrin repeat and SOCS box-containing protein 11
<i>Sall1</i>	-1.5	Sal-like 1 ( <i>Drosophila</i> )
<i>BC016423</i>	-1.6	CDNA sequence BC016423
<i>Mthfd2</i>	-1.6	Methylenetetrahydrofolate dehydrogenase (NAD <sup>+</sup> dependent), methenyltetrahydrofolate cyclohydrolase
<i>Cebpg</i>	-1.6	CCAAT/enhancer binding protein (C/EBP), gamma
<i>Timm8a1</i>	-1.6	Translocase of inner mitochondrial membrane 8 homolog a1 (yeast)
<i>Scpep1</i>	-1.6	Serine carboxypeptidase 1
<i>Glce</i>	-1.6	Glucuronyl C5-epimerase
<i>Slc39a8</i>	-1.6	Solute carrier family 39 (metal ion transporter), member 8
<i>Kcnf1</i>	-1.6	Potassium voltage-gated channel, subfamily F, member 1
<i>Mknk1</i>	-1.6	MAP kinase-interacting serine/threonine kinase 1
<i>1500002C15Rik</i>	-1.6	RIKEN cDNA A930001M12 gene
<i>Grxcr1</i>	-1.6	glutaredoxin, cysteine rich 1
<i>Igf1r</i>	-1.6	Insulin-like growth factor I receptor
<i>Dus4l</i>	-1.6	Dihydrouridine synthase 4-like ( <i>S. cerevisiae</i> )
<i>Eprs</i>	-1.6	Glutamyl-prolyl-tRNA synthetase
<i>Adora3</i>	-1.6	Adenosine A3 receptor
<i>Ankrd10</i>	-1.6	Ankyrin repeat domain 10
<i>Cenpq</i>	-1.6	Centromere protein Q
<i>Olf1322</i>	-1.6	Olfactory receptor 1322
<i>Tsen15</i>	-1.6	RIKEN cDNA 5730449L18 gene
<i>Cntn1</i>	-1.6	Contactin 1
<i>Zfp238</i>	-1.6	Zinc finger protein 238

Appendix

<i>Paqr3</i>	-1.6	Progesterin and adipoQ receptor family member III
<i>Tars</i>	-1.6	Threonyl-tRNA synthetase
<i>Gtpbp2</i>	-1.6	GTP binding protein 2
<i>Tra2a</i>	-1.6	Transformer 2 alpha homolog (Drosophila)
<i>Slc1a4</i>	-1.6	Solute carrier family 1 (glutamate/neutral amino acid transporter), member 4
<i>1810011010Rik</i>	-1.6	RIKEN cDNA 1810011010 gene
<i>Otub2</i>	-1.7	OTU domain, ubiquitin aldehyde binding 2
<i>Chac1</i>	-1.7	ChaC, cation transport regulator-like 1 (E. coli)
<i>Ccdc47</i>	-1.7	Coiled-coil domain containing 47
<i>Akna</i>	-1.7	AT-hook transcription factor
<i>Snord53</i>	-1.7	small nucleolar RNA, C/D box 53
<i>Taf1a</i>	-1.7	TATA box binding protein (Tbp)-associated factor, RNA polymerase I, A
<i>Rpl13</i>	-1.7	Ribosomal protein L13
<i>Etv5</i>	-1.7	Ets variant gene 5
<i>Dapp1</i>	-1.7	Dual adaptor for phosphotyrosine and 3-phosphoinositides 1
<i>Eif2s2</i>	-1.7	Eukaryotic translation initiation factor 2, subunit 2 (beta)
<i>Gm3365</i>	-1.7	predicted gene 3365
<i>Fam135a</i>	-1.7	RIKEN cDNA 4921533L14 gene
<i>Ppp1r16b</i>	-1.7	Protein phosphatase 1, regulatory (inhibitor) subunit 16B
<i>Gm129</i>	-1.7	Gene model 129, (NCBI)
<i>Taf15</i>	-1.7	TAF15 RNA polymerase II, TATA box binding protein (TBP)-associated factor
<i>Cntnap2</i>	-1.7	Contactin associated protein-like 2
<i>Lrrfip2</i>	-1.7	Leucine rich repeat (in FLII) interacting protein 2
<i>Phgdh</i>	-1.7	3-phosphoglycerate dehydrogenase
<i>Angptl6</i>	-1.8	Angiopoietin-like 6
<i>2610044015Rik</i>	-1.8	RIKEN cDNA 2610044015 gene
<i>Slc7a3</i>	-1.8	Solute carrier family 7 (cationic amino acid transporter, y+ system), member 3
<i>Dock5</i>	-1.8	Dedicator of cytokinesis 5
<i>Extl1</i>	-1.8	Exostosin (multiple)-like 1
<i>Lonp1</i>	-1.8	Lon peptidase 1, mitochondrial
<i>Psph</i>	-1.8	Phosphoserine phosphatase
<i>Erlin1</i>	-1.8	ER lipid raft associated 1
<i>Cdh8</i>	-1.8	Cadherin 8
<i>Trpm3</i>	-1.8	Transient receptor potential cation channel, subfamily M, member 3
<i>BC023105</i>	-1.8	cDNA sequence BC023105
<i>Sgcd</i>	-1.8	Sarcoglycan, delta (dystrophin-associated glycoprotein)
<i>Ctnnal1</i>	-1.8	Catenin (cadherin associated protein), alpha-like 1
<i>Zcchc12</i>	-1.8	Zinc finger, CCHC domain containing 12
<i>Slc6a9</i>	-1.9	Solute carrier family 6 (neurotransmitter transporter, glycine), member 9
<i>Gm5246</i>	-1.9	predicted gene 5246
<i>Cyb5r2</i>	-1.9	Cytochrome b5 reductase 2
<i>1700016K19Rik</i>	-1.9	RIKEN cDNA 1700016K19 gene
<i>Vldlr</i>	-1.9	Very low density lipoprotein receptor
<i>Prlr</i>	-1.9	Prolactin receptor
<i>Cdh7</i>	-1.9	Cadherin 7, type 2
<i>Lgi2</i>	-1.9	Leucine-rich repeat LGI family, member 2
<i>Stard5</i>	-1.9	StAR-related lipid transfer (START) domain containing 5
<i>Zdhhc22</i>	-1.9	Zinc finger, DHHC-type containing 22
<i>Gnpat1</i>	-1.9	Glucosamine-phosphate N-acetyltransferase 1
<i>Phf10</i>	-1.9	PHD finger protein 10
<i>Ipcef1</i>	-1.9	RIKEN cDNA A130090K04 gene
<i>4930486G11Rik</i>	-1.9	RIKEN cDNA 4930486G11 gene
<i>lfrd1</i>	-2.0	Interferon-related developmental regulator 1

<i>Cyb5r1</i>	-2.0	Cytochrome b5 reductase 1
<i>Fh1</i>	-2.0	Fumarate hydratase 1
<i>Psat1</i>	-2.0	Phosphoserine aminotransferase 1
<i>Kcnh5</i>	-2.0	Potassium voltage-gated channel, subfamily H (eag-related), member 5
<i>Reln</i>	-2.0	Reelin
<i>Ddit3</i>	-2.1	DNA-damage inducible transcript 3
<i>Nrip2</i>	-2.1	Nuclear receptor interacting protein 2
<i>Anxa10</i>	-2.1	Annexin A10
<i>Aldh1l2</i>	-2.2	Aldehyde dehydrogenase 1 family, member L2
<i>Gm281</i>	-2.2	Gene model 281, (NCBI)
<i>Trib3</i>	-2.3	Tribbles homolog 3 (Drosophila)
<i>Ifit3</i>	-2.3	Interferon-induced protein with tetratricopeptide repeats 3
<i>Tnfrsf23</i>	-2.3	Tumor necrosis factor receptor superfamily, member 23
<i>Myd116</i>	-2.4	Myeloid differentiation primary response gene 116
<i>Lonrf3</i>	-2.4	LON peptidase N-terminal domain and ring finger 3
<i>Fbln5</i>	-2.4	Fibulin 5
<i>E530001K10Rik</i>	-2.5	RIKEN cDNA E530001K10 gene
<i>Napb</i>	-2.5	N-ethylmaleimide sensitive fusion protein attachment protein beta
<i>Dusp4</i>	-2.5	Dual specificity phosphatase 4
<i>Rsad2</i>	-2.9	Radical S-adenosyl methionine domain containing 2
<i>Steap1</i>	-2.9	Six transmembrane epithelial antigen of the prostate 1
<i>Cth</i>	-3.0	Cystathionase (cystathionine gamma-lyase)
<i>Mela</i>	-3.0	Melanoma antigen
<i>Cox6a2</i>	-3.8	Cytochrome c oxidase, subunit VI a, polypeptide 2

**Supplementary Table 2. GeneRanker analysis of the gene set displayed in Supplementary Table 1. Only the most significant tissues, cellular components, and disease are included.**

Tissue	p-value	observed genes
connective tissue	4.73E-33	50
extracellular matrix	1.43E-31	70
<b>Cellular component</b>		
extracellular region	2.50E-50	129
extracellular region part	2.11E-49	97
extracellular space	4.11E-44	81
extracellular matrix	8.14E-33	49
<b>Disease</b>		
fibrosis	5.40E-18	49
rupture	6.14E-17	28

**Supplementary Table 3. Differentially expressed genes in isolated islets from Dll1- $\beta$ KO and CreN mice of the second transcriptomics experiment (4.2.5.2), filtered for a fold change of at least 1.5 (FDR <10%).**

Gene Symbol	Dll1- $\beta$ KO/CreN	Gene Name
<i>Olfm3</i>	3.7	Olfactomedin 3
<i>Tnc</i>	3.3	Tenascin C
<i>Bgn</i>	3.3	Biglycan
<i>Acta2</i>	2.8	Actin, alpha 2, smooth muscle, aorta
<i>Inhba</i>	2.7	Inhibin beta-A
<i>Postn</i>	2.7	Periostin, osteoblast specific factor
<i>Timp1</i>	2.6	Tissue inhibitor of metalloproteinase 1
<i>Ptgs2</i>	2.6	Prostaglandin-endoperoxide synthase 2
<i>Esr1</i>	2.5	Estrogen receptor 1 (alpha)

Appendix

<b>Fgf2</b>	2.5	Fibroblast growth factor 2
<b>Olfml3</b>	2.4	Olfactomedin-like 3
<b>Fn1</b>	2.4	Fibronectin 1
<b>Ankrd34c</b>	2.3	ankyrin repeat domain 34C
<b>Tmem47</b>	2.3	Transmembrane protein 47
<b>Selp</b>	2.3	Selectin, platelet
<b>Pdgfrb</b>	2.3	Platelet derived growth factor receptor, beta polypeptide
<b>Spt1</b>	2.2	Salivary protein 1
<b>Vim</b>	2.2	Vimentin
<b>Serpine1</b>	2.2	Serine (or cysteine) peptidase inhibitor, clade E, member 1
<b>Peg10</b>	2.2	Paternally expressed 10
<b>Dpt</b>	2.2	Dermatopontin
<b>Lgals1</b>	2.1	Lectin, galactose binding, soluble 1
<b>Gfra3</b>	2.1	Glial cell line derived neurotrophic factor family receptor alpha 3
<b>Mfap5</b>	2.1	Microfibrillar associated protein 5
<b>Edn3</b>	2.1	Endothelin 3
<b>H2-Ab1</b>	2.1	Histocompatibility 2, class II antigen A, beta 1
<b>Aldh1a2</b>	2.1	Aldehyde dehydrogenase family 1, subfamily A2
<b>Fbn1</b>	2.1	Fibrillin 1
<b>Folr1</b>	2.0	Folate receptor 1 (adult)
<b>Sfrp1</b>	2.0	Secreted frizzled-related protein 1
<b>Ifitm3</b>	2.0	Interferon induced transmembrane protein 3
<b>Lox</b>	2.0	Lysyl oxidase
<b>Cdh11</b>	2.0	Cadherin 11
<b>Tjpi</b>	2.0	Tissue factor pathway inhibitor
<b>H2-Aa</b>	2.0	Histocompatibility 2, class II antigen A, alpha
<b>Cd44</b>	2.0	CD44 antigen
<b>Pdk4</b>	2.0	Pyruvate dehydrogenase kinase, isoenzyme 4
<b>Gria3</b>	2.0	Glutamate receptor, ionotropic, AMPA3 (alpha 3)
<b>Rcn3</b>	2.0	Reticulocalbin 3, EF-hand calcium binding domain
<b>Igsf21</b>	2.0	Immunoglobulin superfamily, member 21
<b>Phlda3</b>	2.0	Pleckstrin homology-like domain, family A, member 3
<b>Eda2r</b>	2.0	Ectodysplasin A2 isoform receptor
<b>Itga5</b>	2.0	Integrin alpha 5 (fibronectin receptor alpha)
<b>Axl</b>	2.0	AXL receptor tyrosine kinase
<b>Ndst4</b>	2.0	N-deacetylase/N-sulfotransferase (heparin glucosaminyl) 4
<b>Enpp1</b>	2.0	Ectonucleotide pyrophosphatase/phosphodiesterase 1
<b>Dio1</b>	2.0	Deiodinase, iodothyronine, type I
<b>9030617O03Rik</b>	1.9	RIKEN cDNA 9030617O03 gene
<b>Ctsc</b>	1.9	Cathepsin C
<b>Ctgf</b>	1.9	Connective tissue growth factor
<b>Ly6a</b>	1.9	Lymphocyte antigen 6 complex, locus A
<b>Mafb</b>	1.9	V-maf musculoaponeurotic fibrosarcoma oncogene family, protein B (avian)
<b>Fstl1</b>	1.9	Follistatin-like 1
<b>Lhfp</b>	1.9	Lipoma HMGIC fusion partner
<b>Srpx2</b>	1.9	Sushi-repeat-containing protein, X-linked 2
<b>Cnn2</b>	1.9	Calponin 2
<b>Plod2</b>	1.9	Procollagen lysine, 2-oxoglutarate 5-dioxygenase 2
<b>Serpinf1</b>	1.9	Serine (or cysteine) peptidase inhibitor, clade F, member 1
<b>Sgce</b>	1.9	Sarcoglycan, epsilon
<b>Fbp1</b>	1.9	Fructose biphosphatase 1
<b>Vip</b>	1.9	Vasoactive intestinal polypeptide
<b>Avpr1b</b>	1.9	Arginine vasopressin receptor 1B

Appendix

<b><i>Kcnj3</i></b>	1.9	Potassium inwardly-rectifying channel, subfamily J, member 3
<b><i>Col8a1</i></b>	1.9	Collagen, type VIII, alpha 1
<b><i>Cygb</i></b>	1.9	Cytoglobin
<b><i>Lrrc32</i></b>	1.8	leucine rich repeat containing 32
<b><i>Pou3f4</i></b>	1.8	POU domain, class 3, transcription factor 4
<b><i>Cd74</i></b>	1.8	CD74 antigen (invariant polypeptide of major histocompatibility complex, class II antigen-associated)
<b><i>Oxtr</i></b>	1.8	Oxytocin receptor
<b><i>Sparc</i></b>	1.8	Secreted acidic cysteine rich glycoprotein
<b><i>Fkbp10</i></b>	1.8	FK506 binding protein 10
<b><i>Anxa2</i></b>	1.8	Annexin A2
<b><i>Aebp1</i></b>	1.8	AE binding protein 1
<b><i>Gpm6a</i></b>	1.8	Glycoprotein m6a
<b><i>Ncam2</i></b>	1.8	Neural cell adhesion molecule 2
<b><i>Klhl13</i></b>	1.8	Kelch-like 13 (Drosophila)
<b><i>Igfbp4</i></b>	1.8	Insulin-like growth factor binding protein 4
<b><i>Penk</i></b>	1.8	Preproenkephalin
<b><i>Ace2</i></b>	1.8	Angiotensin I converting enzyme (peptidyl-dipeptidase A) 2
<b><i>Maml1</i></b>	1.8	mastermind-like domain containing 1
<b><i>Gatm</i></b>	1.8	Glycine amidinotransferase (L-arginine:glycine amidinotransferase)
<b><i>Gm609</i></b>	1.8	Gene model 609, (NCBI)
<b><i>Hhex</i></b>	1.8	Hematopoietically expressed homeobox
<b><i>Col1a1</i></b>	1.8	Collagen, type I, alpha 1
<b><i>Lum</i></b>	1.8	Lumican
<b><i>Prrx1</i></b>	1.8	Paired related homeobox 1
<b><i>Leprel1</i></b>	1.8	Leprecan-like 1
<b><i>Mgp</i></b>	1.7	Matrix Gla protein
<b><i>Aspn</i></b>	1.7	Asporin
<b><i>9130213B05Rik</i></b>	1.7	RIKEN cDNA 9130213B05 gene
<b><i>Plekhh1</i></b>	1.7	Pleckstrin homology domain containing, family B (evectins) member 1
<b><i>Mctp2</i></b>	1.7	Multiple C2 domains, transmembrane 2
<b><i>Col1a2</i></b>	1.7	Collagen, type I, alpha 2
<b><i>Cryab</i></b>	1.7	Crystallin, alpha B
<b><i>Pgm5</i></b>	1.7	Phosphoglucomutase 5
<b><i>Serpinh1</i></b>	1.7	Serine (or cysteine) peptidase inhibitor, clade H, member 1
<b><i>Gprc5a</i></b>	1.7	G protein-coupled receptor, family C, group 5, member A
<b><i>Sorcs2</i></b>	1.7	Sortilin-related VPS10 domain containing receptor 2
<b><i>Galnt13</i></b>	1.7	UDP-N-acetyl-alpha-D-galactosamine:polypeptide N-acetylgalactosaminyltransferase 13
<b><i>Sulf2</i></b>	1.7	Sulfatase 2
<b><i>Ms4a6c</i></b>	1.7	Membrane-spanning 4-domains, subfamily A, member 6C
<b><i>Pigr</i></b>	1.7	Polymeric immunoglobulin receptor
<b><i>Pla2g2d</i></b>	1.7	Phospholipase A2, group IID
<b><i>Lrrc8b</i></b>	1.7	Leucine rich repeat containing 8 family, member B
<b><i>Gfra1</i></b>	1.7	Glial cell line derived neurotrophic factor family receptor alpha 1
<b><i>Lbp</i></b>	1.7	Lipopolysaccharide binding protein
<b><i>Cfh</i></b>	1.7	Complement component factor h
<b><i>Vwde</i></b>	1.7	von Willebrand factor D and EGF domains
<b><i>Pros1</i></b>	1.7	Protein S (alpha)
<b><i>Cald1</i></b>	1.7	Caldesmon 1
<b><i>Slc38a5</i></b>	1.7	Solute carrier family 38, member 5
<b><i>Itpril2</i></b>	1.7	inositol 1,4,5-triphosphate receptor interacting protein-like 2
<b><i>Osmr</i></b>	1.7	Oncostatin M receptor

<i>Cyr61</i>	1.7	Cysteine rich protein 61
<i>Ccdc80</i>	1.7	Coiled-coil domain containing 80
<i>9030420J04Rik</i>	1.7	RIKEN cDNA 9030420J04 gene
<i>Bcl2</i>	1.7	B-cell leukemia/lymphoma 2
<i>Rbms3</i>	1.7	RNA binding motif, single stranded interacting protein
<i>4930539E08Rik</i>	1.7	RIKEN cDNA 4930539E08 gene
<i>Olfml2b</i>	1.7	Olfactomedin-like 2B
<i>Ccl5</i>	1.7	Chemokine (C-C motif) ligand 5
<i>Ednra</i>	1.7	Endothelin receptor type A
<i>Kcnk3</i>	1.7	Potassium channel, subfamily K, member 3
<i>Tm4sf1</i>	1.7	Transmembrane 4 superfamily member 1
<i>Slco2a1</i>	1.7	Solute carrier organic anion transporter family, member 2a1
<i>Sstr2</i>	1.7	Somatostatin receptor 2
<i>Cyrr1</i>	1.7	Cysteine and tyrosine-rich protein 1
<i>Gpx8</i>	1.7	glutathione peroxidase 8 (putative)
<i>AW551984</i>	1.7	Expressed sequence AW551984
<i>Oat</i>	1.7	Ornithine aminotransferase
<i>Rasgef1a</i>	1.7	RasGEF domain family, member 1A
<i>Ugt2b35</i>	1.7	UDP glucuronosyltransferase 2 family, polypeptide B35
<i>Sema3e</i>	1.7	Sema domain, immunoglobulin domain (Ig), short basic domain, secreted, (semaphorin) 3E
<i>C1qb</i>	1.7	Complement component 1, q subcomponent, beta polypeptide
<i>Gpx3</i>	1.7	Glutathione peroxidase 3
<i>Slc2a3</i>	1.7	Solute carrier family 2 (facilitated glucose transporter), member 3
<i>Has2</i>	1.7	Hyaluronan synthase 2
<i>Thbs1</i>	1.7	Thrombospondin 1
<i>Itga1</i>	1.7	Integrin alpha 1
<i>Ndrp2</i>	1.6	N-myc downstream regulated gene 2
<i>Ache</i>	1.6	Acetylcholinesterase
<i>Calb1</i>	1.6	Calbindin-28K
<i>BC030046</i>	1.6	CDNA sequence BC030046
<i>Wfdc17</i>	1.6	WAP four-disulfide core domain 17
<i>Mpeg1</i>	1.6	Macrophage expressed gene 1
<i>Arg1</i>	1.6	Arginase 1, liver
<i>Angptl2</i>	1.6	Angiopoietin-like 2
<i>Fgf14</i>	1.6	Fibroblast growth factor 14
<i>Msn</i>	1.6	Moesin
<i>Eng</i>	1.6	Endoglin
<i>Aldh1a3</i>	1.6	Aldehyde dehydrogenase family 1, subfamily A3
<i>Mmp14</i>	1.6	Matrix metalloproteinase 14 (membrane-inserted)
<i>Tspan18</i>	1.6	Tetraspanin 18
<i>A430107O13Rik</i>	1.6	RIKEN cDNA A430107O13 gene
<i>Arhgdib</i>	1.6	Rho, GDP dissociation inhibitor (GDI) beta
<i>Layn</i>	1.6	Layilin
<i>Wnk3</i>	1.6	WNK lysine deficient protein kinase 3
<i>Ptprk</i>	1.6	Protein tyrosine phosphatase, receptor type, K
<i>Slc40a1</i>	1.6	Solute carrier family 40 (iron-regulated transporter), member 1
<i>Pla2g4a</i>	1.6	Phospholipase A2, group IVA (cytosolic, calcium-dependent)
<i>Ascl1</i>	1.6	Achaete-scute complex homolog-like 1 (Drosophila)
<i>Fam46d</i>	1.6	family with sequence similarity 46, member D
<i>Klb</i>	1.6	Klotho beta
<i>Ebf1</i>	1.6	Early B-cell factor 1
<i>Pxdn</i>	1.6	Peroxidasin homolog (Drosophila)

<b>Lrp1</b>	1.6	Low density lipoprotein receptor-related protein 1
<b>Tgtp</b>	1.6	T-cell specific GTPase
<b>Nid1</b>	1.6	Nidogen 1
<b>Col6a3</b>	1.6	Collagen, type VI, alpha 3
<b>C1qc</b>	1.6	Complement component 1, q subcomponent, C chain
<b>Stmn2</b>	1.6	Stathmin-like 2
<b>Tgfb1</b>	1.6	Transforming growth factor, beta induced
<b>Runx1</b>	1.6	Runt related transcription factor 1
<b>Mkl2</b>	1.6	MKL/myocardin-like 2
<b>Acp5</b>	1.6	Acid phosphatase 5, tartrate resistant
<b>Ldha</b>	1.6	Lactate dehydrogenase A
<b>Jag1</b>	1.6	Jagged 1
<b>Epas1</b>	1.6	Endothelial PAS domain protein 1
<b>Cxcl14</b>	1.6	Chemokine (C-X-C motif) ligand 14
<b>Eef1a2</b>	1.6	Eukaryotic translation elongation factor 1 alpha 2
<b>Clstn2</b>	1.6	Calsyntenin 2
<b>Large</b>	1.6	Like-glycosyltransferase
<b>Heyl</b>	1.6	Hairy/enhancer-of-split related with YRPW motif-like
<b>Aplnr</b>	1.6	apelin receptor
<b>Ehd2</b>	1.6	EH-domain containing 2
<b>Cd81</b>	1.6	CD 81 antigen
<b>Mest</b>	1.6	Mesoderm specific transcript
<b>Smarca1</b>	1.6	SWI/SNF related, matrix associated, actin dependent regulator of chromatin, subfamily a, member 1
<b>Ptprz1</b>	1.6	Protein tyrosine phosphatase, receptor type Z, polypeptide 1
<b>Ldlrad3</b>	1.6	Low density lipoprotein receptor class A domain containing 3
<b>Tgfb1</b>	1.6	Transforming growth factor, beta 1
<b>Ctss</b>	1.6	Cathepsin S
<b>Piezo1</b>	1.6	piezo-type mechanosensitive ion channel component 1
<b>Des</b>	1.6	Desmin
<b>Ly86</b>	1.6	Lymphocyte antigen 86
<b>Adamts2</b>	1.6	A disintegrin-like and metallopeptidase (reprolysin type) with thrombospondin type 1 motif, 2
<b>Tnr</b>	1.6	Tenascin R
<b>Vcan</b>	1.6	Versican
<b>C8b</b>	1.5	Complement component 8, beta subunit
<b>Epb4.1l2</b>	1.5	Erythrocyte protein band 4.1-like 2
<b>Npr2</b>	1.5	Natriuretic peptide receptor 2
<b>Eltf1</b>	1.5	EGF, latrophilin seven transmembrane domain containing 1
<b>Ppargc1a</b>	1.5	Peroxisome proliferative activated receptor, gamma, coactivator 1 alpha
<b>Cd93</b>	1.5	CD93 antigen
<b>Cdkn1a</b>	1.5	Cyclin-dependent kinase inhibitor 1A (P21)
<b>Tgfb3</b>	1.5	Transforming growth factor, beta 3
<b>Bcat1</b>	1.5	Branched chain aminotransferase 1, cytosolic
<b>Sh2d5</b>	1.5	SH2 domain containing 5
<b>Wisp1</b>	1.5	WNT1 inducible signaling pathway protein 1
<b>Nefl</b>	1.5	Neurofilament, light polypeptide
<b>Cav2</b>	1.5	Caveolin 2
<b>Lin7a</b>	1.5	Lin-7 homolog A (C. elegans)
<b>Maml2</b>	1.5	Mastermind like 2 (Drosophila)
<b>Timp2</b>	1.5	Tissue inhibitor of metalloproteinase 2
<b>Itpr1</b>	1.5	Inositol 1,4,5-triphosphate receptor 1
<b>Oit1</b>	1.5	Oncoprotein induced transcript 1

Appendix

<i>Irx1</i>	1.5	Iroquois related homeobox 1 (Drosophila)
<i>Pdzrn3</i>	1.5	PDZ domain containing RING finger 3
<i>Ddr2</i>	1.5	Discoidin domain receptor family, member 2
<i>Corin</i>	1.5	Corin
<i>Timp3</i>	1.5	Tissue inhibitor of metalloproteinase 3
<i>Cxcl13</i>	1.5	Chemokine (C-X-C motif) ligand 13
<i>Zeb2</i>	1.5	Zinc finger E-box binding homeobox 2
<i>9130409I23Rik</i>	1.5	RIKEN cDNA 9130409I23 gene
<i>Slc16a7</i>	1.5	Solute carrier family 16 (monocarboxylic acid transporters), member 7
<i>Pcolce</i>	1.5	Procollagen C-endopeptidase enhancer protein
<i>Dbpht2</i>	1.5	DNA binding protein with his-thr domain
<i>Plxdc2</i>	1.5	Plexin domain containing 2
<i>1700086L19Rik</i>	1.5	RIKEN cDNA 1700086L19 gene
<i>Slc25a43</i>	1.5	Solute carrier family 25, member 43
<i>Sdc1</i>	1.5	Syndecan 1
<i>Dusp26</i>	1.5	Dual specificity phosphatase 26 (putative)
<i>Nrp1</i>	1.5	Neuropilin 1
<i>Dock1</i>	1.5	Dedicator of cyto-kinesis 1
<i>Col15a1</i>	1.5	Collagen, type XV
<i>Kdr</i>	1.5	Kinase insert domain protein receptor
<i>AI607873</i>	1.5	Expressed sequence AI607873
<i>Klhl32</i>	-1.5	Kelch-like 32 (Drosophila)
<i>Psat1</i>	-1.5	Phosphoserine aminotransferase 1
<i>Snord87</i>	-1.5	small nucleolar RNA, C/D box 87
<i>Snord49b</i>	-1.5	small nucleolar RNA, C/D box 49B
<i>Adora3</i>	-1.5	Adenosine A3 receptor
<i>Gm281</i>	-1.5	Gene model 281, (NCBI)
<i>Myo3a</i>	-1.5	Myosin IIIA
<i>Nrcam</i>	-1.6	Neuron-glia-CAM-related cell adhesion molecule
<i>Pgap1</i>	-1.6	post-GPI attachment to proteins 1
<i>Snord34</i>	-1.6	small nucleolar RNA, C/D box 34
<i>Phgdh</i>	-1.6	3-phosphoglycerate dehydrogenase
<i>Cbs</i>	-1.6	Cystathionine beta-synthase
<i>Hpse</i>	-1.6	Heparanase
<i>Fmo1</i>	-1.6	Flavin containing monooxygenase 1
<i>Tubb2b</i>	-1.6	Tubulin, beta 2b
<i>9530091C08Rik</i>	-1.6	RIKEN cDNA 9530091C08 gene
<i>Snord33</i>	-1.6	small nucleolar RNA, C/D box 33
<i>F630048H11Rik</i>	-1.6	RIKEN cDNA F630048H11 gene
<i>Syt13</i>	-1.6	Synaptotagmin-like 3
<i>Trpm3</i>	-1.6	Transient receptor potential cation channel, subfamily M, member 3
<i>Aldh1l2</i>	-1.6	Aldehyde dehydrogenase 1 family, member L2
<i>Gm10520</i>	-1.6	predicted gene 10520
<i>Steap1</i>	-1.6	Six transmembrane epithelial antigen of the prostate 1
<i>Palmd</i>	-1.6	Palmdelphin
<i>Hist2h3c2</i>	-1.6	Histone cluster 2, H3c2
<i>Il4i1</i>	-1.7	Interleukin 4 induced 1
<i>Gcnt1</i>	-1.7	Glucosaminyl (N-acetyl) transferase 1, core 2
<i>Gm16432</i>	-1.7	predicted gene 16432
<i>Rab3c</i>	-1.7	RAB3C, member RAS oncogene family
<i>Nos2</i>	-1.7	Nitric oxide synthase 2, inducible, macrophage
<i>Gm6999</i>	-1.7	predicted gene 6999
<i>1700084C01Rik</i>	-1.8	RIKEN cDNA 1700084C01 gene

<b><i>Snhg1</i></b>	-1.8	small nucleolar RNA host gene (non-protein coding) 1
<b><i>Kcnh5</i></b>	-1.8	Potassium voltage-gated channel, subfamily H (eag-related), member 5
<b><i>Cox6a2</i></b>	-1.9	Cytochrome c oxidase, subunit VI a, polypeptide 2
<b><i>Cth</i></b>	-1.9	Cystathionase (cystathionine gamma-lyase)
<b><i>Olf1322</i></b>	-2.0	Olfactory receptor 1322
<b><i>Fh1</i></b>	-2.2	Fumarate hydratase 1
<b><i>Mela</i></b>	-2.6	Melanoma antigen
<b><i>Chi3l1</i></b>	-3.3	Chitinase 3-like 1

**Supplementary Table 4. GeneRanker analysis of certified Cre-dependent genes (4.2.5.2).**

<b>Tissue</b>	<b>p-value</b>	<b>observed genes</b>
extracellular matrix	5.16E-38	59
connective tissue	1.57E-34	41
<b>Cellular component</b>		
extracellular region part	7.47E-39	65
extracellular region	7.03E-34	78
extracellular matrix	3.71E-31	38
<b>Disease</b>		
fibrosis	1.62E-17	36

**Supplementary Table 5. Differentially expressed genes in isolated islets from Dll1\_T720A mice and wild-type controls, filtered for a fold change of at least 1.5 and a FDR of <10% (4.3). Acinar-related genes were excluded.**

Gene Symbol	Dll1_T720A/WT	Gene Name
<i>Lox</i>	3.6	lysyl oxidase
<i>Mfap5</i>	3.6	microfibrillar associated protein 5
<i>Serpinf1</i>	3.0	serine (or cysteine) peptidase inhibitor, clade F, member 1
<i>Olfml3</i>	3.0	olfactomedin-like 3
<i>Ly6a</i>	2.9	lymphocyte antigen 6 complex, locus A
<i>Srpx2</i>	2.8	sushi-repeat-containing protein, X-linked 2
<i>Fmod</i>	2.8	fibromodulin
<i>Gpx8</i>	2.8	glutathione peroxidase 8 (putative)
<i>Tnc</i>	2.7	tenascin C
<i>Mmp2</i>	2.7	matrix metalloproteinase 2
<i>Fn1</i>	2.7	fibronectin 1
<i>Ly6c1</i>	2.6	lymphocyte antigen 6 complex, locus C1
<i>Lrrc32</i>	2.6	leucine rich repeat containing 32
<i>Ch25h</i>	2.6	cholesterol 25-hydroxylase
<i>Aebp1</i>	2.5	AE binding protein 1
<i>Inhba</i>	2.4	inhibin beta-A
<i>Ifi204</i>	2.4	interferon activated gene 204
<i>Dpt</i>	2.4	dermatopontin
<i>Fbln2</i>	2.4	fibulin 2
<i>Cxcl14</i>	2.4	chemokine (C-X-C motif) ligand 14
<i>Acta2</i>	2.4	actin, alpha 2, smooth muscle, aorta
<i>Pdpn</i>	2.4	podoplanin
<i>Tnfaip6</i>	2.4	tumor necrosis factor alpha induced protein 6
<i>Ptgs2</i>	2.3	prostaglandin-endoperoxide synthase 2
<i>Thbs1</i>	2.3	thrombospondin 1
<i>Penk</i>	2.3	preproenkephalin
<i>Serpinb9b</i>	2.3	serine (or cysteine) peptidase inhibitor, clade B, member 9b
<i>Has2</i>	2.3	hyaluronan synthase 2
<i>Postn</i>	2.3	periostin, osteoblast specific factor
<i>Fbn1</i>	2.3	fibrillin 1
<i>Gm10334</i>	2.3	predicted gene 10334
<i>Anxa3</i>	2.2	annexin A3
<i>Cdh11</i>	2.2	cadherin 11
<i>Cygb</i>	2.2	cytoglobin
<i>Serpine1</i>	2.2	serine (or cysteine) peptidase inhibitor, clade E, member 1
<i>9030420J04Rik</i>	2.2	RIKEN cDNA 9030420J04 gene
<i>Timp1</i>	2.2	tissue inhibitor of metalloproteinase 1
<i>Slc43a3</i>	2.2	solute carrier family 43, member 3
<i>Osmr</i>	2.1	oncostatin M receptor
<i>Ly6c2</i>	2.1	lymphocyte antigen 6 complex, locus C2
<i>Anxa2</i>	2.1	annexin A2
<i>Tmem47</i>	2.1	transmembrane protein 47
<i>Mmp14</i>	2.1	matrix metalloproteinase 14 (membrane-inserted)
<i>Itga5</i>	2.1	integrin alpha 5 (fibronectin receptor alpha)
<i>Vcan</i>	2.1	versican
<i>Nfib</i>	2.1	nuclear factor I
<i>Antxr1</i>	2.1	anthrax toxin receptor 1
<i>Sparc</i>	2.0	secreted acidic cysteine rich glycoprotein
<i>Lsp1</i>	2.0	lymphocyte specific 1
<i>Col8a1</i>	2.0	collagen, type VIII, alpha 1

Appendix

<b>Tgfb3</b>	2.0	transforming growth factor, beta 3
<b>Gm5409</b>	2.0	predicted gene 5409
<b>Ccdc80</b>	2.0	coiled-coil domain containing 80
<b>Fkbp10</b>	2.0	FK506 binding protein 10
<b>Timp3</b>	2.0	tissue inhibitor of metalloproteinase 3
<b>Cyp1b1</b>	2.0	cytochrome P450, family 1, subfamily b, polypeptide 1
<b>Dpysl3</b>	2.0	dihydropyrimidinase-like 3
<b>Col6a3</b>	2.0	collagen, type VI, alpha 3
<b>Gpm6b</b>	2.0	glycoprotein m6b
<b>F2r</b>	2.0	coagulation factor II (thrombin) receptor
<b>Egr2</b>	2.0	early growth response 2
<b>Colec12</b>	2.0	collectin sub-family member 12
<b>Bgn</b>	2.0	biglycan
<b>Cyr61</b>	1.9	cysteine rich protein 61
<b>Pla2g4a</b>	1.9	phospholipase A2, group IVA (cytosolic, calcium-dependent)
<b>Layn</b>	1.9	layilin
<b>Vim</b>	1.9	vimentin
<b>Prrx1</b>	1.9	paired related homeobox 1
<b>Dab2</b>	1.9	disabled homolog 2 (Drosophila)
<b>Fstl1</b>	1.9	folliculin-like 1
<b>Ccl7</b>	1.9	chemokine (C-C motif) ligand 7
<b>Ctgf</b>	1.9	connective tissue growth factor
<b>Il11</b>	1.9	interleukin 11
<b>Enpp1</b>	1.9	ectonucleotide pyrophosphatase
<b>Loxl1</b>	1.9	lysyl oxidase-like 1
<b>Nes</b>	1.9	nestin
<b>Gfpt2</b>	1.9	glutamine fructose-6-phosphate transaminase 2
<b>Fgf2</b>	1.9	fibroblast growth factor 2
<b>Nkd2</b>	1.9	naked cuticle 2 homolog (Drosophila)
<b>Thbs2</b>	1.9	thrombospondin 2
<b>Col1a1</b>	1.8	collagen, type I, alpha 1
<b>Cd209a</b>	1.8	CD209a antigen
<b>Rnu2</b>	1.8	U2 small nuclear RNA
<b>Ddr2</b>	1.8	discoidin domain receptor family, member 2
<b>Col1a2</b>	1.8	collagen, type I, alpha 2
<b>Cnn2</b>	1.8	calponin 2
<b>Col15a1</b>	1.8	collagen, type XV, alpha 1
<b>Emp3</b>	1.8	epithelial membrane protein 3
<b>Antxr2</b>	1.8	anthrax toxin receptor 2
<b>Msn</b>	1.8	moesin
<b>Ebf1</b>	1.8	early B-cell factor 1
<b>P4ha3</b>	1.8	procollagen-proline, 2-oxoglutarate 4-dioxygenase (proline 4-hydroxylase), alpha polypeptide III
<b>Fscn1</b>	1.8	fascin homolog 1, actin bundling protein (Strongylocentrotus purpuratus)
<b>Cilp</b>	1.8	cartilage intermediate layer protein, nucleotide pyrophosphohydrolase
<b>Nid1</b>	1.8	nidogen 1
<b>Pdgfrb</b>	1.8	platelet derived growth factor receptor, beta polypeptide
<b>Snord116</b>	1.8	small nucleolar RNA, C
<b>Tgfb1</b>	1.8	transforming growth factor, beta 1
<b>Eng</b>	1.8	endoglin
<b>Vgll3</b>	1.8	vestigial like 3 (Drosophila)
<b>Gpnmb</b>	1.8	glycoprotein (transmembrane) nmb
<b>Lhfp</b>	1.8	lipoma HMGIC fusion partner
<b>Rprl1</b>	1.7	ribonuclease P RNA-like 1

<i>Csrp2</i>	1.7	cysteine and glycine-rich protein 2
<i>Mrc2</i>	1.7	mannose receptor, C type 2
<i>Ankrd1</i>	1.7	ankyrin repeat domain 1 (cardiac muscle)
<i>Zeb2</i>	1.7	zinc finger E-box binding homeobox 2
<i>Fam38a</i>	1.7	family with sequence similarity 38, member A
<i>Olfml2b</i>	1.7	olfactomedin-like 2B
<i>1110032E23Rik</i>	1.7	RIKEN cDNA 1110032E23 gene
<i>Sprr2a</i>	1.7	small proline-rich protein 2A
<i>Cmtm3</i>	1.7	CKLF-like MARVEL transmembrane domain containing 3
<i>Myof</i>	1.7	myoferlin
<i>Fxyd5</i>	1.7	FXYD domain-containing ion transport regulator 5
<i>Cmklr1</i>	1.7	chemokine-like receptor 1
<i>Mmp7</i>	1.7	matrix metalloproteinase 7
<i>Npy</i>	1.7	neuropeptide Y
<i>Rai14</i>	1.7	retinoic acid induced 14
<i>Zfp36l1</i>	1.7	zinc finger protein 36, C3H type-like 1
<i>Pcolce</i>	1.7	procollagen C-endopeptidase enhancer protein
<i>Rny3</i>	1.7	RNA, Y3 small cytoplasmic (associated with Ro protein)
<i>Gsta3</i>	1.7	glutathione S-transferase, alpha 3
<i>Pmp22</i>	1.7	peripheral myelin protein 22
<i>Flna</i>	1.7	filamin, alpha
<i>Snora52</i>	1.7	small nucleolar RNA, H
<i>Ano1</i>	1.7	anoctamin 1, calcium activated chloride channel
<i>Itpril2</i>	1.7	inositol 1,4,5-triphosphate receptor interacting protein-like 2
<i>Adamts1</i>	1.7	a disintegrin-like and metalloproteinase (reprolysin type) with thrombospondin type 1 motif, 1
<i>Heyl</i>	1.7	hairly
<i>Sh3pxd2b</i>	1.6	SH3 and PX domains 2B
<i>Mfap4</i>	1.6	microfibrillar-associated protein 4
<i>Cspg4</i>	1.6	chondroitin sulfate proteoglycan 4
<i>Gja1</i>	1.6	gap junction protein, alpha 1
<i>Gpr124</i>	1.6	G protein-coupled receptor 124
<i>Angptl2</i>	1.6	angiopoietin-like 2
<i>Pdzrn3</i>	1.6	PDZ domain containing RING finger 3
<i>Capg</i>	1.6	capping protein (actin filament), gelsolin-like
<i>Lrrc8c</i>	1.6	leucine rich repeat containing 8 family, member C
<i>Nrp1</i>	1.6	neuropilin 1
<i>Cd34</i>	1.6	CD34 antigen
<i>Slf3</i>	1.6	schlafen 3
<i>Plat</i>	1.6	plasminogen activator, tissue
<i>Ngfr</i>	1.6	nerve growth factor receptor (TNFR superfamily, member 16)
<i>Tm4sf1</i>	1.6	transmembrane 4 superfamily member 1
<i>Fkbp7</i>	1.6	FK506 binding protein 7
<i>Mgp</i>	1.6	matrix Gla protein
<i>Vcam1</i>	1.6	vascular cell adhesion molecule 1
<i>Chst2</i>	1.6	carbohydrate sulfotransferase 2
<i>Jag1</i>	1.6	jagged 1
<i>Runx1</i>	1.6	runt related transcription factor 1
<i>Lrp1</i>	1.6	low density lipoprotein receptor-related protein 1
<i>Plk1</i>	1.6	polo-like kinase 1 (Drosophila)
<i>Sema7a</i>	1.6	sema domain, immunoglobulin domain (Ig), and GPI membrane anchor, (semaphorin) 7A
<i>Hspb1</i>	1.6	heat shock protein 1
<i>Mustn1</i>	1.6	musculoskeletal, embryonic nuclear protein 1

Appendix

<i>Sparcl1</i>	1.6	SPARC-like 1
<i>Adamts9</i>	1.6	a disintegrin-like and metallopeptidase (reprolysin type) with thrombospondin type 1 motif, 9
<i>Ltbp4</i>	1.6	latent transforming growth factor beta binding protein 4
<i>Axl</i>	1.5	AXL receptor tyrosine kinase
<i>Adcy7</i>	1.5	adenylate cyclase 7
<i>Ccl11</i>	1.5	chemokine (C-C motif) ligand 11
<i>Pxdn</i>	1.5	peroxidasin homolog (Drosophila)
<i>Adam12</i>	1.5	a disintegrin and metallopeptidase domain 12 (meltrin alpha)
<i>Ltbp2</i>	1.5	latent transforming growth factor beta binding protein 2
<i>Slit3</i>	1.5	slit homolog 3 (Drosophila)
<i>Serpinh1</i>	1.5	serine (or cysteine) peptidase inhibitor, clade H, member 1
<i>Ecm1</i>	1.5	extracellular matrix protein 1
<i>Finc</i>	1.5	filamin C, gamma
<i>Adamts2</i>	1.5	a disintegrin-like and metallopeptidase (reprolysin type) with thrombospondin type 1 motif, 2
<i>Ehd2</i>	1.5	EH-domain containing 2
<i>Col6a2</i>	1.5	collagen, type VI, alpha 2
<i>Notch2</i>	1.5	Notch gene homolog 2 (Drosophila)
<i>Fhl3</i>	1.5	four and a half LIM domains 3
<i>Msrb3</i>	1.5	methionine sulfoxide reductase B3
<i>Tgfb1</i>	1.5	transforming growth factor, beta induced
<i>Ugt2b35</i>	1.5	UDP glucuronosyltransferase 2 family, polypeptide B35
<i>Des</i>	1.5	desmin
<i>Hspg2</i>	1.5	perlecan (heparan sulfate proteoglycan 2)
<i>Plod2</i>	1.5	procollagen lysine, 2-oxoglutarate 5-dioxygenase 2
<i>Palld</i>	1.5	palladin, cytoskeletal associated protein
<i>Tgfb1i1</i>	1.5	transforming growth factor beta 1 induced transcript 1
<i>Pmepa1</i>	1.5	prostate transmembrane protein, androgen induced 1
<i>1700084C01Rik</i>	-1.5	RIKEN cDNA 1700084C01 gene
<i>Neurl3</i>	-1.5	neuralized homolog 3 homolog (Drosophila)
<i>Tnfaip3</i>	-1.5	tumor necrosis factor, alpha-induced protein 3
<i>Stom</i>	-1.6	stomatin
<i>C1rb</i>	-1.6	complement component 1, r subcomponent B
<i>Zc3h12a</i>	-1.6	zinc finger CCCH type containing 12A
<i>Npas2</i>	-1.6	neuronal PAS domain protein 2
<i>5830443L24Rik</i>	-1.7	RIKEN cDNA 5830443L24 gene
<i>Sync</i>	-1.7	syncoilin
<i>Slpi</i>	-1.7	secretory leukocyte peptidase inhibitor
<i>Lyn</i>	-1.7	Yamaguchi sarcoma viral (v-yes-1) oncogene homolog
<i>Tnfrsf11b</i>	-1.7	tumor necrosis factor receptor superfamily, member 11b (osteoprotegerin)
<i>Kl</i>	-1.7	klotho
<i>Irak1</i>	-1.8	interleukin-1 receptor-associated kinase 1
<i>Nfkb1a</i>	-1.8	nuclear factor of kappa light polypeptide gene enhancer in B-cells inhibitor, alpha
<i>Spp1</i>	-1.9	secreted phosphoprotein 1
<i>C3</i>	-1.9	complement component 3
<i>Gbp4</i>	-1.9	guanylate binding protein 4
<i>Gpr182</i>	-1.9	G protein-coupled receptor 182
<i>Pglyrp1</i>	-2.0	peptidoglycan recognition protein 1
<i>1600029D21Rik</i>	-2.0	RIKEN cDNA 1600029D21 gene
<i>Mpa2l</i>	-2.1	macrophage activation 2 like
<i>Serpina3n</i>	-2.1	serine (or cysteine) peptidase inhibitor, clade A, member 3N
<i>Tifa</i>	-2.1	TRAF-interacting protein with forkhead-associated domain

<i>Fgb</i>	-2.1	fibrinogen beta chain
<i>Ltf</i>	-2.1	lactotransferrin
<i>Fgg</i>	-2.1	fibrinogen gamma chain
<i>Nos2</i>	-2.2	nitric oxide synthase 2, inducible
<i>D17H6S56E-5</i>	-2.2	DNA segment, Chr 17, human D6S56E 5
<i>Icam1</i>	-2.2	intercellular adhesion molecule 1
<i>Birc3</i>	-2.2	baculoviral IAP repeat-containing 3
<i>Pigr</i>	-2.2	polymeric immunoglobulin receptor
<i>Saa3</i>	-2.6	serum amyloid A 3
<i>Ccl28</i>	-2.8	chemokine (C-C motif) ligand 28
<i>Orm1</i>	-3.0	orosomucoid 1
<i>Lcn2</i>	-3.7	lipocalin 2
<i>Steap4</i>	-5.1	STEAP family member 4
<i>Cfb</i>	-6.5	complement factor B
<i>Chi3l1</i>	-22.0	chitinase 3-like 1

**Supplementary Table 6. Differentially expressed genes in islets isolated from *Pax6<sup>Leca2</sup>* and wild-type mice aged four weeks, filtered for a fold change of at least 2 and a FDR of <10% (4.4). Acinar-related genes were excluded.**

Gene Symbol	<i>Pax6<sup>Leca2</sup></i> /WT	Gene Name
<i>Tacr3</i>	14.3	tachykinin receptor 3
<b>1810009J06Rik</b>	9.3	RIKEN cDNA 1810009J06 gene
<i>Msln</i>	5.1	mesothelin
<i>Dlk1</i>	5.1	delta-like 1 homolog (Drosophila)
<b>EG436523</b>	4.9	predicted gene, EG436523
<i>Vwde</i>	4.7	von Willebrand factor D and EGF domains
<b>Gm10334</b>	4.3	predicted gene 10334
<i>Cnr1</i>	4.2	cannabinoid receptor 1 (brain)
<i>Slc35f4</i>	4.0	solute carrier family 35, member F4
<i>Iqsec3</i>	3.8	IQ motif and Sec7 domain 3
<i>Dapl1</i>	3.7	death associated protein-like 1
<i>Dpp10</i>	3.7	dipeptidylpeptidase 10
<i>Enpp3</i>	3.6	ectonucleotide pyrophosphatase/phosphodiesterase 3
<i>Slc38a11</i>	3.5	solute carrier family 38, member 11
<i>Cdh9</i>	3.5	cadherin 9
<i>Cybb</i>	3.4	cytochrome b-245, beta polypeptide
<i>Vstm2a</i>	3.4	V-set and transmembrane domain containing 2A
<i>Cd55</i>	3.3	CD55 antigen
<i>Lyz2</i>	3.3	lysozyme 2
<b>1600029D21Rik</b>	3.1	RIKEN cDNA 1600029D21 gene
<i>Csn3</i>	3.1	casein kappa
<i>Ddc</i>	3.1	dopa decarboxylase
<i>Prrg3</i>	3.1	proline rich Gla (G-carboxyglutamic acid) 3 (transmembrane)
<i>Gucy2c</i>	3.1	guanylate cyclase 2c
<i>Rerg</i>	3.1	RAS-like, estrogen-regulated, growth-inhibitor
<i>Egflam</i>	3.0	EGF-like, fibronectin type III and laminin G domains
<b>A430107O13Rik</b>	3.0	RIKEN cDNA A430107O13 gene
<i>Lrch2</i>	3.0	leucine-rich repeats and calponin homology (CH) domain containing 2
<i>Chst8</i>	2.9	carbohydrate (N-acetylgalactosamine 4-0) sulfotransferase 8
<i>Necab2</i>	2.9	N-terminal EF-hand calcium binding protein 2
<i>Dmrt1</i>	2.9	doublesex and mab-3 related transcription factor like family A1
<i>Slc38a1</i>	2.8	solute carrier family 38, member 1

Appendix

<b>Nxph1</b>	2.8	neurexophilin 1
<b>Tmem132b</b>	2.8	transmembrane protein 132B
<b>Ly86</b>	2.8	lymphocyte antigen 86
<b>Hs6st2</b>	2.7	heparan sulfate 6-O-sulfotransferase 2
<b>Trim9</b>	2.7	tripartite motif-containing 9
<b>1100001E04Rik</b>	2.7	RIKEN cDNA 1100001E04 gene
<b>C1ql3</b>	2.7	C1q-like 3
<b>Enpep</b>	2.7	glutamyl aminopeptidase
<b>Nebi</b>	2.6	nebullette
<b>Pgf</b>	2.6	placental growth factor
<b>P2ry13</b>	2.5	purinergic receptor P2Y, G-protein coupled 13
<b>Cd53</b>	2.4	CD53 antigen
<b>Galnt13</b>	2.4	UDP-N-acetyl-alpha-D-galactosamine:polypeptide N-acetylgalactosaminyltransferase 13
<b>Magi2</b>	2.4	membrane associated guanylate kinase, WW and PDZ domain containing 2
<b>4931429I11Rik</b>	2.4	RIKEN cDNA 4931429I11 gene
<b>Tmem110</b>	2.4	transmembrane protein 110
<b>Npnt</b>	2.4	nephronectin
<b>Clec7a</b>	2.3	C-type lectin domain family 7, member a
<b>Stc2</b>	2.3	stanniocalcin 2
<b>Crim1</b>	2.3	cysteine rich transmembrane BMP regulator 1 (chordin like)
<b>Neurog3</b>	2.3	neurogenin 3
<b>Rab38</b>	2.3	RAB38, member of RAS oncogene family
<b>Ankrd34b</b>	2.3	ankyrin repeat domain 34B
<b>Oprl1</b>	2.2	opioid receptor-like 1
<b>Tnr</b>	2.2	tenascin R
<b>6430704M03Rik</b>	2.2	RIKEN cDNA 6430704M03 gene
<b>Gabra3</b>	2.2	gamma-aminobutyric acid (GABA) A receptor, subunit alpha 3
<b>Cntnap5b</b>	2.2	contactin associated protein-like 5B
<b>Fhl2</b>	2.2	four and a half LIM domains 2
<b>Ust</b>	2.2	uronyl-2-sulfotransferase
<b>Il17re</b>	2.2	interleukin 17 receptor E
<b>Lrrn3</b>	2.2	leucine rich repeat protein 3, neuronal
<b>Dbc1</b>	2.2	deleted in bladder cancer 1 (human)
<b>Gpr120</b>	2.1	G protein-coupled receptor 120
<b>Lgi1</b>	2.1	leucine-rich repeat LGI family, member 1
<b>Jam2</b>	2.1	junction adhesion molecule 2
<b>9130213B05Rik</b>	2.1	RIKEN cDNA 9130213B05 gene
<b>Klhl13</b>	2.1	kelch-like 13 (Drosophila)
<b>Gcnt3</b>	2.1	glucosaminyl (N-acetyl) transferase 3, mucin type
<b>Expi</b>	2.1	extracellular proteinase inhibitor
<b>Arap2</b>	2.1	ArfGAP with RhoGAP domain, ankyrin repeat and PH domain 2
<b>Eapp</b>	2.1	E2F-associated phosphoprotein
<b>Myo15b</b>	2.1	myosin XVb
<b>Cecr2</b>	2.1	cat eye syndrome chromosome region, candidate 2 homolog (human)
<b>Fgf14</b>	2.1	fibroblast growth factor 14
<b>Trpm3</b>	2.1	transient receptor potential cation channel, subfamily M, member 3
<b>Rasgrf2</b>	2.1	RAS protein-specific guanine nucleotide-releasing factor 2
<b>Dock3</b>	2.0	dedicator of cyto-kinesis 3
<b>Rasd2</b>	2.0	RASD family, member 2
<b>Cer1</b>	2.0	cerberus 1 homolog (Xenopus laevis)
<b>Itpr1</b>	2.0	inositol 1,4,5-triphosphate receptor 1
<b>Elmod1</b>	2.0	ELMO domain containing 1
<b>C1qc</b>	2.0	complement component 1, q subcomponent, C chain

Appendix

<b>AW551984</b>	2.0	expressed sequence AW551984
<b>Rab17</b>	-2.0	RAB17, member RAS oncogene family
<b>Itpkb</b>	-2.0	inositol 1,4,5-trisphosphate 3-kinase B
<b>Unkl</b>	-2.0	unkempt-like (Drosophila)
<b>L1cam</b>	-2.0	L1 cell adhesion molecule
<b>Sult1c2</b>	-2.0	sulfotransferase family, cytosolic, 1C, member 2
<b>Ucn3</b>	-2.0	urocortin 3
<b>Mlph</b>	-2.0	melanophilin
<b>Itgb8</b>	-2.0	integrin beta 8
<b>Car15</b>	-2.1	carbonic anhydrase 15
<b>Mpp3</b>	-2.1	membrane protein, palmitoylated 3 (MAGUK p55 subfamily member 3)
<b>Muc4</b>	-2.1	mucin 4
<b>Mlxipl</b>	-2.1	MLX interacting protein-like
<b>Camk1g</b>	-2.1	calcium/calmodulin-dependent protein kinase I gamma
<b>AK220484</b>	-2.1	cDNA sequence AK220484
<b>Rab3c</b>	-2.2	RAB3C, member RAS oncogene family
<b>Prlr</b>	-2.2	prolactin receptor
<b>Ttc28</b>	-2.2	tetratricopeptide repeat domain 28
<b>Blnk</b>	-2.2	B-cell linker
<b>BC039632</b>	-2.2	cDNA sequence BC039632
<b>Gpr158</b>	-2.2	G protein-coupled receptor 158
<b>Jph3</b>	-2.2	junctophilin 3
<b>Crybb3</b>	-2.2	crystallin, beta B3
<b>Slc26a1</b>	-2.2	solute carrier family 26 (sulfate transporter), member 1
<b>Calml4</b>	-2.3	calmodulin-like 4
<b>Abcb4</b>	-2.3	ATP-binding cassette, sub-family B (MDR/TAP), member 4
<b>Pcx</b>	-2.3	pyruvate carboxylase
<b>Rnf182</b>	-2.3	ring finger protein 182
<b>Fgb</b>	-2.3	fibrinogen beta chain
<b>Adh1</b>	-2.3	alcohol dehydrogenase 1 (class I)
<b>Ffar3</b>	-2.4	free fatty acid receptor 3
<b>Ttyh1</b>	-2.4	tweety homolog 1 (Drosophila)
<b>Fibin</b>	-2.4	fin bud initiation factor homolog (zebrafish)
<b>Hpse</b>	-2.4	heparanase
<b>Nostrin</b>	-2.4	nitric oxide synthase trafficker
<b>BC023105</b>	-2.4	cDNA sequence BC023105
<b>4930550C14Rik</b>	-2.4	RIKEN cDNA 4930550C14 gene
<b>Slc4a10</b>	-2.4	solute carrier family 4, sodium bicarbonate cotransporter-like, member 10
<b>Vstm2l</b>	-2.5	V-set and transmembrane domain containing 2-like
<b>Adora1</b>	-2.5	adenosine A1 receptor
<b>Fmo1</b>	-2.5	flavin containing monooxygenase 1
<b>Ccl28</b>	-2.5	chemokine (C-C motif) ligand 28
<b>Chi3l1</b>	-2.5	chitinase 3-like 1
<b>Slitrk6</b>	-2.5	SLIT and NTRK-like family, member 6
<b>Pstpip2</b>	-2.8	proline-serine-threonine phosphatase-interacting protein 2
<b>Ipcef1</b>	-2.9	interaction protein for cytohesin exchange factors 1
<b>Grin1</b>	-3.0	glutamate receptor, ionotropic, NMDA1 (zeta 1)
<b>Hspa12a</b>	-3.0	heat shock protein 12A
<b>Gpm6a</b>	-3.1	glycoprotein m6a
<b>Ppp1r1a</b>	-3.2	protein phosphatase 1, regulatory (inhibitor) subunit 1A
<b>Kcnh5</b>	-3.2	potassium voltage-gated channel, subfamily H (eag-related), member 5
<b>Serpina3n</b>	-3.4	serine (or cysteine) peptidase inhibitor, clade A, member 3N
<b>Nrcam</b>	-3.6	neuron-glia-CAM-related cell adhesion molecule
<b>B3galt5</b>	-3.7	UDP-Gal:betaGlcNAc beta 1,3-galactosyltransferase, polypeptide 5

<b>Defb1</b>	-3.7	defensin beta 1
<b>Lyve1</b>	-4.0	lymphatic vessel endothelial hyaluronan receptor 1
<b>G6pc2</b>	-4.0	glucose-6-phosphatase, catalytic, 2
<b>Angptl7</b>	-4.0	angiopoietin-like 7
<b>Spc25</b>	-4.1	SPC25, NDC80 kinetochore complex component, homolog (S. cerevisiae)
<b>Gcgr</b>	-4.1	glucagon receptor
<b>Cdh8</b>	-4.6	cadherin 8
<b>Tmem215</b>	-5.1	transmembrane protein 215
<b>Robo1</b>	-5.2	roundabout homolog 1 (Drosophila)
<b>Nell1</b>	-5.8	NEL-like 1 (chicken)
<b>Serpina7</b>	-6.1	serine (or cysteine) peptidase inhibitor, clade A (alpha-1 antiproteinase, antitrypsin), member 7
<b>Ptprz1</b>	-6.1	protein tyrosine phosphatase, receptor type Z, polypeptide 1
<b>Cntfr</b>	-6.4	ciliary neurotrophic factor receptor
<b>Slco1a5</b>	-6.4	solute carrier organic anion transporter family, member 1a5
<b>Edn3</b>	-7.8	endothelin 3
<b>Ffar1</b>	-23.3	free fatty acid receptor 1

**Supplementary Table 7. Differentially expressed genes in islets isolated from *Pax6*<sup>Leca2/wt</sup> and wild-type mice aged four weeks, filtered for a fold change of at least 2 and a FDR of <10% (4.4). Acinar-related genes were excluded.**

<b>Gene Symbol</b>	<b><i>Pax6</i><sup>Leca2/wt</sup>/WT</b>	<b>Gene Name</b>
<b><i>Tacr3</i></b>	4.4	tachykinin receptor 3
<b><i>Msln</i></b>	3.0	mesothelin
<b><i>Dpp10</i></b>	2.1	dipeptidylpeptidase 10
<b><i>Egflam</i></b>	2.0	EGF-like, fibronectin type III and laminin G domains
<b><i>Cecr2</i></b>	2.0	cat eye syndrome chromosome region, candidate 2 homolog (human)
<b><i>Necab2</i></b>	2.0	N-terminal EF-hand calcium binding protein 2
<b><i>Ceacam1</i></b>	-2.0	carcinoembryonic antigen-related cell adhesion molecule 1
<b><i>Ifit3</i></b>	-2.0	interferon-induced protein with tetratricopeptide repeats 3
<b><i>EG634650</i></b>	-2.0	predicted gene, EG634650
<b><i>Ptgs2</i></b>	-2.0	prostaglandin-endoperoxide synthase 2
<b><i>Selp</i></b>	-2.0	selectin, platelet
<b><i>Ifit2</i></b>	-2.0	interferon-induced protein with tetratricopeptide repeats 2
<b><i>Gpm6a</i></b>	-2.0	glycoprotein m6a
<b><i>Cpb2</i></b>	-2.1	carboxypeptidase B2 (plasma)
<b><i>Nrcam</i></b>	-2.1	neuron-glia-CAM-related cell adhesion molecule
<b><i>Ms4a4d</i></b>	-2.1	membrane-spanning 4-domains, subfamily A, member 4D
<b><i>Gbp5</i></b>	-2.1	guanylate binding protein 5
<b><i>Blnk</i></b>	-2.1	B-cell linker
<b><i>BC057170</i></b>	-2.1	cDNA sequence BC057170
<b><i>Cfb</i></b>	-2.1	complement factor B
<b><i>Rnu73b</i></b>	-2.1	U73B small nuclear RNA
<b><i>Rtp4</i></b>	-2.1	receptor transporter protein 4
<b><i>ligp1</i></b>	-2.2	interferon inducible GTPase 1
<b><i>Rsad2</i></b>	-2.2	radical S-adenosyl methionine domain containing 2
<b><i>Ifi47</i></b>	-2.2	interferon gamma inducible protein 47
<b><i>Sp100</i></b>	-2.2	nuclear antigen Sp100
<b><i>Gm12250</i></b>	-2.2	predicted gene 12250
<b><i>Ptprz1</i></b>	-2.3	protein tyrosine phosphatase, receptor type Z, polypeptide 1
<b><i>Ccl2</i></b>	-2.3	chemokine (C-C motif) ligand 2
<b><i>Trim30</i></b>	-2.3	tripartite motif-containing 30
<b><i>Serpina7</i></b>	-2.3	serine (or cysteine) peptidase inhibitor, clade A (alpha-1 antiproteinase,

		antitrypsin), member 7
<i>Gbp3</i>	-2.3	guanylate binding protein 3
<i>Gm5431</i>	-2.4	predicted gene 5431
<i>Cxcl10</i>	-2.4	chemokine (C-X-C motif) ligand 10
<i>Ifi203</i>	-2.4	interferon activated gene 203
<i>I830012O16Rik</i>	-2.4	RIKEN cDNA I830012O16 gene
<i>Ifi204</i>	-2.5	interferon activated gene 204
<i>Mpa2l</i>	-2.5	macrophage activation 2 like
<i>Gbp1</i>	-2.5	guanylate binding protein 1
<i>Npy</i>	-2.6	neuropeptide Y
<i>Penk</i>	-2.6	preproenkephalin
<i>Zbp1</i>	-2.6	Z-DNA binding protein 1
<i>Ifi44</i>	-2.6	interferon-induced protein 44
<i>D14Ert668e</i>	-2.7	DNA segment, Chr 14, ERATO Doi 668, expressed
<i>H28</i>	-2.9	histocompatibility 28
<i>Ifi205</i>	-2.9	interferon activated gene 205
<i>Tgtp</i>	-3.2	T-cell specific GTPase
<i>Ly6a</i>	-3.2	lymphocyte antigen 6 complex, locus A
<i>Gbp4</i>	-3.3	guanylate binding protein 4
<i>Gbp2</i>	-3.4	guanylate binding protein 2
<i>Zfp125</i>	-3.7	zinc finger protein 125
<i>BC023105</i>	-3.8	cDNA sequence BC023105

**Supplementary Table 8. Differentially expressed genes in islets isolated from *Pax6<sup>Leca2</sup>* and *Pax6<sup>Leca2/wt</sup>* mice aged four weeks, filtered for a fold change of at least 2 and a FDR of <10% (4.4). Acinar-related genes were excluded.**

Gene Symbol	<i>Pax6<sup>Leca2</sup></i> / <i>Pax6<sup>Leca2/wt</sup></i>	Gene Name
<i>Iqsec3</i>	3.6	IQ motif and Sec7 domain 3
<i>Tacr3</i>	3.3	tachykinin receptor 3
<i>Slc35f4</i>	3.2	solute carrier family 35, member F4
<i>Enpp3</i>	3.1	ectonucleotide pyrophosphatase/phosphodiesterase 3
<i>Dlk1</i>	3.0	delta-like 1 homolog (Drosophila)
<i>Cnr1</i>	2.9	cannabinoid receptor 1 (brain)
<i>Chst8</i>	2.8	carbohydrate (N-acetylgalactosamine 4-O) sulfotransferase 8
<i>Tgtp</i>	2.6	T-cell specific GTPase
<i>Vstm2a</i>	2.5	V-set and transmembrane domain containing 2A
<i>Prrg3</i>	2.4	proline rich Gla (G-carboxyglutamic acid) 3 (transmembrane)
<i>Fhl2</i>	2.3	four and a half LIM domains 2
<i>Xdh</i>	2.3	xanthine dehydrogenase
<i>Gabra3</i>	2.3	gamma-aminobutyric acid (GABA) A receptor, subunit alpha 3
<i>Ms4a6b</i>	2.3	membrane-spanning 4-domains, subfamily A, member 6B
<i>Arap2</i>	2.2	ArfGAP with RhoGAP domain, ankyrin repeat and PH domain 2
<i>Dbc1</i>	2.1	deleted in bladder cancer 1 (human)
<i>Gabbrp</i>	2.1	gamma-aminobutyric acid (GABA) A receptor, pi
<i>Dmrta1</i>	2.1	doublesex and mab-3 related transcription factor like family A1
<i>Cp</i>	2.1	ceruloplasmin
<i>Neurog3</i>	2.0	neurogenin 3
<i>Csn3</i>	2.0	casein kappa
<i>Pgf</i>	2.0	placental growth factor
<i>Jam2</i>	2.0	junction adhesion molecule 2
<i>Expi</i>	2.0	extracellular proteinase inhibitor
<i>Ttc28</i>	-2.0	tetratricopeptide repeat domain 28
<i>Kcnh5</i>	-2.1	potassium voltage-gated channel, subfamily H (eag-related), member 5

<i>Skap1</i>	-2.1	src family associated phosphoprotein 1
<i>Dach2</i>	-2.1	dachshund 2 (Drosophila)
<i>Sult1c2</i>	-2.2	sulfotransferase family, cytosolic, 1C, member 2
<i>Ucn3</i>	-2.2	urocortin 3
<i>Fam46d</i>	-2.2	family with sequence similarity 46, member D
<i>Adh1</i>	-2.2	alcohol dehydrogenase 1 (class I)
<i>Grin1</i>	-2.3	glutamate receptor, ionotropic, NMDA1 (zeta 1)
<i>Adora1</i>	-2.3	adenosine A1 receptor
<i>Defb1</i>	-2.4	defensin beta 1
<i>Vstm2l</i>	-2.4	V-set and transmembrane domain containing 2-like
<i>Th</i>	-2.4	tyrosine hydroxylase
<i>Lyve1</i>	-2.6	lymphatic vessel endothelial hyaluronan receptor 1
<i>B3galt5</i>	-2.6	UDP-Gal:betaGlcNAc beta 1,3-galactosyltransferase, polypeptide 5
<i>Ptprz1</i>	-2.7	protein tyrosine phosphatase, receptor type Z, polypeptide 1
<i>Gcgr</i>	-2.7	glucagon receptor
<i>G6pc2</i>	-3.8	glucose-6-phosphatase, catalytic, 2
<i>Angptl7</i>	-3.9	angiopoietin-like 7
<i>Robo1</i>	-4.4	roundabout homolog 1 (Drosophila)
<i>Tmem215</i>	-4.5	transmembrane protein 215
<i>Cntfr</i>	-4.9	ciliary neurotrophic factor receptor
<i>Edn3</i>	-5.6	endothelin 3
<i>Nell1</i>	-5.9	NEL-like 1 (chicken)
<i>Ffar1</i>	-17.5	free fatty acid receptor 1

**Supplementary Table 9. Differentially expressed genes in islets isolated from *Pax6*<sup>Leca2</sup> and wild-type mice aged 20 weeks, filtered for a fold change of at least 2 and a FDR of <10% (4.4). Acinar-related genes were excluded.**

Gene Symbol	<i>Pax6</i> <sup>Leca2</sup> /WT	Gene name
<i>Il6</i>	7.9	interleukin 6
<i>Gcnt3</i>	7.3	glucosaminyl (N-acetyl) transferase 3, mucin type
<i>BC023105</i>	7.2	cDNA sequence BC023105 // cDNA sequence BC023105
<i>Gm10334</i>	7.0	predicted gene 10334
<i>Rasgrp1</i>	6.9	RAS guanyl releasing protein 1
<i>Ilgp1</i>	6.7	interferon inducible GTPase 1
<i>Ms4a4d</i>	6.1	membrane-spanning 4-domains, subfamily A, member 4D
<i>Iqsec3</i>	5.9	IQ motif and Sec7 domain 3
<i>Penk</i>	5.8	preproenkephalin
<i>Gbp4</i>	5.7	guanylate binding protein 4
<i>Plac8</i>	5.7	placenta-specific 8
<i>Tgtp</i>	5.7	T-cell specific GTPase
<i>Enpp3</i>	5.5	ectonucleotide pyrophosphatase/phosphodiesterase 3
<i>Ccl2</i>	5.5	chemokine (C-C motif) ligand 2
<i>Ifi205</i>	5.4	interferon activated gene 205
<i>Cxcl9</i>	5.4	chemokine (C-X-C motif) ligand 9
<i>D14Ert668e</i>	5.3	DNA segment, Chr 14, ERATO Doi 668, expressed
<i>Dlk1</i>	5.1	delta-like 1 homolog (Drosophila)
<i>Ifi203</i>	5.1	interferon activated gene 203
<i>Aldh1a2</i>	5.0	aldehyde dehydrogenase family 1, subfamily A2
<i>Ccl7</i>	5.0	chemokine (C-C motif) ligand 7
<i>Ly6c1</i>	5.0	lymphocyte antigen 6 complex, locus C1
<i>Cnr1</i>	5.0	cannabinoid receptor 1 (brain)
<i>Gm5431</i>	4.9	predicted gene 5431

## Appendix

<b>A430107O13Rik</b>	4.9	RIKEN cDNA A430107O13 gene
<b>Cp</b>	4.9	ceruloplasmin
<b>4930539E08Rik</b>	4.9	RIKEN cDNA 4930539E08 gene
<b>Sp100</b>	4.8	nuclear antigen Sp100
<b>Fhl2</b>	4.7	four and a half LIM domains 2
<b>Gabrp</b>	4.6	gamma-aminobutyric acid (GABA) A receptor, pi
<b>Cpb2</b>	4.6	carboxypeptidase B2 (plasma)
<b>Slc38a1</b>	4.6	solute carrier family 38, member 1
<b>Ly6a</b>	4.6	lymphocyte antigen 6 complex, locus A
<b>Zbp1</b>	4.6	Z-DNA binding protein 1
<b>Trim30</b>	4.6	tripartite motif-containing 30
<b>Ifi202b</b>	4.5	interferon activated gene 202B
<b>Gm4951</b>	4.5	predicted gene 4951
<b>Ifi204</b>	4.5	interferon activated gene 204
<b>Fermt1</b>	4.5	fermitin family homolog 1 (Drosophila)
<b>Fgb</b>	4.5	fibrinogen beta chain
<b>Ptgs2</b>	4.4	prostaglandin-endoperoxide synthase 2
<b>Ifi47</b>	4.4	interferon gamma inducible protein 47
<b>Steap4</b>	4.4	STEAP family member 4
<b>Ms4a4c</b>	4.3	membrane-spanning 4-domains, subfamily A, member 4C
<b>Sprr1a</b>	4.3	small proline-rich protein 1A
<b>Ifit2</b>	4.3	interferon-induced protein with tetratricopeptide repeats 2
<b>Vcam1</b>	4.3	vascular cell adhesion molecule 1
<b>Selp</b>	4.2	selectin, platelet
<b>Muc13</b>	4.2	mucin 13, epithelial transmembrane
<b>Tacr3</b>	4.2	tachykinin receptor 3
<b>1600029D21Rik</b>	4.1	RIKEN cDNA 1600029D21 gene
<b>C3</b>	4.1	complement component 3
<b>Hs6st2</b>	4.1	heparan sulfate 6-O-sulfotransferase 2
<b>C1rb</b>	4.0	complement component 1, r subcomponent B
<b>Dmrta1</b>	4.0	doublesex and mab-3 related transcription factor like family A1
<b>Osmr</b>	4.0	oncostatin M receptor
<b>H28</b>	4.0	histocompatibility 28
<b>Chst8</b>	4.0	carbohydrate (N-acetylgalactosamine 4-O) sulfotransferase 8
<b>1100001E04Rik</b>	3.9	RIKEN cDNA 1100001E04 gene
<b>Gbp2</b>	3.9	guanylate binding protein 2
<b>Tnfsf10</b>	3.9	tumor necrosis factor (ligand) superfamily, member 10
<b>Npas2</b>	3.9	neuronal PAS domain protein 2
<b>Rerg</b>	3.8	RAS-like, estrogen-regulated, growth-inhibitor
<b>Mmp2</b>	3.8	matrix metalloproteinase 2
<b>Il33</b>	3.8	interleukin 33
<b>Dpt</b>	3.8	dermatopontin
<b>Lox</b>	3.8	lysyl oxidase
<b>Mpa2l</b>	3.7	macrophage activation 2 like
<b>Il1rn</b>	3.7	interleukin 1 receptor antagonist
<b>Ankrd1</b>	3.7	ankyrin repeat domain 1 (cardiac muscle)
<b>Gbp1</b>	3.7	guanylate binding protein 1
<b>Il11</b>	3.7	interleukin 11
<b>Ly6c2</b>	3.7	lymphocyte antigen 6 complex, locus C2
<b>Gm12250</b>	3.7	predicted gene 12250
<b>Gfpt2</b>	3.7	glutamine fructose-6-phosphate transaminase 2
<b>Tnc</b>	3.6	tenascin C
<b>Serpinb6b</b>	3.6	serine (or cysteine) peptidase inhibitor, clade B, member 6b

Appendix

<b>Gm7609</b>	3.6	predicted gene 7609
<b>EG634650</b>	3.6	predicted gene, EG634650
<b>Olfml3</b>	3.6	olfactomedin-like 3
<b>Cd55</b>	3.6	CD55 antigen
<b>5830443L24Rik</b>	3.6	RIKEN cDNA 5830443L24 gene
<b>Depdc7</b>	3.6	DEP domain containing 7
<b>Jam2</b>	3.6	junction adhesion molecule 2
<b>Rsad2</b>	3.5	radical S-adenosyl methionine domain containing 2
<b>RP23-395H4.4</b>	3.5	elastase 2A
<b>Dbc1</b>	3.5	deleted in bladder cancer 1 (human)
<b>Pfkfb3</b>	3.5	6-phosphofructo-2-kinase/fructose-2,6-biphosphatase 3
<b>Gfra2</b>	3.5	glial cell line derived neurotrophic factor family receptor alpha 2
<b>Cyp1b1</b>	3.5	cytochrome P450, family 1, subfamily b, polypeptide 1
<b>AI607873</b>	3.5	expressed sequence AI607873
<b>Cfb</b>	3.5	complement factor B
<b>Vstm2a</b>	3.5	V-set and transmembrane domain containing 2A
<b>Mmp3</b>	3.5	matrix metalloproteinase 3
<b>Slfm5</b>	3.5	schlafen 5
<b>Prrx1</b>	3.4	paired related homeobox 1
<b>I830012O16Rik</b>	3.4	RIKEN cDNA I830012O16 gene
<b>A4galt</b>	3.4	alpha 1,4-galactosyltransferase
<b>Dnase1B3</b>	3.4	deoxyribonuclease 1-like 3
<b>Alpl</b>	3.4	alkaline phosphatase, liver/bone/kidney
<b>Gvin1</b>	3.4	GTPase, very large interferon inducible 1
<b>Ccl11</b>	3.3	chemokine (C-C motif) ligand 11
<b>Cxcl10</b>	3.3	chemokine (C-X-C motif) ligand 10
<b>Plscr2</b>	3.3	phospholipid scramblase 2
<b>Xdh</b>	3.3	xanthine dehydrogenase
<b>Pdpr</b>	3.3	podoplanin
<b>Pigr</b>	3.3	polymeric immunoglobulin receptor
<b>Lsp1</b>	3.3	lymphocyte specific 1
<b>Il2ra</b>	3.3	interleukin 2 receptor, alpha chain
<b>Gabra3</b>	3.3	gamma-aminobutyric acid (GABA) A receptor, subunit alpha 3
<b>Pros1</b>	3.3	protein S (alpha)
<b>Tfpi2</b>	3.3	tissue factor pathway inhibitor 2
<b>993011J21Rik</b>	3.3	RIKEN cDNA 993011J21 gene
<b>Cxcl14</b>	3.3	chemokine (C-X-C motif) ligand 14
<b>Pdgfra</b>	3.3	platelet derived growth factor receptor, alpha polypeptide
<b>Ascl1</b>	3.2	achaete-scute complex homolog 1 (Drosophila)
<b>Cnn2</b>	3.2	calponin 2
<b>Abi3bp</b>	3.2	ABI gene family, member 3 (NESH) binding protein
<b>Slc43a3</b>	3.2	solute carrier family 43, member 3
<b>Gpx8</b>	3.2	glutathione peroxidase 8 (putative)
<b>AW551984</b>	3.2	expressed sequence AW551984
<b>Igf3bp3</b>	3.2	insulin-like growth factor binding protein 3
<b>Il7r</b>	3.2	interleukin 7 receptor
<b>C1s</b>	3.2	complement component 1, s subcomponent
<b>Glt25d2</b>	3.2	glycosyltransferase 25 domain containing 2
<b>Rtp4</b>	3.2	receptor transporter protein 4
<b>AW112010</b>	3.2	expressed sequence AW112010
<b>Olfm3</b>	3.2	olfactomedin 3
<b>Sp110</b>	3.1	Sp110 nuclear body protein
<b>BC057170</b>	3.1	cDNA sequence BC057170

## Appendix

<i>Lif</i>	3.1	leukemia inhibitory factor
<i>Ms4a6d</i>	3.1	membrane-spanning 4-domains, subfamily A, member 6D
<i>Itga5</i>	3.1	integrin alpha 5 (fibronectin receptor alpha)
<i>Gpm6b</i>	3.1	glycoprotein m6b
<i>D17H6S56E-5</i>	3.1	DNA segment, Chr 17, human D6S56E 5
<i>Far2</i>	3.1	fatty acyl CoA reductase 2
<i>Gm11428</i>	3.1	predicted gene 11428
<i>Tgm2</i>	3.1	transglutaminase 2, C polypeptide
<i>Ch25h</i>	3.0	cholesterol 25-hydroxylase
<i>Timp1</i>	3.0	tissue inhibitor of metalloproteinase 1
<i>Hbb-b1</i>	3.0	hemoglobin, beta adult major chain
<i>Antxr1</i>	3.0	anthrax toxin receptor 1
<i>Ifi44</i>	3.0	interferon-induced protein 44
<i>Lrrc32</i>	3.0	leucine rich repeat containing 32
<i>Tmem173</i>	3.0	transmembrane protein 173
<i>Lhfp12</i>	3.0	lipoma HMGIC fusion partner-like 2
<i>Has2</i>	3.0	hyaluronan synthase 2
<i>1810009J06Rik</i>	3.0	RIKEN cDNA 1810009J06 gene
<i>Enpp1</i>	3.0	ectonucleotide pyrophosphatase/phosphodiesterase 1
<i>Fstl1</i>	3.0	follistatin-like 1
<i>Ddr2</i>	3.0	discoidin domain receptor family, member 2
<i>Tgfb3</i>	3.0	transforming growth factor, beta 3
<i>H2-gs10</i>	3.0	MHC class I like protein GS10
<i>9130213B05Rik</i>	2.9	RIKEN cDNA 9130213B05 gene
<i>Cd80</i>	2.9	CD80 antigen
<i>Wdr72</i>	2.9	WD repeat domain 72
<i>Rab38</i>	2.9	RAB38, member of RAS oncogene family
<i>Il1rl2</i>	2.9	interleukin 1 receptor-like 2
<i>Tmem47</i>	2.9	transmembrane protein 47
<i>Zfp3611</i>	2.9	zinc finger protein 36, C3H type-like 1
<i>Ebf1</i>	2.9	early B-cell factor 1
<i>Aebp1</i>	2.9	AE binding protein 1
<i>Ccl5</i>	2.9	chemokine (C-C motif) ligand 5
<i>Arhgap10</i>	2.9	Rho GTPase activating protein 10
<i>Taf1d</i>	2.9	TATA box binding protein (Tbp)-associated factor, RNA polymerase I, D
<i>Fam84a</i>	2.9	family with sequence similarity 84, member A
<i>Mfap5</i>	2.9	microfibrillar associated protein 5
<i>Gbp3</i>	2.9	guanylate binding protein 3
<i>Slc35f4</i>	2.9	solute carrier family 35, member F4
<i>Hcn1</i>	2.9	hyperpolarization-activated, cyclic nucleotide-gated K+ 1
<i>Mmp7</i>	2.9	matrix metalloproteinase 7
<i>4931429I11Rik</i>	2.8	RIKEN cDNA 4931429I11 gene
<i>Ifit1</i>	2.8	interferon-induced protein with tetratricopeptide repeats 1
<i>Opcml</i>	2.8	opioid binding protein/cell adhesion molecule-like
<i>Galnt3</i>	2.8	UDP-N-acetyl-alpha-D-galactosamine:polypeptide N-acetylgalactosaminyltransferase 3
<i>Stc2</i>	2.8	stanniocalcin 2
<i>Tnfaip6</i>	2.8	tumor necrosis factor alpha induced protein 6
<i>Irgm2</i>	2.8	immunity-related GTPase family M member 2
<i>Layn</i>	2.8	layilin
<i>Tmem45b</i>	2.8	transmembrane protein 45b
<i>Oas2</i>	2.8	2'-5' oligoadenylate synthetase 2
<i>9030420J04Rik</i>	2.8	RIKEN cDNA 9030420J04 gene
<i>OTTMUSG00000005523</i>	2.8	predicted gene, OTTMUSG00000005523

Appendix

<i>Uchl1</i>	2.8	ubiquitin carboxy-terminal hydrolase L1
<i>Fbn1</i>	2.8	fibrillin 1
<i>9030425E11Rik</i>	2.8	RIKEN cDNA 9030425E11 gene
<i>Tspan8</i>	2.8	tetraspanin 8
<i>Enpep</i>	2.8	glutamyl aminopeptidase
<i>Ms4a6b</i>	2.8	membrane-spanning 4-domains, subfamily A, member 6B
<i>Neb1</i>	2.8	nebulette
<i>Tle4</i>	2.8	transducin-like enhancer of split 4, homolog of Drosophila E(spl)
<i>Stat4</i>	2.8	signal transducer and activator of transcription 4
<i>Csf2rb</i>	2.8	colony stimulating factor 2 receptor, beta, low-affinity (granulocyte-macrophage)
<i>Fkbp10</i>	2.8	FK506 binding protein 10
<i>Cdh11</i>	2.7	cadherin 11
<i>Cidea</i>	2.7	cell death-inducing DNA fragmentation factor, alpha subunit-like effector A
<i>Mmp14</i>	2.7	matrix metalloproteinase 14 (membrane-inserted)
<i>Cntnap5b</i>	2.7	contactin associated protein-like 5B
<i>Pi15</i>	2.7	peptidase inhibitor 15
<i>Rgs4</i>	2.7	regulator of G-protein signaling 4
<i>Mlkl</i>	2.7	mixed lineage kinase domain-like
<i>Inhba</i>	2.7	inhibin beta-A
<i>6330406I15Rik</i>	2.7	RIKEN cDNA 6330406I15 gene
<i>Casp12</i>	2.7	caspase 12
<i>Pla2g4a</i>	2.7	phospholipase A2, group IVA (cytosolic, calcium-dependent)
<i>Slc15a3</i>	2.7	solute carrier family 15, member 3
<i>Ptchd1</i>	2.7	patched domain containing 1
<i>Eef1a2</i>	2.7	eukaryotic translation elongation factor 1 alpha 2
<i>Vsig2</i>	2.7	V-set and immunoglobulin domain containing 2
<i>Dram1</i>	2.7	DNA-damage regulated autophagy modulator 1
<i>H2-T24</i>	2.7	histocompatibility 2, T region locus 24
<i>Ccdc85a</i>	2.7	coiled-coil domain containing 85A
<i>Gprc5a</i>	2.7	G protein-coupled receptor, family C, group 5, member A
<i>Cxcl11</i>	2.7	chemokine (C-X-C motif) ligand 11
<i>Scara3</i>	2.7	scavenger receptor class A, member 3
<i>Procr</i>	2.7	protein C receptor, endothelial
<i>Icam1</i>	2.6	intercellular adhesion molecule 1
<i>Il2rg</i>	2.6	interleukin 2 receptor, gamma chain
<i>Ccr7</i>	2.6	chemokine (C-C motif) receptor 7
<i>H2-M2</i>	2.6	histocompatibility 2, M region locus 2
<i>St3gal4</i>	2.6	ST3 beta-galactoside alpha-2,3-sialyltransferase 4
<i>Anxa2</i>	2.6	annexin A2
<i>Srpx2</i>	2.6	sushi-repeat-containing protein, X-linked 2
<i>Slamf7</i>	2.6	SLAM family member 7
<i>Itgb6</i>	2.6	integrin beta 6
<i>Irgm1</i>	2.6	immunity-related GTPase family M member 1
<i>Cytip</i>	2.6	cytohesin 1 interacting protein
<i>Sema3e</i>	2.6	sema domain, immunoglobulin domain (Ig), short basic domain, secreted, (semaphorin) 3E
<i>Hba-a2</i>	2.6	hemoglobin alpha, adult chain 2
<i>Vcan</i>	2.6	versican
<i>Fgf2</i>	2.6	fibroblast growth factor 2
<i>Phf11</i>	2.6	PHD finger protein 11
<i>Large</i>	2.6	like-glycosyltransferase
<i>Cd14</i>	2.6	CD14 antigen
<i>Cadm2</i>	2.6	cell adhesion molecule 2

<b>9230105E10Rik</b>	2.6	RIKEN cDNA 9230105E10 gene
<b>Plaur</b>	2.6	plasminogen activator, urokinase receptor
<b>Tmprss2</b>	2.6	transmembrane protease, serine 2
<b>Bnc2</b>	2.5	basonuclin 2
<b>Col6a3</b>	2.5	collagen, type VI, alpha 3
<b>Adcyap1r1</b>	2.5	adenylate cyclase activating polypeptide 1 receptor 1
<b>Cyr61</b>	2.5	cysteine rich protein 61
<b>Sdc1</b>	2.5	syndecan 1
<b>Podn</b>	2.5	podocan
<b>Ncam2</b>	2.5	neural cell adhesion molecule 2
<b>Cxcl5</b>	2.5	chemokine (C-X-C motif) ligand 5
<b>Arap2</b>	2.5	ArfGAP with RhoGAP domain, ankyrin repeat and PH domain 2
<b>Prrg3</b>	2.5	proline rich Gla (G-carboxyglutamic acid) 3 (transmembrane)
<b>Cdh9</b>	2.5	cadherin 9
<b>Ifit3</b>	2.5	interferon-induced protein with tetratricopeptide repeats 3
<b>Rbms1</b>	2.5	RNA binding motif, single stranded interacting protein 1
<b>Ccl22</b>	2.5	chemokine (C-C motif) ligand 22
<b>Rdh10</b>	2.5	retinol dehydrogenase 10 (all-trans)
<b>Hba-a1</b>	2.5	hemoglobin alpha, adult chain 1
<b>Epha3</b>	2.5	Eph receptor A3
<b>Cecr2</b>	2.5	cat eye syndrome chromosome region, candidate 2 homolog (human)
<b>Ankrd34c</b>	2.5	ankyrin repeat domain 34C
<b>Lrrn3</b>	2.5	leucine rich repeat protein 3, neuronal
<b>Crim1</b>	2.5	cysteine rich transmembrane BMP regulator 1 (chordin like)
<b>Nfib</b>	2.5	nuclear factor I/B
<b>Cd53</b>	2.5	CD53 antigen
<b>Pdgfrb</b>	2.5	platelet derived growth factor receptor, beta polypeptide
<b>Vwde</b>	2.5	von Willebrand factor D and EGF domains
<b>Oas1g</b>	2.5	2'-5' oligoadenylate synthetase 1G
<b>Freq</b>	2.5	frequenin homolog (Drosophila)
<b>Snai1</b>	2.5	snail homolog 1 (Drosophila)
<b>Entpd1</b>	2.5	ectonucleoside triphosphate diphosphohydrolase 1
<b>Myo15b</b>	2.4	myosin XVB
<b>Runx1</b>	2.4	runt related transcription factor 1
<b>Ifi2712a</b>	2.4	interferon, alpha-inducible protein 27 like 2A
<b>Lrrc8c</b>	2.4	leucine rich repeat containing 8 family, member C
<b>Egr2</b>	2.4	early growth response 2
<b>Cygb</b>	2.4	cytoglobin
<b>Ar</b>	2.4	androgen receptor
<b>Mfge8</b>	2.4	milk fat globule-EGF factor 8 protein
<b>Prrg4</b>	2.4	proline rich Gla (G-carboxyglutamic acid) 4 (transmembrane)
<b>C1r</b>	2.4	complement component 1, r subcomponent
<b>Ccl8</b>	2.4	chemokine (C-C motif) ligand 8
<b>Plod2</b>	2.4	procollagen lysine, 2-oxoglutarate 5-dioxygenase 2
<b>Ldha</b>	2.4	lactate dehydrogenase A
<b>Smad3</b>	2.4	MAD homolog 3 (Drosophila)
<b>Syt17</b>	2.4	synaptotagmin XVII
<b>Crp</b>	2.4	C-reactive protein, pentraxin-related
<b>Elov17</b>	2.4	ELOVL family member 7, elongation of long chain fatty acids (yeast)
<b>Cd302</b>	2.4	CD302 antigen
<b>Fmo2</b>	2.4	flavin containing monooxygenase 2
<b>Slc39a8</b>	2.4	solute carrier family 39 (metal ion transporter), member 8
<b>S1pr3</b>	2.4	sphingosine-1-phosphate receptor 3

<i>Gadd45g</i>	2.4	growth arrest and DNA-damage-inducible 45 gamma
<i>Postn</i>	2.4	periostin, osteoblast specific factor
<i>Fam49a</i>	2.4	family with sequence similarity 49, member A
<i>Ephb4</i>	2.4	Eph receptor B4
<i>Tmem45a</i>	2.4	transmembrane protein 45a
<i>Csf1</i>	2.4	colony stimulating factor 1 (macrophage)
<i>Sh3pxd2b</i>	2.4	SH3 and PX domains 2B
<i>Loxl1</i>	2.4	lysyl oxidase-like 1
<i>Angptl2</i>	2.4	angiopoietin-like 2
<i>Csf2rb2</i>	2.4	colony stimulating factor 2 receptor, beta 2, low-affinity (granulocyte-macrophage)
<i>Rgs1</i>	2.4	regulator of G-protein signaling 1
<i>Apol9a</i>	2.4	apolipoprotein L 9a
<i>Cfh</i>	2.4	complement component factor h
<i>Colec12</i>	2.4	collectin sub-family member 12
<i>Fads3</i>	2.4	fatty acid desaturase 3
<i>Ogn</i>	2.4	osteoglycin
<i>Slc28a3</i>	2.4	solute carrier family 28 (sodium-coupled nucleoside transporter), member 3
<i>Zbtb7c</i>	2.4	zinc finger and BTB domain containing 7C
<i>Tns1</i>	2.4	tensin 1
<i>Gas7</i>	2.4	growth arrest specific 7
<i>Chl1</i>	2.4	cell adhesion molecule with homology to L1CAM
<i>Spred1</i>	2.4	sprouty protein with EVH-1 domain 1, related sequence
<i>Gbp6</i>	2.4	guanylate binding protein 6
<i>Myof</i>	2.4	myoferlin
<i>Bcl2a1a</i>	2.4	B-cell leukemia/lymphoma 2 related protein A1a
<i>Pdzrn3</i>	2.4	PDZ domain containing RING finger 3
<i>Casp4</i>	2.4	caspase 4, apoptosis-related cysteine peptidase
<i>Ptgfrn</i>	2.4	prostaglandin F2 receptor negative regulator
<i>Sparcl1</i>	2.3	SPARC-like 1
<i>Cfi</i>	2.3	complement component factor i
<i>Dhx58</i>	2.3	DEXH (Asp-Glu-X-His) box polypeptide 58
<i>Msn</i>	2.3	moesin
<i>Tm4sf1</i>	2.3	transmembrane 4 superfamily member 1
<i>Adcy2</i>	2.3	adenylate cyclase 2
<i>Ccdc80</i>	2.3	coiled-coil domain containing 80
<i>Ecm1</i>	2.3	extracellular matrix protein 1
<i>Ddx60</i>	2.3	DEAD (Asp-Glu-Ala-Asp) box polypeptide 60
<i>Frmpr4</i>	2.3	FERM and PDZ domain containing 4
<i>Cd38</i>	2.3	CD38 antigen
<i>Olfml2b</i>	2.3	olfactomedin-like 2B
<i>Gucy2c</i>	2.3	guanylate cyclase 2c
<i>Ust</i>	2.3	uronyl-2-sulfotransferase
<i>Bcl2a1b</i>	2.3	B-cell leukemia/lymphoma 2 related protein A1b
<i>Pcolce</i>	2.3	procollagen C-endopeptidase enhancer protein
<i>Gm8995</i>	2.3	predicted gene 8995
<i>Eng</i>	2.3	endoglin
<i>Antxr2</i>	2.3	anthrax toxin receptor 2
<i>Adamts9</i>	2.3	a disintegrin-like and metallopeptidase (reprolysin type) with thrombospondin type 1 motif, 9
<i>C230081A13Rik</i>	2.3	RIKEN cDNA C230081A13 gene
<i>Sh3bgrl2</i>	2.3	SH3 domain binding glutamic acid-rich protein like 2
<i>Kirrel</i>	2.3	kin of IRRE like (Drosophila)
<i>Fbln2</i>	2.3	fibulin 2

<b>Cxcl2</b>	2.3	chemokine (C-X-C motif) ligand 2
<b>Abcb1b</b>	2.3	ATP-binding cassette, sub-family B (MDR/TAP), member 1B
<b>Ngf</b>	2.3	nerve growth factor
<b>Oasl1</b>	2.3	2'-5' oligoadenylate synthetase-like 1
<b>Ehd2</b>	2.3	EH-domain containing 2
<b>Mx2</b>	2.3	myxovirus (influenza virus) resistance 2
<b>Bcl2a1d</b>	2.3	B-cell leukemia/lymphoma 2 related protein A1d
<b>Axl</b>	2.3	AXL receptor tyrosine kinase
<b>Timp3</b>	2.3	tissue inhibitor of metalloproteinase 3
<b>Tspan18</b>	2.3	tetraspanin 18
<b>Xaf1</b>	2.3	XIAP associated factor 1
<b>Cyba</b>	2.3	cytochrome b-245, alpha polypeptide
<b>Sema7a</b>	2.3	sema domain, immunoglobulin domain (Ig), and GPI membrane anchor, (semaphorin) 7A
<b>H2-Ea</b>	2.3	histocompatibility 2, class II antigen E alpha
<b>Wsb1</b>	2.3	WD repeat and SOCS box-containing 1
<b>Bmp2</b>	2.3	bone morphogenetic protein 2
<b>Des</b>	2.3	desmin
<b>Lhfp</b>	2.3	lipoma HMGIC fusion partner
<b>Scn2a1</b>	2.3	sodium channel, voltage-gated, type II, alpha 1
<b>Nhs1</b>	2.2	NHS-like 1
<b>Gdf10</b>	2.2	growth differentiation factor 10
<b>Oasl2</b>	2.2	2'-5' oligoadenylate synthetase-like 2
<b>Pxdn</b>	2.2	peroxidasin homolog (Drosophila)
<b>Gimap4</b>	2.2	GTPase, IMAP family member 4
<b>Rbms3</b>	2.2	RNA binding motif, single stranded interacting protein
<b>Aldh1a3</b>	2.2	aldehyde dehydrogenase family 1, subfamily A3
<b>Ephb2</b>	2.2	Eph receptor B2
<b>Htra1</b>	2.2	HtrA serine peptidase 1
<b>Ppap2a</b>	2.2	phosphatidic acid phosphatase type 2A
<b>Il15</b>	2.2	interleukin 15
<b>Zeb2</b>	2.2	zinc finger E-box binding homeobox 2
<b>Cyrr1</b>	2.2	cysteine and tyrosine-rich protein 1
<b>Serpine1</b>	2.2	serine (or cysteine) peptidase inhibitor, clade E, member 1
<b>Serpinf1</b>	2.2	serine (or cysteine) peptidase inhibitor, clade F, member 1
<b>Oas3</b>	2.2	2'-5' oligoadenylate synthetase 3
<b>Gpr120</b>	2.2	G protein-coupled receptor 120
<b>Flna</b>	2.2	filamin, alpha
<b>Anxa3</b>	2.2	annexin A3
<b>Pld1</b>	2.2	phospholipase D1
<b>Tap1</b>	2.2	transporter 1, ATP-binding cassette, sub-family B (MDR/TAP)
<b>Acer2</b>	2.2	alkaline ceramidase 2
<b>Apof</b>	2.2	apolipoprotein F
<b>Edn1</b>	2.2	endothelin 1
<b>Fos1</b>	2.2	fos-like antigen 1
<b>Mmp19</b>	2.2	matrix metalloproteinase 19
<b>Shisa6</b>	2.2	shisa homolog 6 (Xenopus laevis)
<b>Ms4a6c</b>	2.2	membrane-spanning 4-domains, subfamily A, member 6C
<b>Sema6a</b>	2.2	sema domain, transmembrane domain (TM), and cytoplasmic domain, (semaphorin) 6A
<b>Plekho2</b>	2.2	pleckstrin homology domain containing, family O member 2
<b>Tek</b>	2.2	endothelial-specific receptor tyrosine kinase
<b>Slc38a11</b>	2.2	solute carrier family 38, member 11
<b>Ramp3</b>	2.2	receptor (calcitonin) activity modifying protein 3

<b><i>Klhl29</i></b>	2.2	kelch-like 29 (Drosophila)
<b><i>Cd34</i></b>	2.2	CD34 antigen
<b><i>Tspan4</i></b>	2.2	tetraspanin 4
<b><i>Neurog3</i></b>	2.2	neurogenin 3
<b><i>Stk17b</i></b>	2.2	serine/threonine kinase 17b (apoptosis-inducing)
<b><i>Nid1</i></b>	2.2	nidogen 1
<b><i>Ctla2a</i></b>	2.2	cytotoxic T lymphocyte-associated protein 2 alpha
<b><i>Aplnr</i></b>	2.2	apelin receptor
<b><i>Spp1</i></b>	2.2	secreted phosphoprotein 1
<b><i>Notch2</i></b>	2.2	Notch gene homolog 2 (Drosophila)
<b><i>Cd97</i></b>	2.2	CD97 antigen
<b><i>Myo1g</i></b>	2.2	myosin IG
<b><i>Ammecr1</i></b>	2.2	Alport syndrome, mental retardation, midface hypoplasia and elliptocytosis chromosomal region gene 1 homolog (human)
<b><i>Gna14</i></b>	2.2	guanine nucleotide binding protein, alpha 14
<b><i>Pltp</i></b>	2.2	phospholipid transfer protein
<b><i>Col1a1</i></b>	2.2	collagen, type I, alpha 1
<b><i>Plvap</i></b>	2.2	plasmalemma vesicle associated protein
<b><i>Samsn1</i></b>	2.2	SAM domain, SH3 domain and nuclear localization signals, 1
<b><i>Fscn1</i></b>	2.2	fascin homolog 1, actin bundling protein (Strongylocentrotus purpuratus)
<b><i>Lmcd1</i></b>	2.2	LIM and cysteine-rich domains 1
<b><i>Ehf</i></b>	2.2	ets homologous factor
<b><i>Klhl38</i></b>	2.2	kelch-like 38 (Drosophila)
<b><i>Cldn2</i></b>	2.2	claudin 2
<b><i>Tcr<math>\gamma</math>-V3</i></b>	2.2	T-cell receptor gamma, variable 3
<b><i>Txnip</i></b>	2.2	thioredoxin interacting protein
<b><i>Irf7</i></b>	2.2	interferon regulatory factor 7
<b><i>Fcgr4</i></b>	2.2	Fc receptor, IgG, low affinity IV
<b><i>Cav1</i></b>	2.2	caveolin 1, caveolae protein
<b><i>Igsf6</i></b>	2.1	immunoglobulin superfamily, member 6
<b><i>Lbp</i></b>	2.1	lipopolysaccharide binding protein
<b><i>Tlr7</i></b>	2.1	toll-like receptor 7
<b><i>Heyl</i></b>	2.1	hairy/enhancer-of-split related with YRPW motif-like
<b><i>Tfpi</i></b>	2.1	tissue factor pathway inhibitor
<b><i>Wwc2</i></b>	2.1	WW, C2 and coiled-coil domain containing 2
<b><i>Itpril2</i></b>	2.1	inositol 1,4,5-triphosphate receptor interacting protein-like 2
<b><i>Arntl</i></b>	2.1	aryl hydrocarbon receptor nuclear translocator-like
<b><i>Tnfrsf1b</i></b>	2.1	tumor necrosis factor receptor superfamily, member 1b
<b><i>Ysk4</i></b>	2.1	Yeast Sps1/Ste20-related kinase 4 ( <i>S. cerevisiae</i> )
<b><i>Tmem110</i></b>	2.1	transmembrane protein 110
<b><i>Fkbp7</i></b>	2.1	FK506 binding protein 7
<b><i>Adamts2</i></b>	2.1	a disintegrin-like and metallopeptidase (reprolysin type) with thrombospondin type 1 motif, 2
<b><i>Pcdh24</i></b>	2.1	protocadherin 24
<b><i>Slc7a11</i></b>	2.1	solute carrier family 7 (cationic amino acid transporter, $\gamma$ + system), member 11
<b><i>Magi2</i></b>	2.1	membrane associated guanylate kinase, WW and PDZ domain containing 2
<b><i>Slfn2</i></b>	2.1	schlafen 2
<b><i>Prkch</i></b>	2.1	protein kinase C, eta
<b><i>Fgf14</i></b>	2.1	fibroblast growth factor 14
<b><i>Plk2</i></b>	2.1	polo-like kinase 2 (Drosophila)
<b><i>Stom</i></b>	2.1	stomatin
<b><i>Cpne8</i></b>	2.1	copine VIII
<b><i>Gbp5</i></b>	2.1	guanylate binding protein 5

<b><i>Ampd3</i></b>	2.1	adenosine monophosphate deaminase 3
<b><i>Sulf1</i></b>	2.1	sulfatase 1
<b><i>Gadd45b</i></b>	2.1	growth arrest and DNA-damage-inducible 45 beta
<b><i>Tmem140</i></b>	2.1	transmembrane protein 140
<b><i>Clec4a3</i></b>	2.1	C-type lectin domain family 4, member a3
<b><i>Gm5409</i></b>	2.1	predicted gene 5409
<b><i>Socs3</i></b>	2.1	suppressor of cytokine signaling 3
<b><i>Calcr1</i></b>	2.1	calcitonin receptor-like
<b><i>Gm9907</i></b>	2.1	predicted gene 9907
<b><i>Epb4.1l2</i></b>	2.1	erythrocyte protein band 4.1-like 2
<b><i>Sbno2</i></b>	2.1	strawberry notch homolog 2 (Drosophila)
<b><i>Rapgef5</i></b>	2.1	Rap guanine nucleotide exchange factor (GEF) 5
<b><i>Expi</i></b>	2.1	extracellular proteinase inhibitor
<b><i>Ltbp1</i></b>	2.1	latent transforming growth factor beta binding protein 1
<b><i>Has1</i></b>	2.1	hyaluronan synthase1
<b><i>Anxa10</i></b>	2.1	annexin A10
<b><i>Vgl3</i></b>	2.1	vestigial like 3 (Drosophila)
<b><i>9430031J16Rik</i></b>	2.1	RIKEN cDNA 9430031J16 gene
<b><i>Slc24a3</i></b>	2.1	solute carrier family 24 (sodium/potassium/calcium exchanger), member 3
<b><i>Tlr13</i></b>	2.1	toll-like receptor 13
<b><i>Fam69a</i></b>	2.1	family with sequence similarity 69, member A
<b><i>Odz1</i></b>	2.1	odd Oz/ten-m homolog 1 (Drosophila)
<b><i>Ppap2b</i></b>	2.1	phosphatidic acid phosphatase type 2B
<b><i>Ednra</i></b>	2.1	endothelin receptor type A
<b><i>Ndrp2</i></b>	2.1	N-myc downstream regulated gene 2
<b><i>Rest</i></b>	2.1	RE1-silencing transcription factor
<b><i>Stc1</i></b>	2.1	stanniocalcin 1
<b><i>Nrp2</i></b>	2.1	neuropilin 2
<b><i>Lrch2</i></b>	2.1	leucine-rich repeats and calponin homology (CH) domain containing 2
<b><i>Adap2</i></b>	2.1	ArfGAP with dual PH domains 2
<b><i>2310040G07Rik</i></b>	2.1	RIKEN cDNA 2310040G07 gene
<b><i>Akr1b8</i></b>	2.1	aldo-keto reductase family 1, member B8
<b><i>Flrt2</i></b>	2.1	fibronectin leucine rich transmembrane protein 2
<b><i>Gsta4</i></b>	2.1	glutathione S-transferase, alpha 4
<b><i>Wipf1</i></b>	2.1	WAS/WASL interacting protein family, member 1
<b><i>Ctss</i></b>	2.1	cathepsin S
<b><i>Adamts1</i></b>	2.1	a disintegrin-like and metallopeptidase (reprolysin type) with thrombospondin type 1 motif, 1
<b><i>Selplg</i></b>	2.1	selectin, platelet (p-selectin) ligand
<b><i>Neurl3</i></b>	2.1	neuralized homolog 3 homolog (Drosophila)
<b><i>Arrdc4</i></b>	2.1	arrestin domain containing 4
<b><i>Oprl1</i></b>	2.1	opioid receptor-like 1
<b><i>Tgfb1</i></b>	2.1	transforming growth factor, beta 1
<b><i>Ms4a7</i></b>	2.1	membrane-spanning 4-domains, subfamily A, member 7
<b><i>Gli3</i></b>	2.1	GLI-Kruppel family member GLI3
<b><i>Bmp3</i></b>	2.1	bone morphogenetic protein 3
<b><i>Sgk1</i></b>	2.1	serum/glucocorticoid regulated kinase 1
<b><i>Serpinh1</i></b>	2.1	serine (or cysteine) peptidase inhibitor, clade H, member 1
<b><i>Tgfbr2</i></b>	2.1	transforming growth factor, beta receptor II
<b><i>Gypc</i></b>	2.1	glycophorin C
<b><i>Nckap1l</i></b>	2.0	NCK associated protein 1 like
<b><i>Foxf1a</i></b>	2.0	forkhead box F1a
<b><i>Rbm11</i></b>	2.0	RNA binding motif protein 11
<b><i>Lphn2</i></b>	2.0	latrophilin 2

<i>Dab2</i>	2.0	disabled homolog 2 (Drosophila)
<i>Fli1</i>	2.0	Friend leukemia integration 1
<i>Podxl</i>	2.0	podocalyxin-like
<i>Wisp1</i>	2.0	WNT1 inducible signaling pathway protein 1
<i>Cmklr1</i>	2.0	chemokine-like receptor 1
<i>Bgn</i>	2.0	biglycan
<i>Cd180</i>	2.0	CD180 antigen
<i>Bcl2l14</i>	2.0	BCL2-like 14 (apoptosis facilitator)
<i>Galnt13</i>	2.0	UDP-N-acetyl-alpha-D-galactosamine:polypeptide N-acetylgalactosaminyltransferase 13
<i>Tnfrsf25</i>	2.0	tumor necrosis factor, alpha-induced protein 2
<i>Chrnb4</i>	2.0	cholinergic receptor, nicotinic, beta polypeptide 4
<i>Itga1</i>	2.0	integrin alpha 1
<i>Samd9l</i>	2.0	sterile alpha motif domain containing 9-like
<i>Col1a2</i>	2.0	collagen, type I, alpha 2
<i>C1ql3</i>	2.0	C1q-like 3
<i>5430435G22Rik</i>	2.0	RIKEN cDNA 5430435G22 gene
<i>Stat2</i>	2.0	signal transducer and activator of transcription 2
<i>Fam179a</i>	2.0	family with sequence similarity 179, member A
<i>Serpine2</i>	2.0	serine (or cysteine) peptidase inhibitor, clade E, member 2
<i>Kdr</i>	2.0	kinase insert domain protein receptor
<i>Meox2</i>	2.0	mesenchyme homeobox 2
<i>Herc5</i>	2.0	hect domain and RLD 5
<i>Cald1</i>	2.0	caldesmon 1
<i>Epas1</i>	2.0	endothelial PAS domain protein 1
<i>Apbb1ip</i>	2.0	amyloid beta (A4) precursor protein-binding, family B, member 1 interacting protein
<i>Gng2</i>	2.0	guanine nucleotide binding protein (G protein), gamma 2
<i>Limch1</i>	2.0	LIM and calponin homology domains 1
<i>Car13</i>	2.0	carbonic anhydrase 13
<i>Tubb6</i>	2.0	tubulin, beta 6
<i>Itga2</i>	2.0	integrin alpha 2
<i>Gpc3</i>	2.0	glypican 3
<i>Abcg2</i>	2.0	ATP-binding cassette, sub-family G (WHITE), member 2
<i>Ctgf</i>	2.0	connective tissue growth factor
<i>Lrrc8b</i>	2.0	leucine rich repeat containing 8 family, member B
<i>Cxcl12</i>	2.0	chemokine (C-X-C motif) ligand 12
<i>Pde3a</i>	2.0	phosphodiesterase 3A, cGMP inhibited
<i>Thbs2</i>	2.0	thrombospondin 2
<i>Pknox2</i>	2.0	Pbx/knotted 1 homeobox 2
<i>Parp14</i>	2.0	poly (ADP-ribose) polymerase family, member 14
<i>Ctsk</i>	2.0	cathepsin K
<i>Rnf122</i>	2.0	ring finger protein 122
<i>Renbp</i>	2.0	renin binding protein
<i>Bambi</i>	2.0	BMP and activin membrane-bound inhibitor, homolog (Xenopus laevis)
<i>Cd93</i>	2.0	CD93 antigen
<i>Rai14</i>	2.0	retinoic acid induced 14
<i>Slc7a7</i>	2.0	solute carrier family 7 (cationic amino acid transporter, y+ system), member 7
<i>Cmtm3</i>	2.0	CKLF-like MARVEL transmembrane domain containing 3
<i>Mpzl2</i>	2.0	myelin protein zero-like 2
<i>Papss2</i>	-2.0	3'-phosphoadenosine 5'-phosphosulfate synthase 2
<i>Ttc28</i>	-2.0	tetratricopeptide repeat domain 28
<i>Wnt4</i>	-2.0	wingless-related MMTV integration site 4
<i>Slc35d3</i>	-2.0	solute carrier family 35, member D3

Appendix

<b>Aass</b>	-2.0	aminoadipate-semialdehyde synthase
<b>Crybb3</b>	-2.0	crystallin, beta B3
<b>Rwdd2a</b>	-2.0	RWD domain containing 2A
<b>Coro2b</b>	-2.0	coronin, actin binding protein, 2B
<b>L1cam</b>	-2.0	L1 cell adhesion molecule
<b>Defb1</b>	-2.0	defensin beta 1
<b>Cdh7</b>	-2.0	cadherin 7, type 2
<b>Cdh4</b>	-2.0	cadherin 4
<b>Cnnm1</b>	-2.0	cyclin M1
<b>Aldh1l2</b>	-2.1	aldehyde dehydrogenase 1 family, member L2
<b>Gm6999</b>	-2.1	predicted gene 6999
<b>Fam107a</b>	-2.1	family with sequence similarity 107, member A
<b>Syt4</b>	-2.1	synaptotagmin-like 4
<b>Vsnl1</b>	-2.1	visinin-like 1
<b>Hrh3</b>	-2.1	histamine receptor H3
<b>Ky</b>	-2.1	kyphoscoliosis peptidase
<b>Hsd17b13</b>	-2.1	hydroxysteroid (17-beta) dehydrogenase 13
<b>Akr1c14</b>	-2.1	aldo-keto reductase family 1, member C14
<b>Skap1</b>	-2.1	src family associated phosphoprotein 1
<b>Lmo1</b>	-2.1	LIM domain only 1
<b>1810010H24Rik</b>	-2.2	RIKEN cDNA 1810010H24 gene
<b>Dbp</b>	-2.2	D site albumin promoter binding protein
<b>Mpp3</b>	-2.2	membrane protein, palmitoylated 3 (MAGUK p55 subfamily member 3)
<b>Atp4a</b>	-2.2	ATPase, H <sup>+</sup> /K <sup>+</sup> exchanging, gastric, alpha polypeptide
<b>Akr1c19</b>	-2.2	aldo-keto reductase family 1, member C19
<b>Wdr67</b>	-2.2	WD repeat domain 67
<b>Rab3c</b>	-2.2	RAB3C, member RAS oncogene family
<b>Prom1</b>	-2.2	prominin 1
<b>Fibin</b>	-2.2	fin bud initiation factor homolog (zebrafish)
<b>Fmo1</b>	-2.2	flavin containing monooxygenase 1
<b>Lphn3</b>	-2.2	latrophilin 3
<b>Eapp</b>	-2.3	E2F-associated phosphoprotein
<b>Dsp</b>	-2.3	desmoplakin
<b>Pappa2</b>	-2.3	pappalysin 2
<b>Slitrk6</b>	-2.3	SLIT and NTRK-like family, member 6
<b>Pycr1</b>	-2.3	pyrroline-5-carboxylate reductase 1
<b>Dach2</b>	-2.3	dachshund 2 (Drosophila)
<b>St8sia1</b>	-2.3	ST8 alpha-N-acetyl-neuraminide alpha-2,8-sialyltransferase 1
<b>Trpm5</b>	-2.4	transient receptor potential cation channel, subfamily M, member 5
<b>Tat</b>	-2.4	tyrosine aminotransferase
<b>Slc2a2</b>	-2.4	solute carrier family 2 (facilitated glucose transporter), member 2
<b>AK220484</b>	-2.4	cDNA sequence AK220484
<b>Ntrk2</b>	-2.4	neurotrophic tyrosine kinase, receptor, type 2
<b>Ptprz1</b>	-2.4	protein tyrosine phosphatase, receptor type Z, polypeptide 1
<b>Rab17</b>	-2.4	RAB17, member RAS oncogene family
<b>Mlph</b>	-2.4	melanophilin
<b>Plk3</b>	-2.5	polo-like kinase 3 (Drosophila)
<b>Gmpr</b>	-2.5	guanosine monophosphate reductase
<b>Camk1g</b>	-2.5	calcium/calmodulin-dependent protein kinase I gamma
<b>Pftk2</b>	-2.5	PFTAIRE protein kinase 2
<b>Pstpip2</b>	-2.5	proline-serine-threonine phosphatase-interacting protein 2
<b>Pdyn</b>	-2.6	prodynorphin
<b>Sult1c2</b>	-2.7	sulfotransferase family, cytosolic, 1C, member 2

## Appendix

<b>4930550C14Rik</b>	-2.7	RIKEN cDNA 4930550C14 gene
<b>Cbs</b>	-2.7	cystathionine beta-synthase
<b>Pcx</b>	-2.7	pyruvate carboxylase
<b>Itgb8</b>	-2.8	integrin beta 8
<b>Rasgrf1</b>	-2.8	RAS protein-specific guanine nucleotide-releasing factor 1
<b>BC039632</b>	-2.8	cDNA sequence BC039632
<b>Gpm6a</b>	-2.8	glycoprotein m6a
<b>Ipcef1</b>	-2.8	interaction protein for cytohesin exchange factors 1
<b>Olfm4</b>	-2.9	olfactomedin 4
<b>Rnf182</b>	-2.9	ring finger protein 182
<b>Grin1</b>	-3.0	glutamate receptor, ionotropic, NMDA1 (zeta 1)
<b>Muc4</b>	-3.0	mucin 4
<b>Serpina7</b>	-3.1	serine (or cysteine) peptidase inhibitor, clade A (alpha-1 antiproteinase, antitrypsin), member 7
<b>Degs2</b>	-3.2	degenerative spermatocyte homolog 2 (Drosophila), lipid desaturase
<b>Slco1a6</b>	-3.2	solute carrier organic anion transporter family, member 1a6
<b>Vstm2l</b>	-3.3	V-set and transmembrane domain containing 2-like
<b>Sgcz</b>	-3.4	sarcoglycan zeta
<b>Robo1</b>	-3.4	roundabout homolog 1 (Drosophila)
<b>Ffar3</b>	-3.5	free fatty acid receptor 3
<b>Abcb4</b>	-3.5	ATP-binding cassette, sub-family B (MDR/TAP), member 4
<b>Kcnh5</b>	-3.6	potassium voltage-gated channel, subfamily H (eag-related), member 5
<b>Tex15</b>	-3.6	testis expressed gene 15
<b>MLxipl</b>	-3.6	MLX interacting protein-like
<b>Hspa12a</b>	-3.6	heat shock protein 12A
<b>Cdh8</b>	-3.7	cadherin 8
<b>Jph3</b>	-3.7	junctophilin 3
<b>Adora1</b>	-3.8	adenosine A1 receptor
<b>Star</b>	-3.8	steroidogenic acute regulatory protein
<b>Slc6a19</b>	-3.9	solute carrier family 6 (neurotransmitter transporter), member 19
<b>Slc4a10</b>	-4.0	solute carrier family 4, sodium bicarbonate cotransporter-like, member 10
<b>Adh1</b>	-4.0	alcohol dehydrogenase 1 (class I)
<b>Ucn3</b>	-4.0	urocortin 3
<b>B3gal5</b>	-4.2	UDP-Gal:betaGlcNAc beta 1,3-galactosyltransferase, polypeptide 5
<b>Gcgr</b>	-4.3	glucagon receptor
<b>Cntfr</b>	-4.5	ciliary neurotrophic factor receptor
<b>Th</b>	-4.6	tyrosine hydroxylase
<b>Ppp1r1a</b>	-4.6	protein phosphatase 1, regulatory (inhibitor) subunit 1A
<b>Slco1a5</b>	-4.8	solute carrier organic anion transporter family, member 1a5
<b>Nrcam</b>	-5.5	neuron-glia-CAM-related cell adhesion molecule
<b>Edn3</b>	-6.5	endothelin 3
<b>G6pc2</b>	-6.9	glucose-6-phosphatase, catalytic, 2
<b>Tmem215</b>	-6.9	transmembrane protein 215
<b>Nell1</b>	-7.2	NEL-like 1 (chicken)
<b>Spc25</b>	-8.6	SPC25, NDC80 kinetochore complex component, homolog (S. cerevisiae)
<b>Angptl7</b>	-9.1	angiopoietin-like 7
<b>Ffar1</b>	-17.6	free fatty acid receptor 1

**Supplementary Table 10. List of genes both differentially regulated in 4-weeks old *Pax6<sup>Leca2</sup>* islets and reported by Xie et al.<sup>216</sup> to be directly bound by PAX6. Gene names in bold refer to those promoter regions that were occupied by PAX6 in  $\beta$ -TC3 cells, whereas the rest were bound in chromatin from lens and forebrain.**

Gene Symbol	Gene name
<i>Cnr1</i>	cannabinoid receptor 1 (brain)
<i>Dapl1</i>	death associated protein-like 1
<i>Dpp10</i>	dipeptidylpeptidase 10
<b><i>Nxph1</i></b>	<b>neurexophilin 1</b>
<i>Hs6st2</i>	heparan sulfate 6-O-sulfotransferase 2
<i>C1ql3</i>	C1q-like 3
<b><i>Galnt13</i></b>	<b>UDP-N-acetyl-alpha-D-galactosamine:polypeptide N-acetylgalactosaminyltransferase 13</b>
<i>Magi2</i>	membrane associated guanylate kinase, WW and PDZ domain containing 2
<i>4931429I11Rik</i>	RIKEN cDNA 4931429I11 gene
<i>Tmem110</i>	transmembrane protein 110
<b><i>Clec7a</i></b>	<b>C-type lectin domain family 7, member a</b>
<i>Ankrd34b</i>	ankyrin repeat domain 34B
<i>Gabra3</i>	gamma-aminobutyric acid (GABA) A receptor, subunit alpha 3
<i>Fhl2</i>	four and a half LIM domains 2
<b><i>Lrrn3</i></b>	<b>leucine rich repeat protein 3, neuronal</b>
<i>Lgi1</i>	leucine-rich repeat LGI family, member 1
<i>Trpm3</i>	transient receptor potential cation channel, subfamily M, member 3
<b><i>Elmod1</i></b>	<b>ELMO domain containing 1</b>
<i>AW551984</i>	expressed sequence AW551984
<i>L1cam</i>	L1 cell adhesion molecule
<i>Mlph</i>	melanophilin
<i>Mpp3</i>	membrane protein, palmitoylated 3 (MAGUK p55 subfamily member 3)
<i>Rab3c</i>	RAB3C, member RAS oncogene family
<i>Gpr158</i>	G protein-coupled receptor 158
<i>Jph3</i>	junctophilin 3
<i>Crybb3</i>	crystallin, beta B3
<b><i>Slc26a1</i></b>	<b>solute carrier family 26 (sulfate transporter), member 1</b>
<i>Rnf182</i>	ring finger protein 182
<b><i>Fgb</i></b>	<b>fibrinogen beta chain</b>
<i>Nostrin</i>	nitric oxide synthase trafficker
<i>Vstm2l</i>	V-set and transmembrane domain containing 2-like
<i>Chi3l1</i>	chitinase 3-like 1
<b><i>Slitrk6</i></b>	<b>SLIT and NTRK-like family, member 6</b>
<i>Hspa12a</i>	heat shock protein 12A
<i>Kcnh5</i>	potassium voltage-gated channel, subfamily H (eag-related), member 5
<i>Defb1</i>	defensin beta 1
<i>Cdh8</i>	cadherin 8
<b><i>Nell1</i></b>	<b>NEL-like 1 (chicken)</b>

**Supplementary Table 11. List of genes both differentially regulated in 20-weeks old *Pax6<sup>Leca2</sup>* islets and reported by Xie et al.<sup>216</sup> to be directly bound by PAX6. Gene names in bold refer to those promoter regions that were occupied by PAX6 in  $\beta$ -TC3 cells, whereas the rest were bound in chromatin from lens and forebrain.**

Gene symbol	Gene name
<i>Plac8</i>	placenta-specific 8
<i>Ifi203</i>	interferon activated gene 203
<i>Aldh1a2</i>	aldehyde dehydrogenase family 1, subfamily A2
<i>Ly6c1</i>	lymphocyte antigen 6 complex, locus C1
<i>Cnr1</i>	cannabinoid receptor 1 (brain)

<i>Fhl2</i>	four and a half LIM domains 2
<i>Fermt1</i>	fermitin family homolog 1 (Drosophila)
<b><i>Fgb</i></b>	<b>fibrinogen beta chain</b>
<i>Ifit2</i>	interferon-induced protein with tetratricopeptide repeats 2
<i>Hs6st2</i>	heparan sulfate 6-O-sulfotransferase 2
<b><i>Npas2</i></b>	<b>neuronal PAS domain protein 2</b>
<i>Lox</i>	lysyl oxidase
<i>Gbp1</i>	guanylate binding protein 1
<i>Tnc</i>	tenascin C
<i>EG634650</i>	predicted gene, EG634650
<i>Olfm3</i>	olfactomedin-like 3
<i>Rsad2</i>	radical S-adenosyl methionine domain containing 2
<i>Cfb</i>	complement factor B
<b><i>A4galt</i></b>	<b>alpha 1,4-galactosyltransferase</b>
<i>Cxcl10</i>	chemokine (C-X-C motif) ligand 10
<i>Pdpr</i>	podoplanin
<i>Gabra3</i>	gamma-aminobutyric acid (GABA) A receptor, subunit alpha 3
<i>Pros1</i>	protein S (alpha)
<i>Cxcl14</i>	chemokine (C-X-C motif) ligand 14
<b><i>Abi3bp</i></b>	<b>ABI gene family, member 3 (NESH) binding protein</b>
<i>AW551984</i>	expressed sequence AW551984
<i>Glt25d2</i>	glycosyltransferase 25 domain containing 2
<i>Rtp4</i>	receptor transporter protein 4
<i>Olfm3</i>	olfactomedin 3
<i>Lif</i>	leukemia inhibitory factor
<i>Gpm6b</i>	glycoprotein m6b
<b><i>Lrrc32</i></b>	<b>leucine rich repeat containing 32</b>
<i>Has2</i>	hyaluronan synthase 2
<b><i>Cd80</i></b>	<b>CD80 antigen</b>
<i>Wdr72</i>	WD repeat domain 72
<i>Tmem47</i>	transmembrane protein 47
<i>Ebf1</i>	early B-cell factor 1
<i>Mmp7</i>	matrix metalloproteinase 7
<i>4931429I11Rik</i>	RIKEN cDNA 4931429I11 gene
<b><i>Opcml</i></b>	<b>opioid binding protein/cell adhesion molecule-like</b>
<i>Uchl1</i>	ubiquitin carboxy-terminal hydrolase L1
<i>Tle4</i>	transducin-like enhancer of split 4, homolog of Drosophila E(spl)
<i>Pi15</i>	peptidase inhibitor 15
<i>Inhba</i>	inhibin beta-A
<i>Slc15a3</i>	solute carrier family 15, member 3
<i>Ccdc85a</i>	coiled-coil domain containing 85A
<i>Il2rg</i>	interleukin 2 receptor, gamma chain
<i>Anxa2</i>	annexin A2
<i>Itgb6</i>	integrin beta 6
<i>Irgm1</i>	immunity-related GTPase family M member 1
<i>Fgf2</i>	fibroblast growth factor 2
<i>9230105E10Rik</i>	RIKEN cDNA 9230105E10 gene
<i>Plaur</i>	plasminogen activator, urokinase receptor
<i>Tmprss2</i>	transmembrane protease, serine 2
<i>Bnc2</i>	basonucin 2
<i>Sdc1</i>	syndecan 1
<b><i>Lrrn3</i></b>	<b>leucine rich repeat protein 3, neuronal</b>
<i>Pdgfrb</i>	platelet derived growth factor receptor, beta polypeptide
<i>Oas1g</i>	2'-5' oligoadenylate synthetase 1G

<i>Freq</i>	frequenin homolog (Drosophila)
<i>Runx1</i>	runt related transcription factor 1
<i>Cygb</i>	cytoglobin
<i>C1r</i>	complement component 1, r subcomponent
<b>Syt17</b>	<b>synaptotagmin XVII</b>
<i>Cd302</i>	CD302 antigen
<i>S1pr3</i>	sphingosine-1-phosphate receptor 3
<b>Cfh</b>	<b>complement component factor h</b>
<b>Slc28a3</b>	<b>solute carrier family 28 (sodium-coupled nucleoside transporter), member 3</b>
<i>Sparcl1</i>	SPARC-like 1
<i>Ccdc80</i>	coiled-coil domain containing 80
<b>Bcl2a1b</b>	<b>B-cell leukemia/lymphoma 2 related protein A1b</b>
<i>Pcolce</i>	procollagen C-endopeptidase enhancer protein
<i>Antxr2</i>	anthrax toxin receptor 2
<i>Sh3bgrl2</i>	SH3 domain binding glutamic acid-rich protein like 2
<b>Cxcl2</b>	<b>chemokine (C-X-C motif) ligand 2</b>
<b>Abcb1b</b>	<b>ATP-binding cassette, sub-family B (MDR/TAP), member 1B</b>
<i>Sema7a</i>	sema domain, immunoglobulin domain (Ig), and GPI membrane anchor, (semaphorin) 7A
<i>Bmp2</i>	bone morphogenetic protein 2
<i>Scn2a1</i>	sodium channel, voltage-gated, type II, alpha 1
<i>Gdf10</i>	growth differentiation factor 10
<i>Gimap4</i>	GTPase, IMAP family member 4
<b>Cyrr1</b>	<b>cysteine and tyrosine-rich protein 1</b>
<i>Flna</i>	filamin, alpha
<i>Sema6a</i>	sema domain, transmembrane domain (TM), and cytoplasmic domain, (semaphorin) 6A
<i>Tek</i>	endothelial-specific receptor tyrosine kinase
<i>Nid1</i>	nidogen 1
<b>Spp1</b>	<b>secreted phosphoprotein 1</b>
<i>Ammecr1</i>	Alport syndrome, mental retardation, midface hypoplasia and elliptocytosis chromosomal region gene 1 homolog (human)
<i>Pltp</i>	phospholipid transfer protein
<b>Col1a1</b>	<b>collagen, type I, alpha 1</b>
<i>Irf7</i>	interferon regulatory factor 7
<i>Igsf6</i>	immunoglobulin superfamily, member 6
<i>Tmem110</i>	transmembrane protein 110
<i>Adamts2</i>	a disintegrin-like and metallopeptidase (repolysin type) with thrombospondin type 1 motif, 2
<i>Slc7a11</i>	solute carrier family 7 (cationic amino acid transporter, y+ system), member 11
<i>Magi2</i>	membrane associated guanylate kinase, WW and PDZ domain containing 2
<i>Slfn2</i>	schlafen 2
<i>Prkch</i>	protein kinase C, eta
<i>Ampd3</i>	adenosine monophosphate deaminase 3
<i>Ltbp1</i>	latent transforming growth factor beta binding protein 1
<i>Has1</i>	hyaluronan synthase1
<i>Anxa10</i>	annexin A10
<i>Odz1</i>	odd Oz/ten-m homolog 1 (Drosophila)
<i>Ppap2b</i>	phosphatidic acid phosphatase type 2B
<i>Stc1</i>	stanniocalcin 1
<i>Nrp2</i>	neuropilin 2
<b>Flrt2</b>	<b>fibronectin leucine rich transmembrane protein 2</b>
<i>Adamts1</i>	a disintegrin-like and metallopeptidase (repolysin type) with thrombospondin type 1 motif, 1
<b>Arrdc4</b>	<b>arrestin domain containing 4</b>
<i>Gli3</i>	GLI-Kruppel family member GLI3
<i>Foxf1a</i>	forkhead box F1a
<i>Dab2</i>	disabled homolog 2 (Drosophila)

<b><i>Podxl</i></b>	<b>podocalyxin-like</b>
<b><i>Galnt13</i></b>	<b>UDP-N-acetyl-alpha-D-galactosamine:polypeptide N-acetylgalactosaminyltransferase 13</b>
<i>C1ql3</i>	C1q-like 3
<i>Serpine2</i>	serine (or cysteine) peptidase inhibitor, clade E, member 2
<i>Epas1</i>	endothelial PAS domain protein 1
<b><i>Gng2</i></b>	<b>guanine nucleotide binding protein (G protein), gamma 2</b>
<i>Limch1</i>	LIM and calponin homology domains 1
<i>Car13</i>	carbonic anhydrase 13
<i>Itga2</i>	integrin alpha 2
<i>Ctgf</i>	connective tissue growth factor
<i>Thbs2</i>	thrombospondin 2
<i>Pknx2</i>	Pbx/knotted 1 homeobox 2
<i>Cd93</i>	CD93 antigen
<i>Papss2</i>	3'-phosphoadenosine 5'-phosphosulfate synthase 2
<i>Crybb3</i>	crystallin, beta B3
<b><i>Rwdd2a</i></b>	<b>RWD domain containing 2A</b>
<i>L1cam</i>	L1 cell adhesion molecule
<i>Defb1</i>	defensin beta 1
<b><i>Cnm1</i></b>	<b>cyclin M1</b>
<i>Aldh1l2</i>	aldehyde dehydrogenase 1 family, member L2
<i>Hrh3</i>	histamine receptor H3
<i>Mpp3</i>	membrane protein, palmitoylated 3 (MAGUK p55 subfamily member 3)
<i>Atp4a</i>	ATPase, H <sup>+</sup> /K <sup>+</sup> exchanging, gastric, alpha polypeptide
<b><i>Akr1c19</i></b>	<b>aldo-keto reductase family 1, member C19</b>
<i>Rab3c</i>	RAB3C, member RAS oncogene family
<i>Dsp</i>	desmoplakin
<i>Pappa2</i>	pappalysin 2
<b><i>Slitrk6</i></b>	<b>SLIT and NTRK-like family, member 6</b>
<i>St8sia1</i>	ST8 alpha-N-acetyl-neuraminide alpha-2,8-sialyltransferase 1
<i>Ntrk2</i>	neurotrophic tyrosine kinase, receptor, type 2
<i>Mlph</i>	melanophilin
<i>Olfm4</i>	olfactomedin 4
<i>Rnf182</i>	ring finger protein 182
<i>Vstm2l</i>	V-set and transmembrane domain containing 2-like
<i>Kcnh5</i>	potassium voltage-gated channel, subfamily H (eag-related), member 5
<i>Hspa12a</i>	heat shock protein 12A
<i>Cdh8</i>	cadherin 8
<i>Jph3</i>	junctionophilin 3
<i>Th</i>	tyrosine hydroxylase
<b><i>Nell1</i></b>	<b>NEL-like 1 (chicken)</b>

## 7. References

1. Bray, S. J. Notch signalling: a simple pathway becomes complex. *Nat. Rev. Mol. Cell Biol.* **7**, 678–689 (2006).
2. Lai, E. C. Notch signaling: control of cell communication and cell fate. *Development* **131**, 965–973 (2004).
3. Fischer, A. & Gessler, M. Delta-Notch--and then? Protein interactions and proposed modes of repression by Hes and Hey bHLH factors. *Nucleic Acids Res.* **35**, 4583–4596 (2007).
4. Kopan, R. & Ilagan, M. X. G. The Canonical Notch Signaling Pathway: Unfolding the Activation Mechanism. *Cell* **137**, 216–233 (2009).
5. D'Souza, B., Miyamoto, A. & Weinmaster, G. The many facets of Notch ligands. *Oncogene* **27**, 5148–5167 (2008).
6. Rebay, I. *et al.* Specific EGF repeats of Notch mediate interactions with Delta and Serrate: implications for Notch as a multifunctional receptor. *Cell* **67**, 687–699 (1991).
7. Gordon, W. R. *et al.* Structural basis for autoinhibition of Notch. *Nat. Struct. Mol. Biol.* **14**, 295–300 (2007).
8. Mumm, J. S. *et al.* A ligand-induced extracellular cleavage regulates gamma-secretase-like proteolytic activation of Notch1. *Mol. Cell* **5**, 197–206 (2000).
9. Brou, C. *et al.* A novel proteolytic cleavage involved in Notch signaling: the role of the disintegrin-metalloprotease TACE. *Mol. Cell* **5**, 207–216 (2000).
10. Fortini, M. E. Gamma-secretase-mediated proteolysis in cell-surface-receptor signalling. *Nat. Rev. Mol. Cell Biol.* **3**, 673–684 (2002).
11. Jarriault, S. *et al.* Signalling downstream of activated mammalian Notch. *Nature* **377**, 355–358 (1995).
12. Hsieh, J. J. *et al.* Truncated mammalian Notch1 activates CBF1/RBPJk-repressed genes by a mechanism resembling that of Epstein-Barr virus EBNA2. *Mol. Cell. Biol.* **16**, 952–959 (1996).
13. Sakamoto, K., Ohara, O., Takagi, M., Takeda, S. & Katsube, K. Intracellular cell-autonomous association of Notch and its ligands: a novel mechanism of Notch signal modification. *Dev. Biol.* **241**, 313–326 (2002).
14. Cordle, J. *et al.* A Conserved Face of the Jagged/Serrate DSL Domain is Involved in Notch Trans-Activation and Cis-Inhibition. *Nat Struct Mol Biol* **15**, 849–857 (2008).
15. Sprinzak, D. *et al.* Cis-interactions between Notch and Delta generate mutually exclusive signalling states. *Nature* **465**, 86–90 (2010).
16. Axelrod, J. D. Delivering the lateral inhibition punchline: it's all about the timing. *Sci Signal* **3**, pe38 (2010).
17. Ong, C.-T. *et al.* Target selectivity of vertebrate notch proteins. Collaboration between discrete domains and CSL-binding site architecture determines activation probability. *J. Biol. Chem.* **281**, 5106–5119 (2006).
18. Beatus, P., Lundkvist, J., Oberg, C. & Lendahl, U. The notch 3 intracellular domain represses notch 1-mediated activation through Hairy/Enhancer of split (HES) promoters. *Development* **126**, 3925–3935 (1999).
19. Wu, J. & Bresnick, E. H. Bare rudiments of notch signaling: how receptor levels are regulated. *Trends Biochem. Sci.* **32**, 477–485 (2007).

20. Fortini, M. E. & Bilder, D. Endocytic regulation of Notch signaling. *Curr. Opin. Genet. Dev.* **19**, 323–328 (2009).
21. Le Borgne, R. Regulation of Notch signalling by endocytosis and endosomal sorting. *Curr. Opin. Cell Biol.* **18**, 213–222 (2006).
22. Parks, A. L., Klueg, K. M., Stout, J. R. & Muskavitch, M. A. Ligand endocytosis drives receptor dissociation and activation in the Notch pathway. *Development* **127**, 1373–1385 (2000).
23. Kandachar, V. & Roegiers, F. Endocytosis and control of Notch signaling. *Current Opinion in Cell Biology* **24**, 534–540 (2012).
24. Stanley, P. Regulation of Notch signaling by glycosylation. *Curr. Opin. Struct. Biol.* **17**, 530–535 (2007).
25. Klüppel, M. & Wrana, J. L. Turning it up a Notch: cross-talk between TGF beta and Notch signaling. *Bioessays* **27**, 115–118 (2005).
26. Kamakura, S. *et al.* Hes binding to STAT3 mediates crosstalk between Notch and JAK-STAT signalling. *Nat. Cell Biol.* **6**, 547–554 (2004).
27. Qi, H. *et al.* Processing of the notch ligand delta by the metalloprotease Kuzbanian. *Science* **283**, 91–94 (1999).
28. Mishra-Gorur, K., Rand, M. D., Perez-Villamil, B. & Artavanis-Tsakonas, S. Down-regulation of Delta by proteolytic processing. *J. Cell Biol.* **159**, 313–324 (2002).
29. Sapir, A., Assa-Kunik, E., Tsruya, R., Schejter, E. & Shilo, B.-Z. Unidirectional Notch signaling depends on continuous cleavage of Delta. *Development* **132**, 123–132 (2005).
30. Bland, C. E., Kimberly, P. & Rand, M. D. Notch-induced Proteolysis and Nuclear Localization of the Delta Ligand. *J. Biol. Chem.* **278**, 13607–13610 (2003).
31. Zolkiewska, A. ADAM proteases: ligand processing and modulation of the Notch pathway. *Cell. Mol. Life Sci.* **65**, 2056–2068 (2008).
32. Six, E. *et al.* The Notch ligand Delta1 is sequentially cleaved by an ADAM protease and gamma-secretase. *Proc. Natl. Acad. Sci. U.S.A.* **100**, 7638–7643 (2003).
33. Gravano, D. M. & Manilay, J. O. Inhibition of proteolysis of Delta-like-1 does not promote or reduce T-cell developmental potential. *Immunol. Cell Biol.* **88**, 746–753 (2010).
34. Liebler, S. S. *et al.* No Evidence for a Functional Role of Bi-Directional Notch Signaling during Angiogenesis. *PLoS ONE* **7**, e53074 (2012).
35. Sun, D., Li, H. & Zolkiewska, A. The role of Delta-like 1 shedding in muscle cell self-renewal and differentiation. *J. Cell. Sci.* **121**, 3815–3823 (2008).
36. Kolev, V. *et al.* The intracellular domain of Notch ligand Delta1 induces cell growth arrest. *FEBS Lett.* **579**, 5798–5802 (2005).
37. Hiratochi, M. *et al.* The Delta intracellular domain mediates TGF-beta/Activin signaling through binding to Smads and has an important bi-directional function in the Notch-Delta signaling pathway. *Nucleic Acids Res.* **35**, 912–922 (2007).
38. Pintar, A., De Biasio, A., Popovic, M., Ivanova, N. & Pongor, S. The intracellular region of Notch ligands: does the tail make the difference? *Biol. Direct* **2**, 19 (2007).
39. Pfister, S. *et al.* Interaction of the MAGUK family member Acvrin1 and the cytoplasmic domain of the Notch ligand Delta1. *J. Mol. Biol.* **333**, 229–235 (2003).
40. Wright, G. J., Leslie, J. D., Ariza-McNaughton, L. & Lewis, J. Delta proteins and MAGI proteins: an interaction of Notch ligands with intracellular scaffolding molecules and its significance for zebrafish development. *Development* **131**, 5659–5669 (2004).

41. Six, E. M. *et al.* The notch ligand Delta1 recruits Dlg1 at cell-cell contacts and regulates cell migration. *J. Biol. Chem.* **279**, 55818–55826 (2004).
42. Mizuhara, E. *et al.* MAGI1 Recruits Dll1 to Cadherin-based Adherens Junctions and Stabilizes It on the Cell Surface. *J. Biol. Chem.* **280**, 26499–26507 (2005).
43. Estrach, S., Legg, J. & Watt, F. M. Syntenin mediates Delta1-induced cohesiveness of epidermal stem cells in culture. *J. Cell. Sci.* **120**, 2944–2952 (2007).
44. Wessells, N. K. & Cohen, J. H. Early pancreas organogenesis: Morphogenesis, tissue interactions, and mass effects. *Developmental Biology* **15**, 237–270 (1967).
45. Burlison, J. S., Long, Q., Fujitani, Y., Wright, C. V. E. & Magnuson, M. A. Pdx-1 and Ptf1a concurrently determine fate specification of pancreatic multipotent progenitor cells. *Dev. Biol.* **316**, 74–86 (2008).
46. Gu, G., Dubauskaite, J. & Melton, D. A. Direct evidence for the pancreatic lineage: NGN3+ cells are islet progenitors and are distinct from duct progenitors. *Development* **129**, 2447–2457 (2002).
47. Pictet, R. L., Clark, W. R., Williams, R. H. & Rutter, W. J. An ultrastructural analysis of the developing embryonic pancreas. *Dev. Biol.* **29**, 436–467 (1972).
48. Herrera, P. L. Adult insulin- and glucagon-producing cells differentiate from two independent cell lineages. *Development* **127**, 2317–2322 (2000).
49. Zhou, Q. *et al.* A Multipotent Progenitor Domain Guides Pancreatic Organogenesis. *Developmental Cell* **13**, 103–114 (2007).
50. Villasenor, A., Chong, D. C., Henkemeyer, M. & Cleaver, O. Epithelial dynamics of pancreatic branching morphogenesis. *Development* **137**, 4295–4305 (2010).
51. Schaffer, A. E., Freude, K. K., Nelson, S. B. & Sander, M. Nkx6 transcription factors and Ptf1a function as antagonistic lineage determinants in multipotent pancreatic progenitors. *Dev. Cell* **18**, 1022–1029 (2010).
52. Apelqvist, J. *et al.* Notch signalling controls pancreatic cell differentiation. *Nature* **400**, 877–881 (1999).
53. Gradwohl, G., Dierich, A., LeMeur, M. & Guillemot, F. neurogenin3 is required for the development of the four endocrine cell lineages of the pancreas. *Proc. Natl. Acad. Sci. U.S.A.* **97**, 1607–1611 (2000).
54. Rojas, A. *et al.* Islet cell development. *Adv. Exp. Med. Biol.* **654**, 59–75 (2010).
55. Talchai, C., Xuan, S., Lin, H. V., Sussel, L. & Accili, D. Pancreatic  $\beta$  Cell Dedifferentiation as a Mechanism of Diabetic  $\beta$  Cell Failure. *Cell* **150**, 1223–1234 (2012).
56. Johansson, K. A. *et al.* Temporal control of neurogenin3 activity in pancreas progenitors reveals competence windows for the generation of different endocrine cell types. *Dev. Cell* **12**, 457–465 (2007).
57. Murtaugh, L. C. Pancreas and beta-cell development: from the actual to the possible. *Development* **134**, 427–438 (2007).
58. Oliver-Krasinski, J. M. & Stoffers, D. A. On the origin of the beta cell. *Genes Dev.* **22**, 1998–2021 (2008).
59. Marsich, E., Vetere, A., Di Piazza, M., Tell, G. & Paoletti, S. The PAX6 gene is activated by the basic helix–loop–helix transcription factor NeuroD/BETA2. *Biochemical Journal* **376**, 707 (2003).
60. St-Onge, L., Sosa-Pineda, B., Chowdhury, K., Mansouri, A. & Gruss, P. Pax6 is required for differentiation of glucagon-producing alpha-cells in mouse pancreas. *Nature* **387**, 406–409 (1997).

61. Sander, M. *et al.* Genetic analysis reveals that PAX6 is required for normal transcription of pancreatic hormone genes and islet development. *Genes Dev.* **11**, 1662–1673 (1997).
62. Collombat, P. *et al.* Opposing actions of Arx and Pax4 in endocrine pancreas development. *Genes Dev.* **17**, 2591–2603 (2003).
63. Sosa-Pineda, B., Chowdhury, K., Torres, M., Oliver, G. & Gruss, P. The Pax4 gene is essential for differentiation of insulin-producing beta cells in the mammalian pancreas. *Nature* **386**, 399–402 (1997).
64. Jensen, J. *et al.* Control of endodermal endocrine development by Hes-1. *Nature Genetics* **24**, 36–44 (2000).
65. Fujikura, J. *et al.* Notch/Rbp-j signaling prevents premature endocrine and ductal cell differentiation in the pancreas. *Cell Metabolism* **3**, 59–65 (2006).
66. Murtaugh, L. C., Stanger, B. Z., Kwan, K. M. & Melton, D. A. Notch Signaling Controls Multiple Steps of Pancreatic Differentiation. *PNAS* **100**, 14920–14925 (2003).
67. Hald, J. *et al.* Activated Notch1 prevents differentiation of pancreatic acinar cells and attenuate endocrine development. *Developmental Biology* **260**, 426–437 (2003).
68. Vooijs, M. *et al.* Mapping the consequence of Notch1 proteolysis in vivo with NIP-CRE. *Development* **134**, 535–544 (2007).
69. Esni, F. *et al.* Notch inhibits Ptf1 function and acinar cell differentiation in developing mouse and zebrafish pancreas. *Development* **131**, 4213–4224 (2004).
70. Ahnfelt-Rønne, J. *et al.* Preservation of proliferating pancreatic progenitor cells by Delta-Notch signaling in the embryonic chicken pancreas. *BMC Developmental Biology* **7**, 63 (2007).
71. Jarriault, S. *et al.* Delta-1 activation of notch-1 signaling results in HES-1 transactivation. *Mol. Cell. Biol.* **18**, 7423–7431 (1998).
72. Lee, J. C. *et al.* Regulation of the Pancreatic Pro-Endocrine Gene Neurogenin3. *Diabetes* **50**, 928–936 (2001).
73. Rose, S. D., Swift, G. H., Peyton, M. J., Hammer, R. E. & MacDonald, R. J. The role of PTF1-P48 in pancreatic acinar gene expression. *J. Biol. Chem.* **276**, 44018–44026 (2001).
74. Ghosh, B. & Leach, S. D. Interactions between Hairy/Enhancer of Split-related proteins and the pancreatic transcription factor Ptf1-p48 modulate function of the PTF1 transcriptional complex. *Biochem J* **393**, 679–685 (2006).
75. Georgia, S., Soliz, R., Li, M., Zhang, P. & Bhushan, A. p57 and Hes1 coordinate cell cycle exit with self-renewal of pancreatic progenitors. *Developmental Biology* **298**, 22–31 (2006).
76. Miyamoto, Y. *et al.* Notch mediates TGF alpha-induced changes in epithelial differentiation during pancreatic tumorigenesis. *Cancer Cell* **3**, 565–576 (2003).
77. Maillard, I. & Pear, W. S. Notch and cancer: best to avoid the ups and downs. *Cancer Cell* **3**, 203–205 (2003).
78. Kopinke, D. *et al.* Lineage tracing reveals the dynamic contribution of Hes1+ cells to the developing and adult pancreas. *Development* **138**, 431–441 (2011).
79. Cras-Méneur, C., Li, L., Kopan, R. & Permutt, M. A. Presenilins, Notch dose control the fate of pancreatic endocrine progenitors during a narrow developmental window. *Genes Dev.* **23**, 2088–2101 (2009).
80. Afelik, S. *et al.* Notch-Mediated Patterning and Cell Fate Allocation of Pancreatic Progenitor Cells. *Development* **139**, 1744–1753 (2012).

81. Pandol, S. J. The Exocrine Pancreas. (2010). at <http://www.ncbi.nlm.nih.gov/books/NBK54128/>
82. In't Veld, P. & Marichal, M. Microscopic anatomy of the human islet of Langerhans. *Adv. Exp. Med. Biol.* **654**, 1–19 (2010).
83. Bardeesy, N. & DePinho, R. A. Pancreatic cancer biology and genetics. *Nature Reviews Cancer* **2**, 897–909 (2002).
84. Offield, M. F. *et al.* PDX-1 is required for pancreatic outgrowth and differentiation of the rostral duodenum. *Development* **122**, 983–995 (1996).
85. Harrison, K. A., Thaler, J., Pfaff, S. L., Gu, H. & Kehrl, J. H. Pancreas dorsal lobe agenesis and abnormal islets of Langerhans in Hlxb9-deficient mice. *Nat. Genet.* **23**, 71–75 (1999).
86. Li, H., Arber, S., Jessell, T. M. & Edlund, H. Selective agenesis of the dorsal pancreas in mice lacking homeobox gene Hlxb9. *Nat. Genet.* **23**, 67–70 (1999).
87. Bencosme, S. A. & Liepa, E. Regional differences of the pancreatic islet. *Endocrinology* **57**, 588–593 (1955).
88. Huang, Y. H., Sun, M. J., Jiang, M. & Fu, B. Y. Immunohistochemical localization of glucagon and pancreatic polypeptide on rat endocrine pancreas: coexistence in rat islet cells. *Eur J Histochem* **53**, (2009).
89. Newsholme, P., Gaudel, C. & McClenaghan, N. H. Nutrient regulation of insulin secretion and beta-cell functional integrity. *Adv. Exp. Med. Biol.* **654**, 91–114 (2010).
90. Straub, S. G. & Sharp, G. W. G. Glucose-stimulated signaling pathways in biphasic insulin secretion. *Diabetes Metab. Res. Rev.* **18**, 451–463 (2002).
91. Clark, R. & Proks, P. ATP-sensitive potassium channels in health and disease. *Adv. Exp. Med. Biol.* **654**, 165–192 (2010).
92. Ashcroft, F. M. & Rorsman, P. Diabetes Mellitus and the  $\beta$  Cell: The Last Ten Years. *Cell* **148**, 1160–1171 (2012).
93. Kim, W. & Egan, J. M. The Role of Incretins in Glucose Homeostasis and Diabetes Treatment. *Pharmacol Rev* **60**, 470–512 (2008).
94. Leech, C. A. *et al.* Molecular physiology of glucagon-like peptide-1 insulin secretagogue action in pancreatic  $\beta$  cells. *Prog. Biophys. Mol. Biol.* **107**, 236–247 (2011).
95. Poitout, V. *et al.* Regulation of the insulin gene by glucose and fatty acids. *J. Nutr.* **136**, 873–876 (2006).
96. Halban, P. A. *et al.* The possible importance of contact between pancreatic islet cells for the control of insulin release. *Endocrinology* **111**, 86–94 (1982).
97. Konstantinova, I. *et al.* EphA-Ephrin-A-mediated beta cell communication regulates insulin secretion from pancreatic islets. *Cell* **129**, 359–370 (2007).
98. Nolan, C. J. & Prentki, M. The islet beta-cell: fuel responsive and vulnerable. *Trends Endocrinol. Metab.* **19**, 285–291 (2008).
99. International Diabetes Federation. IDF Diabetes Atlas Update 2012. at <http://www.idf.org/diabetesatlas/5e/Update2012>
100. Resolutions: General Assembly (GA), 61st session: United Nations (UN). at <http://www.un.org/Depts/dhl/resguide/r61.htm>
101. Aronoff, S. L., Berkowitz, K., Shreiner, B. & Want, L. Glucose Metabolism and Regulation: Beyond Insulin and Glucagon. *Diabetes Spectr* **17**, 183–190 (2004).
102. American Diabetes Association. Screening for Type 2 Diabetes. *Dia Care* **26**, s21–s24 (2003).

103. Lacy, P. E., Hegre, O. D., Gerasimidi-Vazeou, A., Gentile, F. T. & Dionne, K. E. Maintenance of normoglycemia in diabetic mice by subcutaneous xenografts of encapsulated islets. *Science* **254**, 1782–1784 (1991).
104. American Diabetes Association. Diagnosis and Classification of Diabetes Mellitus. *Diabetes Care* **34**, S62–S69 (2010).
105. Pozzilli, P. & Buzzetti, R. A new expression of diabetes: double diabetes. *Trends Endocrinol. Metab.* **18**, 52–57 (2007).
106. Pickup, J. C. & Crook, M. A. Is type II diabetes mellitus a disease of the innate immune system? *Diabetologia* **41**, 1241–1248 (1998).
107. Syed, M. A. *et al.* Is type 2 diabetes a chronic inflammatory/autoimmune disease? *Diabetes Nutr. Metab.* **15**, 68–83 (2002).
108. Hyppönen, E., Virtanen, S. M., Kenward, M. G., Knip, M. & Akerblom, H. K. Obesity, increased linear growth, and risk of type 1 diabetes in children. *Diabetes Care* **23**, 1755–1760 (2000).
109. Donath, M. Y. & Halban, P. A. Decreased beta-cell mass in diabetes: significance, mechanisms and therapeutic implications. *Diabetologia* **47**, 581–589 (2004).
110. Kahn, S. E., Hull, R. L. & Utzschneider, K. M. Mechanisms linking obesity to insulin resistance and type 2 diabetes. *Nature* **444**, 840–846 (2006).
111. Kahn, S. E. The Importance of  $\beta$ -Cell Failure in the Development and Progression of Type 2 Diabetes. *JCEM* **86**, 4047–4058 (2001).
112. Butler, A. E. *et al.*  $\beta$ -Cell Deficit and Increased  $\beta$ -Cell Apoptosis in Humans With Type 2 Diabetes. *Diabetes* **52**, 102–110 (2003).
113. Leahy, J. L. Pathogenesis of type 2 diabetes mellitus. *Arch. Med. Res.* **36**, 197–209 (2005).
114. Zeggini, E. *et al.* Meta-analysis of genome-wide association data and large-scale replication identifies additional susceptibility loci for type 2 diabetes. *Nature Genetics* **40**, 638–645 (2008).
115. Grarup, N. *et al.* Association testing of novel type 2 diabetes risk alleles in the JAZF1, CDC123/CAMK1D, TSPAN8, THADA, ADAMTS9, and NOTCH2 loci with insulin release, insulin sensitivity, and obesity in a population-based sample of 4,516 glucose-tolerant middle-aged Danes. *Diabetes* **57**, 2534–2540 (2008).
116. Dror, V. *et al.* Notch signalling suppresses apoptosis in adult human and mouse pancreatic islet cells. *Diabetologia* **50**, 2504–2515 (2007).
117. Efrat, S. Ex-vivo Expansion of Adult Human Pancreatic Beta-Cells. *Rev Diabet Stud* **5**, 116–122 (2008).
118. Weinberg, N., Ouziel-Yahalom, L., Knoller, S., Efrat, S. & Dor, Y. Lineage tracing evidence for in vitro dedifferentiation but rare proliferation of mouse pancreatic beta-cells. *Diabetes* **56**, 1299–1304 (2007).
119. Bar, Y., Russ, H. A., Knoller, S., Ouziel-Yahalom, L. & Efrat, S. HES-1 Is Involved in Adaptation of Adult Human B-Cells to Proliferation In Vitro. *Diabetes* **57**, 2413–2420 (2008).
120. Ball, A. J., Abrahamsson, A. E., Tyrberg, B., Itkin-Ansari, P. & Levine, F. HES6 reverses nuclear reprogramming of insulin-producing cells following cell fusion. *Biochem. Biophys. Res. Commun.* **355**, 331–337 (2007).
121. Darville, M. I. & Eizirik, D. L. Notch signaling: A mediator of  $\beta$ -cell de-differentiation in diabetes? *Biochemical and Biophysical Research Communications* **339**, 1063–1068 (2006).

122. Hanley, S. C. *et al.*  $\beta$ -Cell mass dynamics and islet cell plasticity in human type 2 diabetes. *Endocrinology* **151**, 1462–1472 (2010).
123. Simpson, T. I. & Price, D. J. Pax6; a pleiotropic player in development. *Bioessays* **24**, 1041–1051 (2002).
124. Chi, N. & Epstein, J. A. Getting your Pax straight: Pax proteins in development and disease. *Trends Genet.* **18**, 41–47 (2002).
125. Yusuf, D. *et al.* The Transcription Factor Encyclopedia. *Genome Biology* **13**, R24 (2012).
126. Epstein, J., Cai, J., Glaser, T., Jepeal, L. & Maas, R. Identification of a Pax paired domain recognition sequence and evidence for DNA-dependent conformational changes. *J. Biol. Chem.* **269**, 8355–8361 (1994).
127. Wilson, D., Sheng, G., Lecuit, T., Dostatni, N. & Desplan, C. Cooperative dimerization of paired class homeo domains on DNA. *Genes Dev.* **7**, 2120–2134 (1993).
128. Tang, H. K., Singh, S. & Saunders, G. F. Dissection of the Transactivation Function of the Transcription Factor Encoded by the Eye Developmental Gene PAX6. *J. Biol. Chem.* **273**, 7210–7221 (1998).
129. Epstein, J. A. *et al.* Two independent and interactive DNA-binding subdomains of the Pax6 paired domain are regulated by alternative splicing. *Genes Dev.* **8**, 2022–2034 (1994).
130. Kozmik, Z., Czerny, T. & Busslinger, M. Alternatively spliced insertions in the paired domain restrict the DNA sequence specificity of Pax6 and Pax8. *EMBO J.* **16**, 6793–6803 (1997).
131. Jun, S. & Desplan, C. Cooperative interactions between paired domain and homeodomain. *Development* **122**, 2639–2650 (1996).
132. Thaug, C. *et al.* Novel ENU-induced eye mutations in the mouse: models for human eye disease. *Hum. Mol. Genet.* **11**, 755–767 (2002).
133. Ashery-Padan, R. *et al.* Conditional inactivation of Pax6 in the pancreas causes early onset of diabetes. *Dev. Biol.* **269**, 479–488 (2004).
134. Hart, A. W., Mella, S., Mendrychowski, J., van Heyningen, V. & Kleinjan, D. A. The developmental regulator pax6 is essential for maintenance of islet cell function in the adult mouse pancreas. *PLoS ONE* **8**, e54173 (2013).
135. Graw, J. *et al.* Three novel Pax6 alleles in the mouse leading to the same small-eye phenotype caused by different consequences at target promoters. *Invest. Ophthalmol. Vis. Sci.* **46**, 4671–4683 (2005).
136. Gradinger, D., Cavanna, D. *et al.* Molecular and Histological Comparison of Pancreata from Adult Pax6Leca2 Mutant Mice of Different Ages. *Poster presentation at the 26th International Mammalian Genome Conference* (St Pete Beach, Florida, USA (October 2012)).
137. Dor, Y., Brown, J., Martinez, O. I. & Melton, D. A. Adult pancreatic beta-cells are formed by self-duplication rather than stem-cell differentiation. *Nature* **429**, 41–46 (2004).
138. Hozumi, K. *et al.* Delta-like 1 is necessary for the generation of marginal zone B cells but not T cells in vivo. *Nature Immunology* **5**, 638–644 (2004).
139. Thorel, F. *et al.* Conversion of adult pancreatic alpha-cells to beta-cells after extreme beta-cell loss. *Nature* **464**, 1149–1154 (2010).
140. Soewarto, D. *et al.* The large-scale Munich ENU-mouse-mutagenesis screen. *Mammalian Genome* **11**, 507–510 (2000).

141. Bustin, S. A. *et al.* The MIQE guidelines: minimum information for publication of quantitative real-time PCR experiments. *Clin. Chem.* **55**, 611–622 (2009).
142. Flicek, P. *et al.* Ensembl 2013. *Nucleic Acids Res.* **41**, D48–55 (2013).
143. Gutierrez, L. *et al.* The lack of a systematic validation of reference genes: a serious pitfall undervalued in reverse transcription-polymerase chain reaction (RT-PCR) analysis in plants. *Plant Biotechnol. J.* **6**, 609–618 (2008).
144. Vandesompele, J. *et al.* Accurate normalization of real-time quantitative RT-PCR data by geometric averaging of multiple internal control genes. *Genome Biol.* **3**, RESEARCH0034 (2002).
145. Suslov, O. & Steindler, D. A. PCR inhibition by reverse transcriptase leads to an overestimation of amplification efficiency. *Nucleic Acids Res.* **33**, e181 (2005).
146. Levesque-Sergerie, J.-P., Duquette, M., Thibault, C., Delbecchi, L. & Bissonnette, N. Detection limits of several commercial reverse transcriptase enzymes: impact on the low- and high-abundance transcript levels assessed by quantitative RT-PCR. *BMC Molecular Biology* **8**, 93 (2007).
147. Livak, K. J. & Schmittgen, T. D. Analysis of Relative Gene Expression Data Using Real-Time Quantitative PCR and the 2- $\Delta\Delta$ CT Method. *Methods* **25**, 402–408 (2001).
148. Rainer, J., Sanchez-Cabo, F., Stocker, G., Sturn, A. & Trajanoski, Z. CARMAweb: comprehensive R- and bioconductor-based web service for microarray data analysis. *Nucleic Acids Res.* **34**, W498–503 (2006).
149. Benjamini, Y. & Hochberg, Y. Controlling the False Discovery Rate: A Practical and Powerful Approach to Multiple Testing. *Journal of the Royal Statistical Society. Series B (Methodological)* **57**, 289–300 (1995).
150. Gallagher, S. R. One-dimensional SDS gel electrophoresis of proteins. *Curr Protoc Immunol* **Chapter 8**, Unit 8.4 (2006).
151. Gallagher, S., Winston, S. E., Fuller, S. A. & Hurrell, J. G. R. Immunoblotting and immunodetection. *Curr Protoc Cell Biol* **Chapter 6**, Unit 6.2 (2011).
152. Li, D.-S., Yuan, Y.-H., Tu, H.-J., Liang, Q.-L. & Dai, L.-J. A protocol for islet isolation from mouse pancreas. *Nature Protocols* **4**, 1649–1652 (2009).
153. Carter, J. D., Dula, S. B., Corbin, K. L., Wu, R. & Nunemaker, C. S. A Practical Guide to Rodent Islet Isolation and Assessment. *Biol Proced Online* **11**, 3–31 (2009).
154. Watkins, S. Immunohistochemistry. *Curr Protoc Cytom* **Chapter 12**, Unit 12.16 (2009).
155. Brissova, M. *et al.* Assessment of human pancreatic islet architecture and composition by laser scanning confocal microscopy. *J. Histochem. Cytochem.* **53**, 1087–1097 (2005).
156. Le Marchand, S. J. & Piston, D. W. Glucose suppression of glucagon secretion: metabolic and calcium responses from alpha-cells in intact mouse pancreatic islets. *J. Biol. Chem.* **285**, 14389–14398 (2010).
157. Merglen, A. *et al.* Glucose sensitivity and metabolism-secretion coupling studied during two-year continuous culture in INS-1E insulinoma cells. *Endocrinology* **145**, 667–678 (2004).
158. Madadi, G., Dalvi, P. S. & Belsham, D. D. Regulation of brain insulin mRNA by glucose and glucagon-like peptide 1. *Biochemical and Biophysical Research Communications* **376**, 694–699 (2008).
159. Geling, A., Steiner, H., Willem, M., Bally-Cuif, L. & Haass, C. A  $\gamma$ -secretase inhibitor blocks Notch signaling in vivo and causes a severe neurogenic phenotype in zebrafish. *EMBO Rep* **3**, 688–694 (2002).

160. Sauer, B. & Henderson, N. Site-specific DNA recombination in mammalian cells by the Cre recombinase of bacteriophage P1. *Proc Natl Acad Sci U S A* **85**, 5166–5170 (1988).
161. Sauer, B. & Henderson, N. Cre-stimulated recombination at loxP-containing DNA sequences placed into the mammalian genome. *Nucleic Acids Res.* **17**, 147–161 (1989).
162. Metzger, D., Clifford, J., Chiba, H. & Chambon, P. Conditional site-specific recombination in mammalian cells using a ligand-dependent chimeric Cre recombinase. *Proc. Natl. Acad. Sci. U.S.A.* **92**, 6991–6995 (1995).
163. Feil, R. *et al.* Ligand-activated site-specific recombination in mice. *Proc. Natl. Acad. Sci. U.S.A.* **93**, 10887–10890 (1996).
164. Postic, C. *et al.* Dual roles for glucokinase in glucose homeostasis as determined by liver and pancreatic beta cell-specific gene knock-outs using Cre recombinase. *J. Biol. Chem.* **274**, 305–315 (1999).
165. Lee, J.-Y. *et al.* RIP-Cre revisited, evidence for impairments of pancreatic beta-cell function. *J. Biol. Chem.* **281**, 2649–2653 (2006).
166. Pomplun, D., Florian, S., Schulz, T., Pfeiffer, A. F. H. & Ristow, M. Alterations of pancreatic beta-cell mass and islet number due to Ins2-controlled expression of Cre recombinase: RIP-Cre revisited; part 2. *Horm. Metab. Res.* **39**, 336–340 (2007).
167. Thyagarajan, B., Guimarães, M. J., Groth, A. C. & Calos, M. P. Mammalian genomes contain active recombinase recognition sites. *Gene* **244**, 47–54 (2000).
168. Silver, D. P. & Livingston, D. M. Self-excising retroviral vectors encoding the Cre recombinase overcome Cre-mediated cellular toxicity. *Mol. Cell* **8**, 233–243 (2001).
169. Huh, W. J., Mysorekar, I. U. & Mills, J. C. Inducible activation of Cre recombinase in adult mice causes gastric epithelial atrophy, metaplasia, and regenerative changes in the absence of ‘floxed’ alleles. *Am J Physiol Gastrointest Liver Physiol* **299**, G368–G380 (2010).
170. Schmidt, E. E., Taylor, D. S., Prigge, J. R., Barnett, S. & Capecchi, M. R. Illegitimate Cre-dependent chromosome rearrangements in transgenic mouse spermatids. *PNAS* **97**, 13702–13707 (2000).
171. Loonstra, A. *et al.* Growth inhibition and DNA damage induced by Cre recombinase in mammalian cells. *Proc. Natl. Acad. Sci. U.S.A.* **98**, 9209–9214 (2001).
172. Magnuson, M. A. & Burlison, J. S. Caveats and considerations for performing pancreas-specific gene manipulations in the mouse. *Diabetes Obes Metab* **9 Suppl 2**, 5–13 (2007).
173. Liu, Y. *et al.* Tamoxifen-Independent Recombination in the RIP-CreER Mouse. *PLoS ONE* **5**, e13533 (2010).
174. Kawano, K. *et al.* Spontaneous Long-Term Hyperglycemic Rat With Diabetic Complications: Otsuka Long-Evans Tokushima Fatty (OLETF) Strain. *Diabetes* **41**, 1422–1428 (1992).
175. Movassat, J., Saulnier, C., Serradas, P. & Portha, B. Impaired development of pancreatic beta-cell mass is a primary event during the progression to diabetes in the GK rat. *Diabetologia* **40**, 916–925 (1997).
176. Riccillo, F. L., Bracamonte, M. I., Montenegro, S., Martínez, S. M. & Ronderos, J. R. Progressive histopathological changes and  $\beta$ -cell loss in the pancreas of a new spontaneous rat model of type 2 diabetes. *Tissue and Cell* **44**, 101–110 (2012).
177. Homo-Delarche, F. *et al.* Islet inflammation and fibrosis in a spontaneous model of type 2 diabetes, the GK rat. *Diabetes* **55**, 1625–1633 (2006).

178. Yoshikawa, H. *et al.* Role of TGF- $\beta$ 1 in the development of pancreatic fibrosis in Otsuka Long-Evans Tokushima Fatty rats. *Am J Physiol Gastrointest Liver Physiol* **282**, G549–G558 (2002).
179. Löhr, M. *et al.* Transforming growth factor-beta1 induces desmoplasia in an experimental model of human pancreatic carcinoma. *Cancer Res.* **61**, 550–555 (2001).
180. Gressner, O. A. & Gressner, A. M. Connective tissue growth factor: a fibrogenic master switch in fibrotic liver diseases. *Liver Int.* **28**, 1065–1079 (2008).
181. Kuiper, E. J. *et al.* The angio-fibrotic switch of VEGF and CTGF in proliferative diabetic retinopathy. *PLoS ONE* **3**, e2675 (2008).
182. Sanvito, F. *et al.* TGF-beta 1 overexpression in murine pancreas induces chronic pancreatitis and, together with TNF-alpha, triggers insulin-dependent diabetes. *Biochem. Biophys. Res. Commun.* **217**, 1279–1286 (1995).
183. Ebert, M. P. A. *et al.* Reduced PTEN expression in the pancreas overexpressing transforming growth factor-beta 1. *Br. J. Cancer* **86**, 257–262 (2002).
184. Harper, J. W., Adami, G. R., Wei, N., Keyomarsi, K. & Elledge, S. J. The p21 Cdk-interacting protein Cip1 is a potent inhibitor of G1 cyclin-dependent kinases. *Cell* **75**, 805–816 (1993).
185. Gorospe, M., Wang, X. & Holbrook, N. J. Functional role of p21 during the cellular response to stress. *Gene Expr.* **7**, 377–385 (1999).
186. Cazzalini, O., Scovassi, A. I., Savio, M., Stivala, L. A. & Prosperi, E. Multiple roles of the cell cycle inhibitor p21(CDKN1A) in the DNA damage response. *Mutat. Res.* **704**, 12–20 (2010).
187. Gong, J., Ammanamanchi, S., Ko, T. C. & Brattain, M. G. Transforming growth factor beta 1 increases the stability of p21/WAF1/CIP1 protein and inhibits CDK2 kinase activity in human colon carcinoma FET cells. *Cancer Res.* **63**, 3340–3346 (2003).
188. Bauer, J., Sporn, J. C., Cabral, J., Gomez, J. & Jung, B. Effects of Activin and TGF $\beta$  on p21 in Colon Cancer. *PLoS ONE* **7**, e39381 (2012).
189. Smith, W. L., Garavito, R. M. & DeWitt, D. L. Prostaglandin Endoperoxide H Synthases (Cyclooxygenases)-1 and -2. *J. Biol. Chem.* **271**, 33157–33160 (1996).
190. Sorli, C. H. *et al.* Basal expression of cyclooxygenase-2 and nuclear factor-interleukin 6 are dominant and coordinately regulated by interleukin 1 in the pancreatic islet. *Proc. Natl. Acad. Sci. U.S.A.* **95**, 1788–1793 (1998).
191. Robertson, R. P. Dominance of cyclooxygenase-2 in the regulation of pancreatic islet prostaglandin synthesis. *Diabetes* **47**, 1379–1383 (1998).
192. Tran, P. O., Gleason, C. E., Poitout, V. & Robertson, R. P. Prostaglandin E(2) mediates inhibition of insulin secretion by interleukin-1beta. *J. Biol. Chem.* **274**, 31245–31248 (1999).
193. Tabatabaie, T., Waldon, A. M., Jacob, J. M., Floyd, R. A. & Kotake, Y. COX-2 inhibition prevents insulin-dependent diabetes in low-dose streptozotocin-treated mice. *Biochem. Biophys. Res. Commun.* **273**, 699–704 (2000).
194. Heitmeier, M. R. *et al.* Role of cyclooxygenase-2 in cytokine-induced beta-cell dysfunction and damage by isolated rat and human islets. *J. Biol. Chem.* **279**, 53145–53151 (2004).
195. Shanmugam, N. *et al.* Increased expression of cyclooxygenase-2 in human pancreatic islets treated with high glucose or ligands of the advanced glycation endproduct-specific receptor (AGER), and in islets from diabetic mice. *Diabetologia* **49**, 100–107 (2006).

196. Yeh, T.-S. *et al.* The activated Notch1 signal pathway is associated with gastric cancer progression through cyclooxygenase-2. *Cancer Res.* **69**, 5039–5048 (2009).
197. Tseng, Y.-C. *et al.* Notch2-induced COX-2 expression enhancing gastric cancer progression. *Mol. Carcinog.* **51**, 939–951 (2012).
198. Oström, M. *et al.* Retinoic acid promotes the generation of pancreatic endocrine progenitor cells and their further differentiation into beta-cells. *PLoS ONE* **3**, e2841 (2008).
199. Shimamura, M., Karasawa, H., Sakakibara, S. & Shinagawa, A. Raldh3 expression in diabetic islets reciprocally regulates secretion of insulin and glucagon from pancreatic islets. *Biochem. Biophys. Res. Commun.* **401**, 79–84 (2010).
200. Rhee, E.-J. & Plutzky, J. Retinoid Metabolism and Diabetes Mellitus. *Diabetes & Metabolism Journal* **36**, 167 (2012).
201. Paschaki, M. *et al.* Retinoic Acid-Dependent Signaling Pathways and Lineage Events in the Developing Mouse Spinal Cord. *PLoS ONE* **7**, e32447 (2012).
202. Murata-Ohsawa, M., Tohda, S., Kogoshi, H., Sakano, S. & Nara, N. The Notch ligand, Delta-1, alters retinoic acid (RA)-induced neutrophilic differentiation into monocytic and reduces RA-induced apoptosis in NB4 cells. *Leuk. Res.* **29**, 197–203 (2005).
203. Rathcke, C. N., Johansen, J. S. & Vestergaard, H. YKL-40, a biomarker of inflammation, is elevated in patients with type 2 diabetes and is related to insulin resistance. *Inflamm. Res.* **55**, 53–59 (2006).
204. Rathcke, C. N., Persson, F., Tarnow, L., Rossing, P. & Vestergaard, H. YKL-40, a marker of inflammation and endothelial dysfunction, is elevated in patients with type 1 diabetes and increases with levels of albuminuria. *Diabetes Care* **32**, 323–328 (2009).
205. Schinner, S. *et al.* Regulation of insulin secretion, glucokinase gene transcription and beta cell proliferation by adipocyte-derived Wnt signalling molecules. *Diabetologia* **51**, 147–154 (2008).
206. Bordonaro, M., Tewari, S., Atamna, W. & Lazarova, D. L. The Notch ligand Delta-like 1 integrates inputs from TGFbeta/Activin and Wnt pathways. *Exp. Cell Res.* **317**, 1368–1381 (2011).
207. Pociot, F. & McDermott, M. F. Genetics of type 1 diabetes mellitus. *Genes Immun.* **3**, 235–249 (2002).
208. Hellström, M. *et al.* Dll4 signalling through Notch1 regulates formation of tip cells during angiogenesis. *Nature* **445**, 776–780 (2007).
209. Yan, M. Therapeutic promise and challenges of targeting DLL4/NOTCH1. *Vascular Cell* **3**, 17 (2011).
210. Pellegrinet, L. *et al.* Dll1- and dll4-mediated notch signaling are required for homeostasis of intestinal stem cells. *Gastroenterology* **140**, 1230–1240.e1–7 (2011).
211. Cavanna, D., Gradinger, D., Schieven, N., Przemec, G. K. H. & Hrabé De Angelis, M. Analysis of Delta-like 1 (DLL1) in adult murine islets. *Poster presentation at the 26th International Mammalian Genome Conference* (St Pete Beach, Florida, USA (October 2012)).
212. Pajvani, U. B. *et al.* Inhibition of Notch signaling ameliorates insulin resistance in a FoxO1-dependent manner. *Nat. Med.* **17**, 961–967 (2011).
213. Rubio-Aliaga, I. *et al.* Dll1 Haploinsufficiency in Adult Mice Leads to a Complex Phenotype Affecting Metabolic and Immunological Processes. *PLoS ONE* **4**, e6054 (2009).

214. Ishihara, H. *et al.* Pancreatic beta cell line MIN6 exhibits characteristics of glucose metabolism and glucose-stimulated insulin secretion similar to those of normal islets. *Diabetologia* **36**, 1139–1145 (1993).
215. Ravassard, P. *et al.* A genetically engineered human pancreatic  $\beta$  cell line exhibiting glucose-inducible insulin secretion. *Journal of Clinical Investigation* **121**, 3589–3597 (2011).
216. Xie, Q. *et al.* Pax6 Interactions with Chromatin and Identification of Its Novel Direct Target Genes in Lens and Forebrain. *PLoS ONE* **8**, e54507 (2013).
217. Efrat, S. *et al.* Beta-cell lines derived from transgenic mice expressing a hybrid insulin gene-oncogene. *Proc. Natl. Acad. Sci. U.S.A.* **85**, 9037–9041 (1988).
218. Efrat, S., Surana, M. & Fleischer, N. Glucose induces insulin gene transcription in a murine pancreatic beta-cell line. *J. Biol. Chem.* **266**, 11141–11143 (1991).
219. Walcher, T. *et al.* Functional dissection of the paired domain of Pax6 reveals molecular mechanisms of coordinating neurogenesis and proliferation. *Development* **140**, 1123–1136 (2013).
220. Chauhan, B. K., Yang, Y., Cveklova, K. & Cvekl, A. Functional Properties of Natural Human PAX6 and PAX6(5a) Mutants. *Invest Ophthalmol Vis Sci* **45**, 385–392 (2004).
221. Xu, H. E. *et al.* Crystal structure of the human Pax6 paired domain–DNA complex reveals specific roles for the linker region and carboxy-terminal subdomain in DNA binding. *Genes Dev.* **13**, 1263–1275 (1999).
222. Chauhan, B. K., Yang, Y., Cveklová, K. & Cvekl, A. Functional interactions between alternatively spliced forms of Pax6 in crystallin gene regulation and in haploinsufficiency. *Nucl. Acids Res.* **32**, 1696–1709 (2004).
223. Yamaguchi, Y., Sawada, J., Yamada, M., Handa, H. & Azuma, N. Autoregulation of Pax6 transcriptional activation by two distinct DNA-binding subdomains of the paired domain. *Genes Cells* **2**, 255–261 (1997).
224. Azuma, N., Nishina, S., Yanagisawa, H., Okuyama, T. & Yamada, M. PAX6 missense mutation in isolated foveal hypoplasia. *Nat. Genet.* **13**, 141–142 (1996).
225. Singh, S., Stellrecht, C. M., Tang, H. K. & Saunders, G. F. Modulation of PAX6 Homeodomain Function by the Paired Domain. *J. Biol. Chem.* **275**, 17306–17313 (2000).
226. Singh, S., Stellrecht, C. M., Tang, H. K. & Saunders, G. F. Modulation of PAX6 Homeodomain Function by the Paired Domain. *J. Biol. Chem.* **275**, 17306–17313 (2000).
227. Sharrocks, A. D. The ETS-domain transcription factor family. *Nat. Rev. Mol. Cell Biol.* **2**, 827–837 (2001).
228. Plaza, S., Grevin, D., MacLeod, K., Stehelin, D. & Saule, S. Pax-QNR/Pax-6, a paired- and homeobox-containing protein, recognizes Ets binding sites and can alter the transactivating properties of Ets transcription factors. *Gene Expr.* **4**, 43–52 (1994).
229. Tuoc, T. & Stoykova, A. Er81 is a downstream target of Pax6 in cortical progenitors. *BMC Developmental Biology* **8**, 23 (2008).
230. Fitzsimmons, D. *et al.* Pax-5 (BSAP) recruits Ets proto-oncogene family proteins to form functional ternary complexes on a B-cell-specific promoter. *Genes Dev.* **10**, 2198–2211 (1996).
231. Gosmain, Y. *et al.* Pax6 is crucial for  $\beta$ -cell function, insulin biosynthesis, and glucose-induced insulin secretion. *Mol. Endocrinol.* **26**, 696–709 (2012).

232. Cissell, M. A., Zhao, L., Sussel, L., Henderson, E. & Stein, R. Transcription Factor Occupancy of the Insulin Gene in Vivo EVIDENCE FOR DIRECT REGULATION BY Nkx2.2. *J. Biol. Chem.* **278**, 751–756 (2003).
233. Knepel, W. Transcriptional control of pancreatic islet hormones gene expression. *Exp. Clin. Endocrinol.* **101**, 39–45 (1993).
234. Ritz-Laser, B., Estreicher, A., Klages, N., Saule, S. & Philippe, J. Pax-6 and Cdx-2/3 interact to activate glucagon gene expression on the G1 control element. *J. Biol. Chem.* **274**, 4124–4132 (1999).
235. Grapp, M. *et al.* The homeodomain of PAX6 is essential for PAX6-dependent activation of the rat glucagon gene promoter: evidence for a PHO-like binding that induces an active conformation. *Biochim. Biophys. Acta* **1789**, 403–412 (2009).
236. Wen, J. H. *et al.* Paired box 6 (PAX6) regulates glucose metabolism via proinsulin processing mediated by prohormone convertase 1/3 (PC1/3). *Diabetologia* **52**, 504–513 (2009).
237. Katz, L. S., Gosmain, Y., Marthinet, E. & Philippe, J. Pax6 regulates the proglucagon processing enzyme PC2 and its chaperone 7B2. *Mol. Cell. Biol.* **29**, 2322–2334 (2009).
238. Samaras, S. E. *et al.* Conserved sequences in a tissue-specific regulatory region of the pdx-1 gene mediate transcription in Pancreatic beta cells: role for hepatocyte nuclear factor 3 beta and Pax6. *Mol. Cell. Biol.* **22**, 4702–4713 (2002).
239. Raum, J. C. *et al.* Islet beta-cell-specific MafA transcription requires the 5'-flanking conserved region 3 control domain. *Mol. Cell. Biol.* **30**, 4234–4244 (2010).
240. Dames, P. *et al.* Relative roles of the different Pax6 domains for pancreatic alpha cell development. *BMC Developmental Biology* **10**, 39 (2010).
241. Beimesche, S. *et al.* Tissue-specific transcriptional activity of a pancreatic islet cell-specific enhancer sequence/Pax6-binding site determined in normal adult tissues in vivo using transgenic mice. *Mol. Endocrinol.* **13**, 718–728 (1999).
242. McKinnon, C. M. & Docherty, K. Pancreatic duodenal homeobox-1, PDX-1, a major regulator of beta cell identity and function. *Diabetologia* **44**, 1203–1214 (2001).
243. Barrow, J., Hay, C. W., Ferguson, L. A., Docherty, H. M. & Docherty, K. Transcription factor cycling on the insulin promoter. *FEBS Lett.* **580**, 711–715 (2006).
244. Matsuoka, T. *et al.* Members of the large Maf transcription family regulate insulin gene transcription in islet beta cells. *Mol. Cell. Biol.* **23**, 6049–6062 (2003).
245. Matsuoka, T. *et al.* The MafA transcription factor appears to be responsible for tissue-specific expression of insulin. *Proc. Natl. Acad. Sci. U.S.A.* **101**, 2930–2933 (2004).
246. Zhang, C. *et al.* MafA is a key regulator of glucose-stimulated insulin secretion. *Mol. Cell. Biol.* **25**, 4969–4976 (2005).
247. Itoh, Y. *et al.* Free fatty acids regulate insulin secretion from pancreatic  $\beta$  cells through GPR40. *Nature* **422**, 173–176 (2003).
248. Wagner, R. *et al.* Reevaluation of Fatty acid receptor 1 (FFAR1/GPR40) as drug target for the stimulation of insulin secretion in humans. *Diabetes* (2013). doi:10.2337/db12-1249
249. Sørensen, H. *et al.* Glucagon receptor knockout mice display increased insulin sensitivity and impaired beta-cell function. *Diabetes* **55**, 3463–3469 (2006).
250. Gelling, R. W. *et al.* Pancreatic beta-cell overexpression of the glucagon receptor gene results in enhanced beta-cell function and mass. *Am. J. Physiol. Endocrinol. Metab.* **297**, E695–707 (2009).

251. Johansson, S. M. *et al.* A1 receptor deficiency causes increased insulin and glucagon secretion in mice. *Biochem. Pharmacol.* **74**, 1628–1635 (2007).
252. Salehi, A., Parandeh, F., Fredholm, B. B., Grapengiesser, E. & Hellman, B. Absence of adenosine A1 receptors unmasks pulses of insulin release and prolongs those of glucagon and somatostatin. *Life Sci.* **85**, 470–476 (2009).
253. Huang, C., Snider, F. & Cross, J. C. Prolactin receptor is required for normal glucose homeostasis and modulation of beta-cell mass during pregnancy. *Endocrinology* **150**, 1618–1626 (2009).
254. Jitrapakdee, S. & Wallace, J. C. Structure, function and regulation of pyruvate carboxylase. *Biochem. J.* **340 ( Pt 1)**, 1–16 (1999).
255. Han, J. & Liu, Y. Q. Reduction of islet pyruvate carboxylase activity might be related to the development of type 2 diabetes mellitus in Agouti-K mice. *J. Endocrinol.* **204**, 143–152 (2010).
256. MacDonald, M. J. *et al.* Decreased levels of metabolic enzymes in pancreatic islets of patients with type 2 diabetes. *Diabetologia* **52**, 1087–1091 (2009).
257. Hasan, N. M. *et al.* Impaired Anaplerosis and Insulin Secretion in Insulinoma Cells Caused by Small Interfering RNA-mediated Suppression of Pyruvate Carboxylase. *J. Biol. Chem.* **283**, 28048–28059 (2008).
258. Xu, J., Han, J., Long, Y. S., Epstein, P. N. & Liu, Y. Q. The role of pyruvate carboxylase in insulin secretion and proliferation in rat pancreatic beta cells. *Diabetologia* **51**, 2022–2030 (2008).
259. Jensen, M. V. *et al.* Metabolic cycling in control of glucose-stimulated insulin secretion. *Am J Physiol Endocrinol Metab* **295**, E1287–E1297 (2008).
260. Arden, S. D. *et al.* Molecular cloning of a pancreatic islet-specific glucose-6-phosphatase catalytic subunit-related protein. *Diabetes* **48**, 531–542 (1999).
261. Petrolonis, A. J. *et al.* Enzymatic characterization of the pancreatic islet-specific glucose-6-phosphatase-related protein (IGRP). *J. Biol. Chem.* **279**, 13976–13983 (2004).
262. Rose, C. S. *et al.* A variant in the G6PC2/ABCB11 locus is associated with increased fasting plasma glucose, increased basal hepatic glucose production and increased insulin release after oral and intravenous glucose loads. *Diabetologia* **52**, 2122–2129 (2009).
263. Tam, C. H. T. *et al.* Common Polymorphisms in MTNR1B, G6PC2 and GCK Are Associated with Increased Fasting Plasma Glucose and Impaired Beta-Cell Function in Chinese Subjects. *PLoS ONE* **5**, e11428 (2010).
264. Martin, C. C., Oeser, J. K. & O'Brien, R. M. Differential Regulation of Islet-specific Glucose-6-phosphatase Catalytic Subunit-related Protein Gene Transcription by Pax-6 and Pdx-1. *J. Biol. Chem.* **279**, 34277–34289 (2004).
265. Li, C. *et al.* Urocortin III is expressed in pancreatic beta-cells and stimulates insulin and glucagon secretion. *Endocrinology* **144**, 3216–3224 (2003).
266. Li, C., Chen, P., Vaughan, J., Lee, K.-F. & Vale, W. Urocortin 3 regulates glucose-stimulated insulin secretion and energy homeostasis. *PNAS* **104**, 4206–4211 (2007).
267. Blum, B. *et al.* Functional beta-cell maturation is marked by an increased glucose threshold and by expression of urocortin 3. *Nat. Biotechnol.* **30**, 261–264 (2012).
268. Hou, L.-Q. *et al.* Expression and localization of mesothelin in developing rat pancreas. *Development, Growth & Differentiation* **50**, 531–541 (2008).

269. Nordquist, R. E. *et al.* Characterization of behavioral response to amphetamine, tyrosine hydroxylase levels, and dopamine receptor levels in neurokinin 3 receptor knockout mice. *Behav Pharmacol* **19**, 518–529 (2008).
270. Ustione, A. & Piston, D. W. Dopamine synthesis and D3 receptor activation in pancreatic  $\beta$ -cells regulates insulin secretion and intracellular  $[Ca^{2+}]$  oscillations. *Mol. Endocrinol.* **26**, 1928–1940 (2012).
271. Vilches-Flores, A., Delgado-Buenrostro, N. L., Navarrete-Vázquez, G. & Villalobos-Molina, R. CB1 cannabinoid receptor expression is regulated by glucose and feeding in rat pancreatic islets. *Regul. Pept.* **163**, 81–87 (2010).
272. Li, C., Bowe, J. E., Jones, P. M. & Persaud, S. J. Expression and function of cannabinoid receptors in mouse islets. *Islets* **2**, 293–302 (2010).
273. Kim, W. *et al.* Cannabinoids inhibit insulin receptor signaling in pancreatic  $\beta$ -cells. *Diabetes* **60**, 1198–1209 (2011).
274. Li, C. *et al.* Cannabinoid receptor agonists and antagonists stimulate insulin secretion from isolated human islets of Langerhans. *Diabetes Obes Metab* **13**, 903–910 (2011).
275. Rorsman, F. *et al.* Aromatic-L-amino-acid decarboxylase, a pyridoxal phosphate-dependent enzyme, is a beta-cell autoantigen. *Proc. Natl. Acad. Sci. U.S.A.* **92**, 8626–8629 (1995).
276. Alpert, S., Hanahan, D. & Teitelman, G. Hybrid insulin genes reveal a developmental lineage for pancreatic endocrine cells and imply a relationship with neurons. *Cell* **53**, 295–308 (1988).
277. Baekkeskov, S. *et al.* Identification of the 64K autoantigen in insulin-dependent diabetes as the GABA-synthesizing enzyme glutamic acid decarboxylase. *Nature* **347**, 151–156 (1990).
278. Atouf, F., Czernichow, P. & Scharfmann, R. Expression of neuronal traits in pancreatic beta cells. Implication of neuron-restrictive silencing factor/repressor element silencing transcription factor, a neuron-restrictive silencer. *J. Biol. Chem.* **272**, 1929–1934 (1997).
279. Gao, N. *et al.* Foxa1 and Foxa2 maintain the metabolic and secretory features of the mature beta-cell. *Mol. Endocrinol.* **24**, 1594–1604 (2010).
280. Quintens, R., Hendrickx, N., Lemaire, K. & Schuit, F. Why expression of some genes is disallowed in beta-cells. *Biochem. Soc. Trans.* **36**, 300–305 (2008).
281. Sekine, N. *et al.* Low lactate dehydrogenase and high mitochondrial glycerol phosphate dehydrogenase in pancreatic beta-cells. Potential role in nutrient sensing. *J. Biol. Chem.* **269**, 4895–4902 (1994).
282. Thiel, G. & Schuit, F. No REST for healthy beta cells. *Diabetologia* **51**, 1343–1346 (2008).
283. Martin, D. *et al.* Functional significance of repressor element 1 silencing transcription factor (REST) target genes in pancreatic beta cells. *Diabetologia* **51**, 1429–1439 (2008).
284. Yasuda, T. *et al.* PAX6 mutation as a genetic factor common to aniridia and glucose intolerance. *Diabetes* **51**, 224–230 (2002).
285. White, P. & Kaestner, K. H. Gene expression analysis in diabetes research. *Methods Mol. Biol.* **560**, 239–261 (2009).
286. Rankin, M. M. & Kushner, J. A. Aging induces a distinct gene expression program in mouse islets. *Islets* **2**, 345–352 (2010).

287. Dreja, T. *et al.* Diet-induced gene expression of isolated pancreatic islets from a polygenic mouse model of the metabolic syndrome. *Diabetologia* **53**, 309–320 (2010).
288. MacGregor, R. R. *et al.* Small rat islets are superior to large islets in in vitro function and in transplantation outcomes. *Am. J. Physiol. Endocrinol. Metab.* **290**, E771–779 (2006).
289. Williams, S. J. *et al.* Adhesion of pancreatic beta cells to biopolymer films. *Biopolymers* **91**, 676–685 (2009).
290. Janette Williams, S. *et al.* Reduction of diffusion barriers in isolated rat islets improves survival, but not insulin secretion or transplantation outcome. *Organogenesis* **6**, 115–124 (2010).

## IV. Publications, talks, and posters

Davide Cavanna\*, Daniel Gradinger\*, Nina Schieven, Gerhard K. H. Przemeck, Martin Hrabé de Angelis.

### **$\beta$ -cell dedifferentiation in the *Pax6*<sup>Leca2</sup> ENU-generated mouse line.**

Manuscript in preparation.

\*contributed equally

Davide Cavanna, Daniel Gradinger, Nina Schieven, Gerhard K. H. Przemeck, Martin Hrabé de Angelis.

### **Analysis of Delta-like 1 (DLL1) in adult murine islets.**

26<sup>th</sup> International Mammalian Genome Conference (21/10/2012 St Pete Beach, Florida, USA), oral and poster presentation.

***Prize-winning "Outstanding poster presentation"***

Daniel Gradinger, Davide Cavanna, Christian Cohrs, Nina Schieven, Tanka Becke, Gerhard K. H. Przemeck, Martin Hrabé de Angelis.

### **Molecular and histological comparison of pancreata from adult *Pax6*<sup>Leca2</sup> mice of different ages.**

26<sup>th</sup> International Mammalian Genome Conference (21/10/2012 St Pete Beach, Florida, USA), oral and poster presentation.

***Prize-winning "Outstanding poster presentation"***

### **Analysis of Delta-like 1 (DLL1) in adult murine islets.**

10<sup>th</sup> DZD Workshop, 12/11/2012, München, oral presentation.

### **Gene Expression analyses with isolated murine islets of Langerhans: strategy and caveats.**

8<sup>th</sup> DZD Workshop, 26/03/2012, Tübingen, oral presentation.

## V. Acknowledgments

I am grateful to Prof. Dr. Martin Hrabé de Angelis for the opportunity to perform my doctoral thesis in his esteemed laboratory and with such an interesting topic, as well as for his kindness and charisma as a supervisor. His constant interest in my progress was a source of motivation and support.

I would also like to thank Dr. Gerhard Przemeck for his excellent mentoring and support throughout my thesis, and Prof. Dr. Heiko Lickert for the constructive suggestions and discussions that helped me along the way.

A very special thanks goes to Daniel Gradinger, Nina Schieven, and Dr. Christian Cohrs for the wonderful teamwork. Daniel prepared his doctoral thesis in parallel to and in close collaboration with mine, and I like to think that we were able to produce more than just the sum of two parts. The interchange of ideas and know-how was especially valuable at a time in which the institute was re-orienting itself with a new focus on diabetes research. Nina Schieven provided technical assistance of first-class level and showed a lasting curiosity in my work and progress as well as a willingness to support me in frustrating times that proved invaluable. Dr. Christian Cohrs simply is the most patient and competent individual I had the pleasure to meet in my time on this planet. I am proud to have shared a lab with all three of them.

I would also like to thank Dr. Karin Schwarzenbacher and Dr. Peter Huypens for their readiness to engage in illuminating and helpful discussions about my project and my data. They are both very capable and kind individuals, and their help is greatly appreciated.

I am grateful to Dr. Kerstin Adler, Dr. Jan Rozman, Dr. Peter Huypens, Dr. Susanne Neschen, Barbara Fridrich, Melanie Kahle, Anja Wohlbier, and Dr. Ana Messias and for the training and technical help they provided me with in specific laboratory techniques. I thank Dr. Helmut Fuchs and Dr. Valerie Gailus-Durner for the possibility they granted me to work in the rooms of the German Mouse Clinic.

To all my colleagues here at the IEG I am deeply grateful for the enjoyable and stimulating atmosphere. I can say with certainty that I am not the same person I was before I started working here.

## **VI. Affirmation**

Ich erkläre hiermit an Eides statt, dass ich die vorliegende Arbeit selbstständig, ohne unzulässige fremde Hilfe und ausschließlich mit den angegebenen Quellen und Hilfsmitteln angefertigt habe. Die verwendeten Literaturquellen sind im Literaturverzeichnis (References) vollständig zitiert. Diese Arbeit hat in dieser oder ähnlicher Form noch keiner anderen Prüfungsbehörde vorgelegen.

München, den 25.06.2013

Davide Cavanna